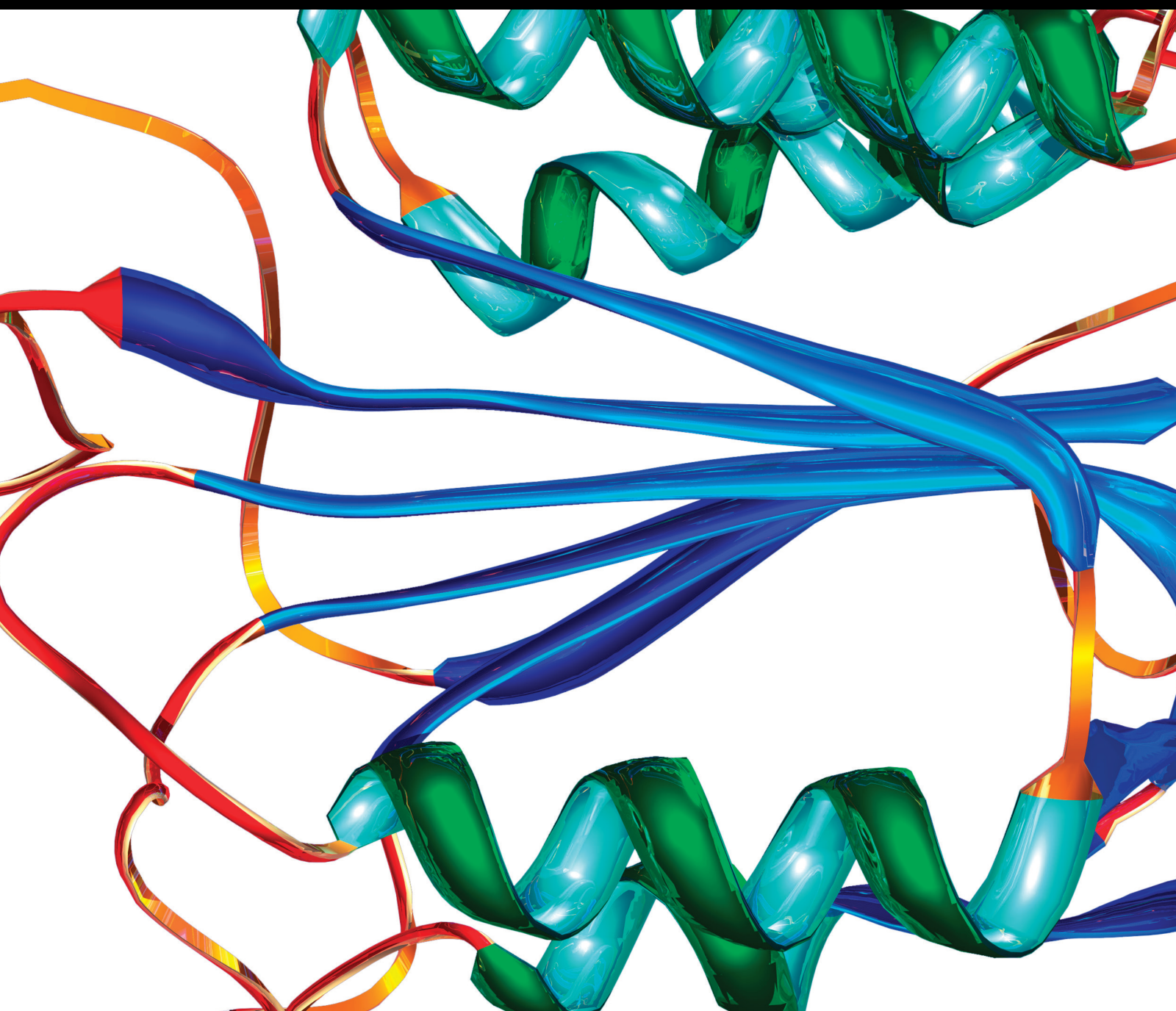# New Therapeutic Targets of Non-Small Cell Lung Cancer

Lead Guest Editor: Cheng Zhan
Guest Editors: Jianrong Zhang, Jiaqi Liang, Ming Li, and Zhijie Xu

New Therapeutic Targets of Non-Small Cell Lung Cancer

New Therapeutic Targets of Non-Small Cell Lung Cancer

Lead Guest Editor: Cheng Zhan
Guest Editors: Jianrong Zhang, Jiaqi Liang, Ming Li, and Zhijie Xu

Chief Editor

Paola Gazzaniga, Italy

Alexander G. Mathioudakis, United Kingdom
Andrea Maugeri, Italy
Prasenjit Mitra, India
Ekansh Mittal, USA
Hiroshi Miyamoto, USA
Naoshad Muhammad, USA
Chiara Nicolazzo, Italy
Xing Niu, China
Dong Pan, USA
Dr.Krupakar Parthasarathy, India
Robert Pichler, Austria
Dimitri Poddighe, Kazakhstan
Roberta Rizzo, Italy
Maddalena Ruggieri, Italy
Tamal Sadhukhan, USA
Pier P. Sainaghi, Italy
Cristian Scheau, Romania
Jens-Christian Schewe, Germany
Alexandra Scholze, Denmark
Shabana, Pakistan
Anja Hviid Simonsen, Denmark
Eric A. Singer, USA
Daniele Sola, Italy
Timo Sorsa, Finland
Yaying Sun, China
Mohammad Tarique, USA
Jayaraman Tharmalingam, USA
Sowjanya Thatikonda, USA
Stamatios E. Theocharis, Greece
Tilman Todenhöfer, Germany
Anil Tomar, India
Alok Tripathi, India
Drenka Trivanović, Germany
Natacha Turck, Switzerland
Azizah Ugusman, Malaysia
Shailendra K. Verma, USA
Aristidis S. Veskoukis, Greece
Arianna Vignini, Italy
Jincheng Wang, Japan
Zhongqiu Xie, USA
Yuzhen Xu, China
Zhijie Xu, China
Guan-Jun Yang, China
Yan Yang, USA

Chengwu Zeng, China
Jun Zhang Zhang, USA
Qun Zhang, China
Changli Zhou, USA
Heng Zhou, China
Jian-Guo Zhou, China

Contents

Research Article

Lower Expression of TWEAK is Associated with Poor Survival and Dysregulate TIICs in Lung Adenocarcinoma

Zhengxi He [ID],[1,2,3,4] **Sai Wang** [ID],[5] **Jinchun Wu,**[1] **Yangchun Xie,**[6] and **Bin Li** [ID][1]

[1]Department of Oncology, Xiangya Hospital, Central South University, Changsha, Hunan 410008, China
[2]Hunan Cancer Hospital and The Affiliated Cancer Hospital of Xiangya School of Medicine, Central South University Changsha, Hunan 410013, China
[3]NHC Key Laboratory of Carcinogenesis, Hunan Cancer Hospital and The Affiliated Cancer Hospital of Xiangya School of Medicine, Central South University, Changsha, Hunan 410013, China
[4]Cancer Research Institute, Basic School of Medicine, Central South University, Changsha, Hunan 410011, China
[5]Department of Neurology, Xiangya Hospital, Central South University, Changsha, Hunan 410008, China
[6]Department of Oncology, The Second Xiangya Hospital, Central South University, Changsha, Hunan 410008, China

Correspondence should be addressed to Zhengxi He; 422594718@qq.com and Bin Li; bincsuxy@csu.edu.cn

Background. Lung cancer remains the leading cause of cancer death worldwide, and the most subtype is lung adenocarcinoma (LUAD). Tumor-infiltrating immune cells (TIICs) greatly impact the prognosis of LUAD. Tumor necrosis factor–like weak inducer of apoptosis (TWEAK), signal via its receptor fibroblast growth factor-inducible 14 (Fn14), dysregulates immune cell recruitment within tumor environment, thus promoting the progression of autoimmune diseases and cancer. We aimed to explore its role in LUAD. *Methods.* The expression level of TWEAK was explored in Tumor Immune Estimation Resource 2.0 (TIMER2.0) and Oncomine databases. The Tumor Immune Dysfunction and Exclusion (TIDE) and Lung Cancer Explorer (LCE) databases were applied to evaluate the survival in correlation to TWEAK expression. TIICs were assessed with TIMER2.0 and TIDE datasets. The expression of TWEAK protein was detected in LUAD cell lines and also in tissue samples from LUAD patients via western blotting or combination with immunochemistry. *Results.* Our results showed that TWEAK was downregulated in LUAD tumors compared to normal tissues in TIMER2.0, Oncomine, cell lines, and clinical specimens. Poor survival was uncovered in lower TWEAK expression of LUAD patients in LCE (meta − HR = 0.84 [95% CI, 0.76-0.92]) and TCGA (Continuous Z = −1.97, $p = 0.0486$) and GSE13213@PRECOG (Continuous Z = −4.25, $p = 2.12e − 5$) in TIDE. Multiple tumor-infiltrating immune cells (TIICs) were found closely correlated with TWEAK expression in LUAD, especially hematopoietic stem cell (Rho = 0.505, $p = 2.78e − 33$), common lymphoid progenitor (Rho = −0.504, $p = 3.79e − 33$), and myeloid-derived suppressor cells (MDSCs) (Rho = −0.615, $p = 1.36e − 52$). *Conclusion.* Lower level of TWEAK was linked with poor survival and aberrant recruitment and phenotype of TIICs in LUAD, which might motivate immune escape and weaken the effects of immunotherapy.

1. Introduction

Lung cancer is a deadly cancer with the highest morbidity and mortality around the world, among which lung adenocarcinoma (LUAD) is the most common pathological type. Currently, the prognosis of LUAD is still not satisfying, and the traditional treatments (including surgery, radiotherapy, and chemotherapy) are limited to a subset of patients

with partial remission. The emerging immunotherapy has achieved encouraging results in certain patients, but the prognosis of LUAD treated with immunotherapy was still varied even in the same TNM (Tumor, regional lymph Node, Metastasis) stage.

Tumor necrosis factor–related weak inducer of apoptosis (TWEAK), also termed TNFSF12, is located in chromosomal 17p13.1. TWEAK encodes many cytokines which is

widely distributed in normal tissues and produces a variety of functions in cancer through combing with Fn14 (TNFRSF12A) such as angiogenesis, proliferation, apoptosis, fibrosis, and epithelial-mesenchymal transform (EMT) [1–3]. Tumor necrosis factor-related weak inducer of apoptosis (TWEAK), also known as TNFSF12, is located on chromosome 17p13.1 and is a member of the TNF superfamily. TWEAK encodes a variety of cytokines, is widely distributed in normal tissues, and binds in cancer by binding to a type I transmembrane protein whose unique receptor, fibroblast growth factor-inducible 14 (Fn14, TNFRSF12A), has so far been reported producing multiple functions by activating the tumor necrosis factor receptor–associated factor (TRAF) signaling pathway and the nuclear factor kappa B (NF-κB) signaling pathway, such as angiogenesis, proliferation, apoptosis, fibrosis, and epithelial-mesenchymal transition (EMT) [1–3]. TWEAK is also the only ligand that binds to Fn14. Recent studies indicate that the aberrant TWEAK/FN14 pathway was engaged in some autoimmune diseases. TWEAK inhibits T helper 1 cells in the innate immune system by hindering IFN-γ and IL-12. Mutant TWEAK causes the lack of antibody by inhibiting the survival of B cells, and TWEAK inhibition can produce an antitumor effect through its regulation on macrophages [4, 5]. Therefore, TWEAK mediates crucial innate and adaptive immune pathways by modulating the function of various TIICs and shows an impact on the efficacy of immunotherapy and compound the prognosis of cancer patients [6–8].

In the present study, we investigated the TWEAK expression in LUAD in TIMER2.0 and TIDE databases and assessed the effect of TWEAK on the survival via TIDE and LCE databases. The relation between TWEAK and TIICs was explored in TIMER2.0 and TIDE. The results shown that low TWEAK expression indicates poor prognosis in LUAD and correlated with various TIICs, possibly due to the defective TWEAK/FN14 pathway.

2. Material and Methods

2.1. The Expression Profiles of TWEAK. The expression levels of TWEAK in cancers were explored from Tumor Immune Estimation Resource 2.0 (TIMER2.0) and Oncomine databases. TIMER2.0 (https://timer.cistrome.org) which based on a deconvolution method is a comprehensive web server which provides tumor-infiltrating immune cell (TIIC) information from gene expression profiles from The Cancer Genome Atlas (TCGA) [9–11]. Oncomine (https://www.oncomine.org/resource/login.html) is an integrated tool to analyze and validate gene expression and targets [12].

2.2. Prognostic Features of TWEAK. The survey of survival information of LUAD patients was carried out though Tumor Immune Dysfunction and Exclusion (TIDE) and Lung Cancer Explorer (LCE) databases. The TIDE database was used to speculate on the functions of genes regulating LUAD immunity and to comprehensively analyze the immune evasion mechanism of immune dysfunction and rejection to LUAD, so as to effectively predict the effect of immune checkpoint inhibition therapy [13]. LCE (https://lce.biohpc.swmed.edu/) is a powerful website to analyze gene expression and related clinical features in lung cancer [14].

2.3. The Correlation between TWEAK and TIICs. To analyze the association between TWEAK and TIICs, TIMER2.0 and TIDE databases were analyzed in this study. The relevance to TIICs (such as B cell, CD4+ T cell, CD8+ T cell, neutrophil, macrophage, and dendritic cell) was carried out via the immune-gene module in TIMER2.0 and query gene module in TIDE (Cytotoxic T lymphocytes, CTL), and all the results from TIMER2.0 were adjusted with purity.

2.4. PPI Network Analysis. To analyze the protein-protein interaction (PPI) network of TWEAK, the STING database was utilized. The STING database (https://string-db.org/) is a database including PPI networks from more than 24584628 proteins of 5090 organisms [15].

2.5. Cell Lines and Cell Culture. The human normal lung epithelial cell line HBE and NSCLC cell lines A549, H1299, H358, SPCA1, PC9, HCC827, and H1993 were purchased from the Cell Biology of Chinese Academy of Science (Shanghai, China). The cells were cultured in RPMI-1640 (Gibco, USA) supplemented with 10% fetal bovine serum (BIOIND, Israel), 100 μg/ml streptomycin, and 100 U/ml penicillin (Gibco, USA) at 37°C in a humidified 5% CO_2. The cells were passaged every 2-3 days by 0.25% trypsin (Gibco) and not cultured for more than 3 months.

2.6. Western Blotting. TWEAK and GAPDH were purchased from ImmunoWay (ImmunoWay Biotechnology Company, Plano, TX). The cells and tissue samples (Department of Thoracic, Xiangya Hospital of Central South University) were harvested and lysed with RIPA protein extraction reagent (Thermo Scientific, USA) supplemented with protease inhibitor cocktail. Approval by the Xiangya Hospital of Central South University Institutional Research Ethics Committee was obtained prior to collecting the archived tissue The protein concentrations were measured using the BCA assay (Pierce, CA, USA). Equal protein amounts were extracts and loaded per well and separated by electrophoresis on 8-10% SDS-PAGE and transferred on to polyvinylidene fluoride (PVDF) membrane (HyClone Laboratories, Logan, UT, USA). The membranes were blocked for 1 h at room temperature in Tris-buffered saline/0.1% Tween 20 (TBST) containing 5% (wt/vol) nonfat milk and then incubated with primary antibodies in TBST containing 5% (wt/vol) nonfat milk at 4°C overnight. The membranes were then incubated with an appropriate secondary antibody coupled to horseradish peroxidase 1 h at 37°C, and the proteins were detected by Luminata Forte western HRP substrate (Millipore, Billerica, MA, USA). Anti-GAPDH levels were detected for normalization.

2.7. Immunohistochemistry. Protein expression detected by IHC was performed on LUAD pathological sections. We obtained formalin-fixed, paraffin-embedded recurrent LUAD specimens (40 patients) from the Department of Pathology, Xiangya Hospital of Central South University and prepared tissue sections (5 μm). Patient characteristics

are summarized in Supplementary Table S1. The specimens were immunostained using the UltraVision Quanto horseradish peroxidase detection system (Thermo Fisher Scientific). After routine deparaffinization with a series of xylene and alcohols, antigen retrieval was performed using 90% formic acid. Slides were then rinsed with distilled H_2O and wash buffer. Endogenous peroxidase activity was blocked with H_2O_2 solution (TA-125-HP, Thermo Fisher Scientific) for 10 min prior to incubation with a rabbit anti-TWEAK monoclonal antibody (ImmunoWay Biotechnology Company, Plano, TX) at 1 : 100 for 60 min at room temperature. The primary antibody signal was developed with Quanto detection reagents and 3,3′-diaminobenzidine chromogen as per the manufacturer's instructions. Virtual slides were produced by scanning the immunohistochemical (IHC) glass slides using the Aperio CS2 digital pathology scanner (Leica Biosystems). Digital quantitative analysis of TWEAK immunoreactivity in cells was performed by an experienced pathologist in a blinded manner with Aperio ImageScope software v12.2.2.5015 (Leica Biosystems) using a customized positive pixel count algorithm. Stain intensity values are provided as a scoring system for each chromophore comprised of staining intensity and extensiveness captured the outcome: 0, negative; 1, weak; 2 moderate; and 3, strong.

2.8. Statistical Analysis. The expression of TWEAK was calculated by the Wilcoxon test, and the purity-adjusted Rho between TWEAK and TIICs was computed by Spearman's correlation coefficient in TIMER2.0. For the TWEAK IHC staining and the western blot signal quantitation results, statistical analysis was performed using 2-way ANOVA and X^2 test. p values <0.05 were considered significant.

3. Results

3.1. The Expression of TWEAK Was Decreased in Tumor Area. To explore the expression of TWEAK in LUAD, TIMER2.0 and Oncomine databases were used. From TIMER2.0, TWEAK expression was drownregulated in LUAD than normal tissues (Figure 1(a)). Similar results were obtained in 15/16(93.75%) datasets from Oncomine (Figure 1(b)).

3.2. Lower Level of TWEAK Correlated to Shorter OS. In order to explore the overall survival (OS) of LUAD patients according to TWEAK expression, the TIDE and LCE databases were analyzed. From TIDE, poorer OS was greatly relevant to lower TWEAK in TCGA (Continuous Z = −1.97, $p = 0.0486$) (Figure 2(a)) and GSE13213@PRECOG (Continuous Z = −4.25, $p = 2.12e − 5$) (Figure 2(b)). Besides, similar outcomes were obtained from the meta-analysis part of LCE (meta − HR = 0.84 [95% CI, 0.76-0.92]) (Figure 2(c)).

3.3. TWEAK Was Highly Related to TIICs. To explore the relationship between TWEAK expressive and TIICs, the TIMER2.0 and TIDE databases were explored (Figure 3). It was revealed from the TIMER2.0 that TWEAK was negatively associated with common lymphoid progenitor, MDSC, mast cell resting, and T cell CD4+Th2, while it was

positively related to hematopoietic stem cell, granulocyte-monocyte progenitor, cancer-associated fibroblast, cancer-switched memory B cell, common myeloid progenitor, T cell NK, endothelial cell, monocyte, eosinophil, and macrophage/monocyte. Besides, by analyzing in TIDE, CTLs also were positively correlated with TWEAK in TCGA ($r = 0.144$, $p = 0.00142$) and GSE13213@PRECOG ($r = 0.255$, $p = 0.00553$). Among these TIICs, hematopoietic stem cell, common lymphoid progenitor, and MDSC were the most closed TIICs ($|Rho| > 0.5$).

3.4. The PPI Network of TWEAK. To explore the downstream targets of TWEAK, the STRING database was applied (Figure 4). From STRING analyses, we found that many genes had intertwined relationships with TWEAK, including TNFRSF12A, TNFRSF25, TNFSF13B, TNFSF11, BIRC2, TRAF2, TNF, TNFRSF1B, TNFRSF13C, and CASP8.

3.5. The Expression of TWEAK in LUAD Cell Lines and Tissues. In order to study the expression of TWEAK in LUAD, first, we tested the expression of TWEAK in fresh lung cancer tissues and normal adjacent tissues (See Supplementary Figure S1 for original results). We found that in 6 pairs of samples, TWEAK was strongly positive in 3 pairs of normal lung tissues (Figure 5(a)). Subsequently, we used western blot analysis to detect normal lung epithelial cell lines HBE and NSCLC cell lines A549, H1299, H358, SPCA1, PC9, HCC827, and H1993, among which lung adenocarcinoma cell lines are A549, H1299, SPCA1, and H1993. The results show that the expression of TWEAK in normal lung epithelial cell lines is relatively higher than its expression in lung adenocarcinoma cell lines, but the expression of TWEAK in other nonsmall cell lung cancers (non-LUAD) is higher than that in normal lung epithelial cell lines (Figure 5(b)). At the same time, we found that the TWEAK protein expression of H1299 is higher than that of HBE. Because the characteristic of the H1299 cell line is p53(-), we speculate that the expression of TWEAK may be related to lymphocyte infiltration and lymph node metastasis. However, more research is needed to explain this issue in the future.

Next, we reviewed 40 LUAD pathological specimens and used IHC analysis to detect the expression of TWEAK in the specimens. The clinicopathological characteristics of the LUAD patients are summarized in Supplementary Table 1. There were 26 female and 14 male patients with a median age of 54 years (range, 36-77 years). Histopathologic diagnosis included the following: well differentiated ($n = 7$, 17.5%), moderately differentiated ($n = 27$, 67.5%), and poorly differentiated ($n = 6$, 15%) tumors. Postoperative staging evaluation demonstrated stage I disease in 14 patients, stage II disease in 6 patients, stage III disease in 19 patients, and stage IV disease in 1 patient. We further detect the TWEAK protein expression in LUAD and the correlation with clinicopathological parameters. In the present study, all of the tumor sections were classified as TWEAK-positive as detected by IHC and positive staining was mainly located in the nucleus (Figure 5(c)). In addition, we found that TWEAK stains deeply (+++) in normal lung epithelial cells, while staining is relatively light
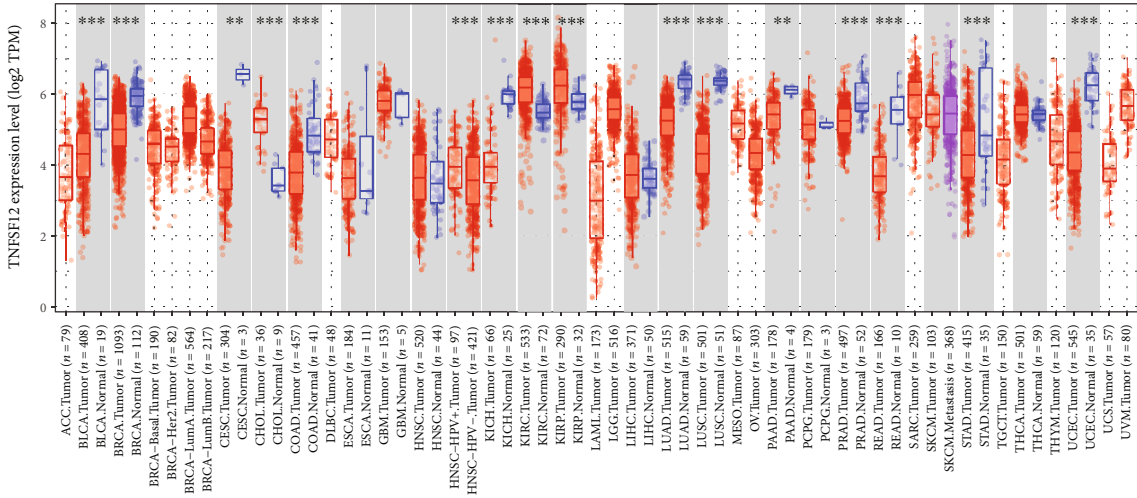
(a)

Comparison of TNFSF12 across 16 analyses
Under-expression/copy number loss

Median rank	*p*- value	Gene
733.0	5.80E-8	TNFSF12

1	2	3	4	5	6	7	8	9	10	11	12	13	14	15	16

Legend

1. Lung Adenocarcinoma vs.Normal
Bhattacharjee lung, *Proc Natl Acad Sci U S A*, 2001

2. Lung Adenocarcinoma vs.Normal
Hou lung, PLoS One, 2010

3. Lung Adenocarcinoma vs.Normal
Landi lung, PLoS One, 2008

4. Lung Adenocarcinoma vs.Normal
Okayama lung, Cancer Res, 2012

5. Lung Adenocarcinoma vs.Normal
Selamat lung, Genome Res, 2012

6. Lung Adenocarcinoma vs.Normal
Stearman lung, Am J Pathol, 2005

7. Lung Adenocarcinoma vs.Normal
Su lung, BMC Genomics, 2007

8. Acinar lung Adenocarcinoma vs.Normal
TCGA lung 2, No associated paper, 2012

9. Lung Adenocarcinoma vs.Normal
TCGA lung 2, No associated paper, 2012

10. Lung Adenocarcinoma, Mixed Subtype vs.Normal
TCGA lung 2, No associated paper, 2012

11. Lung Mucinous Adenocarcinoma, vs. Normal
TCGA lung 2, No associated paper, 2012

12. Micropapillary lung Adenocarcinoma, vs. Normal
TCGA lung 2, No associated paper, 2012

13. Mucinous Bronchiolalveolar Carcinoma, vs. Normal
TCGA lung 2, No associated paper, 2012

14. Non-Mucinous Bronchiolalveolar Carcinoma,vs. Normal
TCGA lung 2, No associated paper, 2012

15. Papillary lung Adenocarcinoma,vs. Normal
TCGA lung 2, No associated paper, 2012

16. Lung Adenocarcinoma vs.Normal
Weiss lung, Sci Transl Med, 2010

1	5	10	25		25	10	5	1	

Not measured

%

The rank for a gene is the median rank that gene across each of the analyses.
The *p*- value for a gene is its *p*- value for the median-ranked analysis

(b)

FIGURE 1: The expression status of TWEAK from TIMER2.0 (a) and Oncomine (b). Note: *p value <0.05; **p value <0.01; and ***p value <0.001.

(a)

(b)

(c)
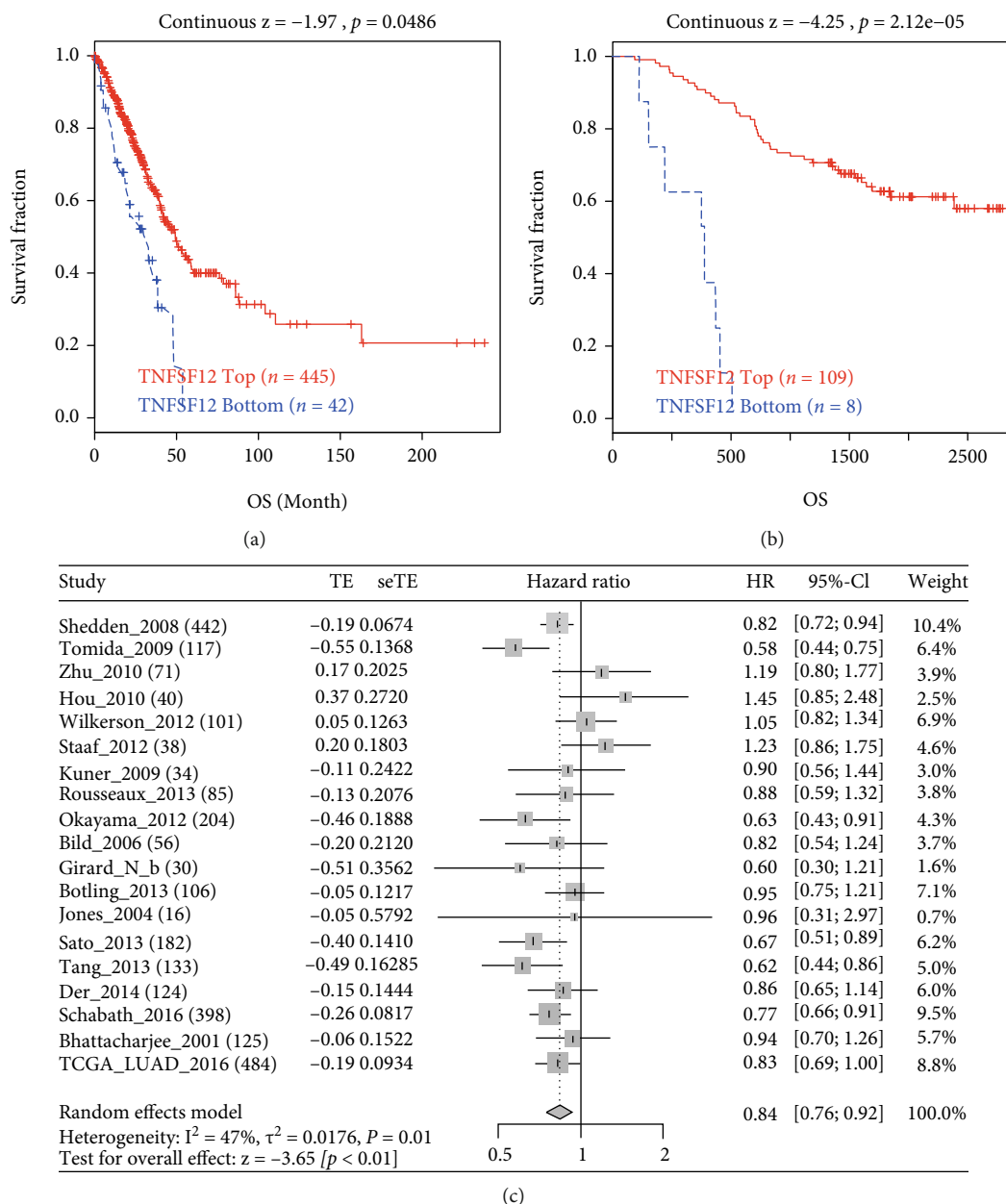
Figure 2: Prognostic value of TWEAK expression in LUAD. TCGA (a), GSE13213@PRECOG, (b) and meta-analyses (c).

(+) in LUAD epithelium. Deep staining of nuclei also appeared in the inflammatory cells of LUAD, suggesting that the expression of TWEAK is also related to inflammation [16]. The correlation of TWEAK expression with clinicopathological parameters was then investigated. TWEAK expression was significantly associated with differentiation, pTNM stage, primary tumor size, lymph node metastasis, and tumor location. No significant relationship was noted between TWEAK 19 expression and gender, age, smoking history, and histological type (Table 1).

4. Discussion

Lung cancer is still the most severe threat to the population around the world due to its high mortality [17]. LUAD is the majority subtype among lung cancer. Immunotherapy has opened a new field for LUAD treatment because of its comparatively higher tolerance and prolonged effectiveness with possible tumor clearance compared with traditional chemotherapy administration. But the act of immunotherapy somewhat depends on the function of immune cells within tumor itself or around tumor microenvironment.

TWEAK is a type II transmembrane protein, belonging to the member of the tumor necrosis factor superfamily (TNFSF) ligands. It plays an important role in the development of cancer through multiple ways including TRAF and NFκB pathways by combining with FN14 [18], such as inflammation [16], proliferation and/or apoptosis of cancer cells, angiogenesis, and epithelial-mesenchymal transform (EMT) [19].

(a)

(b)

(c)

(d)

(e)

(f)

Figure 3: Continued.

(g)

(h)

(i)

(j)

(k)

(l)

Figure 3: Continued.

(m)

(n)

(o)

(p)
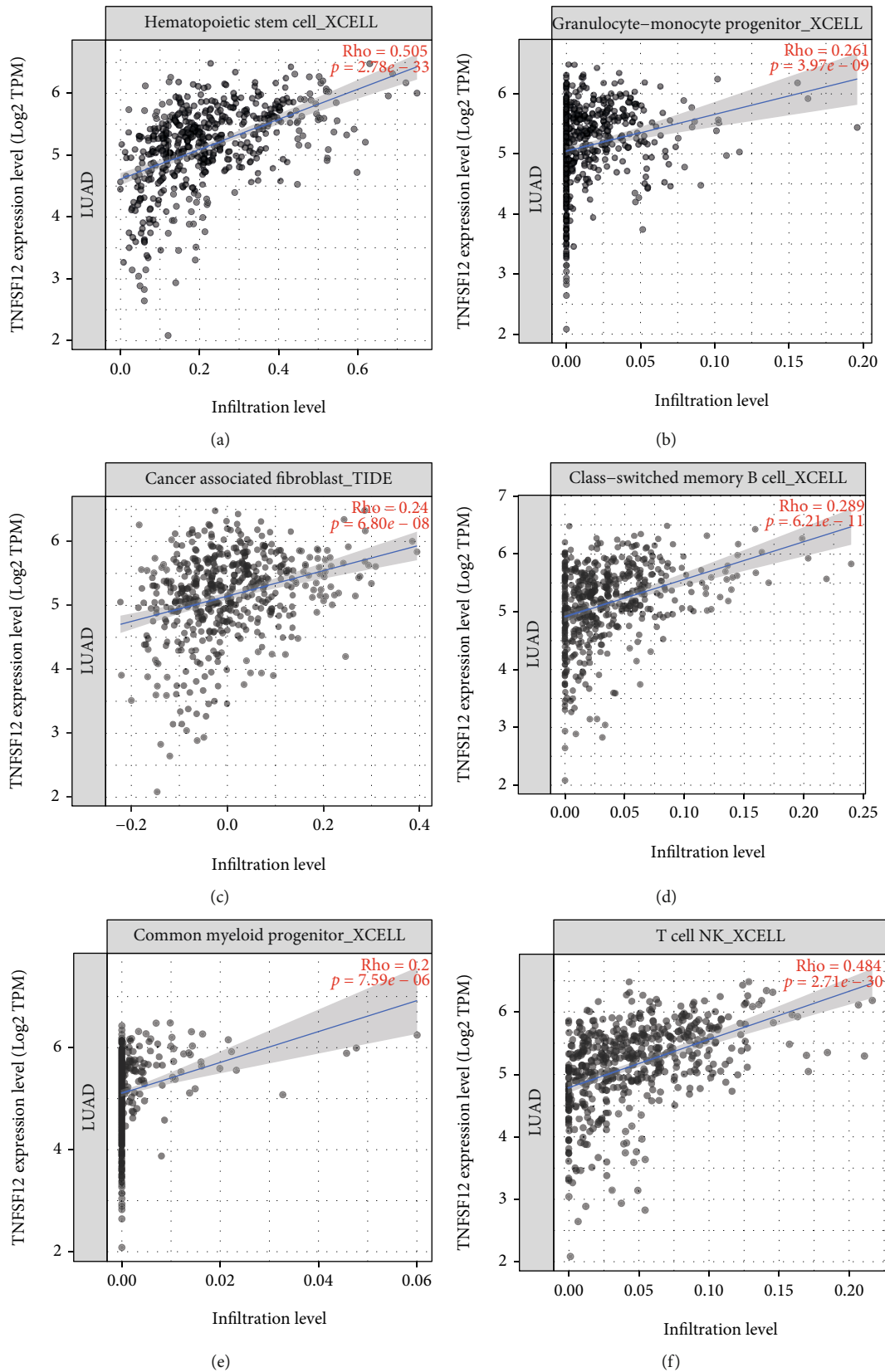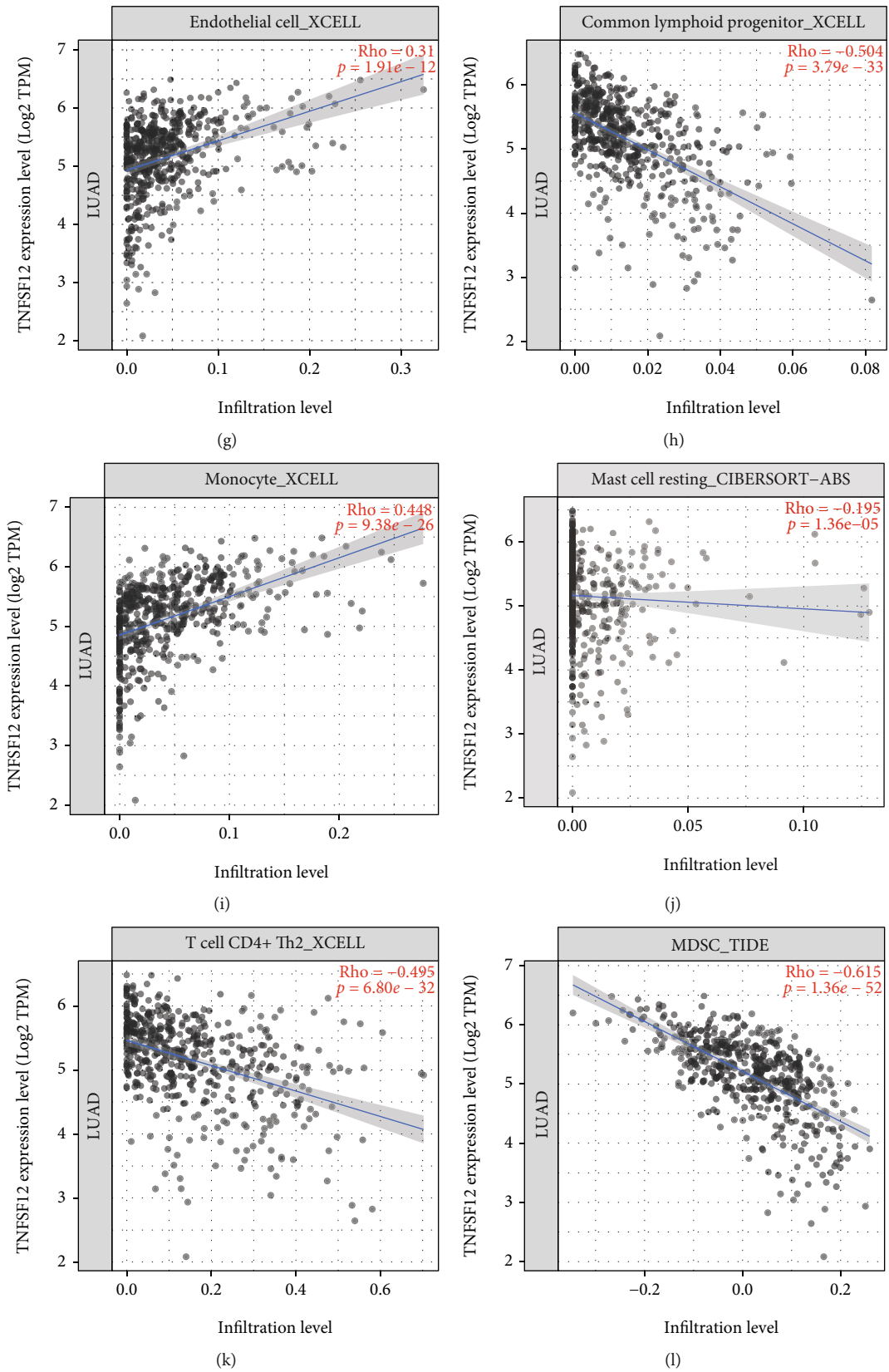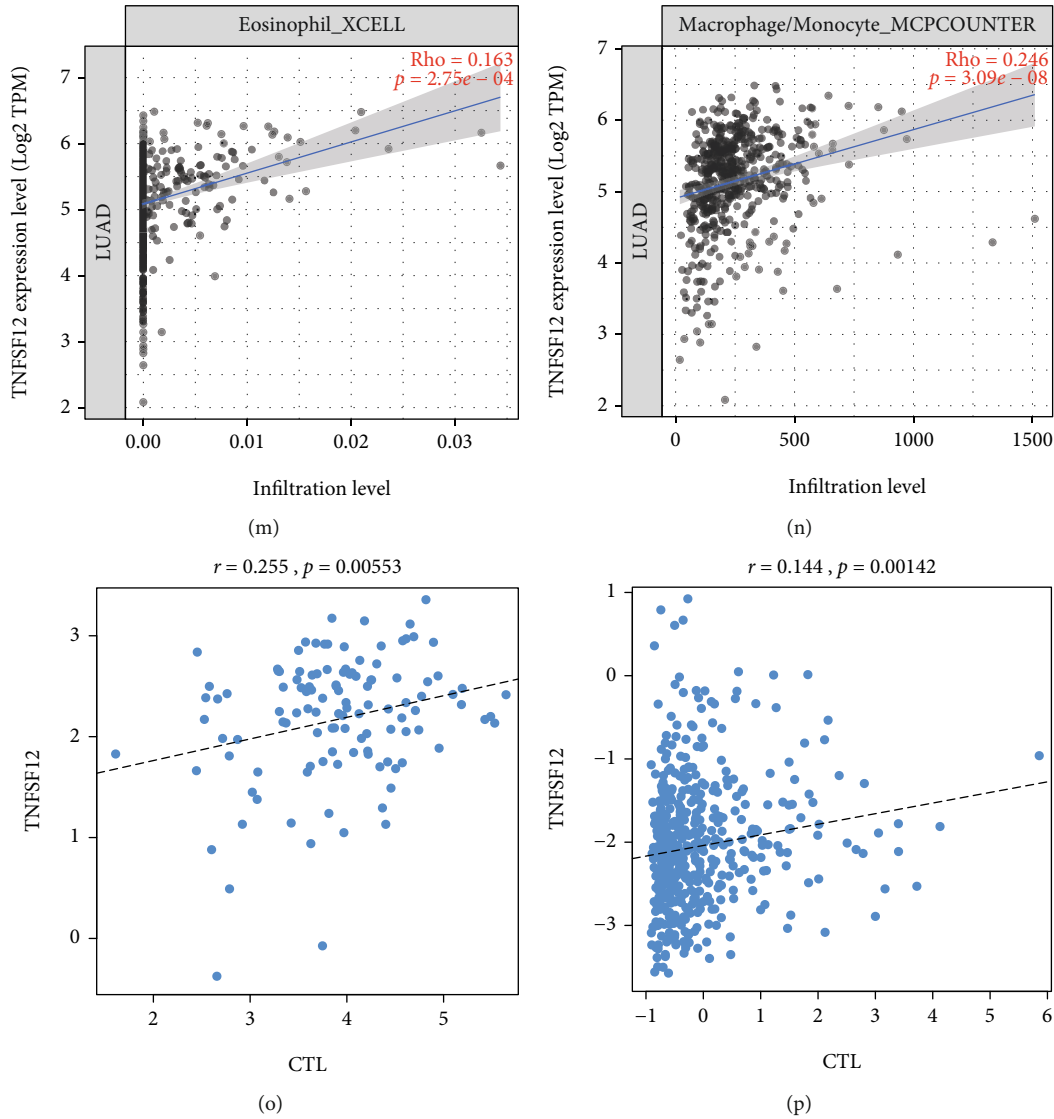
Figure 3: The relationships between TWEAK expression and TIICs in LUAD.
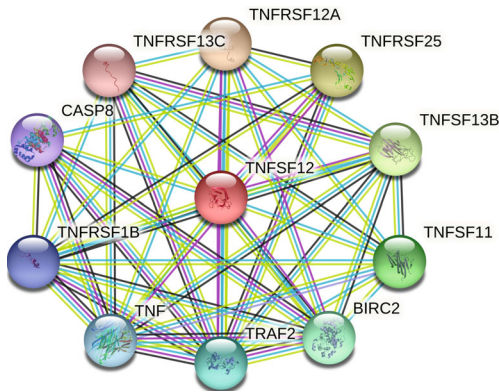
Figure 4: The PPI network of TWEAK. Different color lines: blue: from curated databases; purple: experimentally determined; green: gene neighborhood; black: coexpression; and lavender: protein homology.

Our study revealed that lower expression of TWEAK was connected with worse prognosis. In TIMER2.0 and Oncomine databases, the results showed the decreased TWEAK expression in LUAD tumors compared to normal tissues. Further investigation based on TIDE and LCE suggested that shorter survival appeared in poorer expression of TWEAK in LUA. Therefore, low TWEAK expression was an inferior prognostic biomarker of LUAD.

Besides, less TWEAK is likely to be related with the infiltrations of TIICs in LUAD. According to the TIDE, the CTL was positively related with TWEAK in TIDE. Furthermore, in TIMER2.0, we found that TWEAK shown up in a subtractive relevance to common lymphoid progenitor, MDSC, mast cell resting, and T cell CD4+ Th2 and in a positive correlation with hematopoietic stem cell, granulocyte-monocyte progenitor, cancer-associated fibroblast, cancer-switched memory B cell, common myeloid progenitor, T cell NK, endothelial cell, monocyte, eosinophil, and macrophage/monocyte, especially hematopoietic stem cell, common lymphoid progenitor, and MDSC.

(a)

(b)

(c)
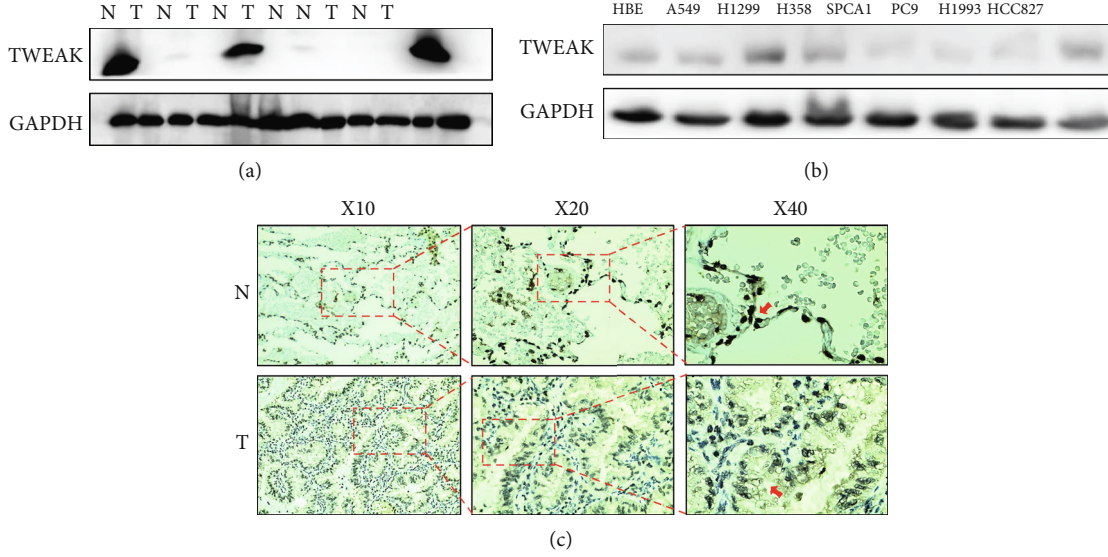
FIGURE 5: TWEAK expression in (a) normal lung epithelium tissue (N) and LUAD tissue (T), (b) normal lung epithelium cell line and LUAD cell line (detected by WB), (c) normal lung epithelium tissue (N), and LUAD tissue (T) (detected by WB and IHC).

Existing researches can be used to help decipher our findings of the role of TWEAK. Although TWEAK is upregulated in many tumors, lower TWEAK level was reported in squamous cervical carcinoma [20], endometrial cancer [21], NSCLS [22], and glioblastoma [23]. Furthermore, poor survival with downregulated TWEAK was proved in head and neck cancer and squamous cervical carcinoma [20, 24]. However, it has not been observed that TWEAK had an impact on the survival in NSCLC.

The poor survival of low TWEAK expression patients might connect with various TIICs. Previous studies found that TWEAK tends to be expressed in a variety of immune cell regions (including dendritic cells, circulating NK cells, and resting and activated monocytes [25]). Many studies have confirmed that TWEAK could induce the death of cancer cells through TWEAK/FN14 pathways, such as apoptosis, necrosis, and indirect cell death [4, 26]. TIICs could also inhibit the survival of cancer cells by surveillance and cytotoxicity [27] of the immune system via TWEAK. For example, macrophages could induce apoptosis by motivating CD4+T Cell through TWEAK pathways [28], whereas longtime of immune infiltrating may transform lesions into the status of chronic inflammation [29] and induce the apoptosis of TIICs themselves [30], which may arouse an environment of immune escape and failure to immunotherapy [31]. On the other hand, the increased inhibitory TIICs could also contribute to the progression of LUAD patients. For instance, MDSCs help cancer cells escape from the immune system and resistant to immunotherapy [32]. In short, the death of cancer cells which might be derived from TIICs and TWEAK/FN14 could account for the difference of prognosis in LUAD.

In addition, it was discovered that TWEAK is positively related with its receptors (FN14, Figure 6(a), and CD163, Figure 6(b)) in TIMER2.0. However, FN14 could accelerate the progression of cancer without the participant of TWEAK [33], which is eccentric to the effects of TWEAK in this

TABLE 1: Association of TWEAK expression with clinicopathological features in LUAD specimens.

Variables	Number	Tweak expression			
		+	++	+++	p value
Sex		23	12	5	
Male	14	7	5	2	0.73
Female	26	16	7	3	
Age (years)					
<58	19	8	7	4	0.28
≥58	21	15	5	1	
Smoking history					
Smoker	19	8	10	1	0.62
Nonsmoker	21	15	2	4	
Differentiation					
Well	7	1	2	4	<0.05 *
Moderate	27	17	9	1	
Poor	6	5	1	0	
pTNM stages					
I-II	19	16	2	1	<0.05 *
III-IV	21	7	10	4	
Primary tumor size(cm)					
<4 cm	15	8	4	3	0.19
≥4 cm	25	15	8	2	
Lymph node metastasis					
Yes	26	16	10	0	<0.05 *
No	14	7	2	5	
Tumor location					
Central	6	3	2	1	<0.05 *
Peripheral	34	20	10	4	

*p value of X^2 test is shown. pTNM: pathological tumor/node metastasis.
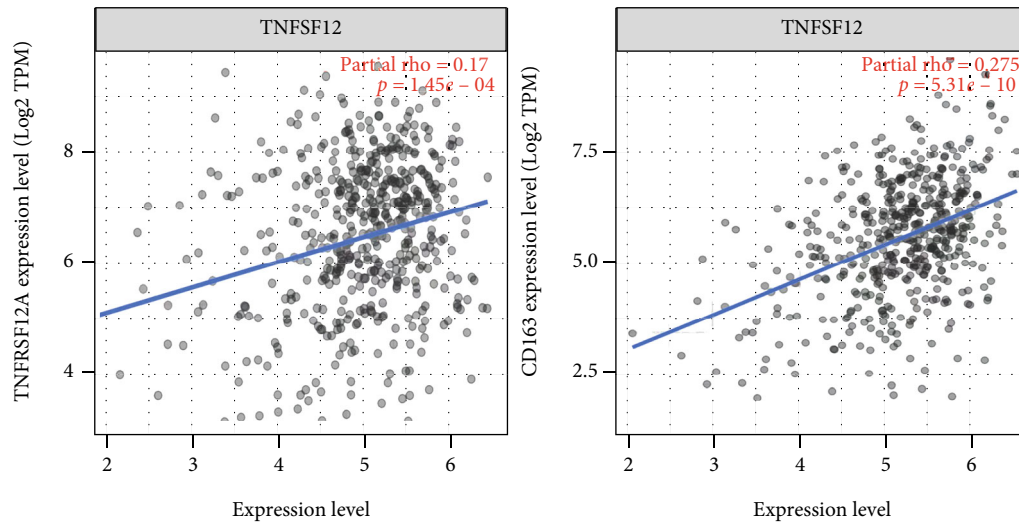
FIGURE 6: The correlations between TNFSF12 and its receptors. FN14 (a) and CD163 (b).

TABLE 2: TWEAK/Fn14 targeting therapeutic agents against cancers.

Target	Agent	Type of agent
Tweak [49–52]	RG7212 (RO5458640)	Neutralizing mAb
	Fn14-TRAIL (kahr-101)	Signal converter protein
	BIIB036 (P4A8)	Agonistic mAb
	I8DI	Agonistic mAb
Fn14 [53–61]	PDLI92	Agonistic mAb
	ITEM4-rGel	Immunotoxin conjugate
	hSGZ	Immunotoxin fusion protein
	Granzyme (GrB)-TWEAK and GrB-Fc-IT4	GrB-containing fusion protein
	Anti-Fn14 antibody conjugated nanoparticles	Drug-loaded nanoparticles

TRAIL: Tumor necrosis factor-related apoptosis-inducing ligand; mAb: Monoclonal antibody.

study. The reported another receptor, CD163, which appeared on the macrophages and monocytes which could promote cell proliferation [34], was also observed with poor survival in cancer [35]. These erratic phenomena need to be clarified and verified.

Since TWEAK is expressed in many types of solid tumors, it exhibits unprecedented potential clinical application value. A new type of human TWEAK receptor antibody (TweakR, Fn14, TNFRSF12A, and CD266) PDL192 was found to directly inhibit tumor cell growth and antibody-dependent cytotoxicity in a variety of mouse xenograft models, showing strong antitumor effects active [36]. Another TWEAK receptor antibody, RG7212, moved from the laboratory to clinical trials. RG7212 inhibits tumor growth by inhibiting tumor cell proliferation and survival signals, enhancing the host's antitumor immune response, but depends on the positive expression of Fn14 [37–39].

We found from the Kaplan-Meier database that the high expression of TweakR (Fn14) suggested poor OS ($n = 719$, $p = 0.0009$), but the expression of TWEAK was not significantly correlated with OS in LUAD patients ($n = 719$, $p = 0.2721$). Lab evidence suggests that low serum levels of TWEAK may be one of the characteristics of NSCLC [40],

and TWEAK/Fn14 induce NSCLC survival rate and treatment response by Mcl-1mediated [41]. Interestingly, among LUAD patients receiving chemotherapy, those with high TWEAK expression levels had poorer OS ($n = 36$, $p = 0.02$), suggesting that TWEAK is related to chemotherapy resistance. In the study of ovarian cancer, Fn14 seems to be able to overcome the resistance of chemotherapy drugs [42] and in gliomas, it is highly expressed in PDX of resistant patients [43]. This seemingly contradictory phenomenon undoubtedly indicates that TWEAK has potentially more unique and unexpected functions.

TWEAK is a type II transmembrane protein, but it can be cleaved by furin to produce soluble cytokines. Therefore, both membrane-anchored and soluble TWEAK can bind to Fn14 [44–46]. TWEAK is a glycoprotein with three parts, including a C-terminal extracellular domain, a transmembrane domain, and an N-terminal intracellular domain. Fn14 contains an extracellular domain that binds to TWEAK and a cytoplasmic tail necessary for signal transduction [47, 48]. Activation of TWEAK/Fn14 signaling triggers intracellular signaling cascades that include regulation of cell death (apoptosis or necrosis), proliferation, differentiation and migration, triggering of angiogenesis, and induction of inflammatory cytokine expression.

TWEAK/Fn14 signaling pathway is involved in tumor pathogenesis. It plays an important role in the growth, invasion, and migration of tumor cells. Furthermore, TWEAK/Fn14 activation triggers downstream signaling to regulate several key events related to tumor inflammation, angiogenesis, and EMT. Given their high tumor-related expression and multiple roles, TWEAK and Fn14 are considered two attractive targets for tumor therapy. Therefore, many drugs targeting TWEAK or Fn14 have been developed by researchers around the world in recent years (Table 2), and some TWEAK and Fn14 targeting drugs have been tested in preclinical trials and showed effective results. They exert antitumor effects through three pathways: neutralize soluble TWEAK, block Fn14 signaling, and directly kill Fn14-positive tumor cells. In the future, we should focus on basic and translational research on the TWEAK-Fn14 axis, which will be a suitable molecular target for the development of new tumor therapies; at the same time, more preclinical studies are needed to explore the safety of TWEAK/Fn14 in clinical practice effective treatment.

5. Conclusions

In this study, we found that lower TWEAK was related to poor prognosis and TIICs in LUAD. And decreased TWEAK was correlated with multiple immune cells in the tumor region. Intimate relationship between FN14 and TWEAK indicated that TWEAK/FN14 pathway possibly plays an important role in the survival of LUAD, but the underlying mechanism needs to be further explored.

Data Availability

The data used to support the findings of this study are available from the corresponding authors upon request.

Conflicts of Interest

The authors report no conflicts of interest in this work.

Authors' Contributions

Zhengxi He and Wang Sai are responsible for the experiments and writing, Jinchun Wu is responsible for data collection and sorting, and Yangchun Xie is responsible for proofreading. Zhengxi He and Bin Li are both the corresponding authors. Zhengxi He and Sai Wang, contributed equally to this work and co-First authors.

Acknowledgments

Supplementary Materials

Figure S1: the original data of TWEAK and GAPDH expression in (A, B) normal lung epithelium tissue (C, D) and normal lung epithelium cell line and LUAD cell line (detected by WB). Table S1: characteristics of LUAD patients. (Supplementary Materials)

References

[1] X. Wang, S. Xiao, and Y. Xia, "Tumor necrosis factor receptor mediates fibroblast growth factor-inducible 14 signaling," Cellular Physiology and Biochemistry, vol. 43, no. 2, pp. 579–588, 2017.

[2] G. Hu, W. Zeng, and Y. Xia, "TWEAK/Fn14 signaling in tumors," Tumour Biology, vol. 39, no. 6, 2017.

[3] Y. Zhang, W. Zeng, and Y. Xia, "TWEAK/Fn14 axis is an important player in fibrosis," Journal of Cellular Physiology, vol. 236, no. 5, pp. 3304–3316, 2021.

[4] Y. Kaduka, K. Takeda, M. Nakayama, K. Kinoshita, H. Yagita, and K. Okumura, "TWEAK mediates anti-tumor effect of tumor-infiltrating macrophage," Biochemical and Biophysical Research Communications, vol. 331, no. 2, pp. 384–390, 2005.

[5] X. Liu, S. Wu, Y. Yang, M. Zhao, G. Zhu, and Z. Hou, "The prognostic landscape of tumor-infiltrating immune cell and immunomodulators in lung cancer," Biomedicine & Pharmacotherapy, vol. 95, pp. 55–61, 2017.

[6] H. Maecker, E. Varfolomeev, F. Kischkel et al., "TWEAK attenuates the transition from innate to adaptive immunity," Cell, vol. 123, no. 5, pp. 931–944, 2005.

[7] S. Ye, M. I. Fox, N. A. Belmar et al., "Enavatuzumab, a humanized anti-tweak receptor monoclonal antibody, exerts antitumor activity through attracting and activating innate immune effector cells," Journal of Immunology Research, vol. 2017, Article ID 5737159, 2017.

[8] X. Yin, L. Luistro, H. Zhong et al., "RG7212 anti-TWEAK mAb inhibits tumor growth through inhibition of tumor cell proliferation and survival signaling and by enhancing the host antitumor immune response," Clinical Cancer Research, vol. 19, no. 20, pp. 5686–5698, 2013.

[9] T. Li, J. Fan, B. Wang et al., "TIMER: a web server for comprehensive analysis of tumor-infiltrating immune cells," Cancer Research, vol. 77, no. 21, pp. e108–e110, 2017.

[10] B. Li, E. Severson, J. C. Pignon et al., "Comprehensive analyses of tumor immunity: implications for cancer immunotherapy," Genome Biology, vol. 17, no. 1, p. 174, 2016.

[11] T. Li, J. Fu, Z. Zeng et al., "TIMER2.0 for analysis of tumor-infiltrating immune cells," Nucleic Acids Research, vol. 48, no. W1, pp. W509–W514, 2020.

[12] D. R. Rhodes, S. Kalyana-Sundaram, V. Mahavisno et al., "Oncomine 3.0: genes, pathways, and networks in a collection of 18,000 cancer gene expression profiles," Neoplasia, vol. 9, no. 2, pp. 166–180, 2007.

[13] P. Jiang, S. Gu, D. Pan et al., "Signatures of T cell dysfunction and exclusion predict cancer immunotherapy response," Nature Medicine, vol. 24, no. 10, pp. 1550–1558, 2018.

[14] L. Cai, S. Lin, L. Girard et al., "LCE: an open web portal to explore gene expression and clinical associations in lung cancer," Oncogene, vol. 38, no. 14, pp. 2551–2564, 2019.

[15] D. Szklarczyk, A. L. Gable, D. Lyon et al., "STRING v11: protein-protein association networks with increased coverage, supporting functional discovery in genome-wide experimental datasets," Nucleic Acids Research, vol. 47, no. D1, pp. D607–D613, 2019.

[16] D. Sidler, P. Wu, R. Herro et al., "TWEAK mediates inflammation in experimental atopic dermatitis and psoriasis," *Nature Communications*, vol. 8, no. 1, article 15395, 2017.

[17] F. Bray, J. Ferlay, I. Soerjomataram, R. L. Siegel, L. A. Torre, and A. Jemal, "Global cancer statistics 2018: GLOBOCAN estimates of incidence and mortality worldwide for 36 cancers in 185 countries," *CA: a Cancer Journal for Clinicians*, vol. 68, no. 6, pp. 394–424, 2018.

[18] M. Bhattacharjee, R. Raju, A. Radhakrishnan et al., "A bioinformatics resource for TWEAK-Fn14 signaling pathway," *Journal of Signal Transduction*, vol. 2012, Article ID 376470, 2012.

[19] Y. Itoigawa, N. Harada, S. Harada et al., "TWEAK enhances TGF-β-induced epithelial-mesenchymal transition in human bronchial epithelial cells," *Respiratory Research*, vol. 16, no. 1, 2015.

[20] H. Zou, D. Wang, X. Gan et al., "Low TWEAK expression is correlated to the progression of squamous cervical carcinoma," *Gynecologic Oncology*, vol. 123, no. 1, pp. 123–128, 2011.

[21] D. Wang, J. N. T. Fung, Y. Tuo, L. Hu, and C. Chen, "TWEAK/Fn14 promotes apoptosis of human endometrial cancer cells via caspase pathway," *Cancer Letters*, vol. 294, no. 1, pp. 91–100, 2010.

[22] W. A. Chang, M. C. Yen, J. Y. HuNg et al., "Investigation of the role of tumor necrosis factor-like weak inducer of apoptosis in non-small cell lung cancer," *Oncology Reports*, vol. 39, no. 2, pp. 573–581, 2018.

[23] N. L. Tran, W. S. McDonough, P. J. Donohue et al., "The human Fn14 receptor gene is up-regulated in migrating glioma cells in vitro and overexpressed in advanced glial tumors," *The American Journal of Pathology*, vol. 162, no. 4, pp. 1313–1321, 2003.

[24] F. X. Avilés-Jurado, X. Terra, D. Gómez et al., "Low blood levels of sTWEAK are related to locoregional failure in head and neck cancer," *European Archives of Oto-Rhino-Laryngology*, vol. 272, no. 7, pp. 1733–1741, 2015.

[25] X. Qi, M. Lei, L. Qin, M. Xie, D. Zhao, and J. Wang, "Endogenous TWEAK is critical for regulating the function of mouse uterine natural killer cells in an immunological model of pregnancy loss," *Immunology*, vol. 148, no. 1, pp. 70–82, 2016.

[26] A. Ikner and A. Ashkenazi, "TWEAK induces apoptosis through a death-signaling complex comprising receptor-interacting protein 1 (RIP1), Fas-associated death domain (FADD), and caspase-8," *The Journal of Biological Chemistry*, vol. 286, no. 24, pp. 21546–21554, 2011.

[27] M. Petitbarat, M. Rahmati, V. Sérazin et al., "TWEAK appears as a modulator of endometrial IL-18 related cytotoxic activity of uterine natural killers," *PLoS One*, vol. 6, no. 1, article e14497, 2011.

[28] M. J. Kaplan, D. Ray, R. R. Mo, R. L. Yung, and B. C. Richardson, "TRAIL (Apo2 ligand) and TWEAK (Apo3 ligand) mediate CD4+T cell killing of antigen-presenting macrophages," *Journal of Immunology*, vol. 164, no. 6, pp. 2897–2904, 2000.

[29] A. Son, T. Oshio, Y. I. Kawamura et al., "TWEAK/Fn14 pathway promotes a T helper 2-type chronic colitis with fibrosis in mice," *Mucosal Immunology*, vol. 6, no. 6, pp. 1131–1142, 2013.

[30] J. Zhu, P. F. Petit, and B. J. Van Den Eynde, "Apoptosis of tumor-infiltrating T lymphocytes: a new immune checkpoint mechanism," *Cancer Immunology, Immunotherapy*, vol. 68, no. 5, pp. 835–847, 2019.

[31] S. Y. Gun, S. W. L. Lee, J. L. Sieow, and S. C. Wong, "Targeting immune cells for cancer therapy," *Redox Biology*, vol. 25, article 101174, 2019.

[32] R. J. Tesi, "MDSC; the most important cell you have never heard of," *Trends in Pharmacological Sciences*, vol. 40, no. 1, pp. 4–7, 2019.

[33] W. Wang, F. Liu, C. Wang, C. Wang, Y. Tang, and Z. Jiang, "Src promotes metastasis of human non-small cell lung cancer cells through Fn14-mediated NF-κB signaling," *Medical Science Monitor*, vol. 24, pp. 1282–1294, 2018.

[34] H. Akahori, V. Karmali, R. Polavarapu et al., "CD163 interacts with TWEAK to regulate tissue regeneration after ischaemic injury," *Nature Communications*, vol. 6, no. 1, p. 7792, 2015.

[35] L. Yang, F. Wang, L. Wang et al., "CD163+ tumor-associated macrophage is a prognostic biomarker and is associated with therapeutic effect on malignant pleural effusion of lung cancer patients," *Oncotarget*, vol. 6, no. 12, pp. 10592–10603, 2015.

[36] J. Michaelson and L. Burkly, "Therapeutic targeting of TWEAK/Fn14 in cancer: exploiting the intrinsic tumor cell killing capacity of the pathway," *Results and Problems in Cell Differentiation*, vol. 49, pp. 145–160, 2009.

[37] T. G. Whitsett, S. P. Fortin Ensign, and H. D. Dhruv, "FN14 expression correlates with MET in NSCLC and promotes MET-driven cell invasion," *Clinical & experimental metastasis*, vol. 31, no. 6, pp. 613–623, 2014.

[38] D. Meulendijks, U. N. Lassen, L. L. Siu et al., "Exposure and tumor Fn14 expression as determinants of pharmacodynamics of the anti-TWEAK monoclonal antibody RG7212 in patients with Fn14-positive solid tumors," *Clinical Cancer Research : an Official Journal of the American Association for Cancer Research*, vol. 22, no. 4, pp. 858–867, 2016.

[39] U. N. Lassen, D. Meulendijks, L. L. Siu et al., "A phase I monotherapy study of RG7212, a first-in-class monoclonal antibody targeting TWEAK signaling in patients with advanced cancers," *Clinical Cancer Research : an Official Journal of the American Association for Cancer Research*, vol. 21, no. 2, pp. 258–266, 2015.

[40] E. Cheng, T. G. Whitsett, N. L. Tran, and J. A. Winkles, "The TWEAK receptor Fn14 is an Src-inducible protein and a positive regulator of Src-driven cell invasion," *Molecular Cancer Research*, vol. 13, no. 3, pp. 575–583, 2015.

[41] T. G. Whitsett, I. T. Mathews, M. H. Cardone et al., "Mcl-1 mediates TWEAK/Fn14-induced non-small cell lung cancer survival and therapeutic response," *Molecular Cancer Research : MCR*, vol. 12, no. 4, pp. 550–559, 2014.

[42] A. Y. Wu, L. Y. Gu, W. Cang et al., "Fn14 overcomes cisplatin resistance of high-grade serous ovarian cancer by promoting Mdm2-mediated p53-R248Q ubiquitination and degradation," *Journal of Experimental & Clinical Cancer Research*, vol. 38, no. 1, p. 176, 2019.

[43] D. S. Hersh, B. G. Harder, A. Roos et al., "The TNF receptor family member Fn14 is highly expressed in recurrent glioblastoma and in GBM patient-derived xenografts with acquired temozolomide resistance," *Neuro-Oncology*, vol. 20, no. 10, pp. 1321–1330, 2018.

[44] C. Bossen, K. Ingold, A. Tardivel et al., "Interactions of tumor necrosis factor (TNF) and TNF receptor family members in the mouse and human∗," *Journal of Biological Chemistry*, vol. 281, no. 20, pp. 13964–13971, 2006.

[45] S. Brown, A. Ghosh, and J. A. Winkles, "Full-length, membrane-anchored TWEAK can function as a juxtacrine

signaling molecule and activate the NF-κB pathway∗," *Journal of Biological Chemistry*, vol. 285, no. 23, pp. 17432–17441, 2010.

[46] C. Roos, A. Wicovsky, N. Müller et al., "Soluble and trans-membrane TNF-like weak inducer of apoptosis differentially activate the classical and noncanonical NF-κB pathway," *Journal of Immunology*, vol. 185, no. 3, pp. 1593–1605, 2010.

[47] J. A. Winkles, N. L. Tran, S. A. Brown, N. Stains, H. E. Cunliffe, and M. E. Berens, "Role of TWEAK and Fn14 in tumor biology," *Frontiers in Bioscience*, vol. 12, no. 1, pp. 2761–2771, 2007.

[48] M. M. Tajrishi, T. S. Zheng, L. C. Burkly, and A. Kumar, "The TWEAK-Fn14 pathway: a potent regulator of skeletal muscle biology in health and disease," *Cytokine & Growth Factor Reviews*, vol. 25, no. 2, pp. 215–225, 2014.

[49] Y. Dong, L. Yang, and P. Li, "Quercetin inhibits the proliferation and metastasis of human non-small cell lung cancer cell line: the key role of Src-mediated fibroblast growth factor-inducible 14 (Fn14)/nuclear factor kappa B (NF-κB) pathway," *Medical science monitor: international medical journal of experimental and clinical research*, vol. 26, Article ID e920537, 2020.

[50] N. Wisniacki, L. Amaravadi, G. R. Galluppi et al., "Safety, tolerability, pharmacokinetics, and pharmacodynamics of anti-TWEAK monoclonal antibody in patients with rheumatoid arthritis," *Clinical therapeutics*, vol. 35, no. 8, pp. 1137–1149, 2013.

[51] W D. Xu, Y. Zhao, and Y. Liu, "Role of the TWEAK/Fn14 pathway in autoimmune diseases," *Immunologic Research*, vol. 64, no. 1, pp. 44–50, 2016.

[52] A. Aronin, S. Amsili, T. B. Prigozhina et al., "Fn14Trail effectively inhibits hepatocellular carcinoma growth," *PLoS One*, vol. 8, no. 10, article e77050, 2013.

[53] J. S. Michaelson, R. Kelly, L. Yang, X. Zhang, K. Wortham, and I. B. Joseph, "The anti-Fn14 antibody BIIB036 inhibits tumor growth in xenografts and patient derived primary tumor models and enhances efficacy of chemotherapeutic agents in multiple xenograft models," *Cancer Biology & Therapy*, vol. 13, no. 9, pp. 812–821, 2014.

[54] J. S. Michaelson, A. Amatucci, R. Kelly et al., "Development of an Fn14 agonistic antibody as an anti-tumor agent," *MAbs*, vol. 3, no. 4, pp. 362–375, 2011.

[55] J. Trebing, I. Lang, M. Chopra et al., "A novel llama antibody targeting Fn14 exhibits anti-metastatic activity in vivo," *MAbs*, vol. 6, no. 1, pp. 297–308, 2014.

[56] L. de Plater, A. Vincent-Salomon, F. Berger et al., "Predictive gene signature of response to the anti-TweakR mAb PDL192 in patient-derived breast cancer xenografts," *PLoS One*, vol. 9, no. 11, article e104227, 2014.

[57] H. Zhou, S. Ekmekcioglu, J. W. Marks et al., "The TWEAK receptor Fn14 is a therapeutic target in melanoma: immuno-toxins targeting Fn14 receptor for malignant melanoma treatment," *Journal of Investigative Dermatology*, vol. 133, no. 4, pp. 1052–1062, 2013.

[58] H. Zhou, W. N. Hittelman, H. Yagita et al., "Antitumor activity of a humanized, bivalent immunotoxin targeting Fn14-positive solid tumors," *Cancer Research*, vol. 73, no. 14, pp. 4439–4450, 2013.

[59] H. Zhou, J. W. Marks, W. N. Hittelman et al., "Development and characterization of a potent immunoconjugate targeting the Fn14 receptor on solid tumor cells," *Molecular Cancer Therapeutics*, vol. 10, no. 7, pp. 1276–1288, 2011.

[60] H. Zhou, K. A. Mohamedali, A. M. Gonzalez-Angulo et al., "Development of human serine protease-based therapeutics targeting Fn14 and identification of Fn14 as a new target over-expressed in TNBC," *Molecular Cancer Therapeutics*, vol. 13, no. 11, pp. 2688–2705, 2014.

[61] C. S. Schneider, J. G. Perez, E. Cheng et al., "Minimizing the non-specific binding of nanoparticles to the brain enables active targeting of Fn14-positive glioblastoma cells," *Biomaterials*, vol. 42, pp. 42–51, 2015.

Research Article

Systemic Analyses of the Expression of TPI1 and Its Associations with Tumor Microenvironment in Lung Adenocarcinoma and Squamous Cell Carcinoma

Xiaodong Yang (iD), **Cong Ye, Hui Zheng, Chenyang Dai** (iD), **and Yuming Zhu** (iD)

Department of Thoracic Surgery, Shanghai Pulmonary Hospital, Tongji University, Shanghai, China

Correspondence should be addressed to Chenyang Dai; daichenyang@tongji.edu.cn and Yuming Zhu; ymzhu2005@aliyun.com

Background. Recent studies have shown that the expression level of triosephosphate isomerase 1 (*TPI1*) may be associated with the occurrence and metastasis of tumors, but the expression level of *TPI1* and its effect on lung adenocarcinoma (LUAD) and squamous cell carcinoma (LUSC) are not yet clear. *Methods*. We comprehensively explored and validated the *TPI1* expression in lung adenocarcinoma and lung squamous cell carcinoma in public datasets. The associations of *TPI1* expression with clinicopathological characteristics and prognosis were also studied in both histological types. Moreover, we analyzed the potential relations of *TPI1* with immunomodulators and immune cell infiltrations in the tumor microenvironment based on previous literatures and bioinformatic tools. *Results*. We found that *TPI1* was significantly overexpressed in LUAD and LUSC. Significant associations of *TPI1* expression were observed regarding age, gender, and pathological stages in LUAD. However, similar trend was only found with respect to age in LUSC. The high expression of *TPI1* was significantly associated with worse survival in LUAD, but not in LUSC. Furthermore, we explored the potential distribution and changes of *TPI1* expression in tumor microenvironment. Pathway enrichment analyses were performed to identify possible roles of *TPI1* in both lung cancers. *Conclusions*. TPI1 was overexpressed in both LUAD and LUSC. Increased *TPI1* expression was correlated with poor prognosis in LUAD and changed immune cell infiltrating in various degrees in both histological types. Our study provides insights in understanding the potential roles of *TPI1* in tumor progression and immune microenvironment.

1. Introduction

Lung cancer is one of the most commonly diagnosed cancers, with over 1,700,000 new cases every year [1, 2]. The current histopathological classification revealed that lung adenocarcinoma (LUAD) and lung squamous cell carcinoma (LUSC) comprise majority of all lung cancers. Cancer metabolism has become the focus in cancer research and clinical oncology, including LUAD and LUSC [3]. Tumor cells are well documented to reprogram their metabolism process to support abnormal proliferation and survival in harsh conditions by mutations in oncogenes and inactivation of tumor suppressor genes [4].

Recent studies have shown that the expression level of triosephosphate isomerase 1 (*TPI1*) may be related to tumorigenesis and metastasis, but the expression level of *TPI1* and its effect on tumors are not clear yet. *TPI1* is located in the cytoplasmic and extracellular regions, which is associated with triosephosphate isomerase deficiency and giardiasis. Previous literature revealed that TP1 is significantly upregulated in intrahepatic cholangiocarcinoma and correlated with high recurrence rate [5]. Kim et al. found that *TP1* may serve as a biomarker for the diagnosis of liver metastasis in colon cancer [6]. Jiang et al. developed a prognostic model for Ewing's sarcoma which comprised *TPI1* [7]. It was also reported that *TPI1* expression was greatly decreased in hepatocellular carcinoma [8]. However, the expression changes and underlying roles of *TPI1* in LUAD and LUSC remain unknown.

Here, we comprehensively explored and validated the *TPI1* expression in LUAD and LUSC using public databases, including The Cancer Genome Atlas (TCGA) and the Gene Expression Omnibus (GEO) datasets. The associations of *TPI1* expression with clinicopathological characteristics and prognosis were also studied in both histological types. Moreover, we analyzed the potential relations of TPI1 with immune cell infiltrations in the tumor microenvironment based on previous literatures and bioinformatic tools. Our study provides insights in understanding the potential roles of *TPI1* in tumor progression and immune microenvironment, which lay the foundation for future clinical research.

2. Methods

2.1. Study Cohort and Data Processing. Level 3 RNA sequencing data of LUAD and LUSC samples were downloaded from TCGA (https://portal.gdc.cancer.gov) before January 27, 2021. We obtained 1122 samples (572 samples of LUAD dataset and 550 samples of LUSC dataset) in total. Baseline clinicopathological factors, treatment, and prognostic information were also downloaded from TCGA.

RNA sequencing data of common lung cancer cell lines (LUAD, LUSC, and small-cell lung cancer) were downloaded from the Cancer Cell Line Encyclopedia (CCLE, https://sites.broadinstitute.org/ccle) [9, 10]. We obtained 154 samples (77 samples of LUAD, 26 samples of LUSC, and 51 samples of small-cell lung cancer) in total.

We adopted the public datasets from GEO (https://www.ncbi.nlm.nih.gov/geo) as the validation cohort. We enrolled GSE30219, GSE50081, and GSE37745 which were all based on the GPL570 genechip for the comparison of *TPI1* expression among LUAD, LUSC, small-cell lung cancer, and normal lung tissue. We used a robust multichip average method by RMAExpress for background adjustment, quantile normalization, and summary to process the gene profiles [11–13]. GSE68465 and GSE157011 datasets were used for the validations of clinical and prognostic values in LUAD and LUSC, respectively. Normalized data were downloaded directly from the GEO database.

The associations of tumor microenvironment with TPI1 expression level were firstly evaluated according to several previous studies. Saltz et al. proposed a leukocyte fraction by estimating tumor-infiltrating leukocytes on hematoxylin and eosin stained slides using deep learning techniques [14]. We also used the "Estimation of STromal and Immune cells in MAlignant Tumours using Expression data (ESTIMATE)" method for the assessment of tumor microenvironment. Moreover, the CIBERSORT method was used to quantify the proportions of the immune cell in both TCGA LUAD and LUSC cohorts [15]. The CIBERSORT is an analytical tool to impute gene expression profiles and provide an estimation of the abundances of member cell types in a mixed cell population. Such mixtures could derive from both patients' solid tissues and blood profiled by array or RNA sequencing [16]. The 22 immune cells are mainly composed of B cells, T cells, macrophages, dendritic cells, plasma cells, natural killer cells, and mast cells. Second, we obtain the list of immunomodulators based on TISIDB (http://cis.hku.hk/

TISIDB/). TISIDB is a web portal for tumor and immune system interaction, which integrates multiple heterogeneous data types [17]. We studied the potential associations of *TPI1* expression with immunomodulators and chemokines in TCGA LUAD and LUSC cohorts. Furthermore, we adopted Tumor Immune Single-Cell Hub (TISCH, https://tisch.comp-genomics.org/) to further explore the expression level of *TPI1* in tumor immune microenvironment. TISCH is a large-scale curated database that integrates single-cell transcriptomic profiles of 2,045,746 cells from 76 high-quality tumor datasets across 28 cancer types [18].

We performed Gene Set Enrichment Analysis (GSEA) to explore the potential effect of *TPI1* expression on LUAD and LUSC. The TCGA datasets were divided into two groups (high and low groups) stratified by *TPI1* expression level, and the enrichment of Hallmark and Kyoto Encyclopedia of Genes and Genomes (KEGG) gene sets was analyzed by GSEA, respectively. Normalized enrichment score > 1, nominal P value < 0.05, and false discovery rate Q value < 0.25 were used as screening thresholds for GSEA.

2.2. Statistical Analysis. All statistical analyses and graphic drawing in this study were performed by R software (version 4.0.3, R Foundation for Statistical Computing, Vienna, Austria), GraphPad Prism 8 (GraphPad Software, San Diego, CA, USA), and IBM SPSS Statistics 23.0 (IBM, Inc., Armonk, NY, USA). In each part of the study, patients were divided into high and low expression groups by the median expression level of the cohort. We adopted the Student t-test to compare the expression of *TPI1* between different groups. Baseline characteristics were compared by the chi-square test. Survival curves were estimated using the Kaplan-Meier method, and the log-rank test was used for comparing survival curves. Comparisons of immunological features and immune cell fractions were performed using the Mann-Whitney U test. In this study, a two-tailed P value of <0.05 was considered statistically significant.

3. Results

Based on TCGA database, we obtained 572 samples (519 tumor samples and 53 lung samples) from patients with LUAD and 550 samples (501 tumor samples and 49 lung samples) from patients with LUSC. The expression level of *TPI1* was explored in both LUAD and LUSC. The results showed that *TPI1* was significantly upregulated in both LUAD and LUSC compared with normal lung tissue ($P < 0.001$ and $P < 0.001$, Figures 1(a) and 1(b)). Similar results of *TPI1* overexpression were found in the combined GEO dataset ($P < 0.001$ and $P < 0.001$, Figure 1(c)). Furthermore, we compared *TPI1* expression among common histological types of lung cancer. The *TPI1* expression of LUSC was significantly higher than that in LUAD and small-cell lung cancer ($P < 0.001$ and $P = 0.017$, Figure 1(c)). The relatively high *TPI1* expression of LUSC was also confirmed using common lung cancer cell lines in CCLE ($P = 0.032$ and $P = 0.050$, Figure 1(d)).

Next, patients with missing clinicopathological information were excluded from further analyses. All patients were
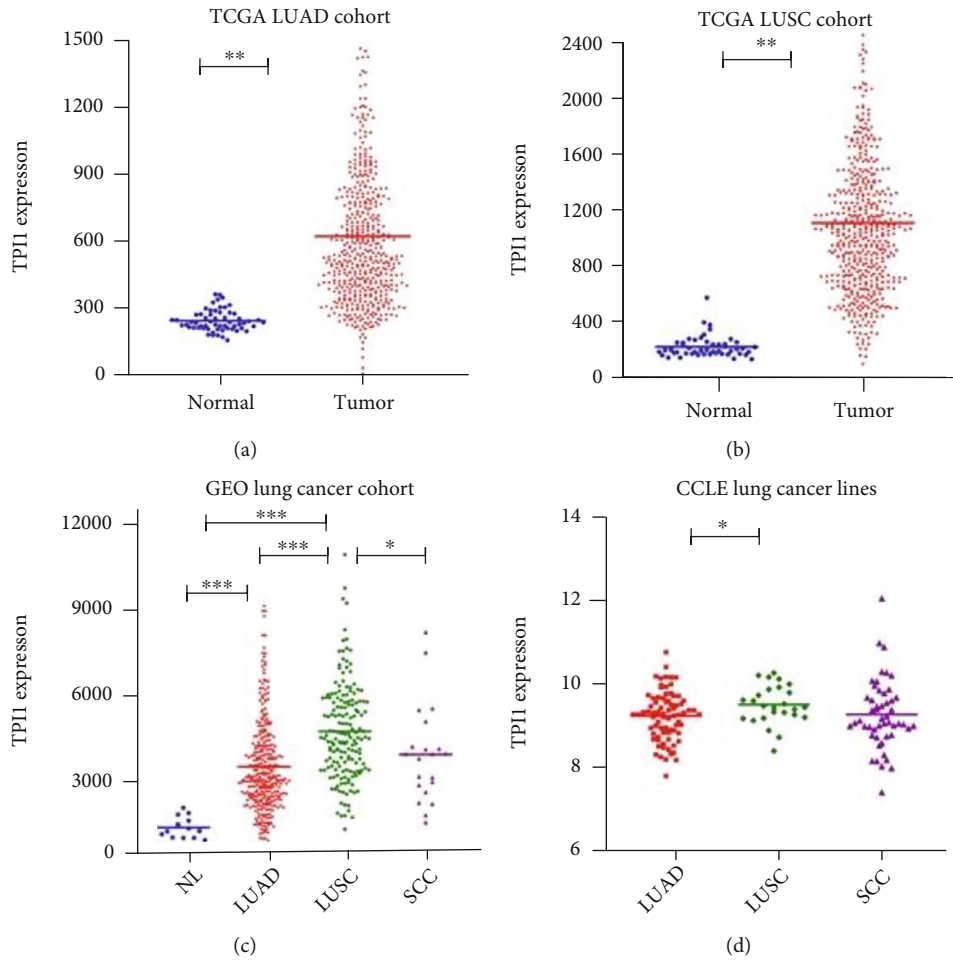
FIGURE 1: Comparison of the *TPI1* expression. (a) *TPI1* was significantly upregulated in LUAD compared with normal lung samples in TCGA ($P < 0.001$). (b) *TPI1* was significantly upregulated in LUSC compared with normal lung samples in TCGA ($P < 0.001$). (c) *TPI1* expression levels in normal lung samples, LUAD, LUSC, and small-cell lung cancer in selected GEO datasets (LUAD vs. normal sample, $P < 0.001$; LUSC vs. normal sample, $P < 0.001$; and LUSC vs. LUAD, $P < 0.001$; LUSC vs. small-cell lung cancer sample, $P = 0.017$). (d) *TPI1* expression levels in LUAD cell lines, LUSC cell lines, and small-cell lung cancer cell lines in the CCLE database (LUSC cell lines vs. LUAD cell lines, $P = 0.032$ and LUSC cell lines vs. small-cell lung cancer cell lines, $P = 0.050$).

divided into high and low expression groups by the median expression level in TCGA LUAD and LUSC cohorts, respectively. We assessed the potential associations of the *TPI1* expression with patients' clinicopathological factors, such as age, gender, tumor stage, and smoking history (Table 1). In TCGA LUAD cohort, we found that patients of *TPI1* low expression group tended to be older ($P = 0.045$) and consisted of more female patients ($P = 0.021$). Higher expression of *TPI1* was associated with more advanced pathological stage in LUAD ($P < 0.001$). There was no statistical difference regarding to patients' smoking history stratified by *TPI1* expression ($P = 0.934$). In TCGA LUSC cohort, similar trend of the association between age and *TPI1* expression was also observed ($P = 0.038$). No significant difference was found with respect to the distribution of patients' gender ($P = 0.098$). Meanwhile, *TPI1* expression did not correlate with the pathological stage of LUSC ($P = 0.680$) and patients' smoking history ($P = 0.542$). The prognostic values of *TPI1* in LUAD and LUSC were also evaluated. We found that high expression of *TPI1* had

adverse effect on patients' survival in TCGA LUAD cohort ($P = 0.006$, Figure 2(a)). In the GEO LUAD (GSE68465) cohort, we observed that higher expression of *TPI1* was associated with worse prognosis, although the difference was not statistically significant ($P = 0.055$, Figure 2(b)). In TCGA LUSC cohort, we found that there was no significant prognostic difference in patients with LUSC stratified by the expression of *TPI1* ($P = 0.963$, Figure 2(c)). Similar result was observed in the GEO LUSC (GSE157011) cohort ($P = 0.571$, Figure 2(d)).

The tumor-infiltrating lymphocyte fractions were compared according to Saltz et al. stratified by the *TPI1* expression [14]. In both TCGA LUAD and LUSC cohorts, we found that higher expression level of *TPI1* were associated with significantly lower lymphocyte fractions ($P = 0.018$ and $P < 0.001$, Figures 3(a)–3(b)). Then, we adopted ESTIMATE method for the evaluations of tumor microenvironment. We observed that lower expression of *TPI1* was related to higher scores in patients with LUAD and LUSC (Figures 3(c) and 3(d)). Then, we studied the potential

TABLE 1: Baseline clinicopathological characteristics stratified by the expression of *TPI1* in lung adenocarcinoma and lung squamous cell carcinoma.

	TCGA LUAD cohort			TCGA LUSC cohort		
	TPI1 low	*TPI1* high	*P* value	*TPI1* low	*TPI* high	*P* value
Age*	66.205 ± 9.663	64.393 ± 10.295	0.045	68.095 ± 8.272	66.481 ± 8.712	0.038
Gender			0.021			0.098
Female	151 (59.2)	125 (49.0)		71 (29.1)	55 (22.5)	
Male	104 (40.8)	130 (51.0)		173 (70.9)	189 (77.5)	
Stage*			<0.001			0.680
Stage I	161 (63.4)	114 (44.7)		121 (49.6)	121 (49.6)	
Stage II	48 (18.9)	77 (30.2)		83 (34)	72 (29.5)	
Stage III	36 (14.2)	47 (18.4)		35 (14.3)	49 (20.1)	
Stage IV	9 (3.5)	17 (6.7)		5 (2)	2 (0.8)	
Smoking status*			0.934			0.542
Nonsmoker	39 (15.9)	35 (14.2)		10 (4.3)	8 (3.4)	
Current smoker	46 (18.8)	73 (29.6)		61 (26)	70 (29.5)	
Reformed smoker (>15 years)	85 (34.7)	49 (19.8)		40 (17)	41 (17.3)	
Reformed smoker (≤15 years)	75 (30.6)	90 (36.4)		124 (52.8)	118 (49.8)	

*Samples with missing value were excluded from the comparison in each analysis.

(a)

(b)

(c)

(d)
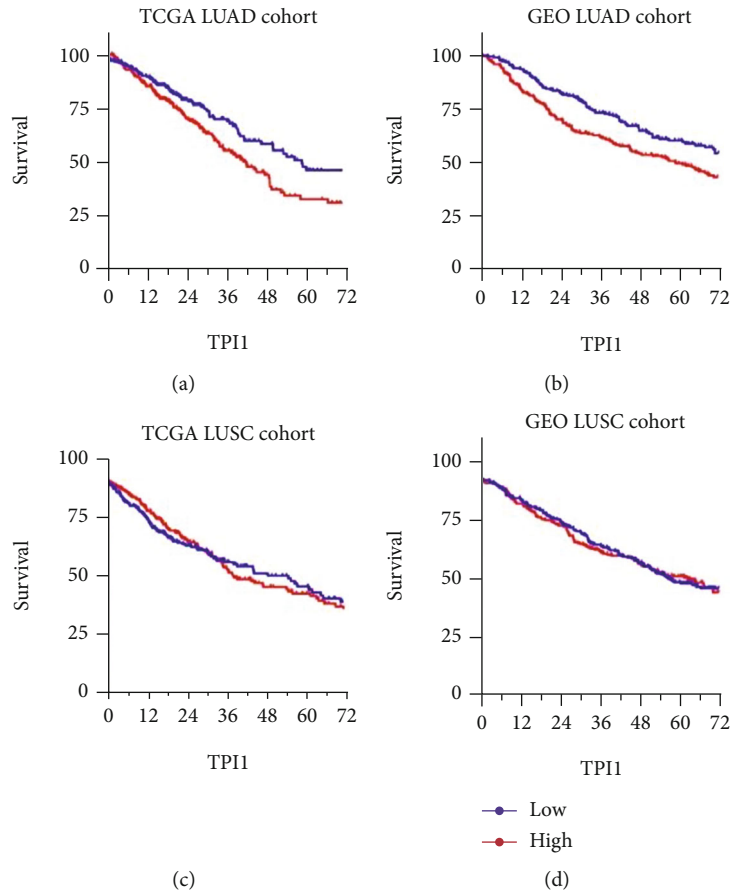
FIGURE 2: Kaplan-Meier survival curves comparing the high and low expression of *TPI1* in lung adenocarcinoma (LUAD) and squamous cell carcinoma (LUSC). (a) Survival curves comparing the *TPI1* expression high and low groups in TCGA LUAD cohort ($P = 0.006$). (b) Survival curves comparing the *TPI1* expression high and low groups in GEO LUAD cohort ($P = 0.055$). (c) Survival curves comparing the *TPI1* expression high and low groups in TCGA LUSC cohort ($P = 0.963$). (d) Survival curves comparing the *TPI1* expression high and low groups in GEO LUSC cohort ($P = 0.571$).

(a)

(b)

(c)

(d)

Figure 3: Continued.

(e)　　　　　　　　　　　　　　　　　　　　　　　(f)

FIGURE 3: (a) Comparison of leukocyte fraction in TCGA LUAD cohort stratified by the expression of *TPI1* ($P = 0.018$). (b) Comparison of leukocyte fraction in TCGA LUSC cohort stratified by the expression of *TPI1* ($P < 0.001$). (c) Comparison of stromal, immune, and ESTIMATE scores in TCGA LUAD cohort stratified by the expression of *TPI1* ($P = 0.001$, $P < 0.001$, and $P < 0.001$). (d) Comparison of stromal, immune, and ESTIMATE scores in TCGA LUSC cohort stratified by the expression of *TPI1* ($P < 0.001$, $P < 0.001$, and $P < 0.001$). (e) Heatmap of associations of *TPI1* expression with immunomodulators and chemokines in TCGA LUAD cohort based on the TISIDB database. (f) Heatmap of associations of *TPI1* expression with immunomodulators and chemokines in TCGA LUSC cohort based on the TISIDB database.

associations of *TPI1* expression with immunomodulators in TCGA LUAD and LUSC cohorts based on the TISIDB database. Significant relations were observed with chemokine, receptor, major histocompatibility complex (MHC), immunoinhibitor, and immunostimulator in both TCGA LUAD and LUSC cohorts (Figures 3(e) and 3(f) and Supplement Table 1), which suggests important roles in both metabolic and immune pathways in LUAD and LUSC. Next, we

explored the potential associations of *TPI1* expression with 22 immune cell infiltrating levels by the CIBERSORT method in TCGA LUAD and LUSC cohorts. We found that *TPI1* expression was significantly associated with subclusters of B cell, T cell CD4+, macrophage, mast cell, eosinophil, and neutrophil in LUAD cohort (Figure 4(a) and Supplement Table 2). However, there were potential relations between *TPI1* expression and subclusters of T cell

(a)

(b)

(c)

FIGURE 4: (a) Bubble plot of associations of *TPI1* expression with immune cell infiltrating level (CIBERSORT method) in TCGA LUAD cohort. (b) Bubble plot of associations of *TPI1* expression with immune cell infiltrating level (CIBERSORT method) in TCGA LUSC cohort. (c) Violin plot displays the distribution of *TPI1* expression in different cells of tumor microenvironment in GSE131907 and GSE127465 based on the TISCH database.

CD4+, T cell regulatory, monocyte, macrophage, mast cell, and eosinophil in LUSC cohort (Figure 4(b) and Supplement Table 2). In the TISCH database, we selected two lung cancer cohorts (GSE131907 and GSE127465). GSE131907 was composed of 44 patients with LUAD, while GSE127465 consists of both LUAD and LUSC patients. We studied the expression of *TPI1* at the single-cell level. The distributions of *TPI1* expression in the above datasets are displayed in Figure 4(c) and Supplement Figure 1. In GSE127465 cohort, *TPI1* was mainly expressed in dendritic cell, macrophage, and tumor cell. Similar results were observed in GSE131907 cohort, which indicated similar distribution of *TPI1* expression in LUAD and LUSC. We performed GSEA in TCGA LUAD and LUSC cohorts stratified by the expression of *TPI1*. In both LUAD and LUSC cohorts, higher *TPI1* expression was related to the enrichment of metabolic pathways and cell cycle process (Supplement Figure 2A-F). However, we noticed that higher *TPI1* expression was also associated with the enrichment of oxidative phosphorylation pathway,

hypoxia-related pathway, and *P53* signaling pathway (Supplement Figure 2G-I).

4. Discussion

Recently, cancer metabolism has become the focus of medical research and the development of potential cancer treatment. More and more evidence indicate that metabolic changes provide cancer cells with growth advantages, especially alterations in glucose metabolism [19]. Previous studies showed that *TPI1* expression may be related to the occurrence and metastasis of tumors, but the expression level of *TPI1* and its effect on tumors are not clear yet. *TPI1*, a key enzyme in the process of carbohydrate metabolism, catalyzes the interconversion of dihydroxyacetone phosphate and D-glyceraldehyde-3-phosphate [20]. Yoshida et al. observed that *TPI1* was significantly upregulated in metastatic tumors than in primary ovarian cancer [21]. Yu et al. found that higher *TPI1* expression may be associated with a higher recurrence rate in intrahepatic

cholangiocarcinoma [5]. Jiang et al. reported that *TPI1* expression was greatly decreased in hepatocellular carcinoma, which was consistent with previous study in osteosarcoma [8, 22]. It was revealed that *TPI1* expression was positively correlated with overall survival and negatively associated with tumor size and histological differentiation [8]. In this study, we adopted public datasets to explore the expression and clinical relevance of *TPI1* in LUAD and LUSC. We found that *TPI1* was significantly overexpressed in both types of lung cancers. Furthermore, *TPI1* was negatively associated with overall survival in patients with LUSC.

TPI1 is primarily associated with triosephosphate isomerase deficiency and giardiasis [7]. *TPI1* catalyzes the stereospecific 1,2-proton shift at dihydroxyacetone phosphate to give (R)-glyceraldehyde 3-phosphate through a pair of isomeric enzyme-bound cis-enediolate phosphate intermediates [23]. The conversion of dihydroxyacetone phosphate to d-3-glyceraldehyde phosphate continues the glycolytic pathway. Therefore, *TPI1* plays an important role in the glycolysis process. Our study indicated that *TPI1* could be a predictive biomarker for LUAD and LUSC. Moreover, the metabolic changes associated with malignancy are not only in cancer cells, but also in tumor microenvironment [24]. We also explored the associations of *TPI1* with tumor microenvironment and its expression levels in various immune cells. However, it is necessary to further study the transcriptional regulation mechanism of *TPI1* and its effect in the relationship between glycolysis and immune-related pathways.

This work systematically studies the associations of *TPI1* expression with LUAD and LUSC, but there are still some shortcomings that should be mentioned. First, *TPI1* expression should be further tested in diverse lung cancer patient cohorts with different therapies. Second, the verifications of expression and the exploration of potential mechanisms require further studies *in vitro* and *in vivo*.

5. Conclusion

TPI1 was significantly upregulated in LUAD and LUSC. Increased *TPI1* expression was correlated with poor prognosis in lLUAD and changed immune cell infiltrating in various degrees in both types of lung cancers. Our study provides insights in understanding the potential roles of *TPI1* in tumor progression and immune microenvironment.

Data Availability

All data could be downloaded from public databases (TCGA and GEO) and previous literatures in the reference.

Conflicts of Interest

The authors declare that they have no conflicts of interest.

Authors' Contributions

Xiaodong Yang and Cong Ye contributed equally to this work.

Supplementary Materials

Supplementary 1. Supplement Table 1: correlations of TPI1 expression with immune cell infiltrating levels in TCGA LUAD and LUSC cohorts.

Supplementary 2. Supplement Table 2: correlations of TPI1 expression with chemokine, receptor, MHC, immunoinhibitor, and immunostimulator in both TCGA LUAD and LUSC cohorts based on the TISIDB database.

Supplementary 3. Supplement Figure 1: (A) single-cell cluster map of TPI1 in GSE131907 based on the TISCH database. (B) Single-cell cluster map of TPI1 in GSE127465 based on the TISCH database.

Supplementary 4. Supplement Figure 2: (A) GSEA showed that higher expression of TPI1 was associated with the enrichment of glycolysis pathway (Hallmark) in TCGA LUAD cohort. (B) GSEA showed that higher expression of TPI1 was associated with the enrichment of pyrimidine metabolism pathway (KEGG) in TCGA LUAD cohort. (C) GSEA showed that higher expression of TPI1 was associated with the enrichment of G2M checkpoint pathway (Hallmark) in TCGA LUAD cohort. (D) GSEA showed that higher expression of TPI1 was associated with the enrichment of citrate cycle TCA cycle pathway (KEGG) in TCGA LUSC cohort. (E) GSEA showed that higher expression of TPI1 was associated with the enrichment of glutathione metabolism pathway (KEGG) in TCGA LUSC cohort. (F) GSEA showed that higher expression of TPI1 was associated with the enrichment of cell cycle pathway (KEGG) in TCGA LUSC cohort. (G) GSEA showed that higher expression of TPI1 was associated with the enrichment of oxidative phosphorylation pathway (Hallmark) in TCGA LUAD cohort. (H) GSEA showed that higher expression of TPI1 was associated with the enrichment of hypoxia (Hallmark) in TCGA LUAD cohort. (I) GSEA showed that higher expression of TPI1 was associated with the enrichment of P53 signaling pathway (KEGG) in TCGA LUAD cohort.

References

[1] F. Bray, J. Ferlay, I. Soerjomataram, R. L. Siegel, L. A. Torre, and A. Jemal, "Global cancer statistics 2018: GLOBOCAN estimates of incidence and mortality worldwide for 36 cancers in 185 countries," *CA: a Cancer Journal for Clinicians*, vol. 68, pp. 394–424, 2018.

[2] H. Sung, J. Ferlay, R. L. Siegel et al., "Global cancer statistics 2020: GLOBOCAN estimates of incidence and mortality worldwide for 36 cancers in 185 countries," *CA: a Cancer Journal for Clinicians*, vol. 71, pp. 209–249, 2021.

[3] J. Kim and R. J. DeBerardinis, "Mechanisms and implications of metabolic heterogeneity in cancer," *Cell Metabolism*, vol. 30, no. 3, pp. 434–446, 2019.

[4] K. Vanhove, G. J. Graulus, L. Mesotten et al., "The metabolic landscape of lung cancer: new insights in a disturbed glucose metabolism," *Frontiers in Oncology*, vol. 9, p. 1215, 2019.

[5] W. L. Yu, G. Yu, H. Dong et al., "Proteomics analysis identified TPI1 as a novel biomarker for predicting recurrence of intrahepatic cholangiocarcinoma," *Journal of Gastroenterology*, vol. 55, pp. 1171–1182, 2020.

[6] E. K. Kim, M. J. Song, Y. Jung, W. S. Lee, and H. H. Jang, "Proteomic analysis of primary colon cancer and synchronous solitary liver metastasis," *Cancer Genomics & Proteomics*, vol. 16, pp. 583–592, 2019.

[7] J. Jiang, X. Zhan, G. Xu et al., "Glycolysis- and immune-related novel prognostic biomarkers of Ewing's sarcoma: glucuronic acid epimerase and triosephosphate isomerase 1," *Aging (Albany NY)*, vol. 13, pp. 17516–17535, 2021.

[8] H. Jiang, N. Ma, Y. Shang et al., "Triosephosphate isomerase 1 suppresses growth, migration and invasion of hepatocellular carcinoma cells," *Biochemical and Biophysical Research Communications*, vol. 482, pp. 1048–1053, 2017.

[9] D. P. Nusinow, J. Szpyt, M. Ghandi et al., "Quantitative proteomics of the Cancer Cell Line Encyclopedia," *Cell*, vol. 180, no. 2, pp. 387–402.e16, 2020.

[10] M. Ghandi, F. W. Huang, J. Jané-Valbuena et al., "Next-generation characterization of the Cancer Cell Line Encyclopedia," *Nature*, vol. 569, no. 7757, pp. 503–508, 2019.

[11] B. M. Bolstad, R. A. Irizarry, M. Astrand, and T. P. Speed, "A comparison of normalization methods for high density oligonucleotide array data based on variance and bias," *Bioinformatics*, vol. 19, pp. 185–193, 2003.

[12] R. A. Irizarry, B. M. Bolstad, F. Collin, L. M. Cope, B. Hobbs, and T. P. Speed, "Summaries of Affymetrix GeneChip probe level data," *Nucleic Acids Research*, vol. 31, no. 4, article e15, pp. 15e–115, 2003.

[13] R. A. Irizarry, B. Hobbs, F. Collin et al., "Exploration, normalization, and summaries of high density oligonucleotide array probe level data," *Biostatistics*, vol. 4, no. 2, pp. 249–264, 2003.

[14] J. Saltz, R. Gupta, L. Hou et al., "Spatial organization and molecular correlation of tumor-infiltrating lymphocytes using deep learning on pathology images," *Cell Reports*, vol. 23, no. 1, pp. 181–193.e7, 2018.

[15] A. M. Newman, C. L. Liu, M. R. Green et al., "Robust enumeration of cell subsets from tissue expression profiles," *Nature Methods*, vol. 12, pp. 453–457, 2015.

[16] X. Yang, Y. Shi, M. Li et al., "Identification and validation of an immune cell infiltrating score predicting survival in patients with lung adenocarcinoma," *Journal of Translational Medicine*, vol. 17, no. 1, p. 217, 2019.

[17] B. Ru, C. N. Wong, Y. Tong et al., "TISIDB: an integrated repository portal for tumor-immune system interactions," *Bioinformatics*, vol. 35, no. 20, pp. 4200–4202, 2019.

[18] D. Sun, J. Wang, Y. Han et al., "TISCH: a comprehensive web resource enabling interactive single-cell transcriptome visualization of tumor microenvironment," *Nucleic Acids Research*, vol. 49, pp. D1420–D1430, 2021.

[19] R. A. Gatenby and R. J. Gillies, "Why do cancers have high aerobic glycolysis?," *Nature Reviews. Cancer*, vol. 4, pp. 891–899, 2004.

[20] W. J. Albery and J. R. Knowles, "Efficiency and evolution of enzyme catalysis," *Angewandte Chemie (International Ed. in English)*, vol. 16, pp. 285–293, 1977.

[21] A. Yoshida, N. Okamoto, A. Tozawa-Ono et al., "Proteomic analysis of differential protein expression by brain metastases of gynecological malignancies," *Human Cell*, vol. 26, pp. 56–66, 2013.

[22] F. Orosz, J. Olah, and J. Ovadi, "Triosephosphate isomerase deficiency: facts and doubts," *IUBMB Life*, vol. 58, pp. 703–715, 2006.

[23] J. P. Richard, "A paradigm for enzyme-catalyzed proton transfer at carbon: triosephosphate isomerase," *Biochemistry*, vol. 51, pp. 2652–2661, 2012.

[24] Y. Yuan, H. Li, W. Pu et al., "Cancer metabolism and tumor microenvironment: fostering each other?," *Science China Life Sciences*, 2021.

Research Article

Pan-Cancer Analysis Reveals FH as a Potential Prognostic and Immunological Biomarker in Lung Adenocarcinoma

Heng Zhang [ID],[1] **Qiang Ju** [ID],[2] **Jing Ji** [ID],[1] **and Yanjie Zhao** [ID][1]

[1]*School of Public Health, Qingdao University, Qingdao, Shandong, China*
[2]*Department of Blood Transfusion, The Affiliated Hospital of Qingdao University, Qingdao, Shandong, China*

Correspondence should be addressed to Yanjie Zhao; zhaoyj@qdu.edu.cn

Fumarate hydratase (FH) is an important enzymatic component in the tricarboxylic acid cycle. Studies have reported that FH plays an important role in hereditary leiomyomatosis and renal cell cancer (HLRCC). However, the role of FH in human different cancers remains unknown. This study is aimed at analyzing the prognostic value of FH and demonstrating the correlation between FH expression and tumor immunity. Results showed that FH was mutated or copy number varied in 27 types of cancer. FH mRNA was abnormally upregulated across various cancers. Survival analysis suggested high expression of FH was associated with poor prognosis in many cancer types, including lung adenocarcinoma (LUAD). Additionally, FH expression was associated with immune infiltration, including B cells, CD4^{+} T cells, CD8^{+} T cells, neutrophils, macrophages, and dendritic cells, especially in liver hepatocellular carcinoma (LIHC), LUAD, and lung squamous cell carcinoma (LUSC). Moreover, FH expression showed a strong correlation with immune checkpoint markers in LUAD and testicular germ cell tumors (TGCT). These results indicate that FH is an immunotherapeutic target and a potential prognostic biomarker in LUAD.

1. Introduction

Cancer is the leading cause of death worldwide, and most existing therapies are low effective [1–3]. Pan-cancer analyses can help us to find common and different characteristics of human malignant tumors [4] and provide novel ideas for the clinical treatment of tumors [5], for example, applying pan-cancer analysis to reveal that immune infiltration influences radiotherapy outcomes [6] and to explore the association between matrisome genes and tumors [7]. In addition, pan-cancer analysis can be used to find valuable prognostic biomarkers [8–10]. Therefore, pan-cancer analysis is an important method for identifying new diagnostic biomarkers and developing more effective molecular targets for cancer treatment.

Fumarate hydratase (FH) is an enzymatic component of the tricarboxylic acid cycle catalyzing fumarate to malate [11]. A growing number of studies have shown that FH is involved in the occurrence and development of certain cancers. For instance, patients with FH gene mutations have a very high risk of hereditary leiomyomatosis and HLRCC

[12]. And gastric cancer patients with high FH expression had a higher risk of death than those with low FH expression [13]. In addition, the loss of FH and the accumulation of fumarate elicit an epithelial-to-mesenchymal-transition (EMT) to promote cancer metastasis [14, 15]. However, the role of FH in pan-cancers needs further study.

The occurrence and development of cancer are closely related to the surrounding stroma. Immune cells play important roles in the occurrence and progression of tumors and are crucial parts of tumor stroma [16, 17]. Tumor-associated macrophages (TAMs) are important immune cells in the tumor microenvironment and play protumoral or antitumoral roles [18, 19]. Therefore, the study of tumor immune microenvironment can provide new clues for understanding the mechanism of tumor occurrence and development and has important value for the clinical treatment of tumors. However, the current research on the role of FH in tumor immunity is still limited.

In this study, we analyzed the expression of FH and evaluated its prognostic value in 33 cancer types. More importantly, we explored the relationship between FH expression

and various tumor immunities. Our results provide new insights into the role of FH in tumors, suggesting that FH is related to the immune infiltration of a variety of tumors and is a potential prognostic biomarker, especially in lung adenocarcinoma (LUAD).

2. Materials and Methods

2.1. Pan-Cancer Analysis of Mutational Data of FH. The mutation and amplification levels of FH in human cancers were evaluated by cBioPortal database (http://www.cbioportal.org/, v3.6.20). By using TCGA database (https://gdc.cancer.gov/access-data/gdc-data-transfer-tool, v23.0), we obtained the mutation levels of five mismatch repair (MMR) genes (MLH1, MSH2, MSH6, PMS2, and EPCAM). The correlation between FH level and MMR gene mutation level was explored by the Pearson correlation analysis.

2.2. Patient Datasets and FH Expression Analysis. The data of the FH expression in tumor and normal tissues of 33 types of cancers were obtained from the Genotype Tissue Expression (GTEx) (https://gtexport.org/home/, v8) and The Cancer Genome Atlas (TCGA). Clinical annotations and RNA sequencing data of 33 cancer types (ACC: adrenocortical carcinoma; BLCA: bladder urothelial carcinoma; BRCA: breast invasive carcinoma; CESC: cervical squamous cell carcinoma; CHOL: cholangiocarcinoma; COAD: colon adenocarcinoma; DLBC: lymphoid neoplasm diffuse large B cell lymphoma; ESCA: esophageal carcinoma; GBM: glioblastoma multiforme; LGG: brain lower grade glioma; HNSC: head and neck squamous cell carcinoma; KICH: kidney chromophobe; KIRC: kidney renal clear cell carcinoma; KIRP: kidney renal papillary cell carcinoma; LAML: acute myeloid leukemia; LIHC: liver hepatocellular carcinoma; LUAD: lung adenocarcinoma; LUSC: lung squamous cell carcinoma; MESO: mesothelioma; OV: ovarian serous cystadenocarcinoma; PAAD: pancreatic adenocarcinoma; PCPG: pheochromocytoma and paraganglioma; PRAD: prostate adenocarcinoma; READ: rectum adenocarcinoma; SARC: sarcoma; SKCM: skin cutaneous melanoma; STAD: stomach adenocarcinoma; TGCT: testicular germ cell tumors; THCA: thyroid carcinoma; THYM: thymoma; UCEC: uterine corpus endometrial carcinoma; UCS: uterine carcinosarcoma; and UVM: uveal melanoma) were obtained from TCGA. All data were normalized as previously described [20, 21].

2.3. Cell Culture and Reagents. BEAS-2B, 16HBE, A549, and H460 were obtained from the American Type Culture Collection (ATCC, Manassas, USA). 16HBE, BEAS-2B, and H460 were cultured in MEM medium (HyClone, Utah, USA) with 10% fetal bovine serum (FBS, Gibco, Amarillo, TX). A549 was cultured in RPMI 1640 medium (Cytiva, Utah, USA) with 10% fetal bovine serum. All cells were cultured in 37°C humidified incubator with 5% CO_2.

2.4. RNA Isolation and Real-Time PCR Analysis. According to the manufacturer's protocol, total RNA was isolated from cell lines by using TRIzol reagent (Invitrogen, USA). Complementary DNA (cDNA) was obtained using a PrimeScript RT reagent kit (TaKaRa, Japan). Real-time PCR was per-

formed using TB Green Premix Ex Taq II (TaKaRa, Japan) in a Light Cycler 480 II Real-Time PCR system. Glyceraldehyde phosphate dehydrogenase (GAPDH) was employed as a control for normalization. The primers were shown as follows: FH forward 5′-CCGCTGAAGTAAACCAGGATT ATG-3′ and FH reverse 5′-ATCCAGTCTGCCATACCAC GAG-3′; and GAPDH forward 5′-GTCTCCTCTGACTT CAACAGCG-3′ and GAPDH reverse 5′-ACCACCCTGTT GCTGTAGCCAA-3.

2.5. Correlation between FH Expression Level and Patients' Prognosis. The relationship between FH expression and OS in 33 types of cancer was analyzed by forest plots and the Kaplan-Meier curves. The hazard ratio (HR) and log-rank P values were acquired by univariate survival analysis.

2.6. Association between FH and Tumor Immunity. The Tumor Immune Estimation Resource (TIMER) database (https://cistrome.shinyapps.io/timer/, v2.0) was used to obtain immune infiltrating cell scores for 33 cancer types. The associations between FH levels and 6 immune infiltrates cells—B cell, CD4$^+$ T cell, CD8$^+$ T cell, neutrophil cell, macrophage cell, and dendritic cell—were evaluated by the Spearman correlation analysis. Moreover, using the Pearson correlation analysis, we examined the correlation between FH level and immune checkpoint marker level.

2.7. Statistical Analysis. The expression level of FH in different tissues was analyzed by t test. The univariate survival analysis and Kaplan-Meier survival analysis were used to analyze the correlation between FH expression and patients' overall survival. $P < 0.05$ were considered significant for all statistical analysis.

3. Results

3.1. Genomic Alterations of FH in Human Pan-Cancer. As we all know, genomic mutation is closely related to tumorigenesis [22]. Using the cBioPortal database, we identified genomic alterations of FH in 32 cancers, including mutations and copy number variations. As a result, FH was mutated or copy number varied in 27 cancers. The results showed that FH mutation frequencies are high in UCEC, BLCA, HNSC, and LAML. Furthermore, FH amplification was one of the significant single factors for alteration in CHOL, USC, PCPG, ESCA, and KIRC (Figure 1(a)). In addition, 73 FH mutations were identified across pan-cancer, and all of them (100%) were missense (Figure 1(b)).

DNA mismatch repair (MMR) maintains genomic stability [23]. Mutations in MMR gene might cause defective mismatch repair, leading to genomic alterations of some genes [24]. Next, we investigated the correlation of four MMR genes' mutation and FH. As shown in Figure 1(c), in most types of cancers, such as LUAD, BLCA, and LUSC, FH expression was significantly related with the mutation level of MMR genes. We next explored the relationship between FH expression and tumor mutational burden (TMB) level. FH expression was associated with TMB in BRCA, COAD, HNSC, LGG, LIHC, LUAD, PAAD, PRAD, SKCM, STAD, THYM,
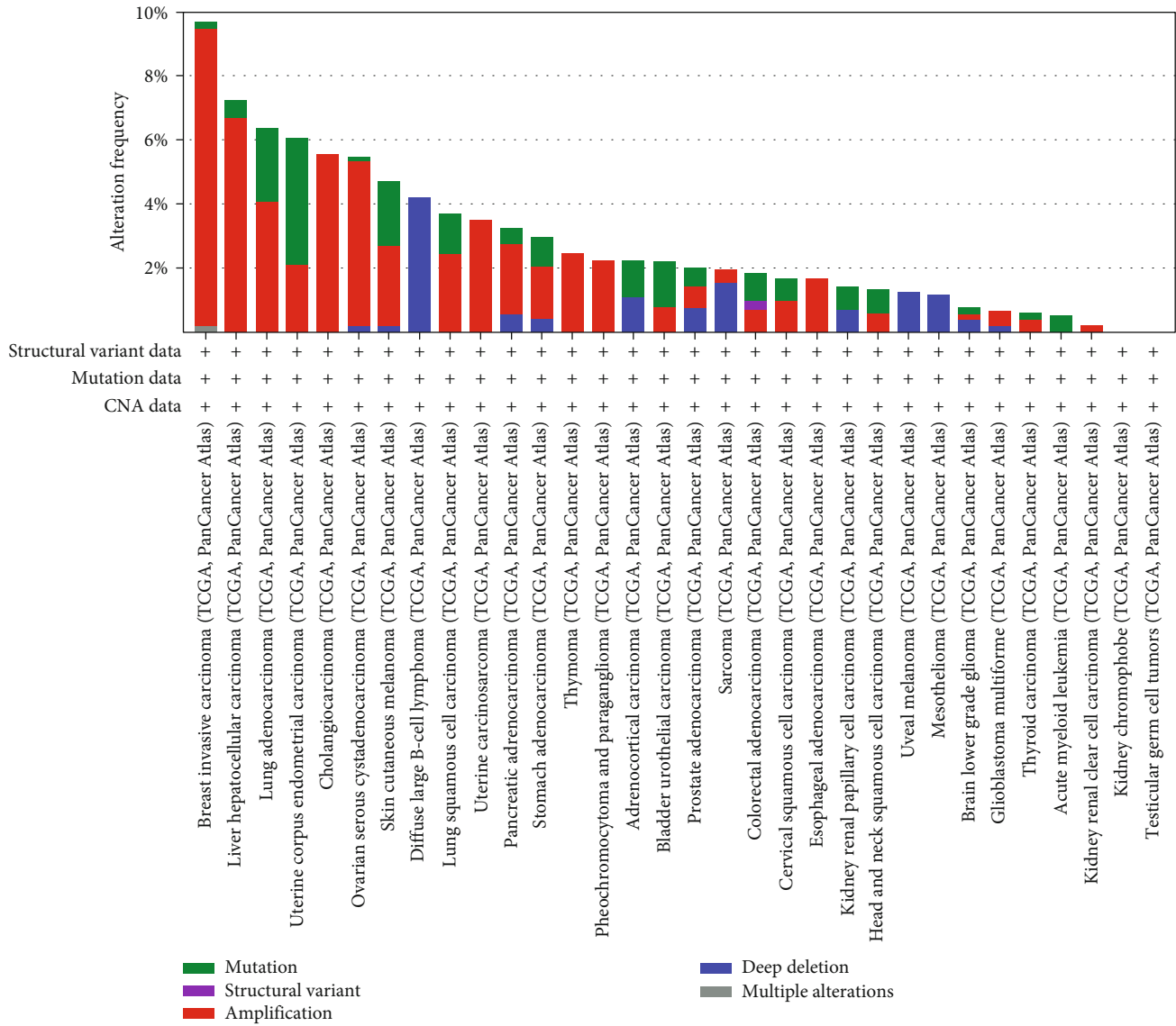
(a)
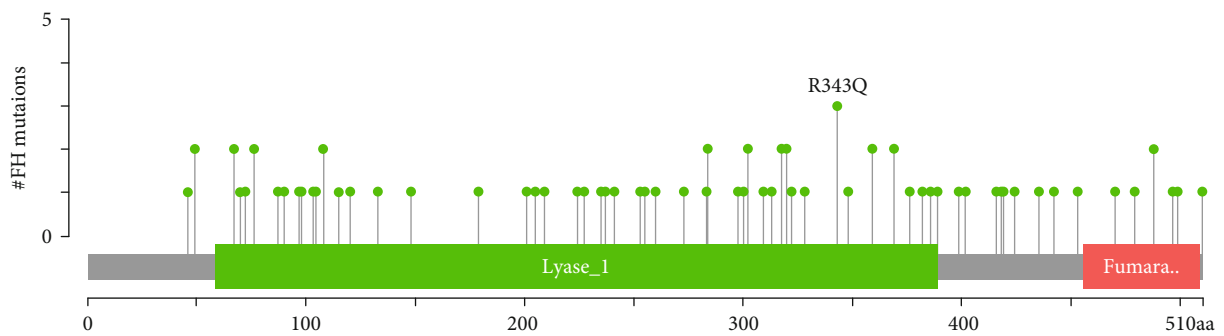
(b)

Figure 1: Continued.

(c)

(d)
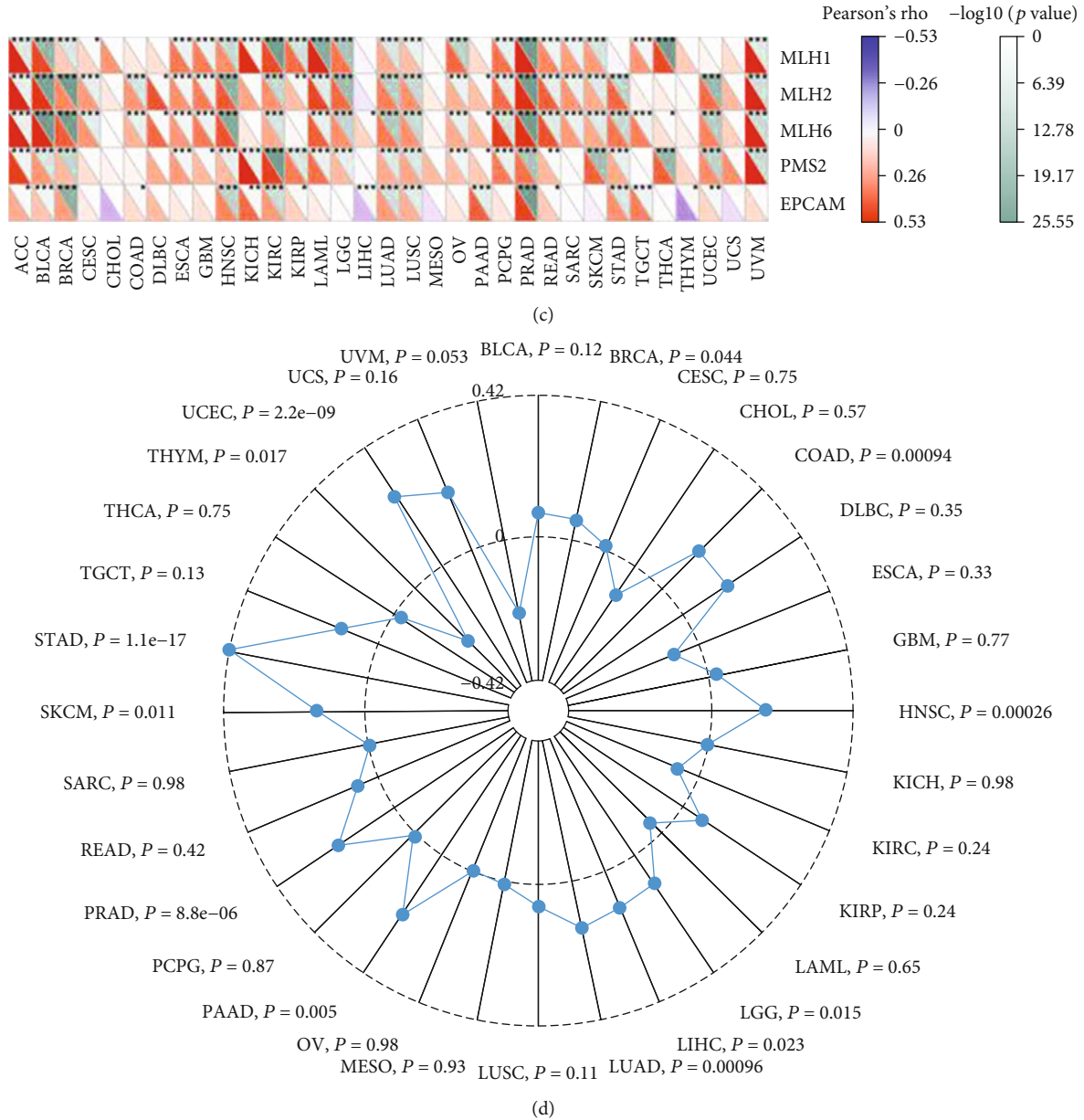
FIGURE 1: Genomic alterations of FH in human pan-cancer. (a) The alteration frequency of FH in human pan-cancer. (b) The types and distributions of FH mutations. X-axis: amino acid; Y-axis: numbers of FH mutations; green/red box: RNA recognition motif (190-248aa, 376-444aa, and 471-527aa); #: number of FH mutations. (c) The association between FH expression level and four MMR genes mutation. (d) Radar map showing the correlation between FH expression and TMB. $^*P < 0.05$, $^{**}P < 0.01$, $^{***}P < 0.001$.

and UCEC (Figure 1(d)). All these results indicate FH shows genomic alterations in many cancers.

3.2. The mRNA Expression of FH in Human Pan-Cancer.

Next, the FH level between tumor tissues and normal tissues in 20 types of cancers was obtained from TCGA database. FH was overexpressed in BRCA, ESCA, GBM, LIHC, LUAD, LUSC, PRAD, STAD, and UCEC tissues compared with normal tissues (Figure 2(a)). In addition, we combined the GTEx database to expand the normal tissue data. Furthermore, the expression level of FH in 27 tumors was analyzed. As shown in Figure 2(b), FH was upregulated in 21 types of cancer tissues, including CC, BLCA, BRCA, CESC, COAD,

ESCA, GBM, KICH, LGG, LIHC, LUAD, LUSC, OV, PAAD, PRAD, SKCM, STAD, TGCT, THCA, UCEC, and UCS. These results suggest that FH is abnormally upregulated in various cancers.

3.3. Prognostic Value Analysis of FH in Human Pan-Cancer.

Next, we investigated whether abnormal expression of FH affects patients' prognosis. By univariate survival analysis, we found that FH expression was associated with patients' OS in 8 cancer types, including ACC, KICH, KIRC, KIRP, LAML, LGG, LUAD, and SKCM (Figure 3(a)). The Kaplan-Meier curves showed that increased FH expression was correlated with poor prognosis in 6 cancer types including ACC
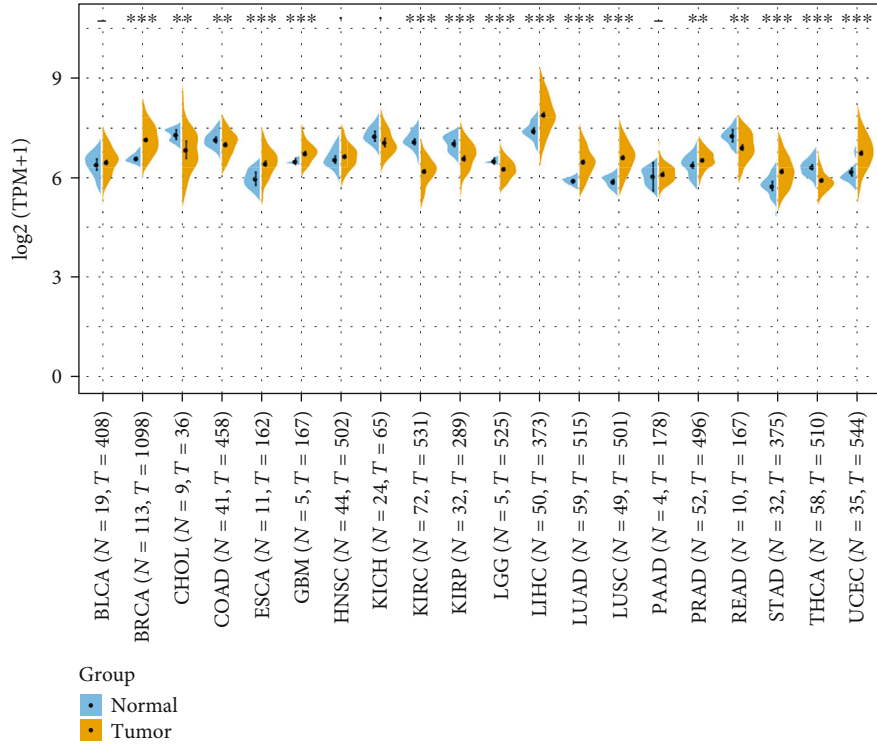
(a)
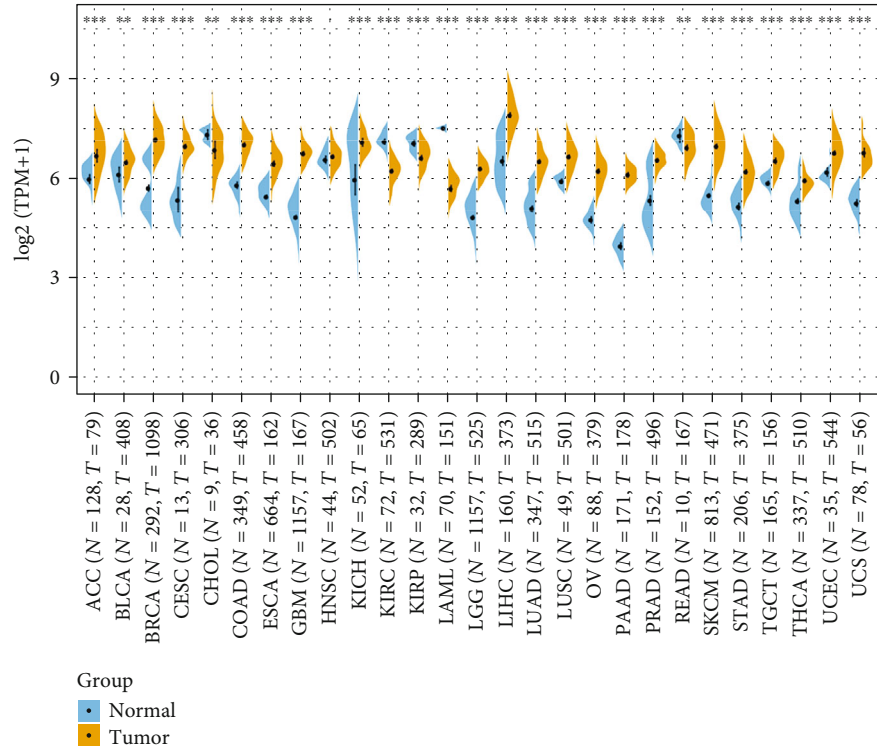
(b)

FIGURE 2: Expression level of FH in different cancer types. (a) Expression level of FH in tumor and normal tissues from TCGA database. (b) Expression level of FH in tumor and normal tissues from TCGA and the GTEx database. $^*P < 0.05$, $^{**}P < 0.01$, $^{***}P < 0.001$.

($P = 0.00069$, HR = 1.01), KICH ($P < 0.0001$, HR = 1.02), LAML ($P < 0.0001$, HR = 1.02), LGG ($P < 0.0001$, HR = 1), LUAD ($P = 0.014$, HR = 1), and SKCM ($P < 0.0001$, HR = 1).

However, KIRC ($P < 0.0001$, HR = 0.99) and KIRP ($P = 0.00016$, HR = 0.99) were exceptions where FH overexpression indicated a better prognosis (Figure 3(b)).

	HR	P value
ACC	1.01 (1 ~ 1.01)	0.02900
BLCA	1 (1 ~ 1.01)	0.15000
BRCA	1 (1 ~ 1)	0.25000
CESC	1 (0.99 ~ 1)	0.42000
CHOL	1 (1 ~ 1.01)	0.18000
COAD	1 (0.99 ~ 1)	0.11000
DLBC	1.01 (0.99 ~ 1.03)	0.23000
ESCA	1.01 (1 ~ 1.01)	0.16000
GBM	1 (0.99 ~ 1.01)	0.76000
HNSC	1 (1 ~ 1.01)	0.13000
KICH	1.02 (1.01 ~ 1.03)	0.00100
KIRC	0.99 (0.99 ~ 1)	0.00210
KIRP	0.99 (0.98 ~ 1)	0.00330
LAML	1.02 (1.01 ~ 1.04)	0.00016
LGG	1 (1 ~ 1.01)	0.00470
LIHC	1 (1 ~ 1)	0.47000
LUAD	1 (1 ~ 1.01)	0.01700
LUSC	1 (1 ~ 1)	0.38000
MESO	1 (1 ~ 1.01)	0.25000
OV	1 (0.99 ~ 1)	0.23000
PAAD	1 (0.99 ~ 1.01)	0.97000
PCPG	1 (0.97 ~ 1.03)	0.94000
PRAD	1 (0.98 ~ 1.03)	0.69000
READ	1 (0.99 ~ 1.01)	0.53000
SARC	1 (1 ~ 1)	0.90000
SKCM	1 (1 ~ 1)	0.00480
STAD	1 (1 ~ 1.01)	0.83000
TGCT	0.98 (0.94 ~ 1.01)	0.18000
THCA	1.01 (0.99 ~ 1.03)	0.24000
THYM	1.01 (0.99 ~ 1.02)	0.26000
UCEC	1 (1 ~ 1)	0.84000
UCS	1 (0.99 ~ 1.01)	0.90000
UVM	1.01 (0.99 ~ 1.02)	0.32000

0.71   HR (95% CI)   1.0

(a)

$P = 0.00069$

$HR = 1.01, 95\%CI (1, 1.01)$

High	15	5	2	0	0	0
Low	64	41	20	8	2	0

Time

FH in ACC exp
- High
- Low

(b)

$P < 0.0001$

$HR = 1.02, 95\%CI (1.01, 1.03)$

High	8	1	0	0	0	0
Low	56	46	35	20	3	0

Time

FH in KICH exp
- High
- Low
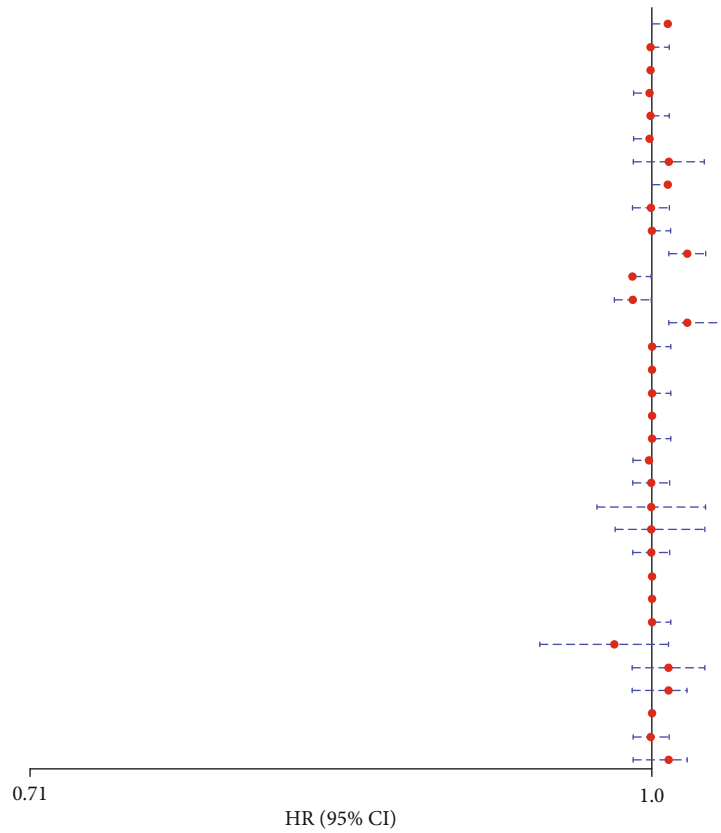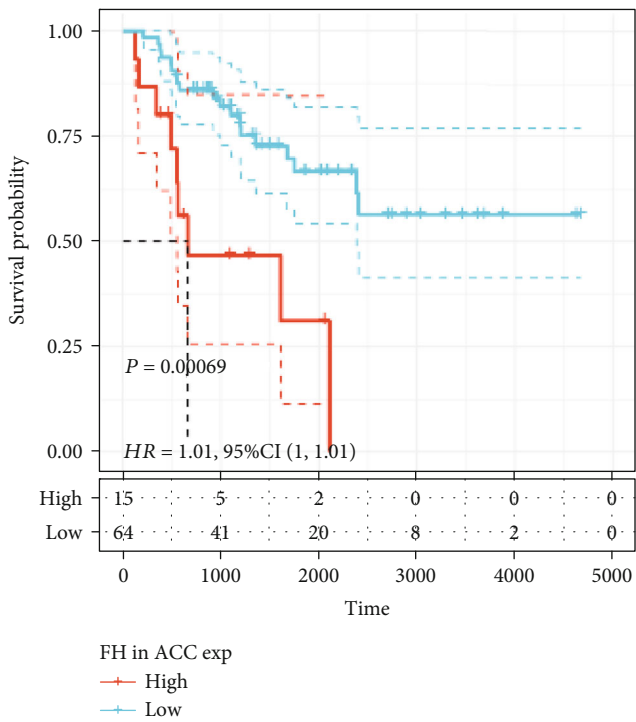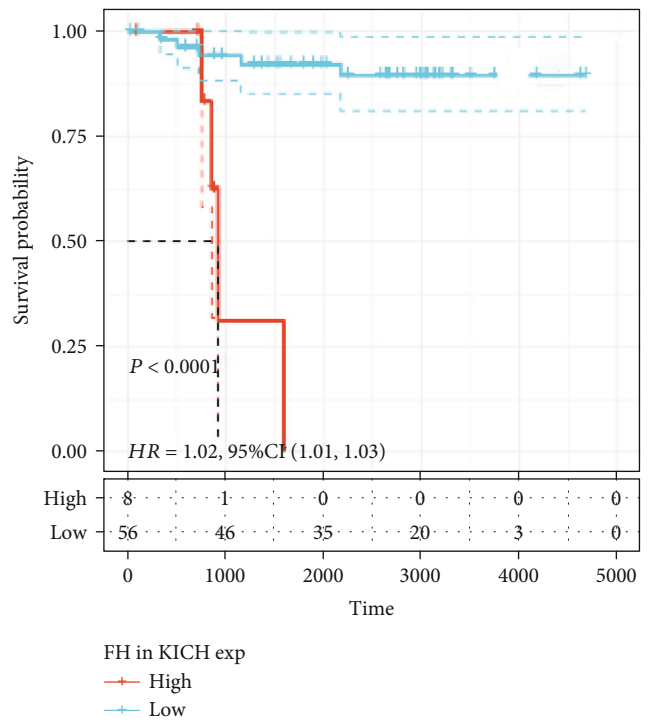
(c)

FIGURE 3: Continued.

(d)

(e)

(f)

(g)

Figure 3: Continued.

(h)

(i)
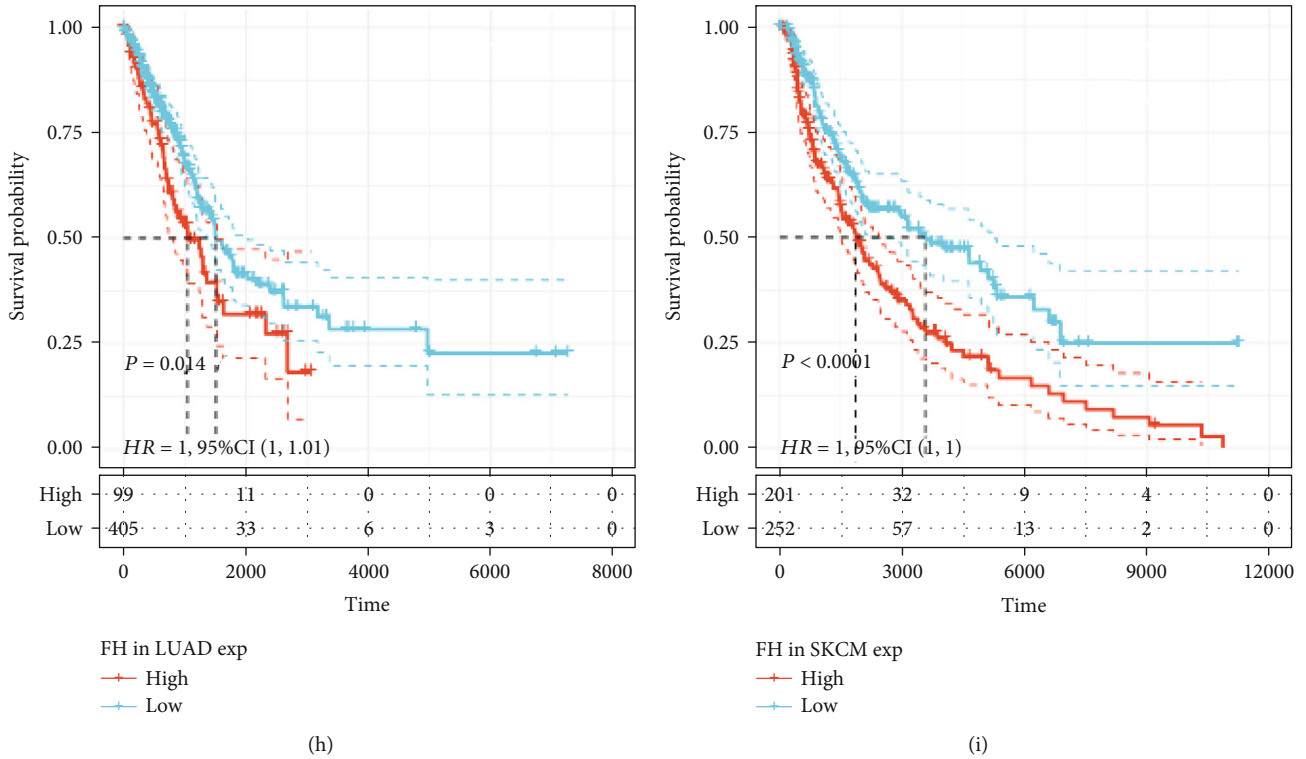
Figure 3: Association between FH expression level and patients' OS. (a) Forest plots of hazard ratios (HRs) of FH expression level in 33 tumor types. (b) The Kaplan-Meier analysis of the correlation between FH expression and patients' OS in ACC, KICH, KIRC, KIRP, LAML, LGG, LUAD, and SKCM.

3.4. The Association between FH Expression and Tumor Immunity.

The immune cells in TME can affect patients' survival [25]. To explore the mechanism of FH affecting patients' prognosis, the correlation between FH expression and immune infiltration in pan-cancer was further investigated. First, we analyzed the scores of 6 types of immune cells (B cell, CD4$^+$ T cell, CD8$^+$ T cell, neutrophil cell, macrophage cell, and dendritic cell) from 33 cancer types through the TIMER database. Notably, FH level was significantly associated with 6 types of immune cells in LIHC, LUAD, and LUSC (Figure 4(a)). To quantify the immune and matrix components in cancers, the immune score (i.e., ImmuneScore), matrix score (i.e., StromalScore), and estimate score (i.e., ESTIMATEScore) were obtained. FH level was significant negatively associated with the ImmuneScore in SARC, BRCA, THCA, StromalScore in THCA, LUAD, TGCT, and ESTIMA-TEScore in THCA, LUAD, and SKCM (Figure 4(b)).

Next, we explored how FH affected immune cells infiltration. The correlation between FH expression and immune checkpoint gene expression was investigated. As shown in Figure 5, we found that in some cancers, especially in LUAD and TGCT, FH expression was significantly correlated with multiple immune checkpoint markers, such as BTLA, TNFRSF14, LAIR1, CD48, and CD28.

4. Discussion

Pan-cancer analysis can reveal similarities and differences in tumors. In recent years, many studies have used pan-cancer analysis to find biomarkers related to cancer prognosis and immunity [26, 27]. FH protein participates in the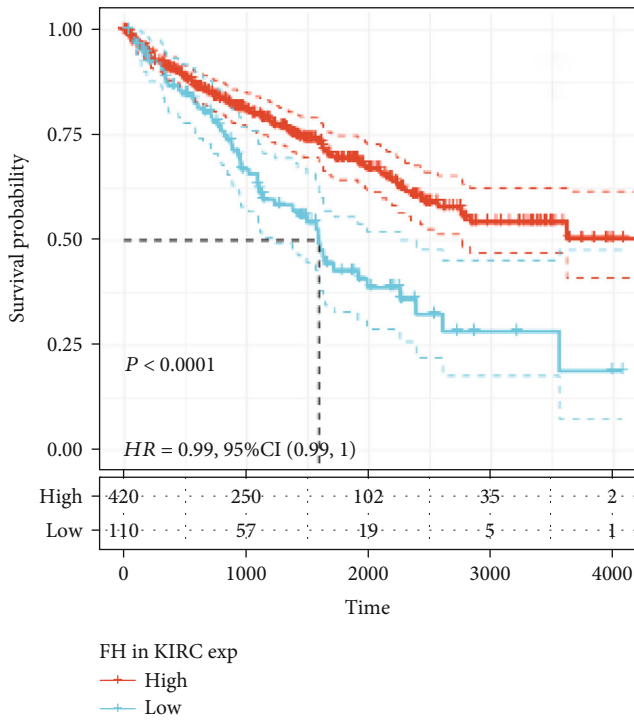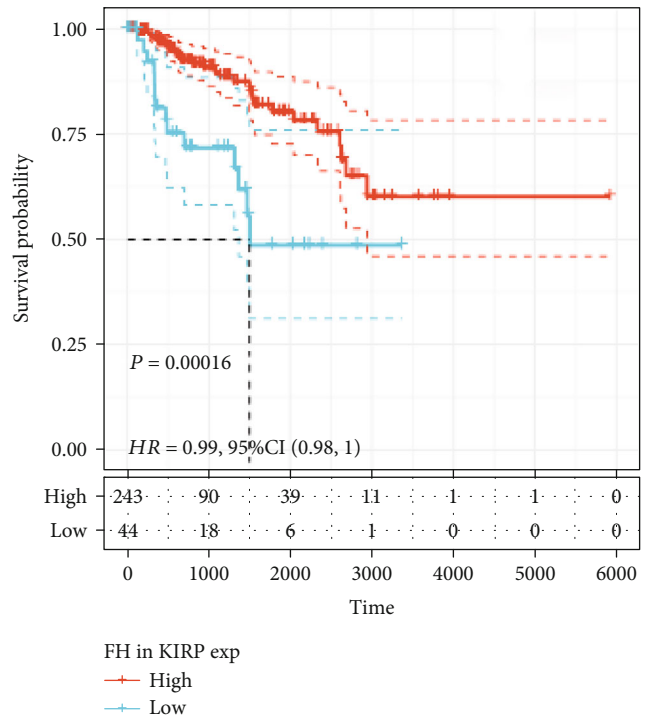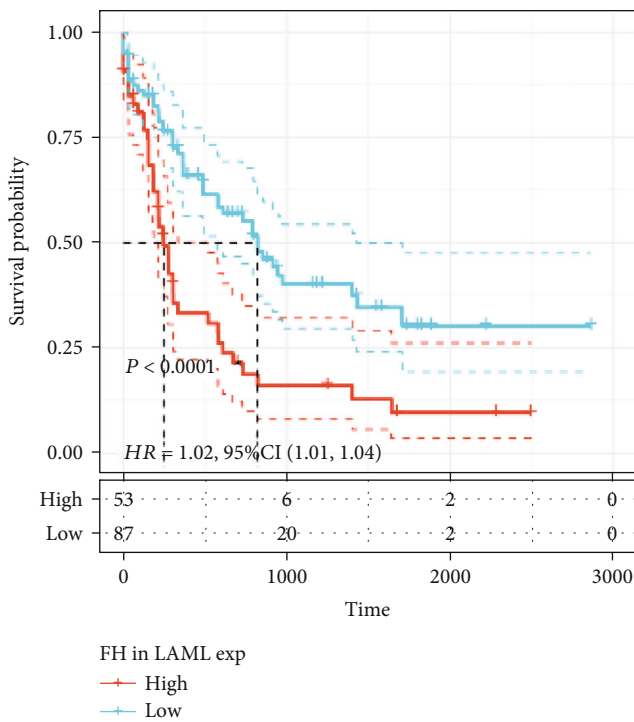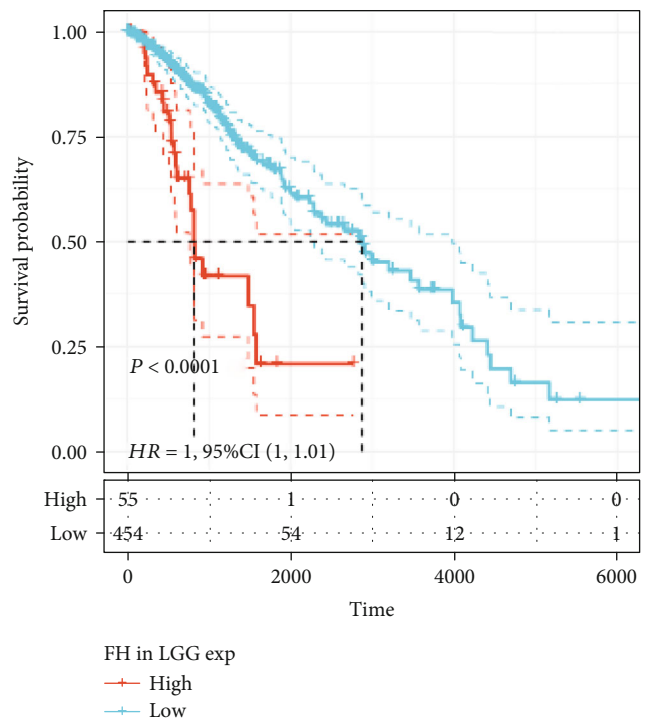 tricarboxylic acid (TCA) cycle, where it catalyzes the reversible hydration of fumarate to malate [28]. At present, many studies have shown that TCA is closely related to the occurrence and development of cancer [29, 30]. Therefore, the role of FH in cancer is worth exploring. Non-small cell lung cancer, especially lung adenocarcinoma, is a serious threat to human health and life. It is becoming more and more important to find new treatment methods and targets to improve the prognosis of lung cancer [31, 32]. In this study, we explored the roles of FH in pan-cancer. On the one hand, we investigated genomic alterations of FH in pan-cancer and identified that there were mutations or copy number variations in FH genome. On the other hand, we found FH was upregulated in 21 types of cancers and related to patients' poor prognosis and immunity in LUAD. These results provide new clues for further research on the roles of FH in cancer.

Genomic instability, including genomic mutations and copy number variants, is the major cause of cancer development [33–36]. And research shows MMR gene mutations are closely related to tumorigenesis [37]. Our results showed FH genome mutation or copy number variation in many types of cancers. And FH expression was found significantly related with the mutation level of MMR genes and TMB level. In brief, our results showed that aberrant FH expression might play an important role in tumorigenesis.

FH has been reported to alter cancer cell migratory potential, and hopefully as a therapeutic target in renal cancer [38].

(a)
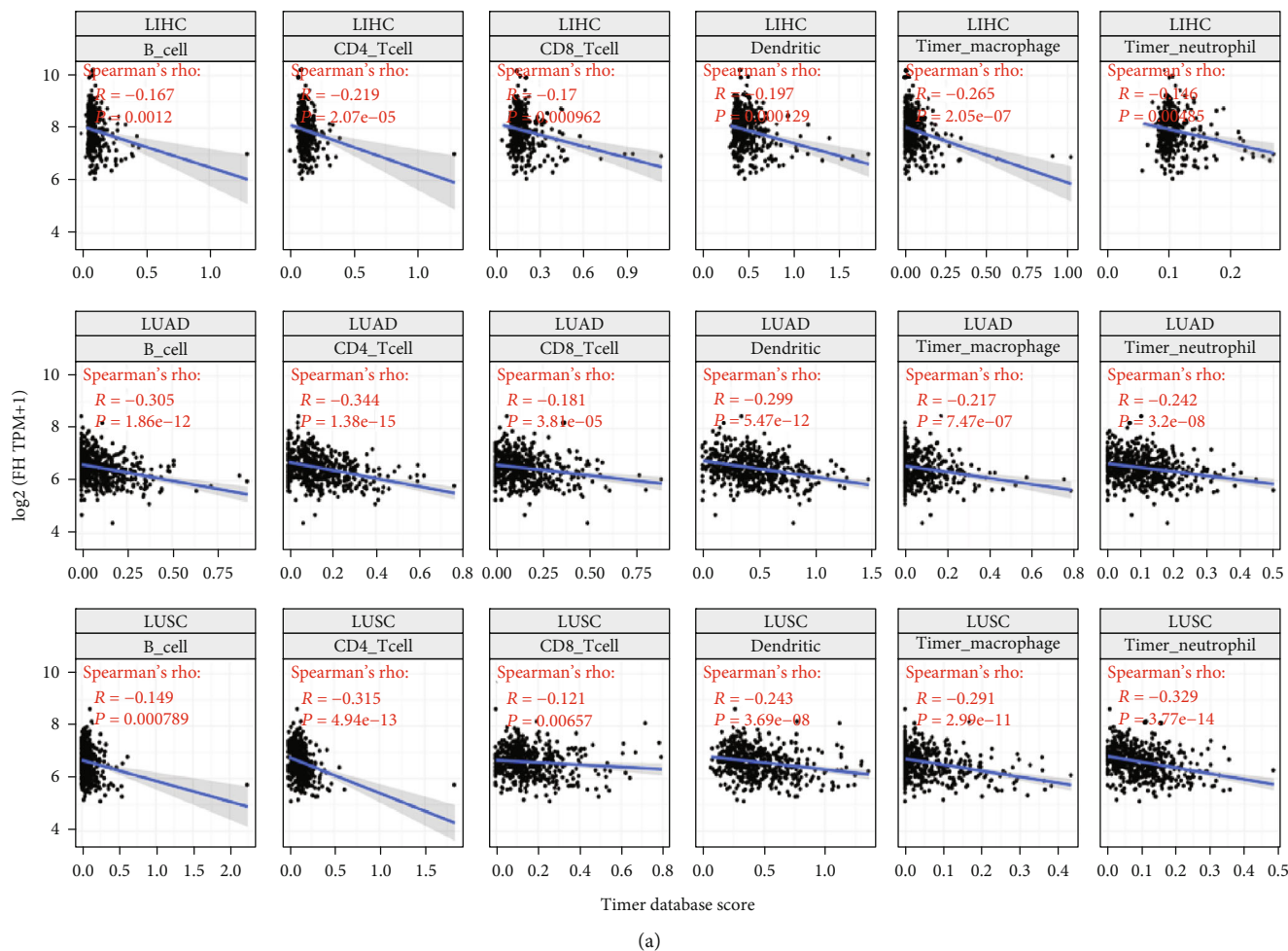
Figure 4: Continued.
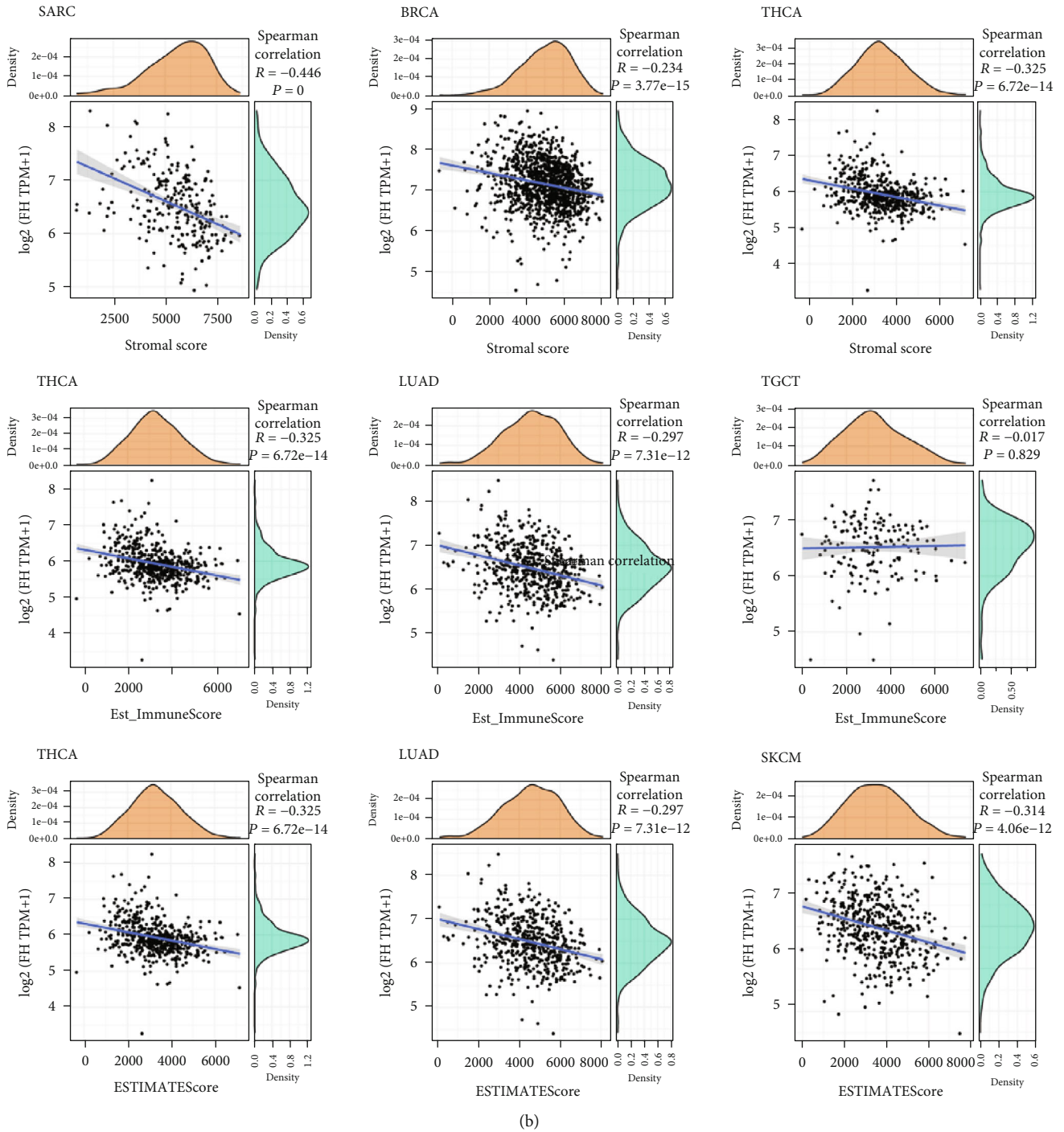
FIGURE 4: The association between FH expression and tumor immunity. (a) Correlation of FH expression with immune infiltration level of 6 types of immune cells in LIHC, LUAD, and LUSC. (b) Correlation analysis between FH expression and ImmuneScore/Stromal Score/ESTIMATEScore in human pan-cancer.

In addition, the inhibition of FH can improve the efficacy of cisplatin-mediated chemotherapy in GC [11]. However, the role of FH in other malignancies remains to be determined. In the present study, we found that FH was upregulated in 21 types of cancers tissues than in normal tissues. To further understand the roles of FH in cancer, we explored the prognostic value of FH in pan-cancer. A high expression level of FH was associated with poor prognosis in several types of cancers, particularly in LUAD. And our experimental results also showed that FH level was significantly upregulated in lung cancer cell lines, including lung adenocarcinoma cell line A549 (Supplementary Figure 1). These results strongly indicated that FH is a significant gene in cancer and may be a potential prognostic marker in patients with LUAD.
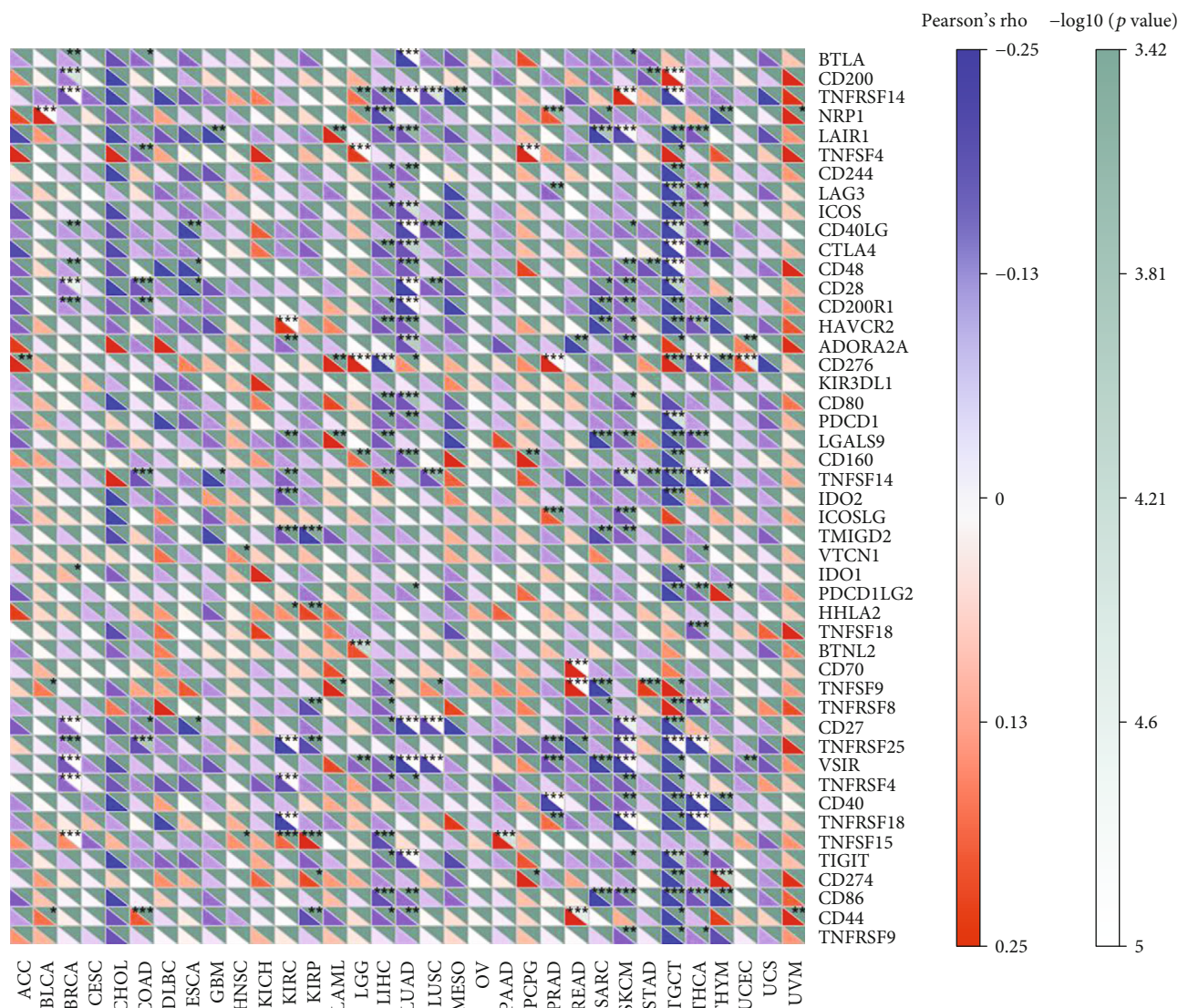
FIGURE 5: Correlation analysis of FH expression levels with 47 immune checkpoints in human pan-cancer. $^*P < 0.05$, $^{**}P < 0.01$, $^{***}P < 0.001$.

Recently, tumor immune microenvironment has received extensive attention, and based on the characteristics of immune cells in the TME, immunotherapy was developed and applied to clinical treatment [39]. Tumor immune microenvironment is a double-edged sword: it can inhibit the development of tumors and can also provide favorable conditions for cancer cells to promote the development of tumors [40]. Tumor-infiltrating immune cells, such as B cells, T cells, neutrophils, macrophages, and dendritic cells, play a significant role in tumor immune microenvironment [41] and can affect the occurrence and development of tumors. For instance, B cells can secret immunoglobulins, promote T cell response, and kill cancer cells to inhibit tumor progression [42]. In advanced ovarian carcinoma, the presence of intratumoral T cells associates with improved survival of patients [43]. Neutrophils can stimulate T cell proliferation [44] to suppress tumor progression. Macrophages and dendritic cells are also closely related to tumor progression [45–47]. Interestingly, in our study, it was found

that FH level was significantly negatively correlated with immune infiltrating cells in LUAD, LIHC, and LUSC. Moreover, we have noticed that immune checkpoint therapy is a hot spot in the treatment of cancer. For example, it can help us to define new means to treat pancreatic cancer [48] and has revolutionized lung cancer treatment paradigms [49]. So, we analyzed the correlations between FH level and immune checkpoint markers; the results showed that FH expression was significantly correlated with a variety of immune checkpoint markers in LUAD and TGCT. However, the results lack validation of clinical specimens, which is the limitation of the study. Overall, our results suggested FH is implicated in cancer immunity, particularly in LUAD.

5. Conclusion

In conclusion, we performed a pan-cancer analysis of the FH and elucidated the prognostic and immune significance of FH expression in human cancers. Our observations

indicated FH may be an immunotherapeutic target and a potential prognostic biomarker, particularly in LUAD. This study provides new insights into the FH in pan-cancer and novel clues for further exploration of the mechanism of FH in cancer.

Data Availability

The datasets presented in this study can be found in online repositories. The names of the repositories can be found in the article material.

Conflicts of Interest

The authors disclose no conflicts.

Acknowledgments

Supplementary Materials

Supplementary Figure 1: Q-PCR analysis of FH expression in normal and lung adenocarcinoma cells. *(Supplementary Materials)*

References

[1] H. Sung, J. Ferlay, R. L. Siegel et al., "Global Cancer Statistics 2020: GLOBOCAN estimates of incidence and mortality worldwide for 36 cancers in 185 countries," *CA: a Cancer Journal for Clinicians*, vol. 71, no. 3, pp. 209–249, 2021.

[2] J. Wei, Y. Yan, X. Chen et al., "The roles of plant-derived triptolide on non-small cell lung cancer," *Oncology Research*, vol. 27, no. 7, pp. 849–858, 2019.

[3] Y. Yan, W. Su, S. Zeng et al., "Effect and mechanism of tanshinone I on the radiosensitivity of lung cancer cells," *Molecular Pharmaceutics*, vol. 15, no. 11, pp. 4843–4853, 2018.

[4] The Cancer Genome Atlas Research Network, J. N. Weinstein, E. A. Collisson et al., "The Cancer Genome Atlas pan-cancer analysis project," *Nature Genetics*, vol. 45, no. 10, pp. 1113–1120, 2013.

[5] J. N. Liu, X. S. Kong, T. Huang, R. Wang, W. Li, and Q. F. Chen, "Clinical implications of aberrant PD-1 and CTLA4 expression for cancer immunity and prognosis: a pan-cancer study," *Frontiers in Immunology*, vol. 11, p. 2048, 2020.

[6] P. Wen, Y. Gao, B. Chen et al., "Pan-cancer analysis of radiotherapy benefits and immune infiltration in multiple human cancers," *Cancers*, vol. 12, no. 4, p. 957, 2020.

[7] V. Izzi, M. N. Davis, and A. Naba, "Pan-cancer analysis of the genomic alterations and mutations of the matrisome," *Cancers*, vol. 12, no. 8, p. 2046, 2020.

[8] Y. Cui, W. Guo, Y. Li, J. Shi, S. Ma, and F. Guan, "Pan-cancer analysis identifies ESM1 as a novel oncogene for esophageal cancer," *Esophagus : official journal of the Japan Esophageal Society*, vol. 18, no. 2, pp. 326–338, 2021.

[9] L. Zhu, W. Wu, S. Jiang et al., "Pan-cancer analysis of the mitophagy-related protein PINK1 as a biomarker for the immunological and prognostic role," *Frontiers in Oncology*, vol. 10, p. 569887, 2020.

[10] Q. Ge, G. Li, J. Chen et al., "Immunological role and prognostic value of APBB1IP in pan-cancer analysis," *Journal of Cancer*, vol. 12, no. 2, pp. 595–610, 2021.

[11] L. Zhang, M. F. Walsh, S. Jairam et al., "Fumarate hydrataseFHc.1431_1433dupAAA (p.Lys477dup) variant is not associated with cancer including renal cell carcinoma," *Human Mutation*, vol. 41, no. 1, pp. 103–109, 2020.

[12] A. Ooi, "Advances in hereditary leiomyomatosis and renal cell carcinoma (HLRCC) research," *Seminars in Cancer Biology*, vol. 61, pp. 158–166, 2020.

[13] H. E. Yu, F. Wang, F. Yu et al., "Suppression of fumarate hydratase activity increases the efficacy of cisplatin-mediated chemotherapy in gastric cancer," *Cell Death & Disease*, vol. 10, no. 6, p. 413, 2019.

[14] M. Sciacovelli, E. Gonçalves, T. I. Johnson et al., "Fumarate is an epigenetic modifier that elicits epithelial-to-mesenchymal transition," *Nature*, vol. 537, no. 7621, pp. 544–547, 2016.

[15] M. Suarez-Carmona, J. Lesage, D. Cataldo, and C. Gilles, "EMT and inflammation: inseparable actors of cancer progression," *Molecular Oncology*, vol. 11, no. 7, pp. 805–823, 2017.

[16] D. C. Hinshaw and L. A. Shevde, "The tumor microenvironment innately modulates cancer progression," *Cancer Research*, vol. 79, no. 18, pp. 4557–4566, 2019.

[17] X. Lei, Y. Lei, J. K. Li et al., "Immune cells within the tumor microenvironment: biological functions and roles in cancer immunotherapy," *Cancer Letters*, vol. 470, pp. 126–133, 2020.

[18] L. Yang and Y. Zhang, "Tumor-associated macrophages: from basic research to clinical application," *Journal of Hematology & Oncology*, vol. 10, no. 1, p. 58, 2017.

[19] L. Cassetta and J. W. Pollard, "Tumor-associated macrophages," *Current Biology : CB*, vol. 30, no. 6, pp. R246–r248, 2020.

[20] Q. Ju, Y. J. Zhao, S. Ma et al., "Genome-wide analysis of prognostic-related lncRNAs, miRNAs and mRNAs forming a competing endogenous RNA network in lung squamous cell carcinoma," *Journal of Cancer Research and Clinical Oncology*, vol. 146, no. 7, pp. 1711–1723, 2020.

[21] Y. Zhao, H. Zhang, Q. Ju, X. Li, and Y. Zheng, "Comprehensive analysis of survival-related lncRNAs, miRNAs, and mRNAs forming a competing endogenous RNA network in gastric cancer," *Frontiers in Genetics*, vol. 12, p. 610501, 2021.

[22] S. A. Martin, M. Hewish, C. J. Lord, and A. Ashworth, "Genomic instability and the selection of treatments for cancer," *The Journal of Pathology*, vol. 220, pp. 281–289, 2010.

[23] R. Ijsselsteijn, J. G. Jansen, and N. de Wind, "DNA mismatch repair-dependent DNA damage responses and cancer," *DNA Repair*, vol. 93, p. 102923, 2020.

[24] J. Peña-Diaz and L. J. Rasmussen, "Approaches to diagnose DNA mismatch repair gene defects in cancer," *DNA Repair*, vol. 38, pp. 147–154, 2016.

[25] Y. Qin, X. Zheng, W. Gao, B. Wang, and Y. Wu, "Tumor microenvironment and immune-related therapies of head and neck squamous cell carcinoma," *Molecular therapy oncolytics*, vol. 20, pp. 342–351, 2021.

[26] Q. Ju, X. Li, H. Zhang, S. Yan, Y. Li, and Y. Zhao, "NFE2L2 is a potential prognostic biomarker and is correlated with immune infiltration in brain lower grade glioma: a pan-cancer analysis," *Oxidative Medicine and Cellular Longevity*, vol. 2020, Article ID 3580719, 26 pages, 2020.

[27] Q. Ju, X. M. Li, H. Zhang, and Y. J. Zhao, "BRCA1-associated protein is a potential prognostic biomarker and is correlated with immune infiltration in liver hepatocellular carcinoma: a pan-cancer analysis," *Frontiers in Molecular Biosciences*, vol. 7, p. 573619, 2020.

[28] C. Schmidt, M. Sciacovelli, and C. Frezza, "Fumarate hydratase in cancer: a multifaceted tumour suppressor," *Seminars in Cell & Developmental Biology*, vol. 98, pp. 15–25, 2020.

[29] Z. Cai, C. F. Li, F. Han et al., "Phosphorylation of PDHA by AMPK drives TCA cycle to promote cancer metastasis," *Molecular Cell*, vol. 80, no. 2, pp. 263–278.e7, 2020.

[30] N. M. Anderson, P. Mucka, J. G. Kern, and H. Feng, "The emerging role and targetability of the TCA cycle in cancer metabolism," *Protein & Cell*, vol. 9, no. 2, pp. 216–237, 2018.

[31] S. Zhou, Y. Yan, X. Chen et al., "Roles of highly expressed PAICS in lung adenocarcinoma," *Gene*, vol. 692, pp. 1–8, 2019.

[32] Y. Yan, Z. Xu, X. Hu et al., "SNCA is a functionally low-expressed gene in lung adenocarcinoma," *Genes*, vol. 9, no. 1, p. 16, 2018.

[33] U. Ben-David, R. Beroukhim, and T. R. Golub, "Genomic evolution of cancer models: perils and opportunities," *Nature Reviews. Cancer*, vol. 19, no. 2, pp. 97–109, 2019.

[34] S. Negrini, V. G. Gorgoulis, and T. D. Halazonetis, "Genomic instability – an evolving hallmark of cancer," *Nature Reviews. Molecular Cell Biology*, vol. 11, no. 3, pp. 220–228, 2010.

[35] D. L. Keefe, "Telomeres and genomic instability during early development," *European Journal of Medical Genetics*, vol. 63, no. 2, p. 103638, 2020.

[36] E. Sanz-Garcia, G. Argiles, E. Elez, and J. Tabernero, "BRAF mutant colorectal cancer: prognosis, treatment, and new perspectives," *Annals of Oncology : official journal of the European Society for Medical Oncology*, vol. 28, no. 11, pp. 2648–2657, 2017.

[37] M. Baretti and D. T. Le, "DNA mismatch repair in cancer," *Pharmacology & Therapeutics*, vol. 189, pp. 45–62, 2018.

[38] P. Kancherla, M. Daneshvar, R. A. Sager, M. Mollapour, and G. Bratslavsky, "Fumarate hydratase as a therapeutic target in renal cancer," *Expert Opinion on Therapeutic Targets*, vol. 24, no. 9, pp. 923–936, 2020.

[39] K. E. Yost, A. T. Satpathy, D. K. Wells et al., "Clonal replacement of tumor-specific T cells following PD-1 blockade," *Nature Medicine*, vol. 25, no. 8, pp. 1251–1259, 2019.

[40] R. D. Schreiber, L. J. Old, and M. J. Smyth, "Cancer immunoediting: integrating immunity's roles in cancer suppression and promotion," *Science*, vol. 331, no. 6024, pp. 1565–1570, 2011.

[41] S. S. Wang, W. Liu, D. Ly, H. Xu, L. Qu, and L. Zhang, "Tumor-infiltrating B cells: their role and application in anti-tumor immunity in lung cancer," *Cellular & Molecular Immunology*, vol. 16, no. 1, pp. 6–18, 2019.

[42] M. Horikawa, V. Minard-Colin, T. Matsushita, and T. F. Tedder, "Regulatory B cell production of IL-10 inhibits lymphoma depletion during CD20 immunotherapy in mice," *The Journal of Clinical Investigation*, vol. 121, no. 11, pp. 4268–4280, 2011.

[43] L. Zhang, J. R. Conejo-Garcia, D. Katsaros et al., "Intratumoral T cells, recurrence, and survival in epithelial ovarian cancer," *The New England Journal of Medicine*, vol. 348, no. 3, pp. 203–213, 2003.

[44] E. B. Eruslanov, P. S. Bhojnagarwala, J. G. Quatromoni et al., "Tumor-associated neutrophils stimulate T cell responses in early-stage human lung cancer," *The Journal of Clinical Investigation*, vol. 124, no. 12, pp. 5466–5480, 2014.

[45] Y. Komohara, Y. Fujiwara, K. Ohnishi, and M. Takeya, "Tumor-associated macrophages: potential therapeutic targets for anti-cancer therapy," *Advanced Drug Delivery Reviews*, vol. 99, pp. 180–185, 2016.

[46] F. Veglia and D. I. Gabrilovich, "Dendritic cells in cancer: the role revisited," *Current Opinion in Immunology*, vol. 45, pp. 43–51, 2017.

[47] M. Hansen and M. H. Andersen, "The role of dendritic cells in cancer," *Seminars in Immunopathology*, vol. 39, no. 3, pp. 307–316, 2017.

[48] E. S. Knudsen, V. Kumarasamy, S. Chung et al., "Targeting dual signalling pathways in concert with immune checkpoints for the treatment of pancreatic cancer," *Gut*, vol. 70, no. 1, pp. 127–138, 2021.

[49] L. Long, C. Zhao, M. Ozarina, X. Zhao, J. Yang, and H. Chen, "Targeting immune checkpoints in lung cancer: current landscape and future prospects," *Clinical Drug Investigation*, vol. 39, no. 4, pp. 341–353, 2019.

Research Article

Identification and Validation of a Proliferation-Associated Score Model Predicting Survival in Lung Adenocarcinomas

Yunyi Bian ⓘ, Qihai Sui, Guoshu Bi, Yuansheng Zheng, Mengnan Zhao, Guangyu Yao, Liang Xue, Yi Zhang ⓘ, and Hong Fan ⓘ

Department of Thoracic Surgery, Zhongshan Hospital, Fudan University, Shanghai, China

Correspondence should be addressed to Yi Zhang; zhang.yi@zs-hospital.sh.cn and Hong Fan; fan.hong@zs-hospital.sh.cn

Aim. This study is aimed at building a risk model based on the genes that significantly altered the proliferation of lung adenocarcinoma cells and exploring the underlying mechanisms. *Methods*. The data of 60 lung adenocarcinoma cell lines in the Cancer Dependency Map (Depmap) were used to identify the genes whose knockout led to dramatical acceleration or deacceleration of cell proliferation. Then, univariate Cox regression was performed using the survival data of 497 patients with lung adenocarcinoma in The Cancer Genome Atlas (TCGA). The least absolute shrinkage and selection operator (LASSO) model was used to construct a risk prediction score model. Patients with lung adenocarcinoma from TCGA were classified into high- or low-risk groups based on the scores. The differences in clinicopathologic, genomic, and immune characteristics between the two groups were analyzed. The prognosis of the genes in the model was verified with immunohistochemical staining in 100 samples from the Department of Thoracic Surgery, Zhongshan Hospital, and the alteration in the proliferation rate was checked after these genes were knocked down in lung adenocarcinoma cells (A549 and H358). *Results*. A total of 55 genes were found to be significantly related to survival by combined methods, which were crucial to tumor progression in functional enrichment analysis. A six-gene-based risk prediction score, including the proteasome subunit beta type-6 (PSMB6), the heat shock protein family A member 9 (HSPA9), the deoxyuridine triphosphatase (DUT), the cyclin-dependent kinase 7 (CDK7), the polo-like kinases 1 (PLK1), and the folate receptor beta 2 (FOLR2), was built using the LASSO method. The high-risk group classified with the score model was characterized by poor overall survival (OS), immune infiltration, and relatively higher mutation load. A total of 9864 differentially expressed genes and 138 differentially expressed miRNAs were found between the two groups. Also, a nomogram comparing score model, age, and the stage was built to predict OS for patients with lung adenocarcinoma. Using immunohistochemistry, the expression levels of PSMB6, HSPA9, DUT, CDK7, and PLK1 were found to be higher in lung adenocarcinoma tissues of patients, while the expression of FOLR2 was low, which was consistent with survival prediction. The knockdown of PSMB6 and HSPA9 by siRNA significantly downregulated the proliferation of A549 and H358 cells. *Conclusion*. The proposed score model may function as a promising risk prediction tool for patients with lung adenocarcinoma and provide insights into the molecular regulation mechanism of lung adenocarcinoma.

1. Introduction

Lung cancer is one of the most common malignant cancers characterized by a high incidence and the highest mortality worldwide, with an average 5-year survival rate of <15% [1, 2]. Lung adenocarcinoma (LUAD) is currently the major subtype of lung cancer, accounting for nearly 60% of new

cases, characterized by poor survival [3]. Early surgical excision is the standard treatment strategy now. For patients with high-risk LUAD, they should receive radiation, chemotherapy, or targeted immunotherapy after surgery to improve survival [2]. Nearly 50% of patients are at risk of postoperative recurrence, and tumor recurrence in high-risk patients is an important cause of death [4, 5]. Therefore,

accurate identification of high-risk patients and early intervention with adjuvant therapy mentioned earlier are very important for improving the prognosis.

Currently, the TNM staging system plays a critical role in risk assessment and therapy guidance. However, these risk assessment factors based on clinical pathological characteristics can not achieve early identification of patients with poor prognosis and can not be accurate to predict patients' response to adjuvant treatment; more precise risk prediction models need to be established, such as scoring models that contain molecular characteristics of LUAD.

In recent years, public databases such as The Cancer Genome Atlas (TCGA) and Gene Expression Omnibus (GEO) provide large lung cancer datasets. At the same time, techniques such as high-throughput sequencing, combined with machine learning methods, have been used to explore more types of biomarkers, identify the signaling pathways, reveal molecular mechanisms, and make clinical prognosis predictions based on large datasets [6]. Several prognostic models for LUAD based on the above techniques have been published, but these models still have limitations. The biomarkers selected had a minimal relationship with tumor proliferation and cannot fully reflect the proliferation potential of LUAD [7–9]. The cancer dependence of genes is the basis of prognosis prediction and drug target research.

Recently, the Cancer Dependency Map (DEPMAP), using genome-scale CRISPR screens in hundreds of cell lines, was used to establish a comprehensive and systematic identification of the genetic and pharmacological dependence of cancer and its prediction biomarkers [10–12]. Therefore, genes closely related to LUAD's proliferation were identified from DEPMAP, and a risk prediction score model was built based on the expression of these genes and survival information in this study. The proposed model could successfully predict prognosis in patients from TCGA and GEO. According to the model, somatic mutations, differentially expressed genes, microRNAs, and immune infiltration patterns were further analyzed to reveal the regulatory factors, cellular processes, and signaling pathways associated with the model-related genes in LUAD. Finally, the effects of some model-related genes on tumor proliferation were verified *in vitro*. The study was meaningful for elucidating the molecular mechanism of proliferation in LUAD and accurately predicting patient prognosis to provide individualized treatment.

2. Materials and Methods

2.1. Data Preprocessing. First, data of 60 LUAD cell lines and the CERES dependency score of genes from DEPMAP (https://depmap.org/) were obtained. The CERES dependency score of the genes represented the effect on cell survival by knocking out individual genes with CRISPR-Cas9 genetic perturbation reagents. A lower CERES score indicated a higher likelihood that the gene of interest was essential in a given cell line. A score of 0 indicated that a gene was not essential; correspondingly, a score of -1 was comparable to the median of all pan-essential genes [13].

The public datasets of LUAD patients ($n = 497$) were downloaded from the UCSC Xena Browser, and the expression data (FPKM form) was matched with patients' survival information downloaded from TCGA. The patients with missing survival data were excluded. The miRNA data, the somatic mutation data, and the copy numbers' variation were obtained from the Xena Browser.

The public datasets from the GEO (https://www.ncbi.nlm.nih.gov/geo/) were used for the validation cohort. A total of 930 samples from the datasets GSE30219 [14], GSE31210 [15, 16], GSE3141 [17], GSE37745 [18–21], GSE50081 [22], and GSE68465 [23] representing different independent studies of LUAD were enrolled. The batch effect caused by the heterogeneity among different studies was eliminated with the COMBAT empirical Bayes method using the sva package [24], and background adjustments and quantile normalization were conducted using the limma package [25].

Next, paraffin-embedded specimens of the tumor and adjacent healthy tissues were collected from 100 patients with LUAD who underwent radical surgery in the Department of Thoracic Surgery, Zhongshan Hospital, Fudan University, from September to November 2015. The survival information of the 100 patients was collected by the follow-up until December 2020, excluding the ones who succumbed. All participants signed informed consent according to the ethical requirements in the Declaration of Helsinki. Ethics approved by the ethical committees of Zhongshan Hospital (B2019-035).

2.2. Gene Selection and Prediction Score Model Construction. The data were processed by the R software (Version 3.5.3) and the GraphPad Prism software (version 7.0). The independent hazard rate of each gene was calculated using univariate Cox regression with the survival package in R, and P value < 0.05 was considered statistically significant. The ClusterProfiler package [26] was also adopted to analyze the functional enrichment of the selected genes. The cutoff of GO and KEGG terms comprised the adjusted P value < 0.05 and the false discovery rate (FDR) < 0.05.

The LASSO Cox regression analysis, a penalized method to select data with high dimensions and reduce the impact of overfitting, was used to build the predictive score model [27, 28]. Tenfold cross-validation was adopted using the glmnet package [29] in R to determine the optimal model parameter λ and corresponding coefficients. The optimal λ was determined as the smallest partial likelihood deviance. A multivariate Cox regression of the six genes was conducted, and their coefficients were applied to build the score model. Harrell's concordance index (C-index) [30] was applied to measure the predictive accuracy of the score model preliminarily.

2.3. Survival Data Analysis. The survival curves were visualized using the ggplot2 package by the Kaplan–Meier method. Log-rank tests exhibited the difference in overall survival (OS). The rms package in R was used to build a nomogram of the 497 LUAD samples from TCGA, and the calibration plots were shown. The univariate and

multivariate Cox proportional risk analyses were conducted to show the score model's prognostic value when age, gender, and stage were adjusted. C-index was also calculated to identify the value of the score model.

2.4. Differentially Expressed Genes, microRNAs (miRNAs), and Somatic Mutation Distribution.

The limma package [25] was adopted to identify differentially expressed genes (DEGs) and miRNAs between high and low score groups. The moderated t-test was used to calculate DEGs and miRNA expression changes, and the P value was adjusted as FDR by Benjamini and Hochberg method [31]. The log fold change was set as >0.5 and the adjusted P value < 0.05 as the cutoff criteria.

We used the maftools package basing on the Kruskal-Wallis test to compare the distribution of somatic mutations and the types of copy number variations. The adjusted P value < 0.01 was used to assess the significance of the mutational frequency.

2.5. Immune Cell Infiltration in the Two Groups.

We selected the gene markers reported by Bindea et al. according to the previous studies [32–34]. A synopsis of genes associated with microenvironment cell sets was constructed precisely, which contained 585 genes depicting 24 tumor microenvironment- (TME-) infiltration cell populations related to innate immunity and adaptive immunity. The subsets included B cells, dendritic cells (DCs), immature DCs, activated DCs, neutrophils, mast cells, eosinophils, macrophages, natural killer (NK) cells, NK CD56bright cells, NK CD56dim cells, cytotoxic cells, T cells, CD8 T cells, and Th1, Th2, Th17, Tfh, Tgd, T$\gamma\delta$, T helper, Tcm, Tem, and Treg cells (Table S1). We employed a seven-gene panel introduced in the POPLAR (patients with previously treated non-small-cell lung cancer) trial as a surrogate index to identify infiltration pattern of effector T-cell (CD8A and CXCL10) and IFN-γ associated cytotoxicity (IFNG, GZMA, GZMB, EOMES, and TBX21) [35]. The CYT (cytolytic activity) score was defined by Rooney et al. [36]. We used it to calculate the geometrical mean of PRF1 and GZMA, which can reflect the significance of the response to antitumor. The pheatmap package was used to plot the 24 immune cell infiltrating patterns from different patients.

2.6. Immunohistochemistry.

The tissue specimens were collected from both tumor and tumor-adjacent areas of 100 patients with LUAD who received lung surgery from September to November 2015 in the Zhongshan Hospital. The paraffin-embedded tissues were dewaxed, rehydrated, and stained using a GTVision + Detection System/Mo&Rb Immunohistochemistry kit (GK500710, GeneTech, Shanghai, China) following the manufacturer's protocol. Anti-PSMB6 (1 : 50, abs116436, Absin Bioscience Inc., Shanghai, China), anti-HSPA9 (1 : 50, abs135628, Absin), anti-DUT (1 : 50, abs102198, Absin), anti-CDK7 (1 : 50, abs136079, Absin), anti-PLK1 (1 : 100, ab17056, Abcam, Cambridge, UK), and anti-FOLR2 antibodies (1 : 50, abs107177, Absin) were used. The detailed procedure can be found in a previous study [37].

2.7. Cell Culture and siRNA Transfection.

Two LUAD cell lines (A549 and H358) were purchased from the Chinese Academy of Science Cell Bank and cultured in high glucose Dulbecco's Modified Eagle's Medium (Hyclone, UT, USA) supplemented with 10% fetal bovine serum (Every Green, Hangzhou, Zhejiang, China), 100 U/mL penicillin, 0.1 mg/mL streptomycin, and 0.25 μg/mL amphotericin B (Sangon Biotech, Shanghai, China) in a humidified 5% CO_2 atmosphere at 37°C.

Two small interfering RNAs (siRNAs) targeting PSMB6 (si-PSMB6-1 and si-PSMB6-2), two siRNAs targeting HSPA9 (si-HSPA9-1 and si-HSPA9-2), and two negative control siRNAs (siCtrl-1 and siCtrl-2) were designed and purchased by Guangzhou RiboBio Co., Ltd. (RiboBio). Target sequences of the siRNAs can be found in Table S7. SiRNAs were transfected with a 100 nM Lipo8000 transfect reagent (Beyotime, Haimen, Zhejiang, China) and Opti-MEM (Thermo Fisher Scientific, MA, USA) following the manufacturer's protocol.

2.8. RNA Extraction and Quantitative Real-Time Polymerase Chain Reaction.

TRIzol reagent (Tiangen Biotechnology Co., Beijing, China) served as an RNA extraction reagent. A PrimeScript RT Reagent Kit (TaKaRa, Tokyo, Japan) was used to synthesize the cDNA template, and SYBR Premix Ex Taq (TaKaRa) was used to perform quantitative real-time polymerase chain reaction following the manufacturer's protocol. All reactions were analyzed in a QuantStudio 5 (Thermo Fisher Scientific). The $2^{-\Delta\Delta CT}$ method using GAPDH as an endogenous calibrator was adopted to relatively quantify the mRNA. All primers were synthesized by Sangon Biotech, and the sequences can be seen in Table S2.

2.9. Western Blot Analysis.

Western blot analysis was performed as described earlier [37]. RIPA buffer (Beyotime) with protease and phosphatase inhibitor cocktail (Topscience Co., Shanghai, China) was used to extract proteins from cells. Proteins were quantified using an Enhanced BCA Protein Assay Kit (Beyotime), separated with SDS-PAGE, and transferred onto polyvinylidene fluoride membranes (Merck-Millipore, MA, USA). Furthermore, 10% nonfat milk was used to block the membranes for 2 h and then incubated with specific primary antibodies for 12 h at 4°C. Tris-buffered saline-Tween 20 (TBST) solution was used to wash the membranes three times, and the secondary antibody dilutions were incubated on the membranes at room temperature for 1 h. Finally, the protein bands were visualized using a Moon Chemiluminescence Reagent kit (Beyotime). In this study, the following antibodies were used: anti-HSPA9 (1 : 1000, abs135628), anti-PSMB6 (1 : 1000, abs135628), anti-tubulin (1 : 1,000, AT-819, Beyotime), horseradish peroxidase- (HRP-) labeled goat anti-mouse IgG (H + L) (1 : 1,000, A0216, Beyotime), and HRP-labeled goat anti-rabbit IgG (H + L) (1 : 1,000, A0208, Beyotime).

2.10. Cell Proliferation Analysis.

Green fluorescent protein- (GFP-) overexpressing cells were first transfected with siRNAs (si-PSMB6-1, si-PSMB6-2, si-HSPA9-1, si-HSPA9-2,

(a)

HR_group
● Higher risk
● Lower risk
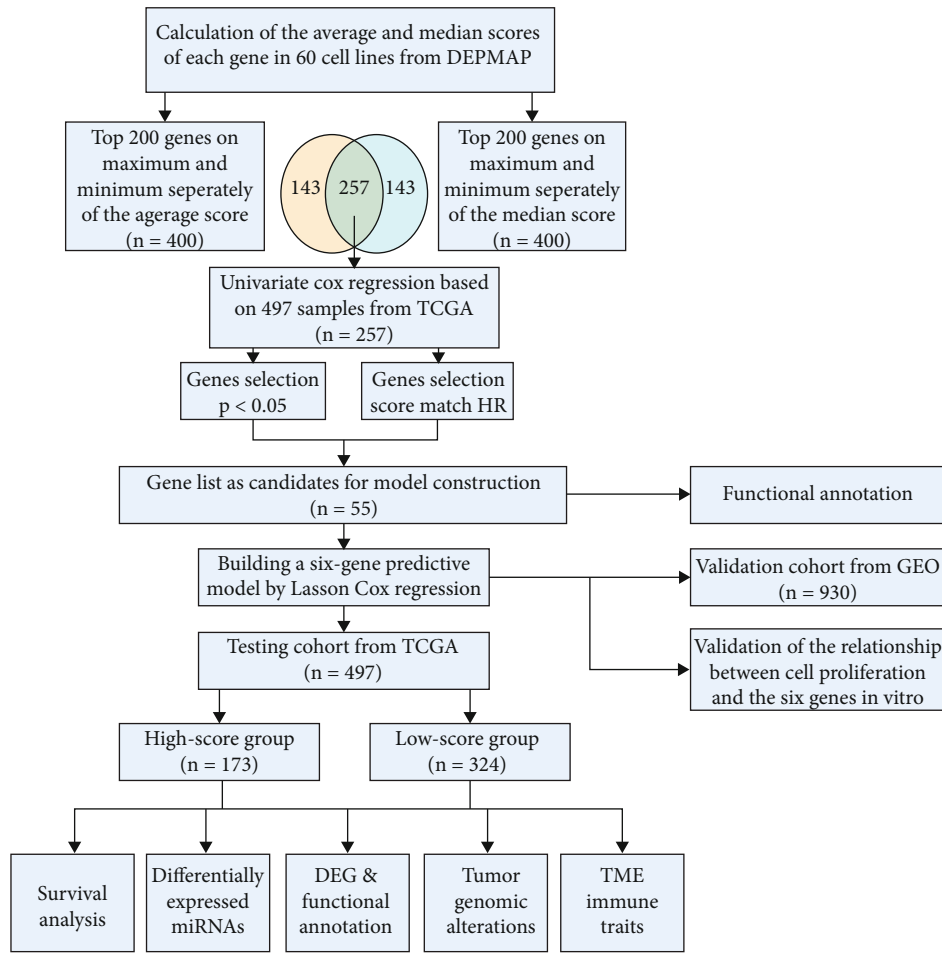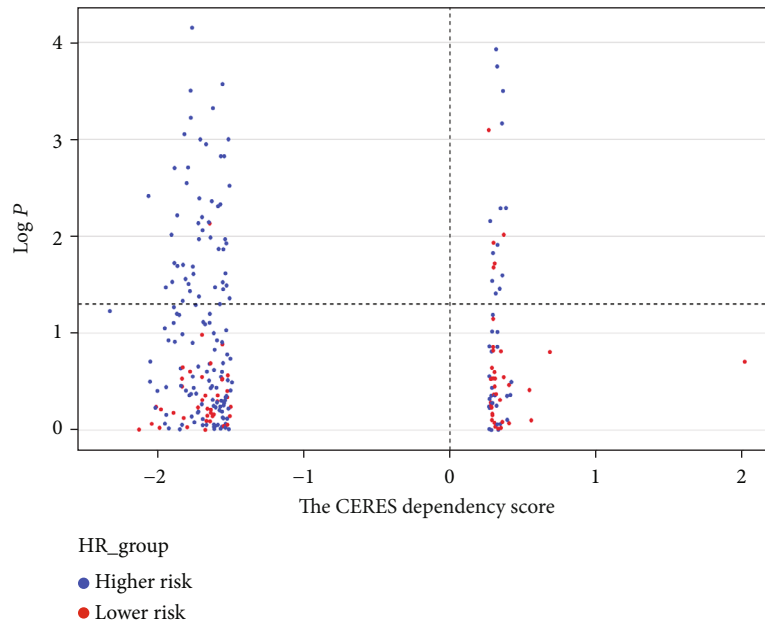
(b)

FIGURE 1: (a) Design of the study. (b) The scatter dot plots show the relationship between the CERES dependency scores and the *P* value of the 257 genes we selected before.

(a)

R-HSA-1640170: Cell cycle
GO:0006260: DNA replication
GO:0044770: Cell cycle phase transition
GO:0051301: Cell division
R-HSA-453279: Mitotic G1 phase and G1/s transition
GO:0000075: Cell cycle checkpoint
R-HSA-8953854: Metabolism of RNA
ko00240: Pyrimidine metabolism
GO:0071103: DNA conformation change
GO:0034502: protein localization to chromosome
R-HSA-176974: Unwinding of DNA
R-HSA-1538133: G0 and early G1
R-HSA-8950505: Gene and protein expression by JAK STAT signaling after interleukin-12 stimulation
GO:0065004: protein-DNA complex assembly
GO:0007080: mitotic metaphase plate congression
R-HSA-6791226: Major pathway of rRNA processing in the nucleolus and cytosol

(b)

(c)

FIGURE 2: Continued.

(d)

(e)

FIGURE 2: (a) The network showed the interactions among the enriched pathways of the 55 genes. The circle nodes' size represents the number of input genes that fall into that pathway, and its color represents its cluster identity. The description of each cluster was shown in the label. The same enrichment network has its nodes colored by P value, as shown in the legend. The dark the color, the more statistically significant the node is (see legend for P value ranges). (b) GO and KEGG functional enrichment analyses of the enriched terms. (c) Coefficient profiles of variables in the LASSO Cox regression model. (d) Tenfold cross-validation for turning parameter selection in the LASSO Cox regression model. λ is the turning parameter. The partial likelihood deviance is plotted in $\log(\lambda)$, in which vertical lines are shown at the optimal values by minimum criteria and $1 - SE$ criteria. (e) Kaplan-Meier curves of overall survival (OS) stratified by the six genes in TCGA.
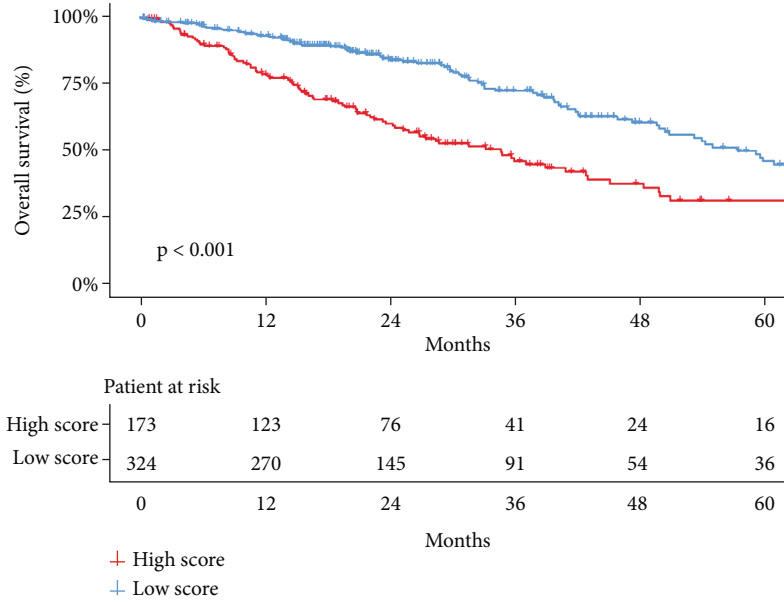
(a)
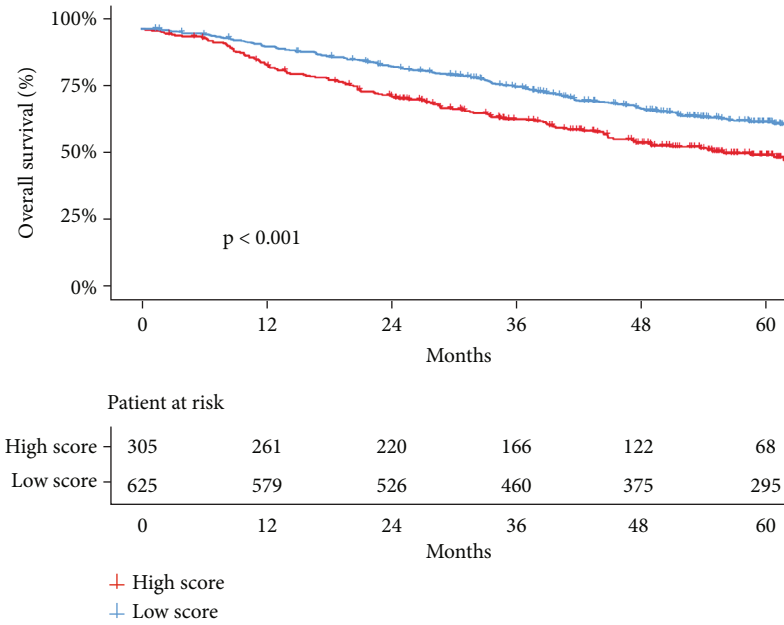
(b)
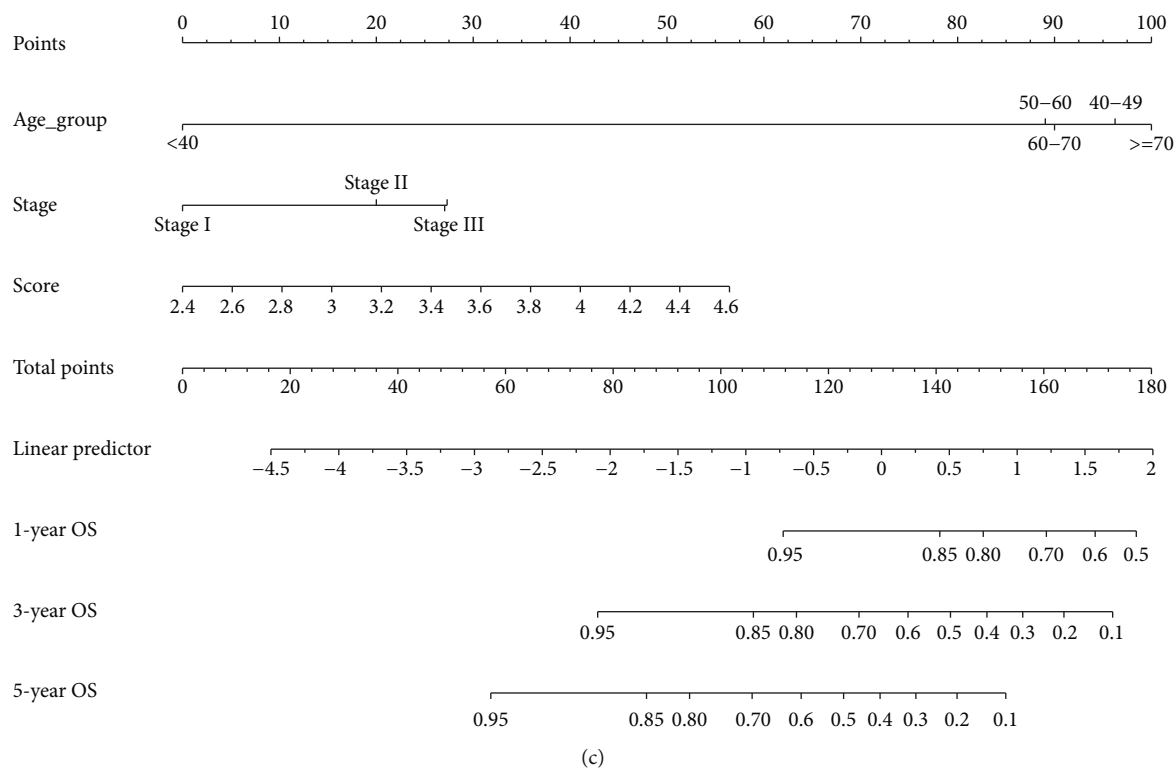
FIGURE 3: Continued.

FIGURE 3: Continued.

(d)
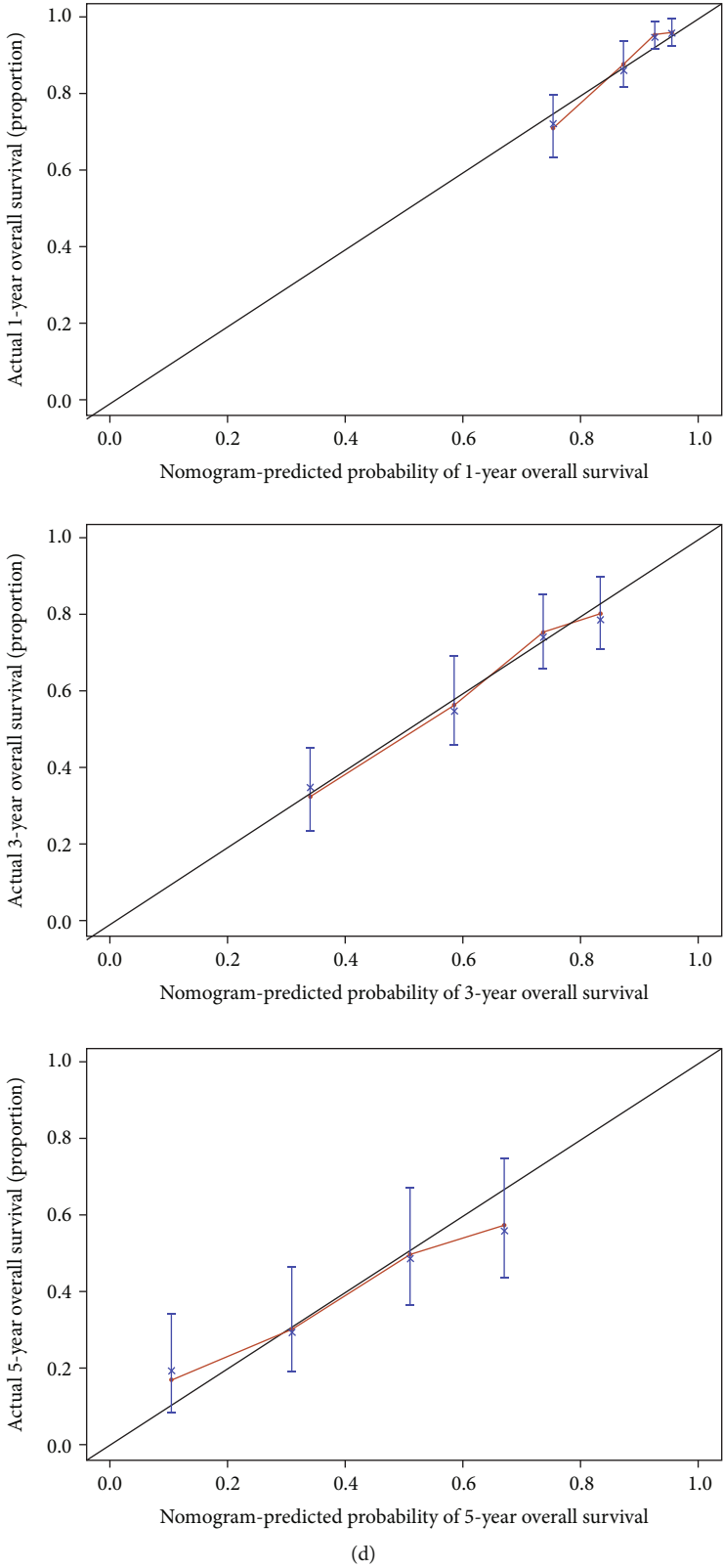
FIGURE 3: (a) Kaplan–Meier curves of OS in patients from TCGA in the two groups. (b) Kaplan–Meier curves of OS in patients from GEO in the two groups. (c) The nomogram of the overall survival prediction model. (d) Calibration plots for the nomogram: 1-, 3-, and 5-year nomogram.

TABLE 1: Univariate and multivariate analysis of overall survival in LUAD patients from TCGA database.

	Univariable		Multivariable	
	HR (95% CI)	*P* value	HR (95% CI)	*P* value
Age				
<60	—	—	—	
60-70	0.82 (0.56-1.19)	0.29	0.97 (0.66-1.43)	0.88
>70	1.26 (0.87-1.83)	0.22	1.61 (1.09-2.36)	0.02
Stage				
Stage I	—	—	—	—
Stage II	2.32 (1.60-3.36)	<0.001	2.35 (1.61-3.43)	<0.001
Stage III	3.30 (2.24-4.85)	<0.001	2.91 (1.96-4.32)	<0.001
Stage IV	3.61 (2.08-6.26)	<0.001	3.20 (1.82-5.62)	<0.001
Gender				
Female	—	—	—	—
Male	1.09 (0.81-1.46)	0.59	0.92 (0.68-1.25)	0.595
Score groups (high vs. low)	2.83 (1.95-4.11)	<0.001	2.86 (1.94-4.22)	<0.001

TABLE 2: Comparison of the accuracy of survival prediction between the factors with and without the score.

|	Age + gender+stage		Score + age + gender +stage	
	C-index	95% CI	C-index	95% CI
Training cohort	0.678	0.632-0.723	0.711	0.667-0.756

si-NC-1, and si-NC-2) at a 100 nM final concentration using Lipo8000 transfection reagent (Beyotime) and Opti-MEM (Thermo Fisher Scientific). Then, 1,500 cells in the logarithmic growth phase were digested and inoculated in blank 96-well plates (Life Science, NY, USA) with 100 μL of cell suspension in every well. Following incubation for 24, 48, 72, 96, and 120 h at 37°C, cell proliferation was measured according to corresponding fluorescence intensity using a Celigo cytometer (Cyntellect Inc., CA, USA), which was equipped with a 4-megapixel CCD camera with an F-theta scan lens.

3. Results

3.1. Gene Selection. The design of this study is shown in Figure 1(a). First, the CERES dependency score of genes with 60 LUAD cell lines from DEPMAP was obtained. A score less than zero showed that the gene knockout inhibited cell proliferation; the smaller the score, the more pronounced the effect. A score greater than zero showed the opposite effect.

The average and median scores of each gene were calculated in 60 cell lines. The top 400 genes on the minimum and maximum of the average and median, respectively, were selected to match, and 257 genes were finally obtained, which meant that cell proliferation was dramatically accelerated or deaccelerated when the genes were knockout. Next, univariate Cox regression was performed on the 257 genes in 497 samples from TCGA. The genes significantly related to survival were retained ($P < 0.05$). The genes that showed the same tendency in cell proliferation (the CERES dependency score) and survival (HR) were matched, and 55 genes finally remained (Figure 1(b), Table S3). The results showed that all these genes greatly influenced cell proliferation and significantly correlated with the survival of LUAD patients.

The analysis of the enrichment of GO and KEGG on these 55 genes was performed using the R cluster profile package. These genes were significantly related to tumor progression, including DNA replication, nuclear division, and cell cycle (Figures 2(a) and 2(b)).

3.2. Construction of the Score Model. After LASSO Cox analysis, six genes, including PSMB6, HSPA9, DUT, CDK7, PLK1, and FOLR2 (Figures 2(c) and 2(d), Table S4), were selected to construct the optimal prognostic model. All the six genes were significantly related to survival (Figure 2(e)). The CERES dependency scores and HRs from univariate Cox regression of the six genes indicated that PSMB6, HSPA9, DUT, CDK7, and PLK1 served as oncogenes, while FOLR2 served as a tumor-suppressor gene. The expression values of most of them were significantly correlated ($P < 0.05$) (Fig. S1A). The correlation between clinical characteristics (sex, age, stage, and smoking) and gene expression is shown in Figure S1B.

A risk-predicted score model was built based on their coefficients with multivariate Cox regression (Additional file 1). Based on the risk predicting score model, 497 patients with LUAD from TCGA were assigned to low score ($n = 324$) and high score ($n = 173$) groups by the optimal cutoff value (3.539). Patients with a high score had a significantly poorer OS (P value < 0.0001, Figure 3(a)) compared with those with a low score, indicating the accuracy of the prediction model.

3.3. Validation and Clinical Significance of the Score Model. The univariate and multivariate Cox regression analyses were performed to demonstrate that the score model was an independent prognostic factor in patients with LUAD

(a)

(b)

FIGURE 4: Continued.

(c)
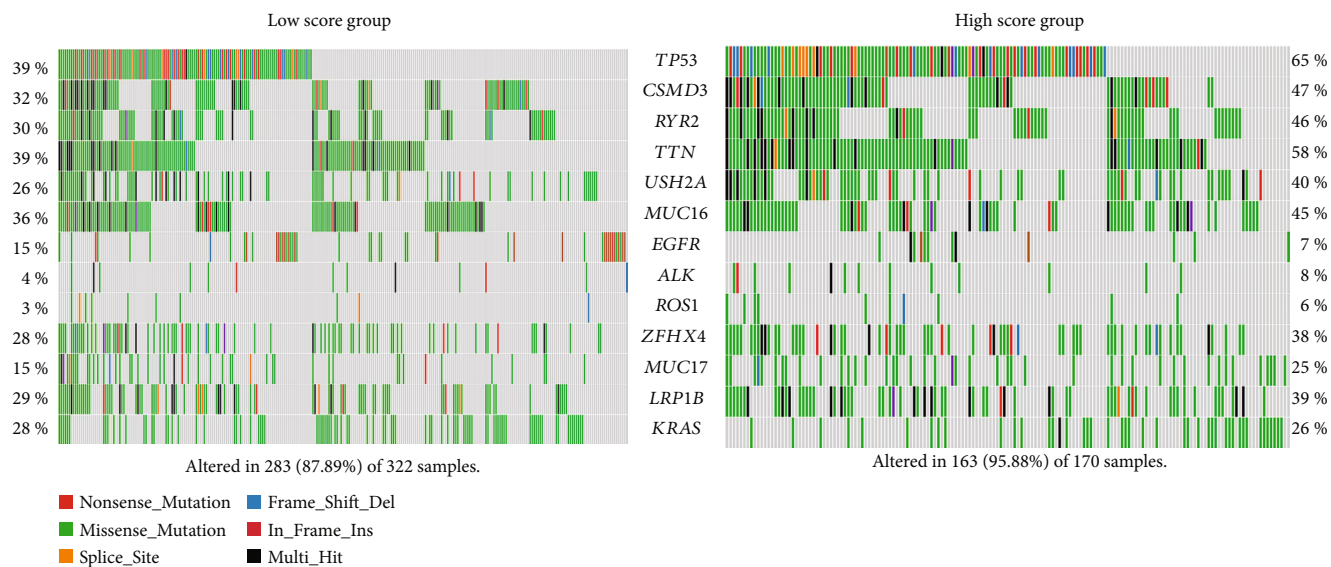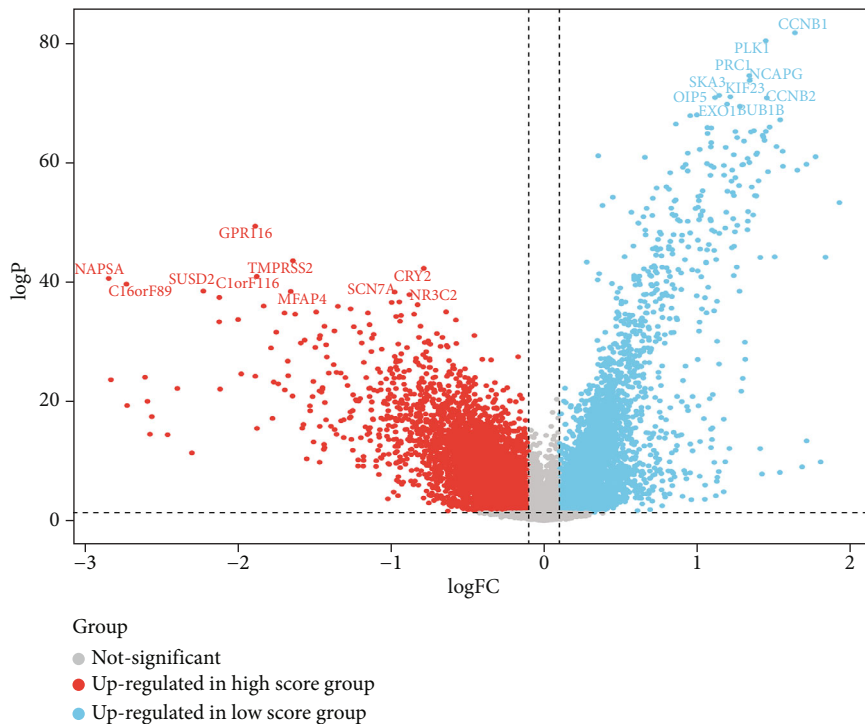
(d)
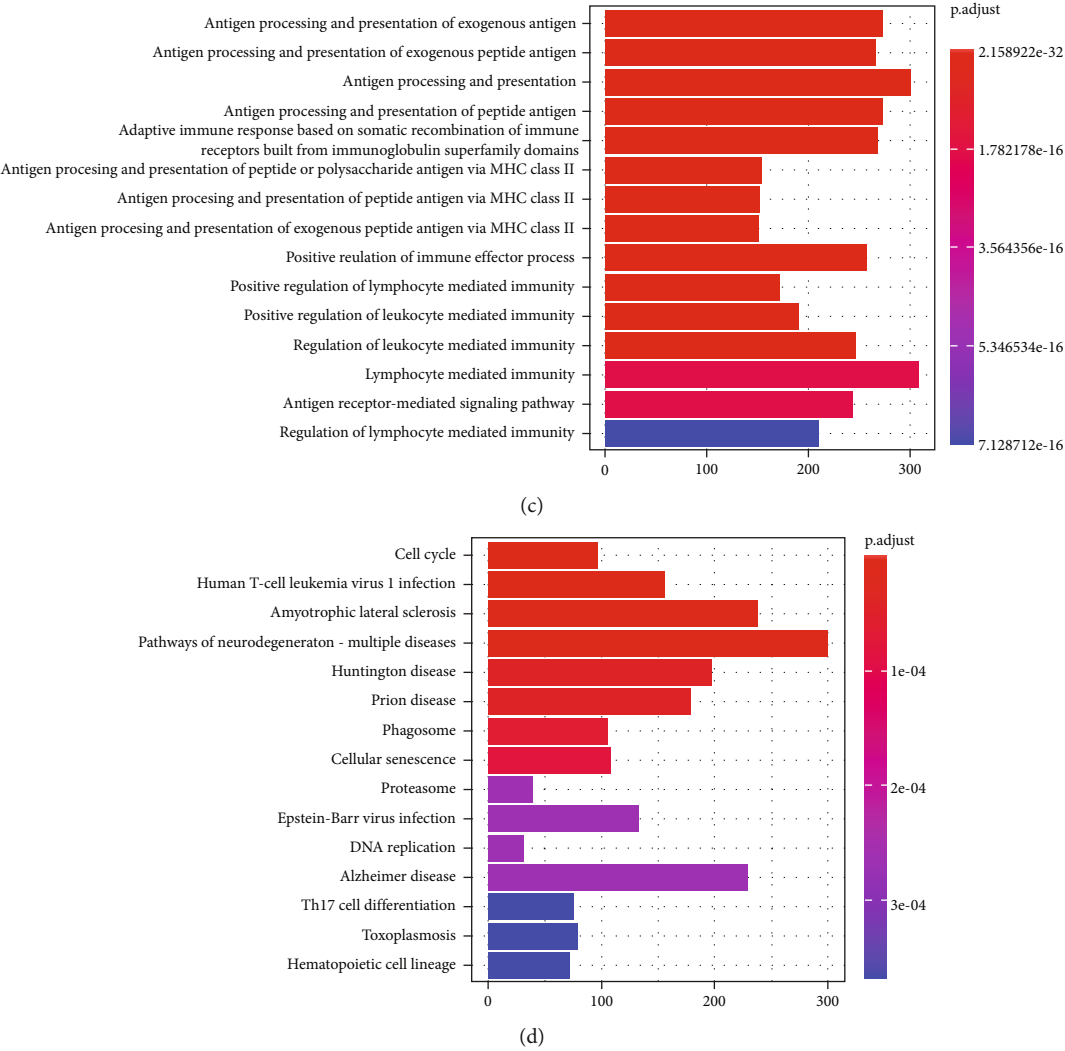
Figure 4: (a) The waterfall plots show the somatic mutations and copy numbers' variations in the two groups. (b) The volcano plot displays the DEGs of the two groups. (c, d) GO (c) and KEGG (d) functional enrichment analyses of the DEGs.

compared with other clinicopathological factors such as age and stage (Table 1). A nomogram based on the multivariate analysis ($P < 0.05$) of the OS of patients with LUAD from TCGA was used to show the prediction (Figure 3(c)). Great calibration plots were shown for the 1-, 3-, and 5-year OS rates of patients with LUAD (Figure 3(d)). The corresponding C-index showed that the combination of the score model, age, and stage performed remarkably (Table 2).

The results of immunohistochemistry further demonstrated the functions of genes. The overexpression of PSMB6, HSPA9, DUT, CDK7, and PLK1 was seen in resected tumor tissues compared with adjacent normal tissues, while FOLR2 was expressed more in normal tissues (Figure 6(d)). One hundred patients from the institution were divided into high and low expression groups according to the expression of the six genes. Patients with high expression of PSMB6, HSPA9, DUT, CDK7, and PLK1 had a significantly poorer OS (P value < 0.0001, Figure 6(e)), while patients with high expression of FOLR2 showed the opposite result.

GEO samples were obtained to verify the score model. Furthermore, 930 patients with LUAD from GEO were also classified into high and low score groups; the survival analysis showed a significant difference in OS between the two groups (P value < 0.0001, Figure 3(b)), which was consistent with the data from TCGA.

3.4. Somatic Mutation, DEGs, and Differentially Expressed microRNA (miRNA) in the Two Groups. As reported before, the number of somatic mutations had relationships with survival. The distribution of somatic genomic mutations and the copy numbers' variation in the high and low score groups were analyzed. The average somatic mutation numbers of each sample in high and low score groups were 95.88 and 87.89, respectively (Figure 4(a)). TP53 was highly mutated in the high score group (65% in the high score group, 39% in the low score group, P value < 0.001). Other genes, such as EGFR (15% in the low score group, 7% in the high score group, P value = 0.013), had lower mutation rates in the high score group (Figure 4(a) and Table S5).
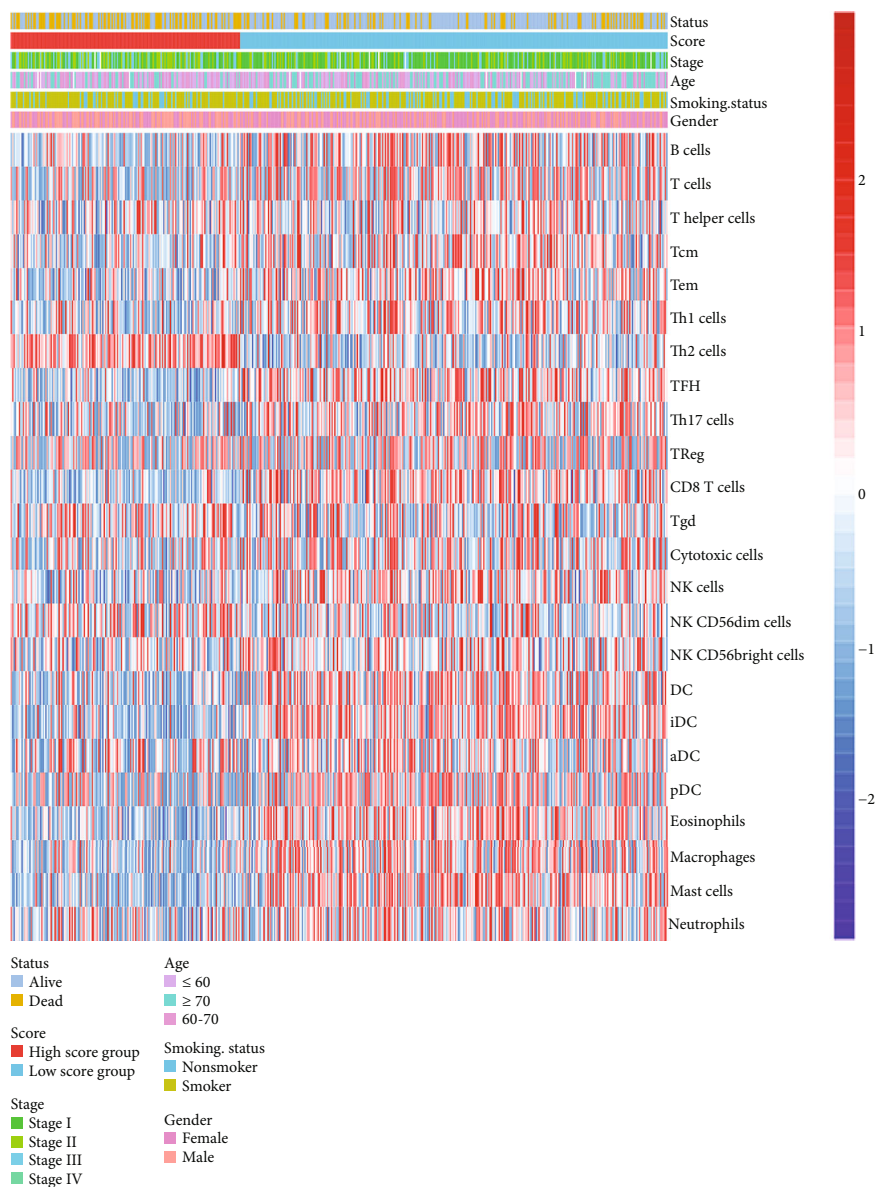
(a)

Figure 5: Continued.
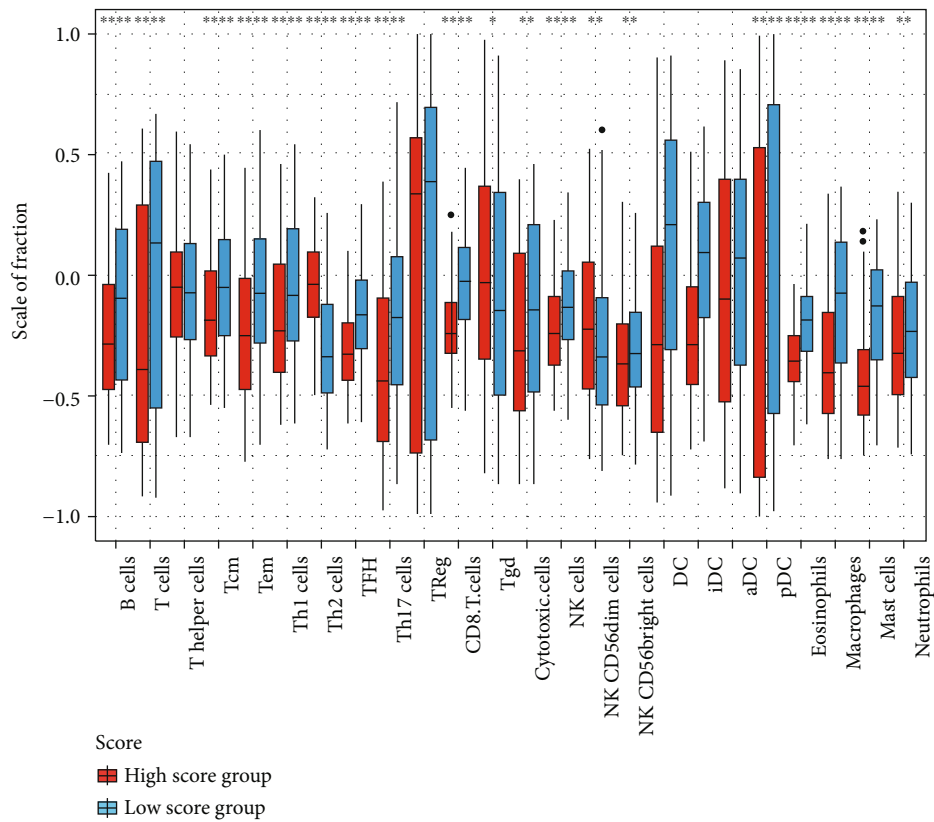
(b)

FIGURE 5: Continued.

(c)
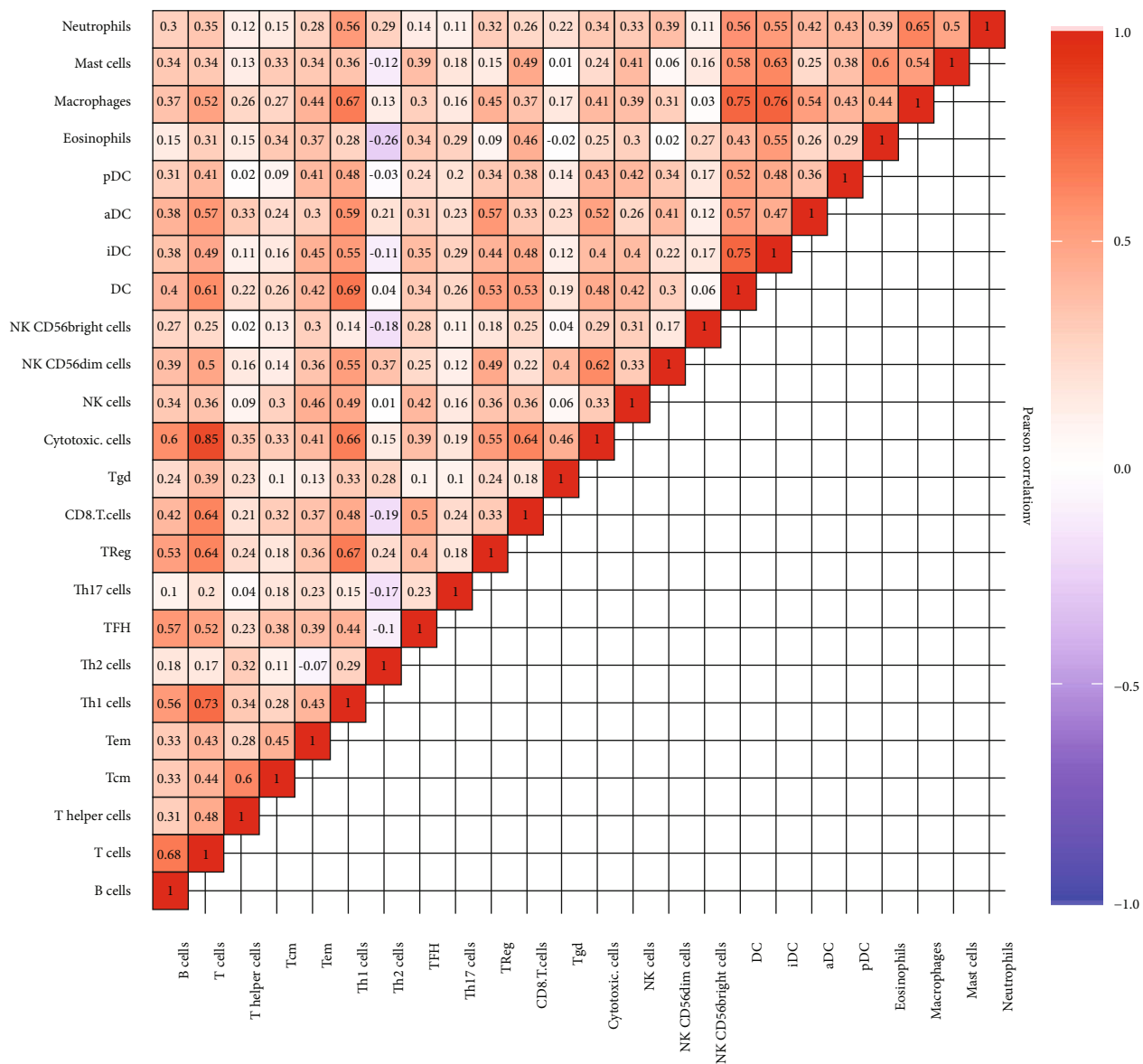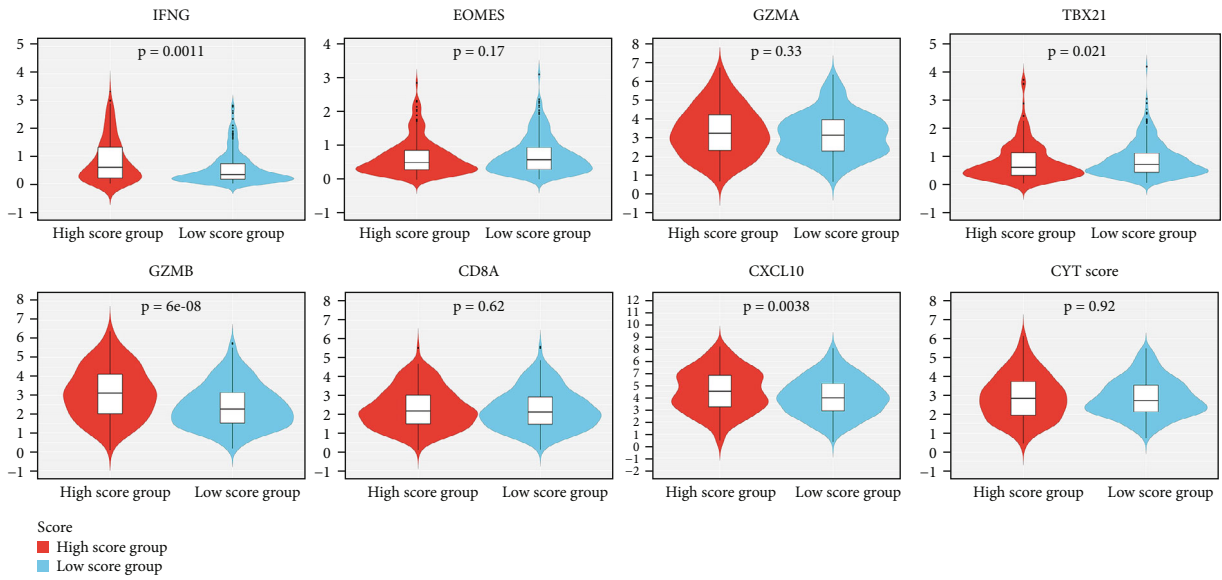
FIGURE 5: Continued.

(d)
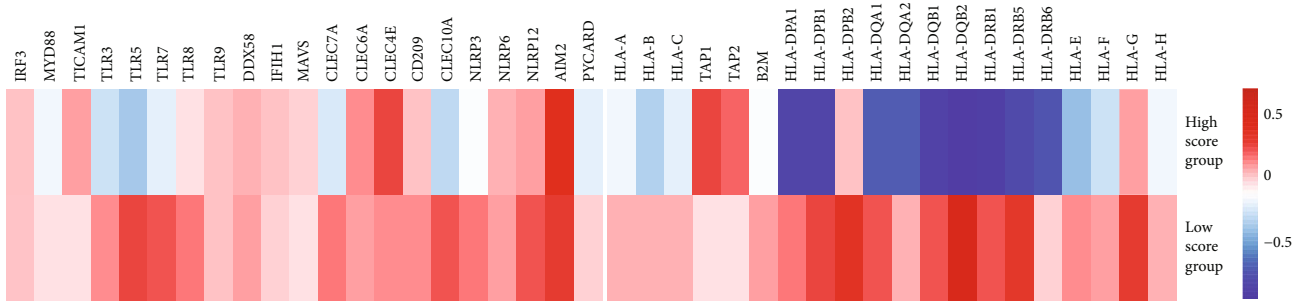
(e)
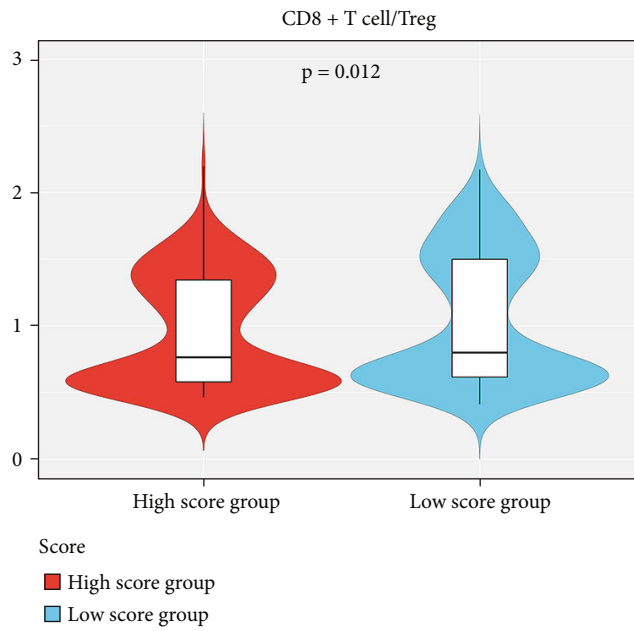
(f)

Figure 5: Continued.

(g)
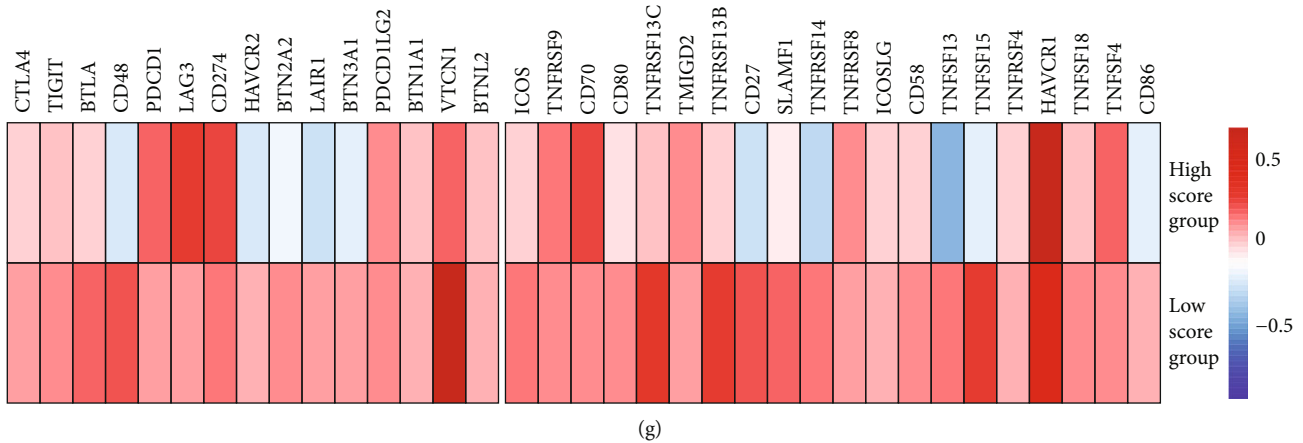
FIGURE 5: TME characteristics of the two groups. (a) Infiltration patterns of immune cells for 497 LUAD patients from TCGA. Clinical and pathological features contain age, gender, stage, smoking status, and score groups. (b) The proportion of immune cells in the two groups. The scattered dots show the immune cells' score. The median, third, and first quartile values are shown in the boxplots. $^*P < 0.05$; $^{**}P < 0.01$; $^{***}P < 0.001$; $^{****}P < 0.0001$. (c) Relationships between the 24 immune cells in LUAD patients from TCGA. (d) Violin plots show the expression profiling of the f7 immune-related genes in the POPLAR study and cytolytic activity (CYT) score. (e) Relative expression level of molecules associated with the innate immune activity (shown at left) and MHC-I/II antigen-presenting process (shown at right). (f) Violin plots displaying the CD8+ T cells/Treg ratio of the infiltration groups. (g) Relative expression level of immune coinhibitors (shown at left) and costimulators (shown at right).

The expression of DEGs was analyzed to draw the landscape of the difference in biological characteristics between the two groups. In total, 4,863 genes, including GPR116, TMPRSS2, and CYR2, were upregulated (all adjusted $P < 0.01$) while 5,001 were downregulated in the high score group, including CCNB1, PLK1, and PRC1 (Figure 4(b), Table S6). Functional enrichment of GO and KEGG in the 9864 DEGs was analyzed, and the pathways were related to the high score group. The antigen processing and presentation and positive regulation of the immune effector process corresponded to the high score group (Figures 4(c) and 4(d)). Several classic metabolic pathways ranked top in the low score group.

Also, the miRNA expression and distribution of somatic mutations were analyzed. In conclusion, 75 miRNAs, including miR-99a-5p, miR-497-5p, and miR-29c-3p, were upregulated (all adjusted $P < 0.01$), and 63 were downregulated in the high score group, including miR-106b-5p and miR-128-1-5p (Fig. S1C and Table S7).

3.5. TME Infiltration Characteristics in the Two Groups. Based on the high scores and low scores of 497 patients from TCGA, the infiltration patterns of each patient in 24 immune cell populations associated with innate immune and adaptive immune processes were determined.

The results showed high infiltration of T cells ($P = 1.26E^{-06}$), Th1.cells ($P = 1.62E^{-05}$), cytotoxic cells ($P = 0.001491$), and pDC cells ($P = 3.54E^{-07}$), except for Th2.cells ($4.45E^{-26}$), which exhibited low infiltration in the low score group (Figures 5(a) and 5(b)). The Wilcoxon test was used to verify the different infiltration patterns (Table S8). The nearly comprehensively positive relativity among the enrichment level of 24 microenvironment cell populations can be seen in Figure 5(c), which was related to the coinfiltration effect.

The TME characteristics in the high and low score groups were described by conducting a full analysis of the expression level of several genes and cytokines associated with immunity from the data of 497 patients with LUAD. A seven-gene panel designed in the POPLAR trial was chosen as a substitute indicator to quantify the cytotoxicity related to IFN-γ (IFNG, EOMES, GZMA, TBX21, and GZMB) and effector T cells (CD8A and CXCL10) [36]. Then, the score was examined according to the score of cytolytic activity reported previously [38], representing the geometric meaning of GZMA and PRF1, to reflect the importance of the antitumor response (Figure 5(d)). The high score group had higher expression levels of GZMA, IFNG, GZMB, CD8A, and CXCL10. (most $P < 0.05$), demonstrating that these patients had a more efficient cytotoxic function. As for the molecules, the low score group showed more activity of the innate immune response. TLR9, AIM2, and NLRP6 showed similar tendencies (Figure 5(e), left). Furthermore, compared with the high score group, the low score group had an enriched abundance of MHC-I/MHC-II-related antigen-presenting molecules(most $P < 0.001$; Figure 5(e), right).

The low score group had enrichment with active innate and adaptive immune cells and immunosuppressor cells such as Tregs and iDCs (Figures 5(a) and 5(c)). Based on this result, the CD8+ T cell/Treg cell ratio was used to estimate the importance of activated and suppressed immunity (Figure 5(f)). The low score group had a higher ratio, which meant that the TME in the low score group was more activated. To verify the result, the expression of several immunoregulators in the two groups was revealed, which included checkpoint molecules ($n = 15$) (Figure 5(g), left) and costimulating molecules ($n = 20$) (Figure 5(g), right). The heat map showed that more costimulating molecules and coinhibitory molecules were expressed in the low score

(a)

(b)
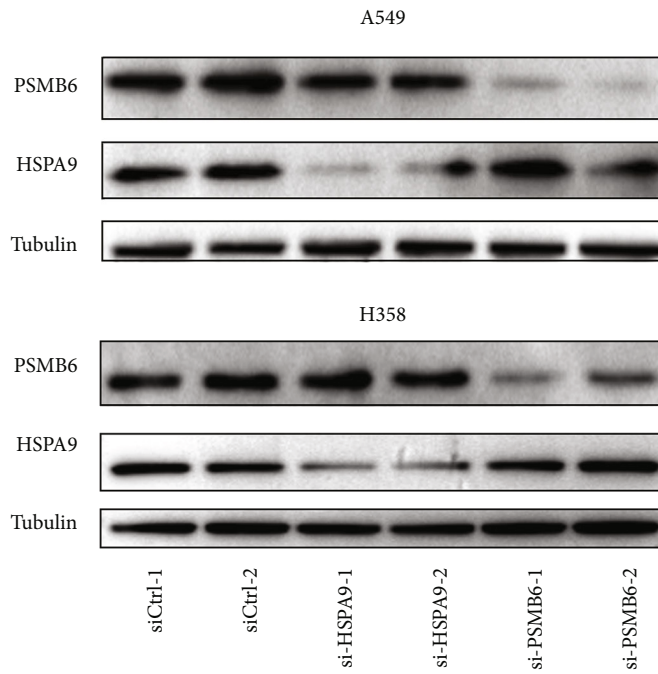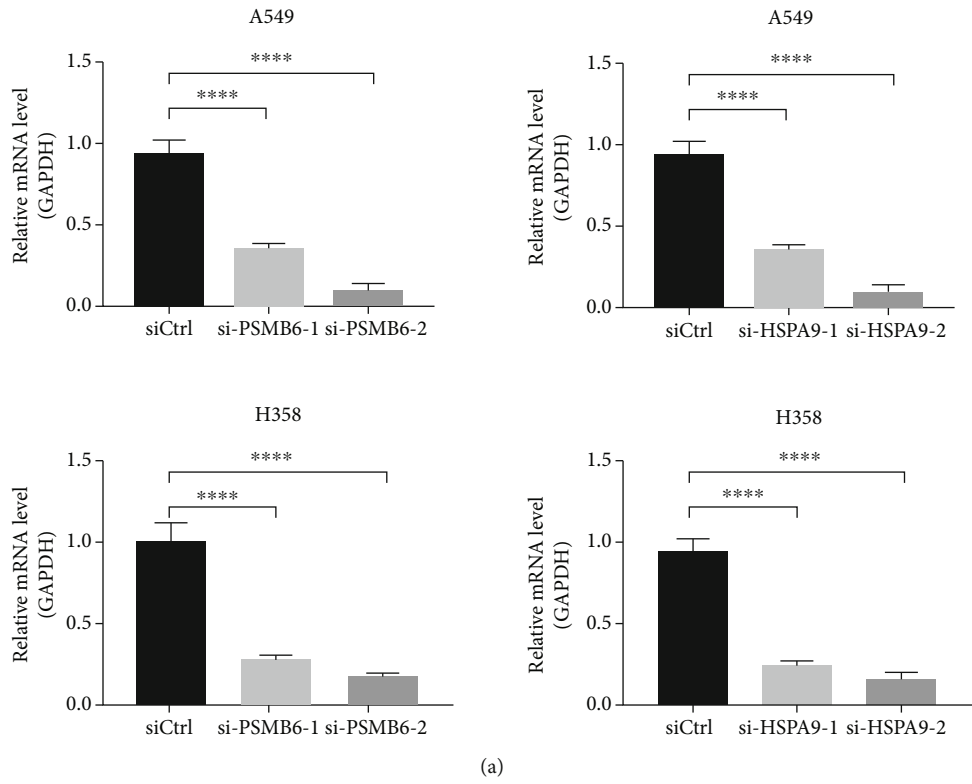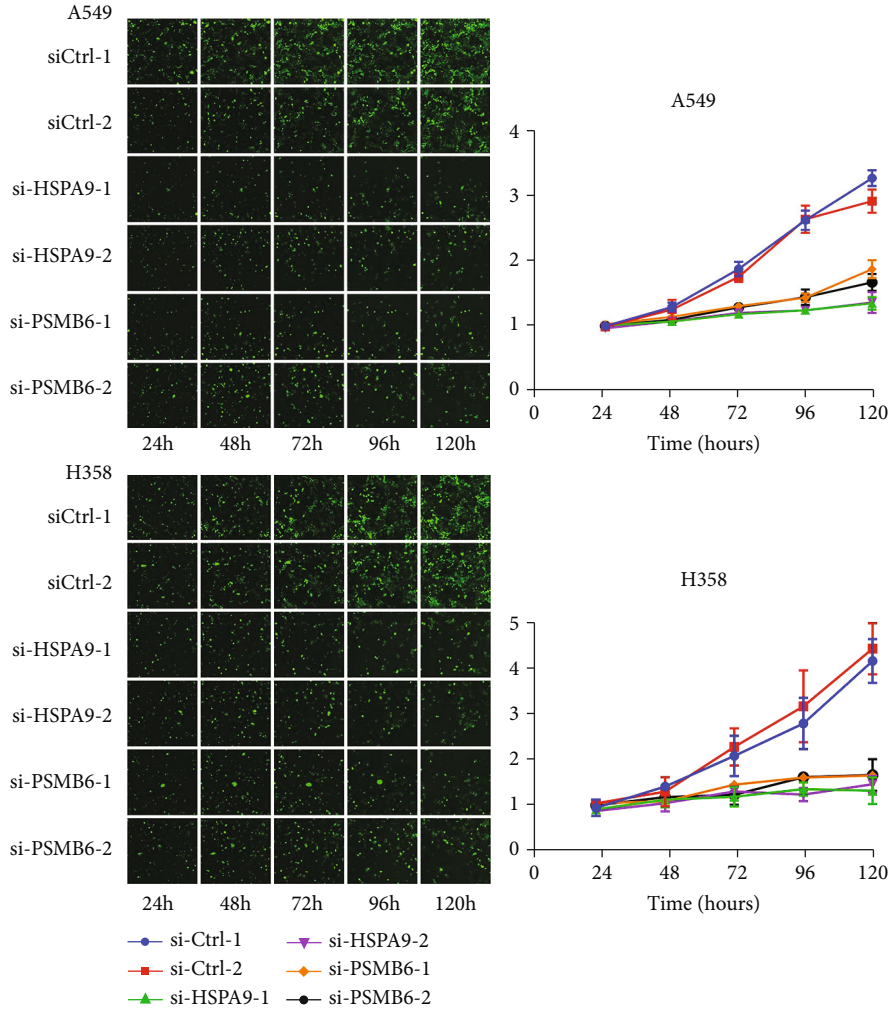
Figure 6: Continued.

(c)

Figure 6: Continued.
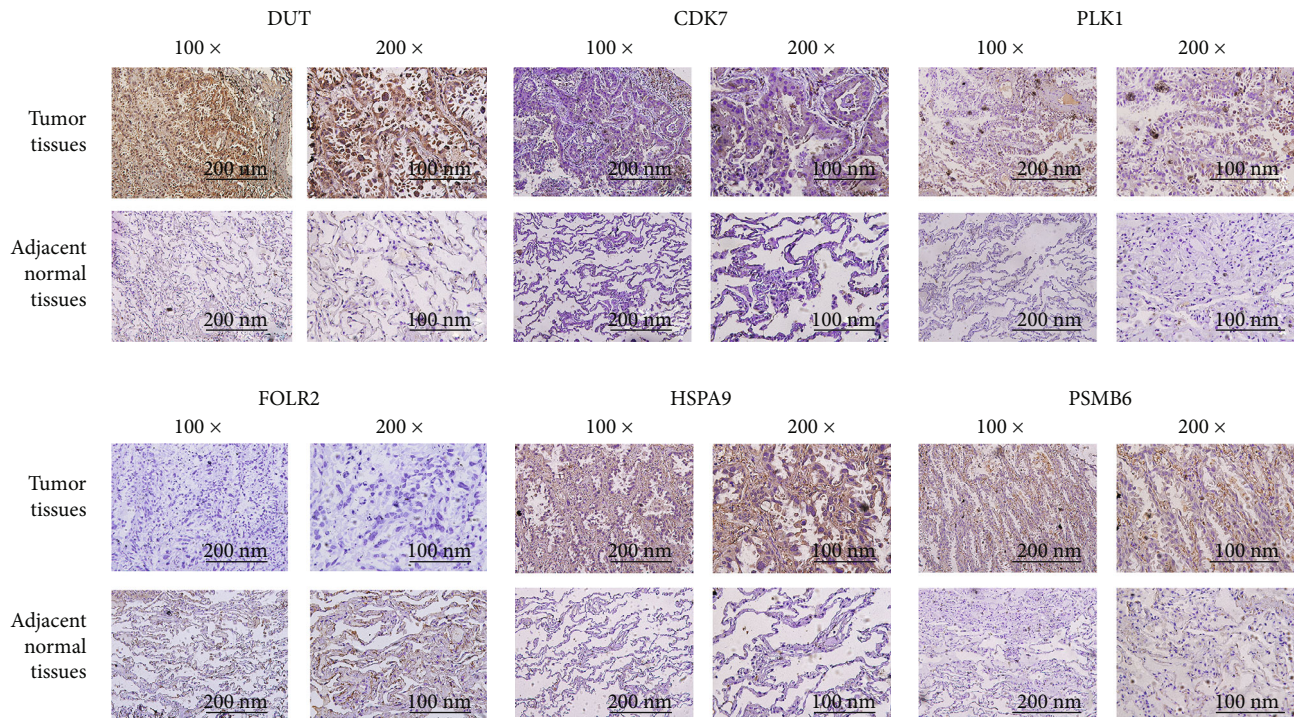
(d)

FIGURE 6: Continued.

(e)
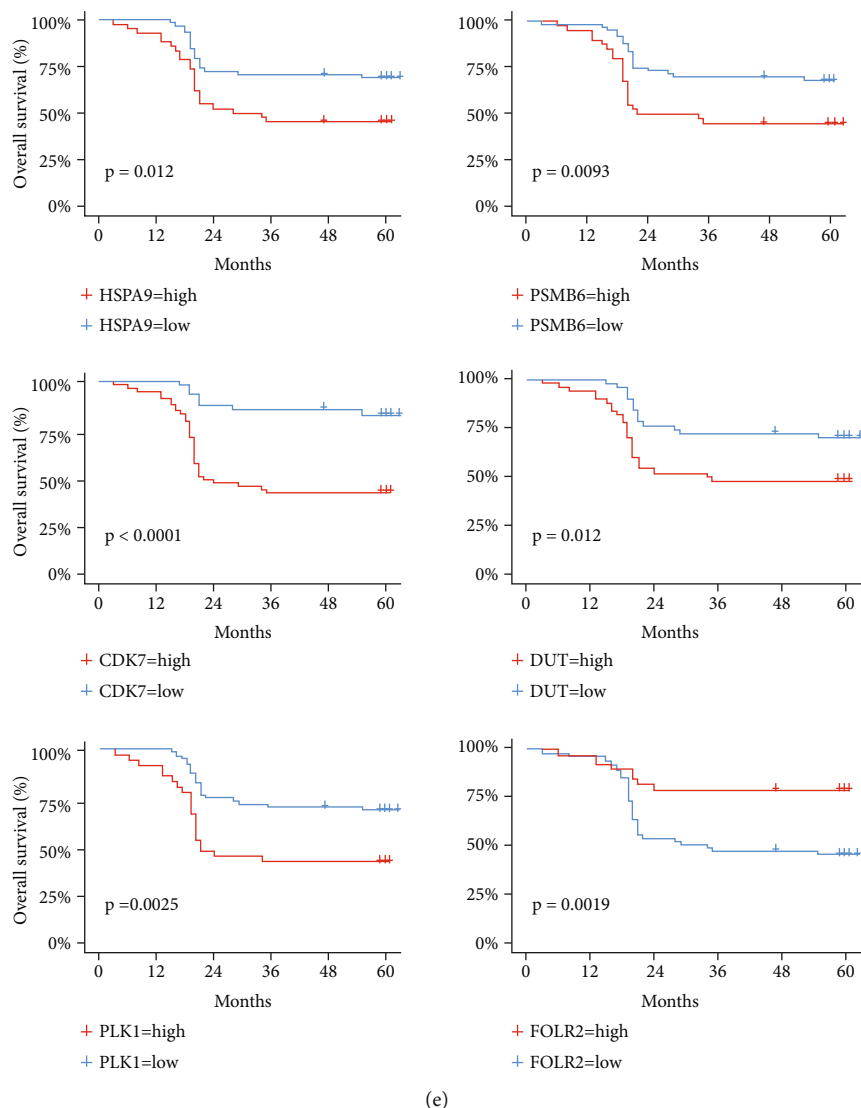
FIGURE 6: (a, b) Quantitative RT-PCR (a) and western blotting analyses (b) verifying the PSMB6 and HSPA9 knockdown efficiency in A549 and H358 cells. (c) The effects of PSMB6 and HSPA9 knockdown on cell proliferation in A549 and H1299 cells. ****$P < 0.0001$. (d) Representative IHC staining images indicating the expression of the six genes in lung adenocarcinoma and adjacent normal tissues. (e) Kaplan-Meier curves of overall survival according to immunohistochemical staining of the six genes in patients from our institution.

group (most $P < 0.05$). Based on the result, it was concluded that patients in the low score group might benefit from immune checkpoint inhibitors (ICI).

3.6. Silencing of PSMB6 and HSPA9 Inhibited the Proliferation of LUAD Cells. According to the CERES dependency score from DEPMAP, the perturbation of PSMB6 and HSPA9 by knockout in different LUAD cell lines inhibited proliferation. To validate the result and explore the function of PSMB6 and HSPA9 in tumor formation and growth, siRNAs targeting PSMB6 and two siRNAs targeting HSPA9 each were transfected into two LUAD cell lines (A549 and H358). Two different siRNAs targeting each gene were used to attenuate the off-target effects. The stable knockdown efficiencies of siRNAs were verified by comparing them with those in the control cells at both mRNA and protein levels (Figures 6(a) and 6(b)). The results of cell counting demonstrated that the proliferation ability of A549 and H358 cell lines after PSMB6 and HSPA9 knockdown significantly decreased compared with that in the control cells (Figure 6(c)).

4. Discussion

In this study, six genes were identified via comprehensive analysis, including PSMB6, HSPA9, DUT, CDK7, PLK1, and FOLR2, which were significantly related to cell proliferation, to construct a risk prediction score model used as an independent predictor. The prediction score model based on these six genes predicted the prognosis of patients with LUAD accurately in the testing cohort from TCGA and the verifying cohorts from GEO. Based on previous findings, it was concluded that silencing the least reported genes

PSMB6 and HSPA9 inhibited cell proliferation *in vitro*, consistent with the results of DEPMAP.

The DEPMAP was created to systematically identify genetic alterations of cancer and their influence by collecting genetic information of hundreds of cancer cell line models [12]. Project Achilles provided the foundation for DEPMAP, which systematically identified and cataloged the essentiality of genes across hundreds of genomically characterized cancer cell lines. Lentiviral-based pooled RNAi or CRISPR/Cas9 libraries were used as highly standardized genome-scale pooled loss-of-function screening, which guaranteed the stable suppression of individual genes. Computational models such as DEMETER [39] for RNAi screening and CERES [13] for CRISPR screening were adopted to determine gene essentiality more accurately. Recently, Szalai et al. [40] explored the mechanisms behind cell death and confounding factors of transcriptomic perturbation screens based on Project Achilles of the DEPMAP. Also, Zhou et al. [41] used the CERES score to identify the prognostic values of solute carrier (SLC) family genes for patients with LUAD. Other studies related to oncology drug discovery were dependent on the DEPMAP [11, 12].

In this study, the six genes used to build the predicted model strongly correlated with cell proliferation and survival of patients with LUAD. As previously reported, high levels of CDK7 mRNA and protein and overexpression of PLK1 were related to poor prognosis in NSCLC [42, 43]. The CDK7 and PLK1 inhibitors played a critical role in immunotherapies for lung cancer [44, 45]. PSMB6 regulated proteasome structure and function, variations in which affected the treatment of multiple myeloma [46]. Shi et al. [47] demonstrated that PSMB6 played a more important role in the proteasome structure than in functional activity. The mitochondrial HSP70 chaperone mortalin (HSPA9/GRP75) was often upregulated in MEK/ERK-deregulated tumors [48]. Wu et al. [49] demonstrated that the depletion effect of HSPA9 was sensitized by KRAS activity, suggesting that HSPA9 was a potential target for KRAS-mutated tumors.

The "cold tumor" in the high score group had a low level of infiltration. In contrast, the low score group was enriched in cytotoxic T cells (as immune activation) and Tregs and others (as immune suppression). As for immunomodulators, the high score group had a relatively low level while the low score group was abundant in immune-related cytokines or markers reported earlier [36, 38, 50, 51]. As showed earlier [38, 52], preexisting immunity, defined by the presence or absence of CD8+ T effector cells, can be used to discriminate immunotherapy-sensitive versus insensitive patients. In summary, we speculated that patients in the low score group could reap more benefits from ICI, and restoring preexisting immunity was crucial to a higher response rate. However, we fail to reveal the relationship between the mutation load and the cytotoxic factors. The low score group had a lower level of genomic mutation but higher immune infiltration comparing with the high score group. As reported before, mutational burden of the tumor may affect the ICI efficiency by enhancing tumor immunogenicity [53, 54].

This study had several limitations. First, although hundreds of samples from the GEO database and the institution were used as validation cohorts, more patients in prospective cohorts are still needed to verify the proposed risk prediction model. Also, the identification of immune subtypes in clinical samples was required to be performed to validate the function of immune cells in the training cohort. Besides, the roles of these genes and the molecular mechanisms in the tumorigenesis of LUAD could not be further explored due to the limitations on research funds and time in the present study. Future research should explore the interaction relationship between the relevant genes in the model and the pathways involved and downstream signaling factors.

In summary, the CERES score of genes from DEPMAP was used to identify six genes with a combination strategy and build a risk prediction score model that could effectively predict the survival of patients with LUAD from TCGA, GEO, and the institution. The study demonstrated that the genes in the prediction model were significantly related to cell proliferation *in vitro*. Moreover, the study described a comprehensive landscape of the regulator factors, signaling pathways, and immune infiltration patterns behind the model, which might help identify the high-risk patients and interfere with individualized treatment early.

Data Availability

All datasets were adopted in this study are available in the TCGA (http://portal.gdc.cancer.gov/), GEO (http://www.ncbi.nlm.nih.gov/geo/), and DEPMAP (https://depmap.org/).

Ethical Approval

All methods were carried out in accordance with relevant guidelines and regulations. All participants signed informed consent according to the ethical requirements in the Declaration of Helsinki. Ethics approved by the ethical committees of Zhongshan Hospital (B2019-035).

Consent

No consent was necessary.

Disclosure

The same title was presented in "ASCVTS 2021 ON-LINE CONFERENCE" according to the following link: "https://ascvts2021.org/program_0605_2021.php" [55].

Conflicts of Interest

The authors declare that they have no conflict of interests.

Authors' Contributions

Yunyi Bian, Qihai Sui, Guoshu Bi, Yi Zhang, and Hong Fan contributed to the conceptualization. Yunyi Bian, Guoshu Bi, and Qihai Sui contributed to the methodology. Yunyi Bian, Guoshu Bi, and Qihai Sui contributed to the software. Yunyi Bian, Guoshu Bi, and Qihai Su contributed to the validation.

Guoshu Bi and Yuansheng Zhen contributed to the formal analysis. Guangyu Yao and Liang Xue contributed to the investigation. Mengnan Zhao contributed to the resources. Yunyi Bian, Guoshu Bi, and Qihai Sui contributed to the data curation. Yunyi Bian and Guoshu Bi contributed to the writing—original draft preparation. Yunyi Bian and Qihai Sui contributed to the writing—review and editing. Yunyi Bian, Guoshu Bi, and Qihai Sui contributed to the visualization. Yi Zhang and Hong Fan contributed to the supervision. Yi Zhang and Hong Fan contributed to the project administration. All authors have read and agreed to the published version of the manuscript. Bian Yunyi, Qihai Sui, and Guoshu Bi contributed equally to this work.

Acknowledgments

Supplementary Materials

Supplementary 1. Additional file 1 score: the score was used in the risk-predicted model to calculate the score of patients with LUAD.

Supplementary 2. Table S1: the table showed genes associated with microenvironment of the 24 immune cell subsets. Table S2: the table showed the sequences of all the siRNAs and primers used in this study. Table S3: the table showed 55 genes selected for LASSO Cox regression; all the 55 genes showed the same tendency in cell proliferation (the CERES dependency score) and survival (HR). Table S4: the table showed six genes used in the model and their LASSO coefficient after LASSO Cox regression. Table S5: the table showed the summary of genomic alterations in the two groups, including the somatic mutation numbers of each gene in high and low score groups. Table S6: the table showed the differentially expressed genes (DEGs) between high score group and low score group identified by limma. Table S7: the table showed the differentially expressed miRNAs between high score group and low score group identified by limma. Table S8: the table showed the comparison the abundance of 24 types of immune cells between the two groups by Wilcoxon test.

Supplementary 3. Figure S1 (A–C) (A) The scatter dot plots show the relationships of expression values between the six genes we selected in the score models. (B) The correlation between clinical characteristics (sex, age, stage, and smoking) and gene expression. The scattered dots show the immune cells' score. The median, third, and first quartile values are shown in the boxplots. $*P < 0.05$; $**P < 0.01$; $***P < 0.001$; $****P < 0.0001$. (C) The volcano plot displays the differentially expressed miRNAs of the two groups.

References

[1] H. Sung, J. Ferlay, R. L. Siegel et al., "Global Cancer Statistics 2020: GLOBOCAN estimates of incidence and mortality worldwide for 36 cancers in 185 countries," *CA: a Cancer Journal for Clinicians*, vol. 71, no. 3, pp. 209–249, 2021.

[2] K. D. Miller, L. Nogueira, A. B. Mariotto et al., "Cancer treatment and survivorship statistics, 2019," *CA: a Cancer Journal for Clinicians*, vol. 69, pp. 363–385, 2019.

[3] T. Lu, X. Yang, Y. Huang et al., "Trends in the incidence, treatment, and survival of patients with lung cancer in the last four decades," *Cancer Management and Research*, vol. 11, pp. 943–953, 2019.

[4] L. Crino, W. Weder, J. van Meerbeeck, and E. Felip, "Early stage and locally advanced (non-metastatic) non-small-cell lung cancer: ESMO Clinical Practice Guidelines for diagnosis, treatment and follow-up," *Annals of Oncology*, vol. 21, no. 5, pp. v103-v115, 2010.

[5] Y. Yan, W. Su, S. Zeng et al., "Effect and mechanism of tanshinone I on the radiosensitivity of lung cancer cells," *Molecular Pharmaceutics*, vol. 15, no. 11, pp. 4843–4853.

[6] M. W. Libbrecht and W. S. Noble, "Machine learning applications in genetics and genomics," *Nature Reviews. Genetics*, vol. 16, pp. 321–332, 2015.

[7] J. Z. Xu, C. Gong, Z. F. Xie, and H. Zhao, "Development of an Oncogenic Driver Alteration Associated Immune-Related Prognostic Model for Stage I-II Lung Adenocarcinoma," *Frontiers in Oncology*, vol. 10, 2020.

[8] X. Yang, Y. Shi, M. Li et al., "Identification and validation of an immune cell infiltrating score predicting survival in patients with lung adenocarcinoma," *Journal of translational medicine*, vol. 17, p. 217, 2019.

[9] X. Shi, H. Tan, X. Le et al., "An expression signature model to predict lung adenocarcinoma-specific survival," *Cancer Management and Research*, vol. 10, pp. 3717–3732, 2018.

[10] K. Han, S. E. Pierce, A. Li et al., "CRISPR screens in cancer spheroids identify 3D growth-specific vulnerabilities," *Nature*, vol. 580, pp. 136–141, 2020.

[11] F. Vazquez and J. S. Boehm, "The Cancer Dependency Map enables drug mechanism-of-action investigations," *Molecular Systems Biology*, vol. 16, article e9757, 2020.

[12] L. Dwane, F. M. Behan, E. Goncalves et al., "Project Score database: a resource for investigating cancer cell dependencies and prioritizing therapeutic targets," *Nucleic Acids Research*, vol. 49, pp. D1365–D1372, 2021.

[13] R. M. Meyers, J. G. Bryan, M. F. JM et al., "Computational correction of copy number effect improves specificity of CRISPR-Cas9 essentiality screens in cancer cells," *Nature Genetics*, vol. 49, pp. 1779–1784, 2017.

[14] S. Rousseaux, A. Debernardi, B. Jacquiau et al., "Ectopic activation of germline and placental genes identifies aggressive metastasis-prone lung cancers," *Science translational medicine*, vol. 5, pp. 166r–186r, 2013.

[15] H. Okayama, T. Kohno, Y. Ishii et al., "Identification of genes upregulated in ALK-positive and EGFR/KRAS/ALK-negative lung adenocarcinomas," *Cancer Research*, vol. 72, pp. 100–111, 2012.

[16] M. Yamauchi, R. Yamaguchi, A. Nakata et al., "Epidermal growth factor receptor tyrosine kinase defines critical prognostic genes of stage I lung adenocarcinoma," *PLoS One*, vol. 7, article e43923, 2012.

[17] A. H. Bild, G. Yao, J. T. Chang et al., "Oncogenic pathway signatures in human cancers as a guide to targeted therapies," *Nature*, vol. 439, pp. 353–357, 2006.

[18] J. Botling, K. Edlund, M. Lohr et al., "Biomarker discovery in non-small cell lung cancer: integrating gene expression profiling, meta-analysis, and tissue microarray validation," *Clinical Cancer Research*, vol. 19, pp. 194–204, 2013.

[19] V. Jabs, K. Edlund, H. Konig et al., "Integrative analysis of genome-wide gene copy number changes and gene expression in non-small cell lung cancer," *PLoS One*, vol. 12, article e187246, 2017.

[20] M. Lohr, B. Hellwig, K. Edlund et al., "Identification of sample annotation errors in gene expression datasets," *Archives of Toxicology*, vol. 89, pp. 2265–2272, 2015.

[21] T. Goldmann, S. Marwitz, D. Nitschkowski et al., "PD-L1 amplification is associated with an immune cell rich phenotype in squamous cell cancer of the lung," *Cancer Immunology, Immunotherapy*, vol. 70, pp. 2577–2587, 2021.

[22] S. D. Der, J. Sykes, M. Pintilie et al., "Validation of a histology-independent prognostic gene signature for early-stage, non-small-cell lung cancer including stage IA patients," *Journal of Thoracic Oncology*, vol. 9, pp. 59–64, 2014.

[23] K. Shedden, J. M. Taylor, S. A. Enkemann et al., "Gene expression-based survival prediction in lung adenocarcinoma: a multi-site, blinded validation study," *Nature medicine*, vol. 14, pp. 822–827, 2008.

[24] W. E. Johnson, C. Li, and A. Rabinovic, "Adjusting batch effects in microarray expression data using empirical Bayes methods," *Biostatistics*, vol. 8, pp. 118–127, 2007.

[25] M. E. Ritchie, B. Phipson, D. I. Wu et al., "limma powers differential expression analyses for RNA-sequencing and microarray studies," *Nucleic acids research*, vol. 43, no. 7, pp. e47–e47, 2015.

[26] G. Yu, L. Wang, Y. Han, and Q. He, "clusterProfiler: an R package for comparing biological themes among gene clusters," *Omics : a journal of integrative biology*, vol. 16, pp. 284–287, 2012.

[27] R. Tibshirani, "Regression shrinkage and selection via the LASSO," *Journal of the Royal Statistical Society: Series B (Statistical Methodology)*, vol. 73, pp. 273–282, 1996.

[28] M. M. Vasquez, C. Hu, D. J. Roe, Z. Chen, M. Halonen, and S. Guerra, "Least absolute shrinkage and selection operator type methods for the identification of serum biomarkers of overweight and obesity: simulation and application," *BMC medical research methodology*, vol. 16, p. 154, 2016.

[29] R. Tibshirani, "The LASSO method for variable selection in the Cox model," *Statistics in medicine*, vol. 16, pp. 385–395, 1997.

[30] F. E. Harrell, "Evaluating the Yield of Medical Tests," *Jama*, 1982.

[31] K. Kato, B. C. Cho, M. Takahashi et al., "Nivolumab versus chemotherapy in patients with advanced oesophageal squamous cell carcinoma refractory or intolerant to previous chemotherapy (ATTRACTION-3): a multicentre, randomised, open-label, phase 3 trial," *The Lancet Oncology*, vol. 20, pp. 1506–1517, 2019.

[32] G. Bindea, B. Mlecnik, M. Tosolini et al., "Spatiotemporal dynamics of intratumoral immune cells reveal the immune landscape in human cancer," *Immunity*, vol. 39, pp. 782–795, 2013.

[33] G. Bi, Z. Chen, X. Yang et al., "Identification and validation of tumor environment phenotypes in lung adenocarcinoma by integrative genome-scale analysis," *Cancer Immunology, Immunotherapy*, vol. 69, pp. 1293–1305, 2020.

[34] Y. Bian, G. Bi, T. Wei et al., "Integrative genome-scale analysis of immune infiltration in esophageal carcinoma," *International Immunopharmacology*, vol. 93, p. 107371, 2021.

[35] K. Kato, B. C. Cho, M. Takahashi et al., "Atezolizumab versus docetaxel for patients with previously treated non-small-cell lung cancer (POPLAR): a multicentre, open-label, phase 2 randomised controlled trial," *Lancet (London, England)*, vol. 387, pp. 1837–1846, 2016.

[36] M. S. Rooney, S. A. Shukla, C. J. Wu, G. Getz, and N. Hacohen, "Molecular and genetic properties of tumors associated with local immune cytolytic activity," *Cell*, vol. 160, pp. 48–61, 2015.

[37] H. Niu, Y. Huang, L. Yan et al., "Knockdown of SMAD3 inhibits the growth and enhances the radiosensitivity of lung adenocarcinoma via p21 in vitro and in vivo," *International journal of biological sciences*, vol. 16, no. 6, p. 1010, 2020.

[38] L. Fehrenbacher, A. Spira, M. Ballinger et al., "Atezolizumab versus docetaxel for patients with previously treated non-small-cell lung cancer (POPLAR): a multicentre, open-label, phase 2 randomised controlled trial," *The Lancet*, vol. 387, pp. 1837–1846, 2016.

[39] A. Tsherniak, F. Vazquez, P. G. Montgomery et al., "Defining a cancer dependency map," *CELL*, vol. 170, pp. 564–576, 2017.

[40] B. Szalai, V. Subramanian, C. H. Holland, R. Alföldi, L. G. Puskás, and J. Saez-Rodriguez, "Signatures of cell death and proliferation in perturbation transcriptomics data-from confounding factor to effective prediction," *Nucleic Acids Research*, vol. 47, pp. 10010–10026, 2019.

[41] H. Zhou, Y. Zhu, H. Qi et al., "Evaluation of the prognostic values of solute carrier (SLC) family 39 genes for patients with lung adenocarcinoma," *Aging*, vol. 12, 2021.

[42] J. Wang, R. Zhang, Z. Lin et al., "CDK7 inhibitor THZ1 enhances antiPD-1 therapy efficacy via the p38α/MYC/PD-L1 signaling in non-small cell lung cancer," *Journal of Hematology & Oncology*, vol. 13, p. 99, 2020.

[43] G. Wolf, R. Elez, A. Doermer et al., "Prognostic significance of polo-like kinase (PLK) expression in non-small cell lung cancer," *Oncogene*, vol. 14, pp. 543–549, 1997.

[44] H. Zhang, C. L. Christensen, R. Dries et al., "CDK7 inhibition potentiates genome instability triggering anti-tumor immunity in small cell lung cancer," *CANCER CELL*, vol. 37, pp. 37–54, 2020.

[45] M. Sebastian, M. Reck, C. F. Waller et al., "The efficacy and safety of BI 2536, a novel Plk-1 inhibitor, in patients with stage IIIB/IV non-small cell lung cancer who had relapsed after, or failed, chemotherapy: results from an open-label, randomized phase II clinical trial," *Journal of Thoracic Oncology*, vol. 5, pp. 1060–1067, 2010.

[46] D. I. Lichter, H. Danaee, M. D. Pickard et al., "Sequence analysis of β-subunit genes of the 20S proteasome in patients with relapsed multiple myeloma treated with bortezomib or dexamethasone," *BLOOD*, vol. 120, pp. 4513–4516, 2012.

[47] C. X. Shi, Y. X. Zhu, L. A. Bruins et al., "Proteasome subunits differentially control myeloma cell viability and proteasome inhibitor sensitivity," *Molecular Cancer Research*, vol. 18, pp. 1453–1464, 2020.

[48] P. K. Wu, S. K. Hong, W. Chen et al., "Mortalin (HSPA9) facilitates BRAF-mutant tumor cell survival by suppressing ANT3-mediated mitochondrial membrane permeability," *Science Signaling*, vol. 13, 2020.

[49] P. K. Wu, S. K. Hong, D. Starenki et al., "Mortalin/HSPA9 targeting selectively induces KRAS tumor cell death by perturbing mitochondrial membrane permeability," *Oncogene*, vol. 39, pp. 4257–4270, 2020.

[50] A. Petretto, G. Carbotti, E. Inglese et al., "Proteomic analysis uncovers common effects of IFN-γ and IL-27 on the HLA class I antigen presentation machinery in human cancer cells," *Oncotarget*, vol. 7, pp. 72518–72536, 2016.

[51] Y. Zhu, M. Li, D. Mu et al., "CD8+/FOXP3+ ratio and PD-L1 expression associated with survival in pT3N0M0 stage esophageal squamous cell cancer. International Journal of Radiation Oncology∗Biology∗Physics," vol. 98, p. 228, 2017.

[52] P. C. Tumeh, C. L. Harview, J. H. Yearley et al., "PD-1 blockade induces responses by inhibiting adaptive immune resistance," *Nature*, vol. 515, pp. 568–571, 2014.

[53] J. Wei, Y. Yan, X. Chen, L. Qian, and Z. Xu, "The roles of plant-derived triptolide on non-small cell lung cancer," *Oncology Research Featuring Preclinical and Clinical Cancer Therapeutics*, vol. 27, 2019.

[54] J. Liang, M. Li, Q. Sui et al., "Compare the efficacy and safety of programmed cell death-1 (PD-1) and programmed cell death ligand-1 (PD-L1) inhibitors for advanced non-small cell lung cancer: a Bayesian analysis," *Translational Lung Cancer Research*, vol. 9, pp. 1302–1323, 2020.

[55] Y. Bian, Q. Sui, G. Bi et al., "Identification and validation of a proliferation-associated score model predicting survival in lung adenocarcinomas," *The 29th Meeting of the Asian Society for Cardiovascular & Thoracic Surgery (ASCVTS)*, 2021.

Research Article

Multiomics Differences in Lung Squamous Cell Carcinoma Patients with High Radiosensitivity Index Compared with Those with Low Radiosensitivity Index

Yajing Du [ID], **Sujuan Yuan, Xibing Zhuang, Qi Zhang, and Tiankui Qiao** [ID]

Center for Tumor Diagnosis and Therapy, Jinshan Hospital, Shanghai 201508, China

Correspondence should be addressed to Tiankui Qiao; qiaotk@163.com

Objectives. Radiosensitivity Index (RSI) can predict intrinsic radiotherapy sensitivity. We analyzed multiomics characteristics in lung squamous cell carcinoma between high and low RSI groups, which may help understand the underlying molecular mechanism of radiosensitivity and guide optional treatment for patients in the future. *Methods*. The Cancer Genome Atlas (TCGA) and the Gene Expression Omnibus (GEO) data were used to download clinical data, mRNA, microRNA, and lncRNA expression. Differential analyses, including mRNA, miRNA, lncRNA, and G.O. and KEGG, and GSVA analyses, were performed with R. Gene set enrichment analysis was done by GSEA. miRNA-differentially expressed gene network and ceRNA network were analyzed and graphed by the Cytoscape software. *Results*. In TCGA data, 542 patients were obtained, including 171 in the low RSI group (LRSI) and 371 in the high RSI group (HRSI). In RNAseq, 558 significantly differentially expressed genes (DEGs) were obtained. KRT6A was the most significantly upregulated gene and IDO1 was the most significantly downregulated gene. In miRNAseq, miR-1269a was the most significantly upregulated. In lncRNAseq, LINC01871 was the most upregulated. A 66-pair interaction between differentially expressed genes and miRNAs and an 11-pair interaction between differential lncRNAs and miRNAs consisted of a ceRNA network, of which miR-184 and miR-490-3p were located in the center. In the GEO data, there were 40 DEGs. A total of 17 genes were founded in both databases, such as ADAM23, AHNAK2, BST2, COL11A1, CXCL13, FBN2, IFI27, IFI44L, MAGEA6, and PTGR1. GSVA analysis revealed 31 significant pathways. GSEA found 87 gene sets enriched in HRSI and 91 gene sets in LRSI. G.O. and KEGG of RNA expression levels revealed that these genes were most enriched in T cell activation and cytokine–cytokine receptor interaction. *Conclusions*. Patients with lung squamous cell carcinoma have different multiomics characteristics between two groups. These differences may have an essential significance with radiotherapy effect.

1. Introduction

Lung cancer, the first killer globally, was estimated at 131,880 deaths in 2021 [1]. Lung squamous cell carcinoma (LUSC) accounts for 20–30% of NSCLCs [2].

Radiotherapy is one of the effective cancer treatments. Radiosensitivity Index (RSI) is a novel model of tumor radiosensitivity. Based on the expression of 10 genes (JUN, STAT1, SUMO1, IRF1, HDAC9, ABL1, CDK1, RELA, PRRT2, and AR), RSI could predict intrinsic radiotherapy sensitivity and treatment response [3]. This model is widely used in cancer, such as breast cancer and NSCLCs [4–6].

Our study analyzed mRNA, miRNA, lncRNA, methylation, somatic mutations, copy number variations, and clinical data between high RSI and low RSI groups in LUSC patients. This research may reference precision radiotherapy research and help build personalized precision management of patients in clinical applications.

2. Material

2.1. TCGA Data. The data were downloaded from The Cancer Genome Atlas (TCGA) data portal (https://portal.gdc.cancer.gov/)(TCGA-LUSC) through https://xenabrowser.
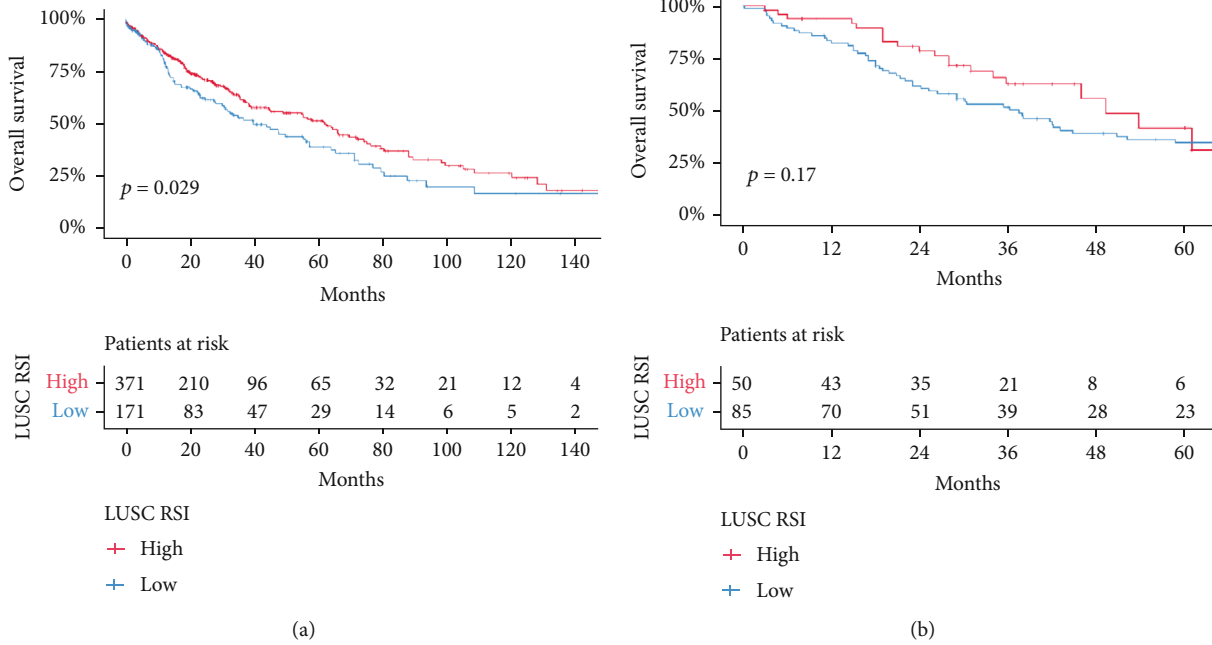
FIGURE 1: (a) Survival analysis of high and low RSI groups in TCGA dataset. (b) Survival analysis of high and low RSI groups in the GEO dataset.

TABLE 1: Clinical characteristics of TCGA samples.

Characteristics	RSI high expression group ($n = 368$)		RSI low expression group ($n = 170$)		p value
Age	67.44		67.08		0.65
Sex					
Female	95	(25.8)	46	(27.1)	0.842
Male	273	(74.2)	124	(72.9)	
Anatomic location					
Bronchial	6	(1.6)	4	(2.4)	0.755
Left	155	(42.1)	68	(40.0)	
Right	197	(53.5)	91	(53.5)	
Other (please specify)	7	(1.9)	3	(1.8)	
NA	2	(0.5)	3	(1.8)	
Discrepancy					
Stage					
Stage I	180	(48.9)	85	(50.0)	0.252
Stage II	125	(34.0)	48	(28.2)	
Stage III	57	(15.5)	31	(18.2)	
Stage IV	5	(1.4)	3	(1.8)	
Discrepancy	1	(0.3)	3	(1.8)	
Histological type					
LUSC	349	(94.8)	165	(97.1)	0.325
Basaloid LUSC	12	(3.3)	4	(2.4)	
Papillary LUSC	6	(1.6)	0	(0.0)	
Small cell LUSC	1	(0.3)	1	(0.6)	

TABLE 2: Clinical characteristics of the GEO samples.

Characteristics	RSI high expression group ($n = 50$)		RSI low expression group ($n = 85$)		p value
Age	61.28		63.66		0.166
Sex					
Female	1	(2.0)	23	(27.1)	0.001
Male	49	(98.0)	62	(72.9)	
Stage					
Stage I	7	(14.0)	36	(42.4)	0.001
Stage I or stage II	14	(28.0)	8	(9.4)	
Stage II	16	(32.0)	20	(23.5)	
Stage III	13	(26.0)	21	(24.7)	

net/datapages/, including mRNA and miRNA expression data, methylation array, mutation profiles, copy number variation, and clinical data [7]. After matching clinical data, 363 cases of mRNA, 542 instances of miRNA, 542 cases of lncRNA, 362 cases of DNA methylation, 480 cases of somatic mutation, and 490 cases of copy number variation were selected for further analysis between the RSI high score group (HRSI) and the low score group (LRSI).

2.2. GEO Data. mRNA data was downloaded from the Gene Expression Omnibus (GEO) database (http://www.ncbi.nlm.nih.gov/geo/).

GSE73403 and GSE37745 datasets were collected for the differential gene expression analysis. GSE73403 dataset contains 69 samples from the LUSC patients, published on Sep

(a)

(b)

(c)
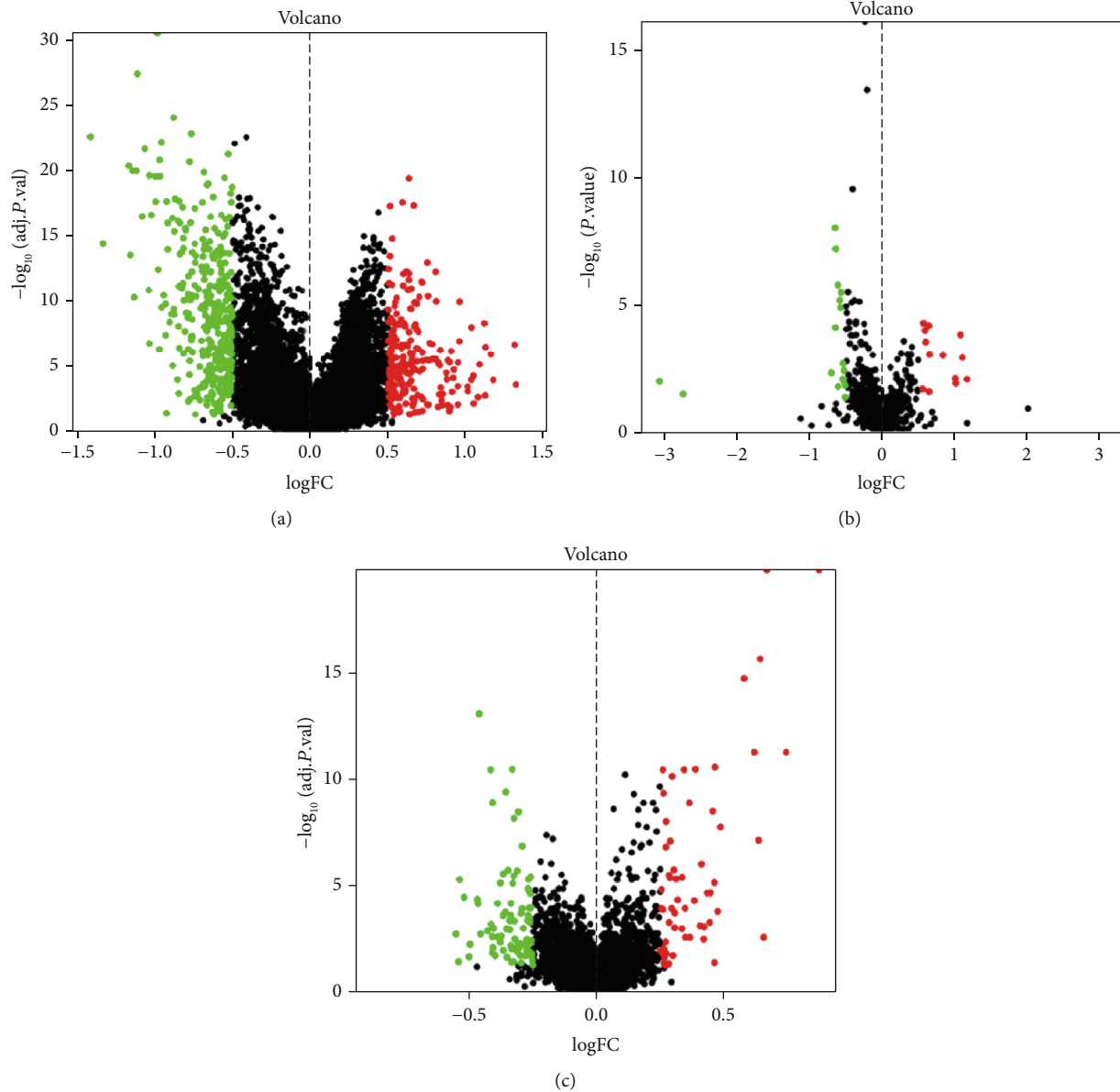
Figure 2: (a) Volcano map of differential expression mRNAs, (b) volcano map of differential expression miRNAs, and (c) volcano map of differential expression lncRNAs.

25, 2015, and GSE37745 includes 66 samples, released on Oct 12, 2012.

3. Statistical Methods

3.1. Statistics of Group. According to previous studies, ten genes (JUN, STAT1, SUMO1, IRF1, HDAC9, ABL1, CDK1, RELA, PRRT2, and AR) were picked out for each sample to calculate RSI (Radiosensitivity Index). The equation is as follows:

$$RSI = -0.0098009 * AR + 0.0128283 * JUN + 0.0254552 \\ * STAT1 - 0.0017589 * PRRT2 - 0.0038171 * RELA + \\ 0.1070213 * ABL1 - 0.0002509 * SUMO1 - 0.0092431 * \\ CDK1 - 0.0204469 * HDAC9 - 0.0441683 * IRF1.$$

The R software (version 4.0.0) was applied to statistical analyses. Cutpoint of RSI was performed by the survminer

package of R with the function of surv_cutpoint, which was design to determine the optimal cutpoint for continuous variables.

3.2. Differential mRNA, miRNAs, lncRNAs, and ceRNA Analysis. In TCGA dataset, after normalization, differential gene analyses, including mRNAseq, miRNAseq, and lncRNAseq, were done by the R limma package. For mRNAseq, the absolute logfoldchange ($|logFC|$) > 0.5 and the adjusted $p < 0.05$ were considered to be significant. For miRNAseq, $|logFC| > 0.5$ and $p < 0.05$ were significant in statistics science. As for lncRNAseq, $|logFC| > 0.25$ and adjusted $p < 0.05$ were statistically significant. For mRNAseq from the GEO dataset, $|logFC| > 0.5$ and the $p < 0.05$ were statistically significant.

Differential lncRNAs targeted miRNAs were achieved through http://mircode.org/index.php.

(a)

(b)

Figure 3: (a) MicroRNAs-differentially expressed gene (miRNA-DEG) pairs. (b) ceRNA network of differential lncRNA-differential miRNA-differentially expressed gene (miRNA-DEG and lncRNA-DEG) pairs.

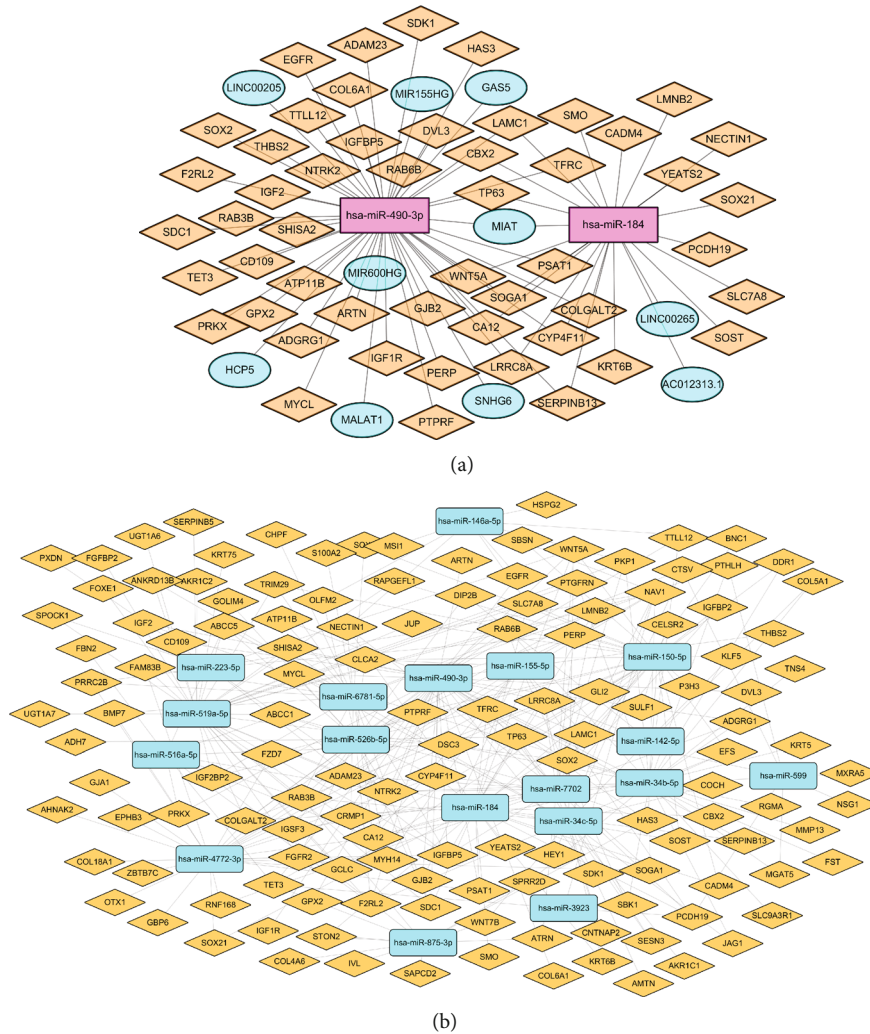Differential miRNAs targeted mRNAs were achieved through http://mirwalk.umm.uni-heidelberg.de/search_mir nas. These data and differential mRNAs were intersected, consisting of a ceRNA network. The Cytoscape software (version 3.7.1) was used to analyze and graph a miRNA-differentially expressed gene network and ceRNA network.

Gene Ontology (G.O.) and Kyoto Encyclopedia of Genes and Genomes (KEGG) were performed by the ClusterProfiler package for the mRNAs, miRNAs, and lncRNAs between HRSI and LRSI patients. Gene set variation analysis was done by the GSVA package. Gene set enrichment (GSEA) was carried out by GSEA (version 4.0.0).

3.3. Copy Number Variation and Somatic Mutation Analysis.
Significantly mutated genes, pfamDomains were done by the maftools package of R. The threshold for significant mutated genes, pfamDomains was $p < 0.05$.

3.4. DNA Methylation Analysis.
Differentially methylated regions, differentially methylated positions, and differentially methylated gene analyses were performed by the minif pack-

age. $p < 0.05$ was considered statistically significant for methylated genes, while adjusted $p < 0.05$ was for methylated regions. In differentially methylated positions, the adjusted $p < 0.05$ was considered to be statistically significant.

Differentially methylated genes and differentially expressed genes were jointly analyzed to find methylation driver genes.

4. Results

4.1. Clinical Characteristics and Survival Analyses.
In TCGA data, based on RSI scores (0.50 tangents), 542 LUSC patients were divided into RSI high grouping (HRSI) and low grouping (LRSI), of which 171 were in LRSI and 371 were in HRSI. The results showed that there was an obvious survival difference between HRSI and LRSI ($p = 0.029$). In two GEO datasets, the cutpoint of RSI was 0.54 and 0.55. We merged two GEO datasets and found the survival of patients with high RSI scores in the GEO database was still better than those with low scores, though not significant ($p = 0.17$) but possibly due to the small number of the patients (50 patients in HRSI vs. 85 patients in LRSI) (Figures 1(a) and 1(b)).

(a)

(b)

FIGURE 4: Continued.

(c)
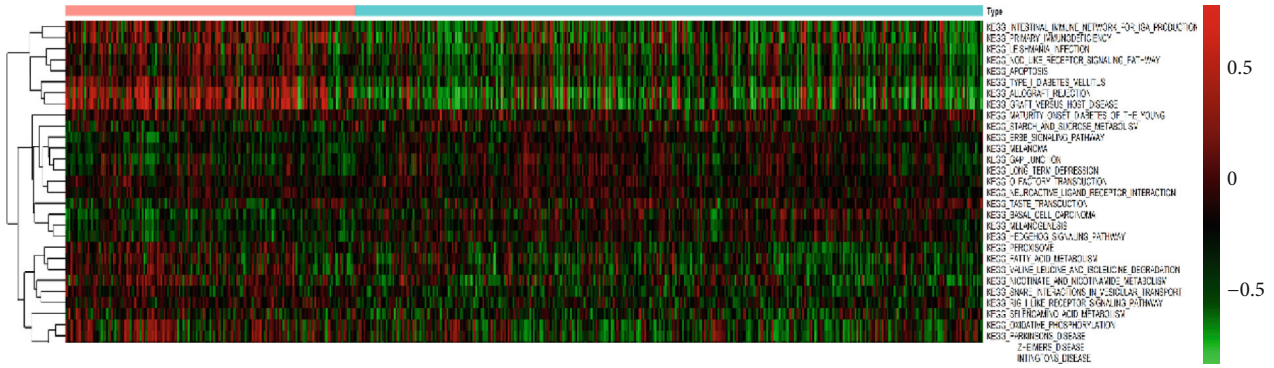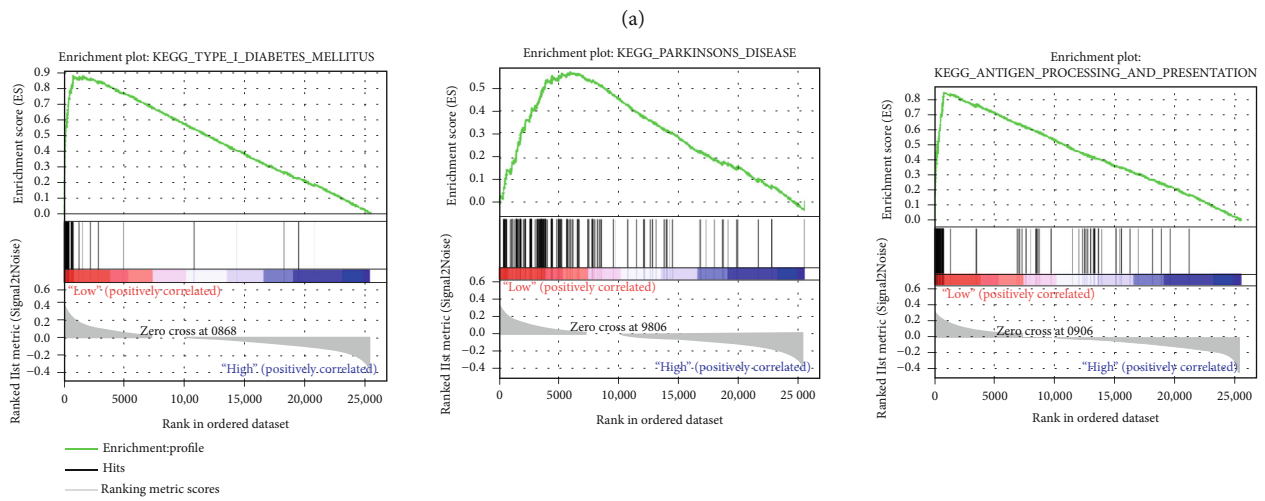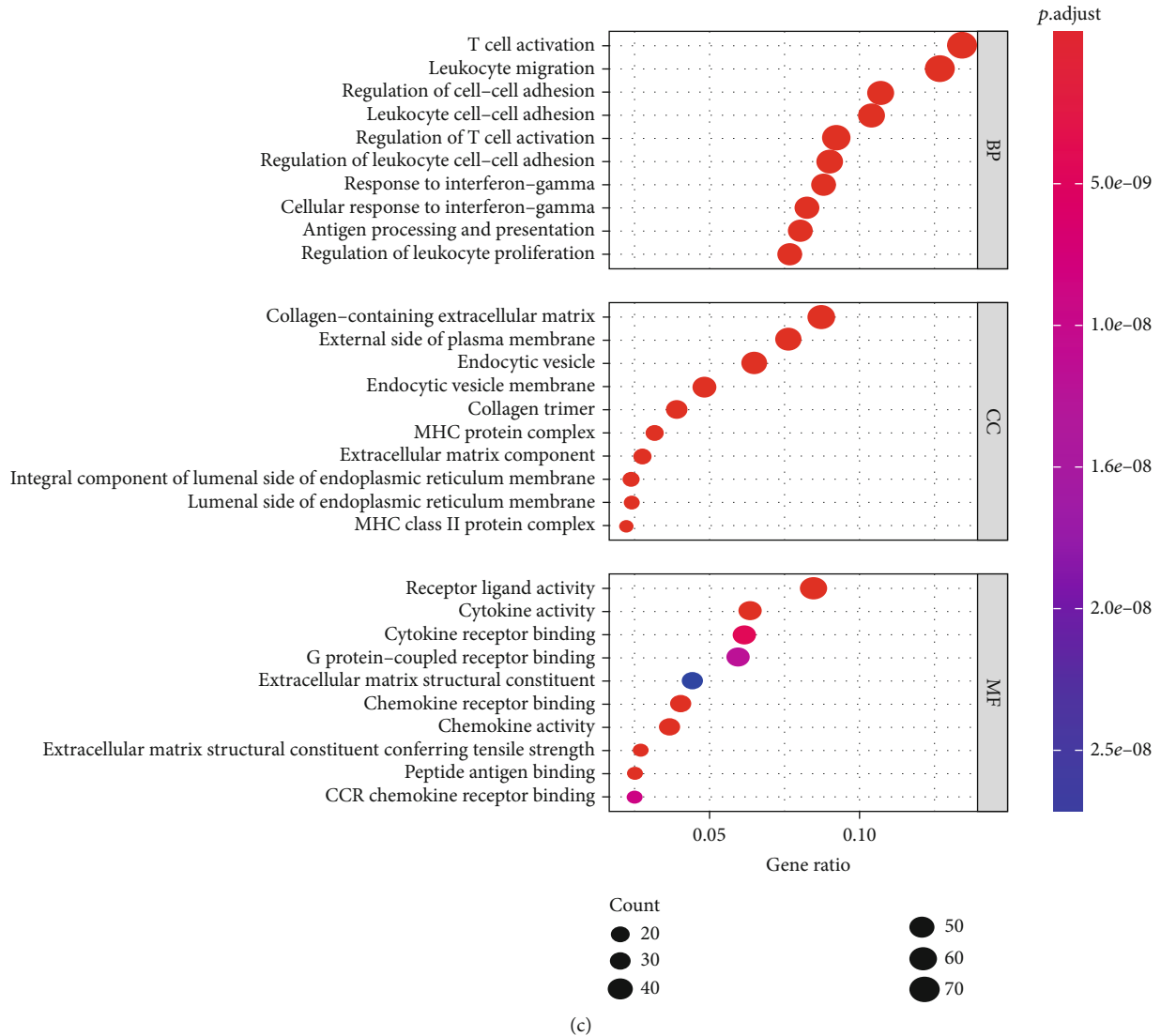
Figure 4: (a) Heatmap of gene set variation analysis for GSVA. (b) The three most significant pathways of GSEA. (c) Dotplot of significantly different pathways from G.O.

Clinical characteristics of patients in the HRSI and LRSI groups are shown in Tables 1 and 2.

4.2. Differentially Expressed Genes, miRNAs, lncRNAs, and ceRNA Network. The low RSI group was used as a reference in the analyses. In RNAseq, 558 significantly differentially expressed genes (DEGs) were obtained; 334 were upregulated, and 224 were downregulated (Figure 2(a)). KRT6A and IDO1 were the most significantly upregulated (logFC = 1.32, adj.p = 0.0002) and downregulated (logFC = −1.42, adj.p < 0.0001) genes, respectively.

In the GEO database, there were 12 upregulated genes and 28 downregulated genes. FBN2 and MAGEA6 were the most significantly upregulated (logFC = 0.85, p value = 0.001) and downregulated (logFC = −1.02, p value = 0.01) genes, respectively.

After intersecting the DEGs in the two databases, we found the total of 17 genes in both databases, including

ADAM23, AHNAK2, BST2, COL11A1, CXCL10, CXCL11, CXCL13, FBN2, HAS3, IFI27, IFI44L, IFIT1, IFIT3, MAGEA6, MMP13, NEFL, and PTGR1.

In TCGA database, 31 differentially expressed miRNAs (DEMs) were obtained. (Figure 2(a)). miR-1269a was the most significantly upregulated (logFC = 1.17, p = 0.0089), while miR-875-3p was the most significantly downregulated (logFC = −3.06, p = 0.0089). And in lncRNAseq (Figure 2(c)), the number of differentially expressed lncRNAs (DELs) was 145, in which LINC01871 was the most significantly upregulated (logFC = 0.87, adj.p < 0.0001) and AL049555.1 was the most significantly downregulated (logFC = −0.55, adj.p = 0.0016).

We used a website http://mirwalk.umm.uni-heidelberg.de/search_mirnas/, predicting miRNAs' target genes, and intersected with the DEGs to draw miRNA-target maps. A 66-pair interaction between differentially expressed genes and miRNAs and an 11-pair interaction between

FIGURE 5: Somatic mutation waterfall map of the most significant genes between HRSI and LRSI.

differentially lncRNAs and miRNAs consisted of a ceRNA network, of which miR-184 and miR-490-3p were located in the center. These miRNAs may play critical roles in radiosensitivity (Figures 3(a) and 3(b)).

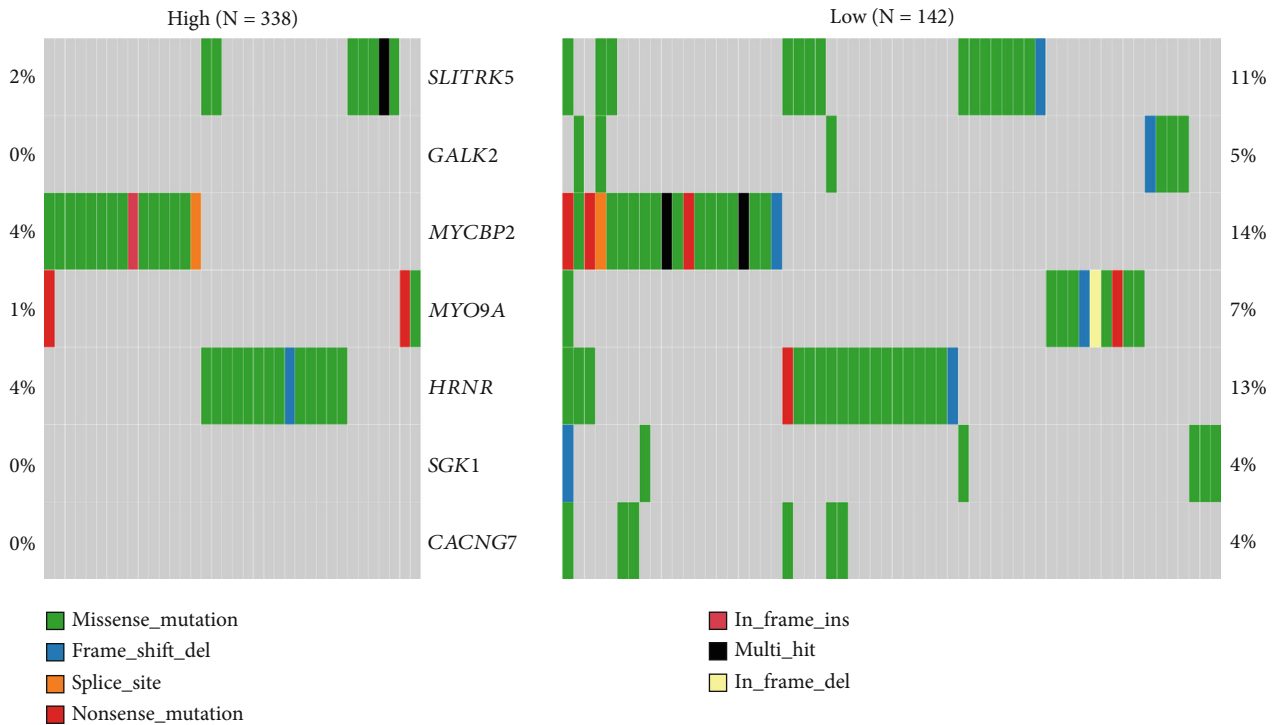4.3. Functional Analysis. GSVA analysis revealed 31 significant pathways, including hedgehog_signaling_pathway, erbb_signaling_pathway, and apoptosis. GSEA found that 87 gene sets were enriched in the HRSI group, including hedgehog_signaling_pathway, while 91 gene sets were enriched in the LRSI group, including natural_killer_cell_mediated_cytotoxicity, toll_like_receptor_signaling_pathway, and cytosolic_DNA_sensing_pathway (Figures 4(a) and 4(b)).

G.O. and KEGG of RNA expression levels revealed that these genes were most significantly enriched in T cell activation and cytokine–cytokine receptor interaction (Figure 4(c)).

4.4. SNV and CNV Analysis. In 480 LUSC patients, the mutation proportion of the most significant genes (SLITRK5, GALK2, MYCBP2, MYO9A, HRNR, SGK1, and CACNG7) between the two groups of HRSI ($n = 338$) and LRSI ($n = 142$) is shown in Figure 5.

After using the mafCompare function, we obtained 212 differential mutation genes, and most of the differential mutation genes in the LRSI group had higher mutation rates. In terms of cancer-driven mutations, the HRSI group has two significant mutations, including HRAS and KLF5, while the LRSI group has three significant mutations, including ATP6V0A2, BSX, and VNN1 (Figures 6 and 7).

We analyzed changes in chromosomal regions in two groups. There are statistical differences between 876 deletion

fragments and 239 amplification fragments ($p < 0.05$). MN1 was the most significant amplification fragments ($p = 0.004$), and SGCD was the deletion fragments ($p = 0.0007$). Most of amplification regions were located on chromosome 2, 5, 7, 18, and 22, while most of the deletion regions were on chromosomes 4, 5, 10, 15, 18, and X. As is shown in the figure, in the HRSI group, deletion regions were most evident on chromosome 5 (Figure 8).

4.5. DNA Methylation Analysis. After quality control, there were 35 upregulated and 231 downregulated methylation positions detected in the HRSI group. Then, we analyzed the differential methylation regions (DMRs). 70 DMRs were obtained, and we used the DMRs to annotate the functional consequences of genetic variation through http://wannovar.wglab.org/. It showed that the most significant DMR was ZFP36L2. We analyzed the methylation genes and mRNAs to obtain methylation-driven genes in the HRSI group. It showed a total of 8 significant genes, including PSMB8, AIM2, GBP4, ACSL5, CD74, OAS2, TRAF2, and ZBTB24, in which PSMB8 is the most significant driven gene (Figures 9 and 10).

5. Discussion

Personalized and precise treatment of cancer patients is a medicine goal at present. RSI is of great significance to the individualization of tumor radiation therapy.

Our study used TCGA and GEO databases to determine the relationship between RSI score and multiomics genetic differences in LUSC patients. In differentially expressed mRNA analyses, we found gene expression, such as KRT6A
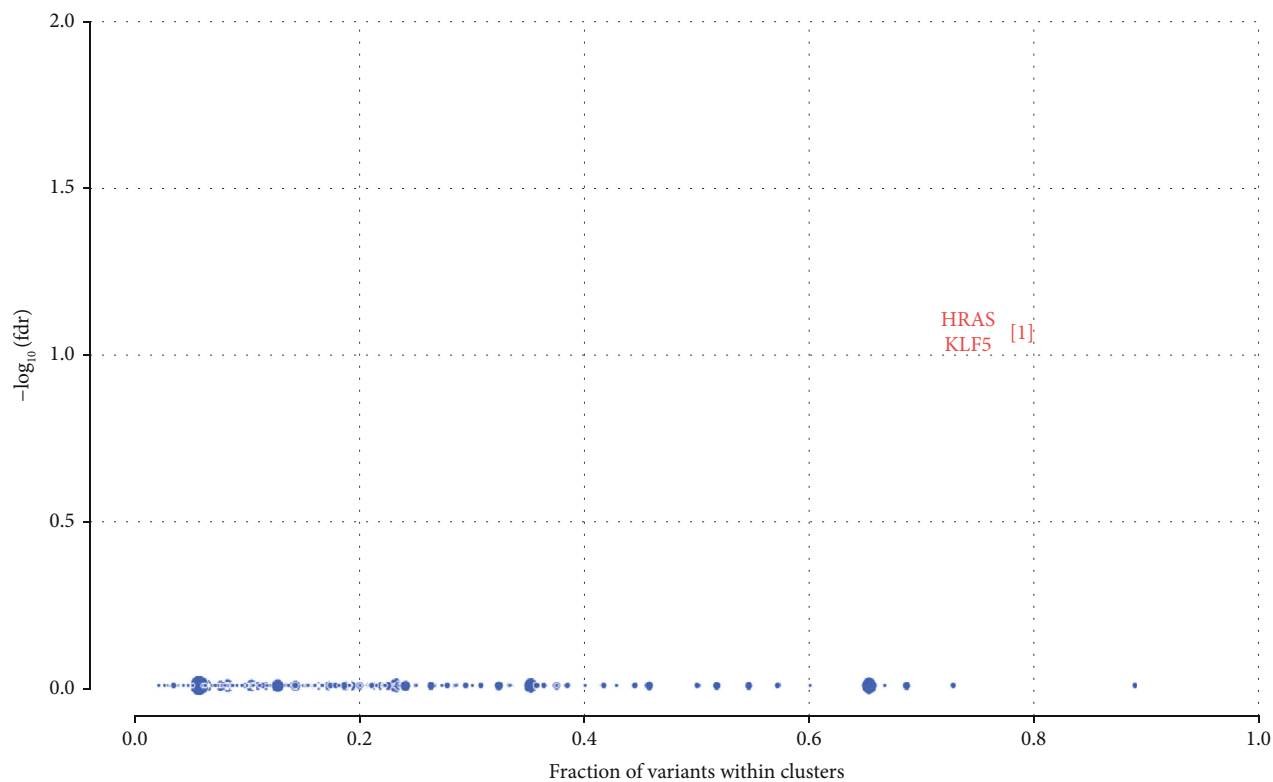
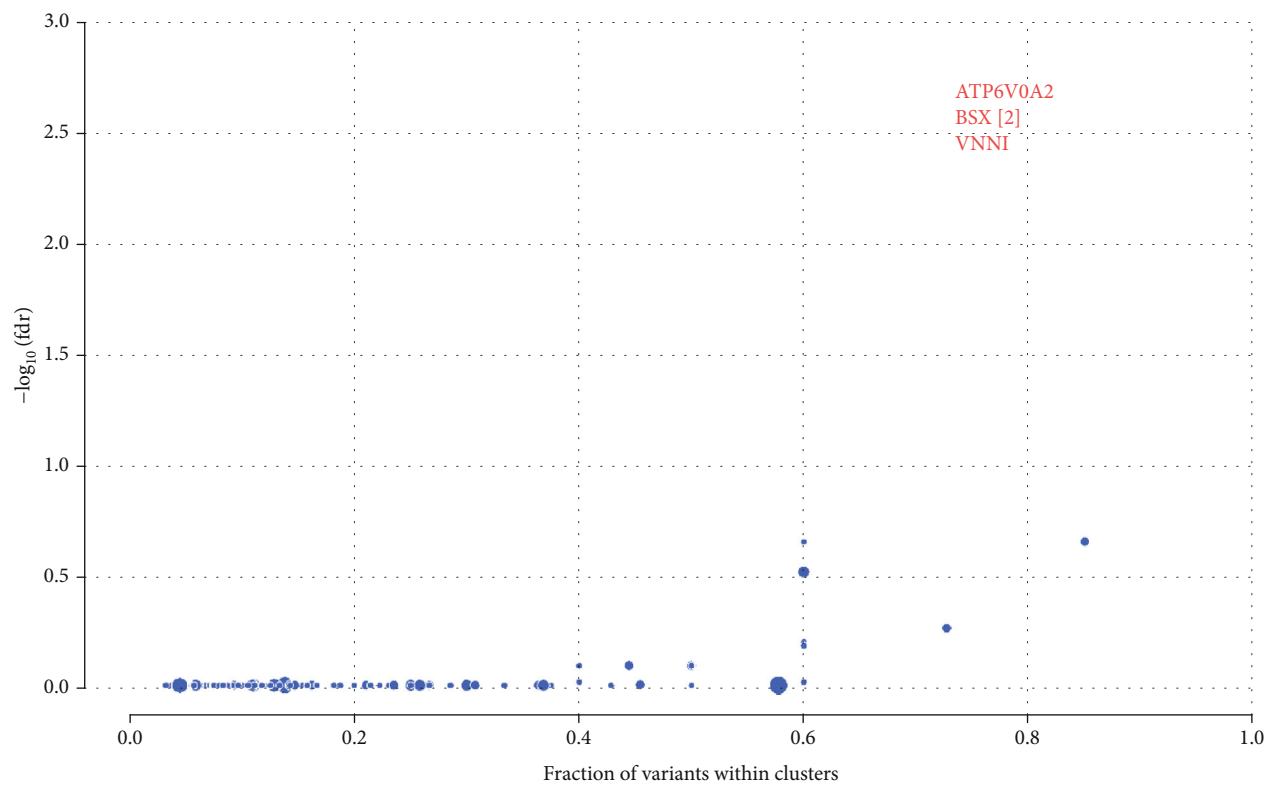FIGURE 6: Cancer-driven mutations in the HRSI group.

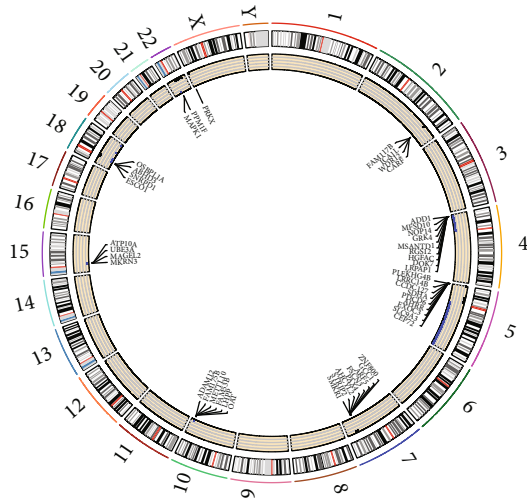FIGURE 7: Cancer-driven mutations in the LRSI group.

FIGURE 8: The differences in CNV between the two groups. The black dots indicate the copy number amplified regions, and the blue dots indicate the copy number deletion regions in the HRSI group.
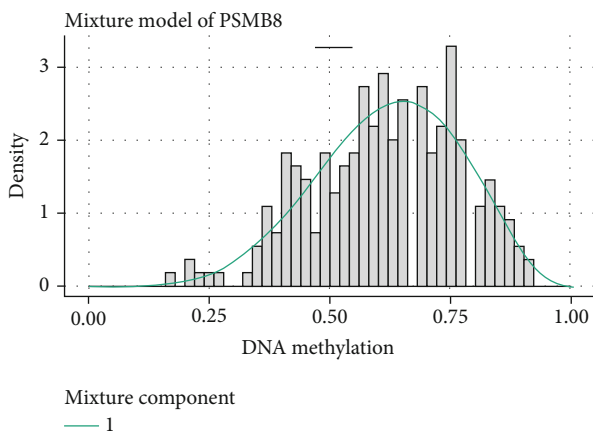

FIGURE 9: A PSMB8 methylation level distribution curve.

and IDO1, is the most significant mRNAs. As is shown in the results, compared with the LRSI group, IDO1 expression in the HRSI group was upregulated. The level of gene transcription of IDO1 is closely related to T cell infiltration [8–12]. In some studies, IDO1 enzymatic activity can directly influence radiation sensitivity, such as colorectal cancer [13–17]. We found some genes in TCGA and GEO databases are related to radiation therapy, including FBN2, IFI27, and IFIT1. Forrester et al. found that FBN2 was associated with radiation-induced fibrosis [18]. STAT1, associated with increased resistance to radiation, regulated IFI27 and IFIT1, which indicated that IFI27 and IFIT1 might be involved in radiation sensitivity.

In differentially expressed miRNA analyses, miR-1269a is the most significant miRNAs. miR-1269a is significantly more expressed in NSCLC tissue than in adjacent tissue. miR-1269a expression upregulation enhances cell proliferation and cluster formation and induces cell cycle conversion. miR-1269a could function as an onco-miRNA in NSCLC
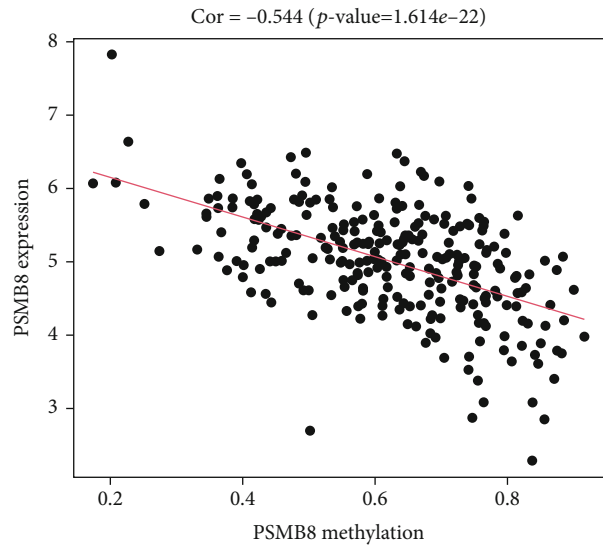
FIGURE 10: Relationship between PSMB8 methylation level and gene expression.

and promote NSCLC growth via downregulating SOX6 [19]. SOX6 suppresses the cell cycle of lung adenocarcinoma by regulating cyclin D1, which indicated miR-1269a might be involved in radiation sensitivity [20]. In lncRNA analyses, LINC01871 was the most significant one. LINC01871 was related to the immunotherapeutic strategy and was used to predict the prognosis of patients with cervical cancer. Radiotherapy combined with immunity will be the next oncology practice [21].

We enriched the function of genes, and the results showed that the upregulated gene pathways in the HRSI group have a stronger relationship with cytosolic_DNA_sensing_pathway. That implied that differences might relate to the sensitivity of radiotherapy.

In SNV and CNV analysis, the mutation proportion of the most significant genes included SLITRK5, SGK1, and CACNG7. SLITRK5 involved radioresistance in nasopharyngeal carcinoma [22]. Several studies have shown that SGK1 can increase radiotherapy sensitivity through various means, in multiple cancers, such as lung cancer, glioblastoma, and synovial sarcoma [22–29].

In DNA methylation analyses, ZFP36L2 is the most significant differential methylation region. A recent study shows that ZFP36L2 inhibited cell proliferation through the cell cycle, which implied that it might be involved in radiation sensitivity [30]. Immune proteasome (PSMB8) is the most significant regional methylation gene between the two groups. PSMB8 is associated with proliferation and apoptosis and is considered a novel prognostic indicator in patients [31]. Ha et al. thought PSMB8 was a predictive marker of preoperative radiosensitivity [32]. Compared with the LRSI group, KLF5 was the most significant gene for CNV in the HRSI group. KLF5 plays an important role in the DNA damage response by regulating DNA damage checkpoint proteins and is associated with cisplatin DDP resistance [33–35]. The relationship between KLF5 and radiotherapy sensitivity needs to be discovered.

Finally, there are some flaws in our experiment. Because the GEO database lacks methylation datasets, we cannot use GEO data to compare methylation mutations. There is also a lack of clinical samples for radiation therapy, so we cannot verify that the differences we find are related to radiation sensitivity.

6. Conclusion

In summary, our study used TCGA and GEO data to investigate multicomponent differences between patients with LUSC high and low RSI. Our research can refer to precision radiotherapy studies and help build personalized precision management for patients in clinical applications.

Data Availability

TCGA data: the data were downloaded from The Cancer Genome Atlas (TCGA) data portal (https://portal.gdc.cancer.gov/)(TCGA-LUSC) through https://xenabrowser.net/datapages/, including mRNA and miRNA expression data, methylation array, mutation profiles, copy number variation, and clinical data. After matching clinical data, 363 cases of mRNA, 542 instances of miRNA, 542 cases of lncRNA, 362 cases of DNA methylation, 480 cases of somatic mutation, and 490 cases of copy number variation were selected for further analysis between the RSI high score group (HRSI) and the low score group (LRSI). GEO data: mRNA data was downloaded from the Gene Expression Omnibus (GEO) database (http://www.ncbi.nlm.nih.gov/geo/). GSE73403 and GSE37745 datasets were collected for the differential gene expression analysis. GSE73403 dataset contains 69 samples from the LUSC patients, published on Sep 25, 2015, and GSE37745 includes 66 samples, released on Oct 12, 2012.

Conflicts of Interest

The authors have no conflicts of interest to declare.

Authors' Contributions

Conception, design, data curation, and formal analysis were carried out by Yajing Du; funding acquisition was done by Yajing Du; writing-original draft was done by Yajing Du and Sujuan Yuan; writing-review and editing was completed by Yajing Du, Qi Zhang, and Xibing Zhuang; final approval of the manuscript and submission was made by all authors.

Acknowledgments

References

[1] R. L. Siegel, K. D. Miller, H. E. Fuchs, and A. Jemal, "Cancer statistics, 2021," *CA: a Cancer Journal for Clinicians*, vol. 71, no. 1, pp. 7–33, 2021.

[2] M. Choi, H. Kadara, J. Zhang et al., "Mutation profiles in early-stage lung squamous cell carcinoma with clinical follow-up and correlation with markers of immune function," *Annals of Oncology*, vol. 28, no. 1, pp. 83–89, 2017.

[3] S. A. Eschrich, J. Pramana, H. Zhang et al., "A gene expression model of intrinsic tumor radiosensitivity: prediction of response and prognosis after chemoradiation," *International Journal of Radiation Oncology • Biology • Physics*, vol. 75, no. 2, pp. 489–496, 2009.

[4] K. A. Ahmed, G. D. Grass, A. G. Orman et al., "Personalizing radiation treatment delivery in the Management of Breast Cancer," *International Journal of Breast Cancer*, vol. 2018, 8 pages, 2018.

[5] J. Meehan, M. Gray, C. Martínez-Pérez et al., "Precision medicine and the role of biomarkers of radiotherapy response in breast cancer," *Frontiers in Oncology*, vol. 10, p. 628, 2020.

[6] W. C. Yang, F. M. Hsu, and P. C. Yang, "Precision radiotherapy for non-small cell lung cancer," *Journal of Biomedical Science*, vol. 27, no. 1, p. 82, 2020.

[7] Z. Hu, G. Bi, Q. Sui et al., "Analyses of multi-omics differences between patients with high and low PD1/PDL1 expression in lung squamous cell carcinoma," *International Immunopharmacology*, vol. 88, p. 106910, 2020.

[8] L. Zhai, E. Ladomersky, A. Lenzen et al., "IDO1 in cancer: a Gemini of immune checkpoints," *Cellular & Molecular Immunology*, vol. 15, no. 5, pp. 447–457, 2018.

[9] J. M. Romero, B. Grünwald, G. H. Jang et al., "A four-chemokine signature is associated with a T-cell-inflamed phenotype in primary and metastatic pancreatic cancer," *Clinical Cancer Research*, vol. 26, no. 8, pp. 1997–2010, 2020.

[10] T. Vidotto, F. P. Saggioro, T. Jamaspishvili et al., "PTEN-deficient prostate cancer is associated with an immunosuppressive tumor microenvironment mediated by increased expression of IDO1 and infiltrating FoxP3+ T regulatory cells," *Prostate*, vol. 79, no. 9, pp. 969–979, 2019.

[11] Z. Y. Xu-Monette, M. Xiao, Q. Au et al., "Immune profiling and quantitative analysis decipher the clinical role of immune-checkpoint expression in the tumor immune microenvironment of DLBCL," *Cancer Immunology Research*, vol. 7, no. 4, pp. 644–657, 2019.

[12] S. Zhang, E. Zhang, J. Long et al., "Immune infiltration in renal cell carcinoma," *Cancer Science*, vol. 110, no. 5, pp. 1564–1572, 2019.

[13] B. Chen, D. M. Alvarado, M. Iticovici et al., "Interferon-induced IDO1 mediates radiation resistance and is a therapeutic target in colorectal cancer," *Cancer Immunology Research*, vol. 8, no. 4, pp. 451–464, 2020.

[14] S. Choudhary, S. C. Burns, H. Mirsafian et al., "Genomic analyses of early responses to radiation inglioblastoma reveal new alterations at transcription, splicing, and translation levels," *Scientific Reports*, vol. 10, no. 1, p. 8979, 2020.

[15] P. Kesarwani, S. Kant, A. Prabhu, and P. Chinnaiyan, "The interplay between metabolic remodeling and immune regulation in glioblastoma," *Neuro-Oncology*, vol. 19, no. 10, pp. 1308–1315, 2017.

[16] J. le Naour, L. Galluzzi, L. Zitvogel, G. Kroemer, and E. Vacchelli, "Trial watch: IDO inhibitors in cancer therapy," *OncoImmunology*, vol. 9, no. 1, 2020.

[17] A. Li, H. B. Barsoumian, J. E. Schoenhals et al., "IDO1 inhibition overcomes radiation-induced "rebound immune suppression" by reducing numbers of IDO1-expressing myeloid-

derived suppressor cells in the tumor microenvironment," *International Journal of Radiation Oncology • Biology • Physics*, vol. 104, no. 4, pp. 903–912, 2019.

[18] H. B. Forrester, J. Li, T. Leong, M. J. McKay, and C. N. Sprung, "Identification of a radiation sensitivity gene expression profile in primary fibroblasts derived from patients who developed radiotherapy-induced fibrosis," *Radiotherapy and Oncology*, vol. 111, no. 2, pp. 186–193, 2014.

[19] R. H. Jin, D. J. Yu, and M. Zhong, "MiR-1269a acts as an onco-miRNA in non-small cell lung cancer via down-regulating SOX6," *European Review for Medical and Pharmacological Sciences*, vol. 22, no. 15, pp. 4888–4897, 2018.

[20] L. Lv, M. Zhou, J. Zhang et al., "SOX6 suppresses the development of lung adenocarcinoma by regulating expression of p53, p21CIPI, cyclin D1 and β-catenin," *FEBS Open Bio*, vol. 10, no. 1, pp. 135–146, 2020.

[21] F. G. Herrera, J. Bourhis, and G. Coukos, "Radiotherapy combination opportunities leveraging immunity for the next oncology practice," *CA: a Cancer Journal for Clinicians*, vol. 67, no. 1, pp. 65–85, 2017.

[22] G. Li, Y. Liu, C. Liu et al., "Genome-wide analyses of long non-coding RNA expression profiles correlated with radioresistance in nasopharyngeal carcinoma via next-generation deep sequencing," *BMC Cancer*, vol. 16, no. 1, p. 719, 2016.

[23] F. Chen, X. Chen, Y. Ren et al., "Radiation-induced glucocorticoid receptor promotes CD44+ prostate cancer stem cell growth through activation of SGK1-Wnt/β-catenin signaling," *Journal of Molecular Medicine (Berlin, Germany)*, vol. 97, no. 8, pp. 1169–1182, 2019.

[24] F. Lang, J. Rajaxavier, Y. Singh, S. Y. Brucker, and M. S. Salker, "The enigmatic role of serum & glucocorticoid inducible kinase 1 in the endometrium," *Frontiers in Cell and Development Biology*, vol. 8, p. 556543, 2020.

[25] J. E. Sagers, R. L. Beauchamp, Y. Zhang et al., "Combination therapy with mTOR kinase inhibitor and dasatinib as a novel therapeutic strategy for vestibular schwannoma," *Scientific Reports*, vol. 10, no. 1, p. 4211, 2020.

[26] C. Talarico, L. D'Antona, D. Scumaci et al., "Preclinical model in HCC: the SGK1 kinase inhibitor SI113 blocks tumor progression in vitro and in vivo and synergizes with radiotherapy," *Oncotarget*, vol. 6, no. 35, pp. 37511–37525, 2015.

[27] C. Talarico, V. Dattilo, L. D'Antona et al., "SI113, a SGK1 inhibitor, potentiates the effects of radiotherapy, modulates the response to oxidative stress and induces cytotoxic autophagy in human glioblastoma multiforme cells," *Oncotarget*, vol. 7, no. 13, pp. 15868–15884, 2016.

[28] Z. Tang, Q. Shen, H. Xie et al., "Serum and glucocorticoid-regulated kinase 1 (SGK1) is a predictor of poor prognosis in non-small cell lung cancer, and its dynamic pattern following treatment with SGK1 inhibitor and γ-ray irradiation was elucidated," *Oncology Reports*, vol. 39, no. 3, pp. 1505–1515, 2018.

[29] C. Zhou, W. Xiao, T. Jiang et al., "Targeting SGK1 enhances the efficacy of radiotherapy in locally advanced rectal cancer," *Biomedicine & Pharmacotherapy*, vol. 125, p. 109954, 2020.

[30] F. M. Suk, C. C. Chang, R. J. Lin et al., "ZFP36L1 and ZFP36L2 inhibit cell proliferation in a cyclin D-dependent and p53-independent manner," *Scientific Reports*, vol. 8, no. 1, p. 2742, 2018.

[31] B. Y. Yang, J. W. Song, H. Z. Sun et al., "PSMB8 regulates glioma cell migration, proliferation, and apoptosis through mod-ulating ERK1/2 and PI3K/AKT signaling pathways," *Biomedicine & Pharmacotherapy*, vol. 100, pp. 205–212, 2018.

[32] Y. J. Ha, K. H. Tak, C. W. Kim et al., "PSMB8 as a candidate marker of responsiveness to preoperative radiation therapy in rectal cancer patients," *International Journal of Radiation Oncology • Biology • Physics*, vol. 98, no. 5, pp. 1164–1173, 2017.

[33] H. Zhang, F. Shao, W. Guo, Y. Gao, and J. He, "Knockdown of KLF5 promotes cisplatin-induced cell apoptosis via regulating DNA damage checkpoint proteins in non-small cell lung cancer," *Thoracic Cancer*, vol. 10, no. 5, pp. 1069–1077, 2019.

[34] T. Gong, L. Cui, H. Wang, H. Wang, and N. Han, "Knockdown of KLF5 suppresses hypoxia-induced resistance to cisplatin in NSCLC cells by regulating HIF-1α-dependent glycolysis through inactivation of the PI3K/Akt/mTOR pathway," *Journal of Translational Medicine*, vol. 16, no. 1, p. 164, 2018.

[35] J. Shi, C. Yang, J. An et al., "KLF5-induced BBOX1-AS1 contributes to cell malignant phenotypes in non-small cell lung cancer via sponging miR-27a-5p to up-regulate MELK and activate FAK signaling pathway," *Journal of Experimental & Clinical Cancer Research*, vol. 40, no. 1, p. 148, 2021.

Research Article

Comprehensive Analysis of YTH Domain Family in Lung Adenocarcinoma: Expression Profile, Association with Prognostic Value, and Immune Infiltration

Kuan Hu ,[1] **Lei Yao** ,[1] **Yuanliang Yan** ,[2,3] **Lei Zhou** ,[4] **and Juanni Li** [5]

[1]*Department of Hepatobiliary Surgery, Xiangya Hospital, Central South University, Changsha, 410008 Hunan, China*
[2]*Department of Pharmacy, Xiangya Hospital, Central South University, Changsha, 410008 Hunan, China*
[3]*National Clinical Research Center for Geriatric Disorders, Xiangya Hospital, Central South University, Changsha, 410008 Hunan, China*
[4]*Department of Anesthesiology, Third Xiangya Hospital of Central South University, Changsha, 410008 Hunan, China*
[5]*Department of Pathology, Xiangya Hospital, Central South University, Changsha, 410008 Hunan, China*

Correspondence should be addressed to Juanni Li; lijuanni2014@csu.edu.cn

Background. All YTH domain family members are m^{6}A reader proteins accounting for the methylation modulation involved in the process of tumorgenesis and tumor progression. However, the expression profiles and roles of the YTH domain family in lung adenocarcinoma (LUAD) remain to be further illustrated. *Methods*. GEPIA2 and TNMplot databases were used to generate the expression profiles of the YTH family. Kaplan-Meier plotter database was employed to analysis the prognostic value of the YTH family. Coexpression profiles and genetic alterations analysis of the YTH family were undertaken using the cBioPortal database. YTH family protein-associated protein-protein interaction (PPI) network was identified by using STRING. Functional enrichment analysis was performed with the help of the WebGestalt database. The correlation analysis between the YTH family and immune cell infiltration in LUAD was administrated by using the TIMER2.0 database. *Results*. mRNA expression of YTHDC1 and YTHDC2 was significantly lower in LUAD, whereas YTHDF1, YTHDF2, and YTHDF3 with apparently higher expression. YTHDF2 expression was observed to be the highest in the nonsmoker subgroup, and its expression gradually decreased with the increased severity of smoking habit. LUAD patients with low expression of YTHDC2, YTHDF1, and YTHDF2 were correlated with a better overall survival (OS) time. The YTHDF1 genetic alteration rate was 26%, which was the highest in the YTH family. The major cancer-associated functions of YTH family pointed in the direction of immunomodulation, especially antigen processing and presentation. Most of the YTH family members were significantly correlated with the infiltration of CD4+ T cells, CD8+ T cells, macrophages, and neutrophils, indicating the deep involvement of the YTH domain family in the immune cell infiltration in LUAD. *Conclusion*. The molecular and expression profiles of the YTH family were dysregulated in LUAD. YTH family members (especially YTHDC2) were promising biomarkers and potential therapeutic targets that may bring benefit for the patients with LUAD.

1. Introduction

As the leading cause of cancer-related deaths in global, lung cancer is composed of two major subtypes lung squamous cell carcinoma (LUSC) and lung adenocarcinoma (LUAD), with LUAD exhibits relatively higher incidence and mortality [1–3]. While tremendous efforts have been made in drug discovery against LUAD, the clinical outcomes of most patients with LUAD remain to be poor [4]. Hence, exploring novel biomarkers and molecular targets is of great value for the development of the LUAD therapeutic strategy.

Dysregulation of RNA methylation has frequently been reported to be implicated in the initiation and progression of cancer [5–7]. N6-Methyladenosine (m6A) modification,

as the most common RNA methylation, has received intensive attention these days and is expected to be a promising therapeutic target against cancer [8]. With the function of recognizing m6A-modified mRNA and regulating the expression of target genes, the YT521-B homology (YTH) family as the major reading proteins (known as "readers") is composed of five proteins that carry the highly conserved YTH domain in common. These proteins are further classified into three categories: YTH domain-containing 1 (YTHDC1), YTH domain-containing 2 (YTHDC2), and YTH m6A-binding protein (YTHDF) including YTHDF1-3. Accumulative studies have shown the robust association between YTH family members and various types of cancer [9]. For instance, there was proved to be a positive correlation between YTHDF1 overexpression and poor prognosis in patients with liver cancer [10]. In addition, the silence of YTHDF2 resulted in the increased invasion of tumor cells in pancreatic cancer [11]. Furthermore, it was reported that YTHDC2 could promote radiotherapy resistance of nasopharyngeal carcinoma via activation of the AKT signal pathway [12]. However, the expression signatures and function of YTH family proteins in LUAD initiation and progression is still lacking.

In the present study, we aimed to further broaden the understanding of the role of the YTH family in LUAD through various public databases, thereby providing novel insights into the diagnosis and treatment of LUAD. The expression profiles, prognostic value, and functional enrichment analysis of YTH family members in LUAD were evaluated, and the correlation of immune cell infiltration with the YTH family was also discussed.

2. Materials and Methods

2.1. GEPIA2 and TNMplot. Gene Expression Profiling Interactive Analysis (GEPIA) 2.0 and TNMplot are two databases that support comprehensive expression analyses based on TCGA and GTEx data [13–15]. The expression profiles of YTH family members in LAUD and normal lung tissue were retrieved from these two databases. A cutoff of 0.05 in p value was set as statistical significance. The relative expression of each YTH in LUAD was compared using GEPIA2. The color density of each block represents the median expression value of each YTH member in LUAD tumor tissue, normalized by the maximum median expression value across all blocks. All the databases used in our study were summarized in Supplementary Table S1.

2.2. UALCAN. UALCAN is a portal for tumor subgroup analysis of different gene expressions [16]. In this study, UALCAN database was also applied to analysis the different expressions of YTH family members based on smoking habits. A cutoff of 0.05 in p value was set as statistical significance.

2.3. Kaplan-Meier Plotter. Kaplan-Meier plotter database is used for evaluating the prognostic role of the expression level of specific gene [17]. In this study, overall survival (OS), first progression (FP), and postprogression survival (PPS) of LUAD patients with different expressions of each

YTH family member were compared, respectively, through the Kaplan-Meier plotter database. A cutoff of 0.05 in p value was set as statistical significance.

2.4. cBioPortal. cBioPortal is a database of cancer genomics which provides download and analysis of genomic alteration data of diverse types of cancer [18, 19]. A dataset of 230 patients with LUAD (TCGA, Firehose Legacy) from cBioPortal was used for the analyses of coexpression and genetic alterations of the YTH family.

2.5. STRING and Cytoscape. Probable protein-protein interactions (PPIs) among YTH family members were predicted using STRING, and a database provides an interactive network among interested proteins [20, 21]. In addition, 152 YTH-associated genes were selected from cBioPortal, then, Cytoscape was used to generate the molecular interaction networks [22].

2.6. WebGestalt. WebGestalt is a comprehensive tool online that supports gene set enrichment analysis and network topology analysis [23]. Kyoto Encyclopedia of Genes and Genomes (KEGG) pathway and Gene Ontology (GO) enrichment analyses were performed by using WebGestalt to get the enrichment pathways correlated to the YTH family in LUAD.

2.7. TIMER2.0. TIMER2.0 is a public resource that offers comprehensive analyses of immune cells infiltration in various types of cancer [24]. Here, we conduct the "immune association" module to obtain the scatterplots which show the association between the expression of YTH family proteins and different types of infiltrated immune cells (CD4+ T cells, CD8+ T cells, B cells, dendritic cells, macrophages, and neutrophils).

3. Results

3.1. Expression Profiles of YTH Domain Family in Patients with LUAD. Data returned from both GEPIA2 and TNMplot databases demonstrated that the mRNA expression of YTH domain family members in LUAD tissues was of widely divergence comparing with that in adjacent normal tissues, especially in the cases of YTHDC2 with significantly lower expression, and YTHDF1, YTHDF2, and YTHDF3 with apparently higher expression only in TNMplot database (Figures 1(a) and 1(b)). Moreover, the expression abundance of each YTH member in LUAD varied. The results showed that the relative expression of YTHDC2 was the lowest in the YTH domain family, while the expression of YTHDF3 was the highest (Figure 1(c)).

There was no significant difference in the expression of YTH family molecules in the four clinical stage subgroups of LUAD (data no shown). While intriguingly, based on the classification of the status of smoking habits (nonsmoker, smoker, reformed smoker1 (who are current reformed smokers for ≤15 years) and reformed smoker2 (who are current reformed smokers for >15 years)) in LUAD patients, YTHDC2 expression was observed to be the highest in nonsmoker subgroup, and its expression
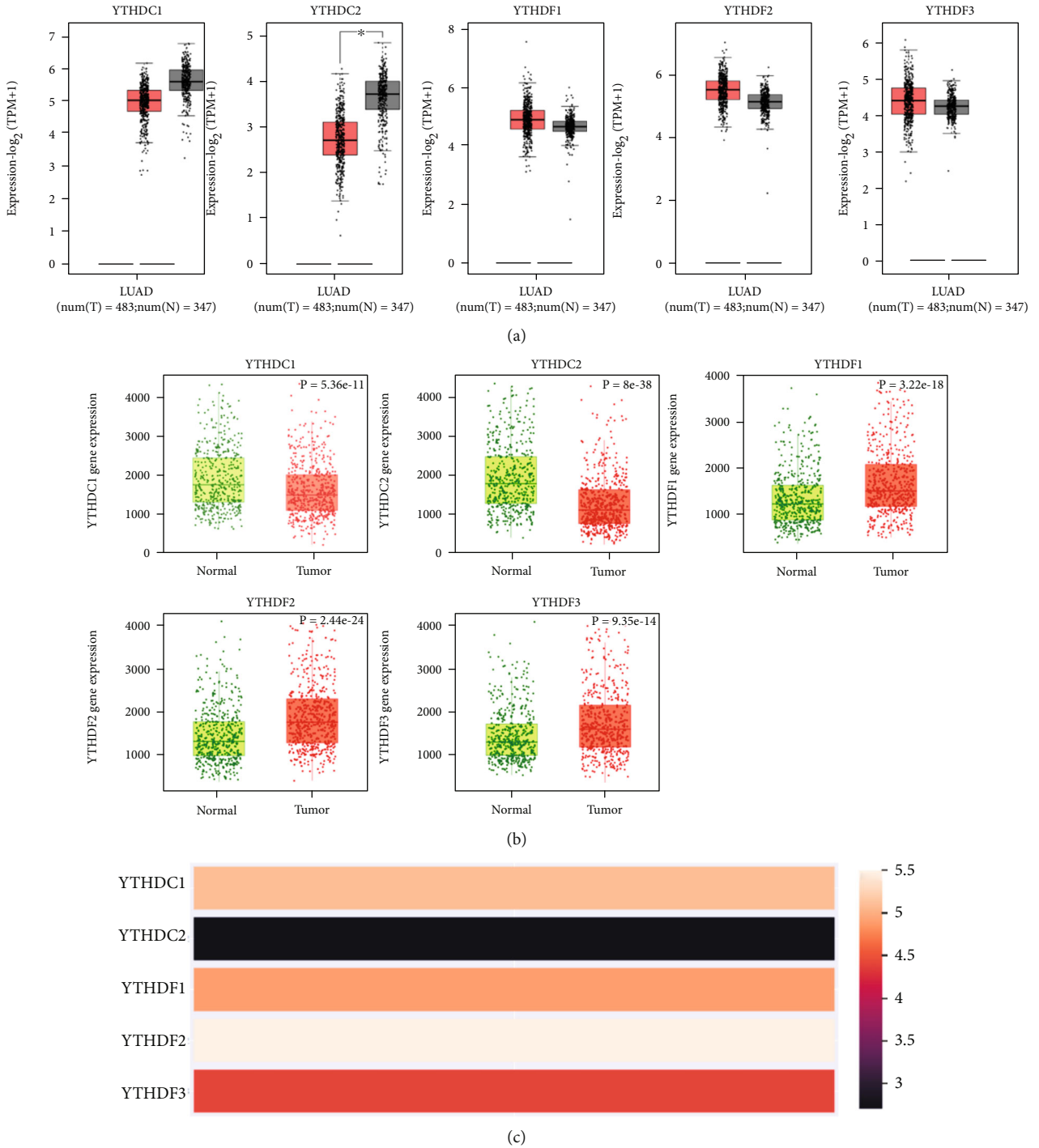
FIGURE 1: The mRNA expression levels of the YTH family in LUAD were compared with that in normal lung tissues. (a) Data were retrieved from the GEPIA2 database. (b) Data were retrieved from the TNMplot database. (c) The relative expression levels of each YTH family member in LUAD patients (GEPIA2). $*p < 0.05$.

gradually decreased with the increased severity of smoking habit, suggesting that the smoking habits might reflect the expression of YTHDC2 level, and even for the LUAD patient with smoking, smoking cessation can effectively reduce YTHDC2 expression (Figure 2). Moreover, we made the logistic regression analysis using LUAD data from TCGA, and the results showed that the relationship between

smoking and YTHDC2 expression was not statistically significant, indicating that more samples are needed to verify the relationship between them (Supplementary Table S3). Furthermore, we analyzed the prognostic effect of YTHDC2 on both smoking and nonsmoking LUAD patients and found that both smoking and nonsmoking patients with high expression of YTHDC2 showed better
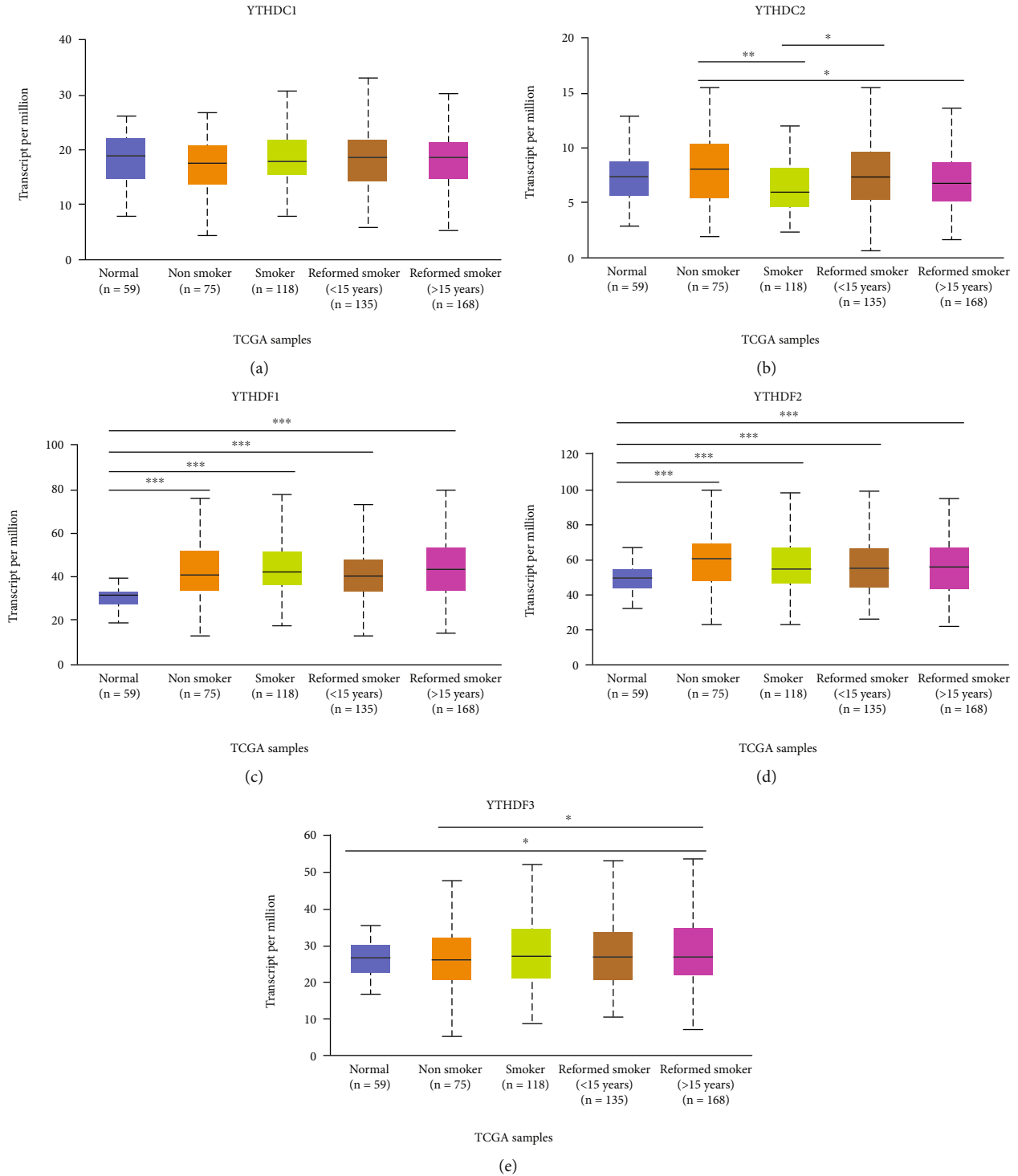
FIGURE 2: The association between the expression of YTH family members and different smoking habits from UALCAN (nonsmoker, smoker, reformed smoker). $^*p < 0.05$, $^{**}p < 0.01$, $^{***}p < 0.001$.

prognosis (HR = 0.65, $p = 0.0011$; HR = 0.19, $p = 5.8e − 08$;, respectively) (Supplementary Figure S1).

3.2. YTH Domain Family in Prognosis of LUAD Patients. To assess the prognostic value of the YTH domain family in LUAD, the correlations between the expression of YTH family members and survival endpoints like overall survival

(OS), first progression (FP), and postprogression survival (PPS) were further analyzed through Kaplan-Meier plotter website. As a consequence, LUAD patients with low expression of YTHDC2 ($p < 0.001$), YTHDF1 ($p < 0.05$), and YTHDF2 ($p < 0.01$) were correlated with a better OS time (Figure 3). Similarly, low expression of YTHDC1 ($p < 0.001$), YTHDC2 ($p < 0.001$), YTHDF2 ($p < 0.001$),
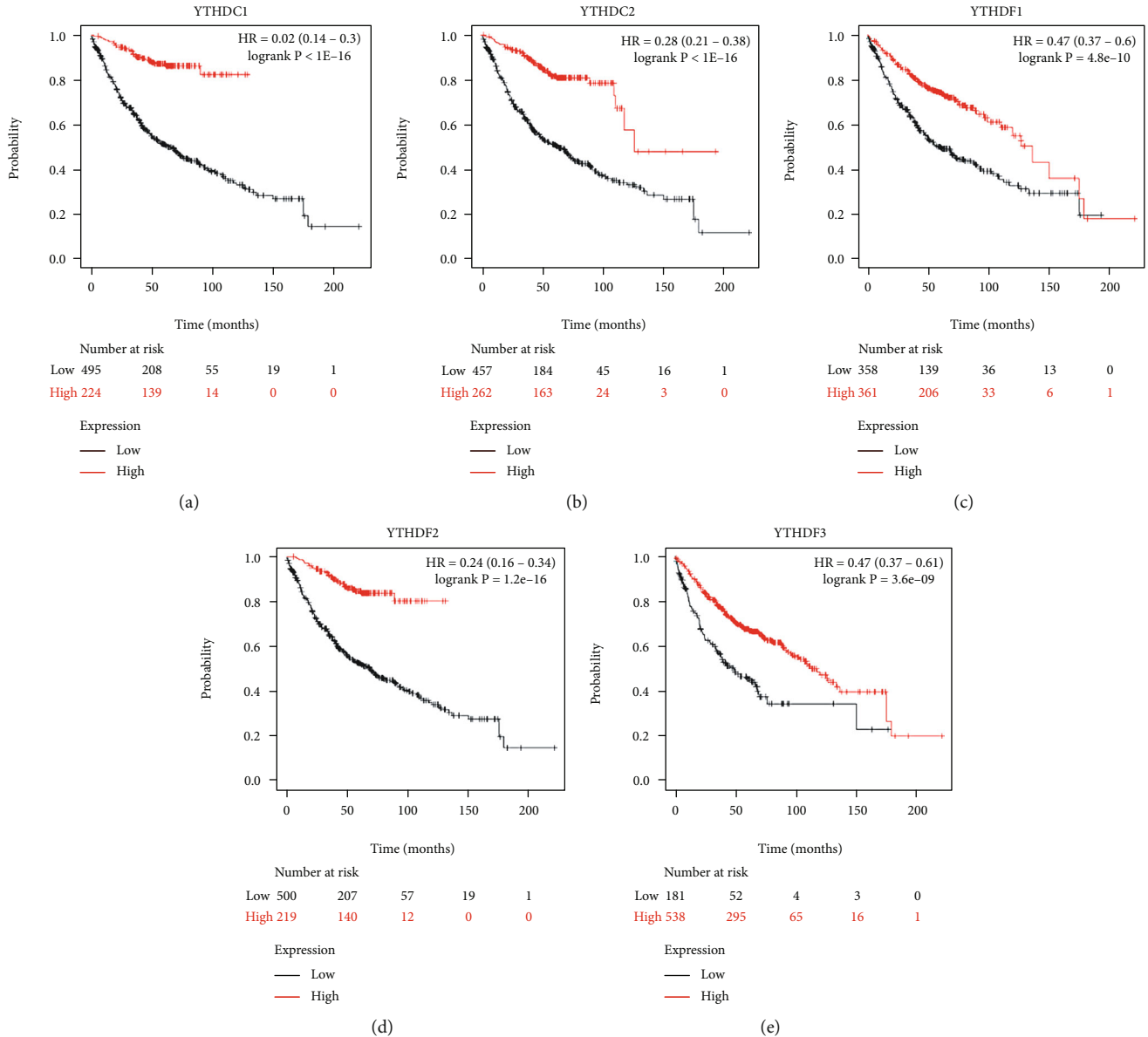
FIGURE 3: The correlations between the expression of YTH family members and overall survival (OS) of LUAD patients were analyzed through the Kaplan-Meier plotter website.

and YTHDF3 ($p < 0.05$) were associated with a better FP time (Figure 4). As for the PPS, it was YTHDC1 ($p < 0.001$), YTHDC2 ($p < 0.001$), and YTHDF2 ($p < 0.005$) that linked to a better prognosis (Figure 5).

3.3. Genetic Alterations of YTH Domain Family in LUAD.

The frequency and types of genetic alterations in the YTH domain family in LUAD were obtained through the TCGA database and cBioPortal tool. As presented in Figure 6(a), the YTHDF1 genetic alteration rate was 26%, which was the highest in the YTH family. Genetic alteration rates of the other family members are 13% (for YTHDC1, YTHDC2, and YTHDF2) and 22% (YTHDF3). In the aspect of types of genetic alterations, gene amplification, missence mutation, truncating mutation, and mRNA high/low were the main genetic alterations in YTHDC1, YTHDF1, and YTHDF2.

Whereas barely missence mutation was observed in YTHDC2, and scarcely missence and truncating mutation were found in YTHDF3 (Figure 6(a)).

3.4. Interactive Network Analyses of YTH Domain Family and Associated Molecules.

The interactive network of the YTH domain family generated by the STRING database demonstrated that YTHDF1, YTHDF2, and YTHDF3 were concordantly interacted with YTHDC1, revealing YTHDC1 acted as the hub node in this interactive network (Figure 6(b)). However, YTHDC2 was relatively dissociated from its family members in terms of the functional network of interactive molecules. Furthermore, 152 most frequent genes with changed expression level and concomitantly with close correlation to YTH domain family were identified from the cBioPortal database (Supplementary Table S2). Then, the
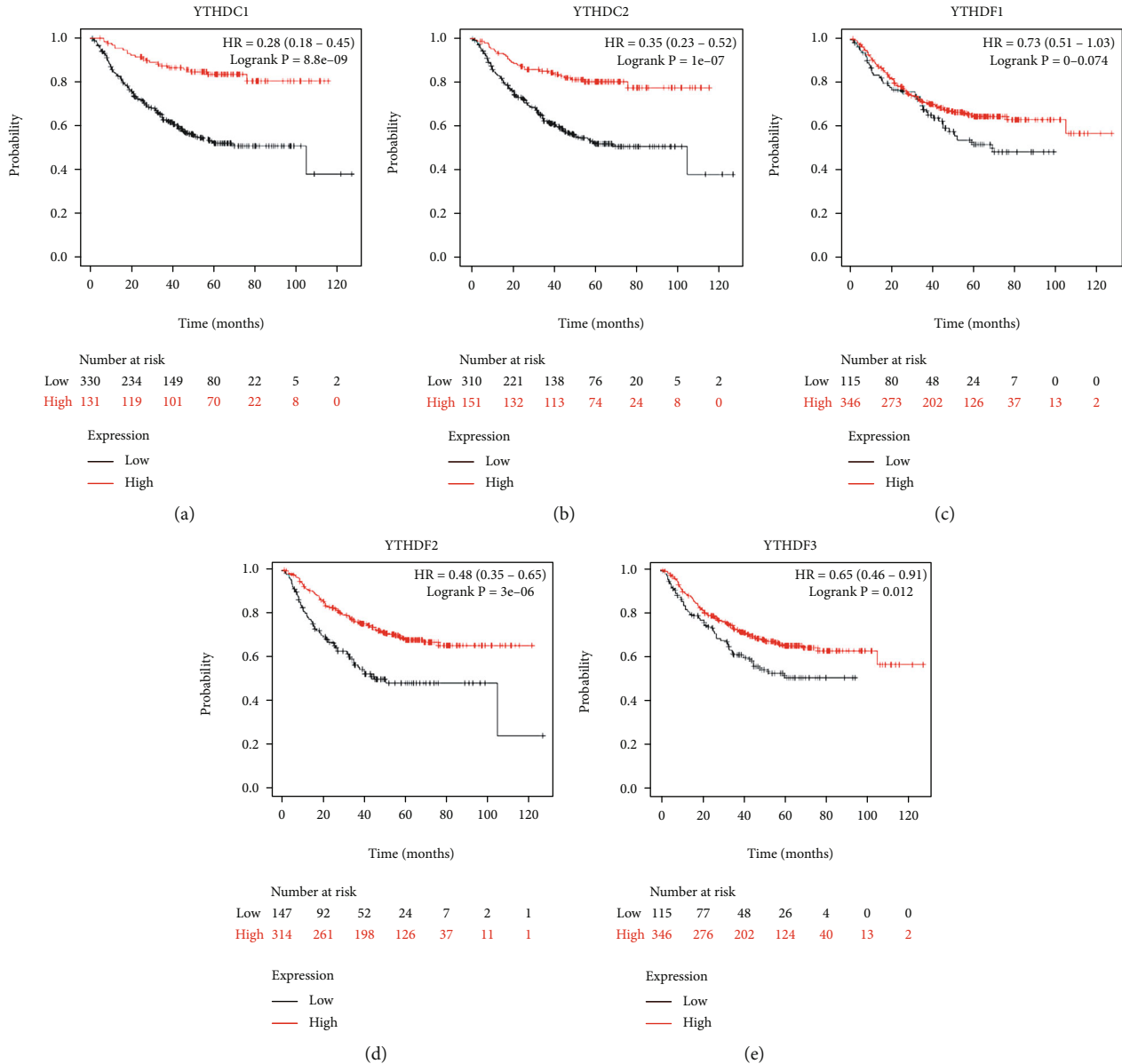
FIGURE 4: The correlations between the expression of YTH family members and first progression (FP) of LUAD patients were retrieved from the Kaplan-Meier plotter website.

interactive network of these 152 genes was established, which further suggested that molecules including MMP1, HP, MRC1, COL7A1, KRT14, ITGB4, CASR, and COL17A1 may serve as hub genes participating in the biological processes of the YTH domain family in LUAD (Figure 6(c)).

To further understand what kinds of functions are induced by the YTH domain family, the functional enrichment analysis was performed on the basis of the 152 YTH-associated genes by using the WebGestalt database. Consequently, YTH domain family members were mainly enriched in biological functions such as biological regulation, response to stimulus, metabolic process, multicellular organismal process, and developmental process. Moreover, YTH domain family members were also found to be highly enriched in the following cellular component, including membrane, vesicle, extracellular space, endomembrane system, nucleus, protein-containing complex, and membrane-enclosed lumen, and so on. As for the enrichment of molecular function, protein binding, ion binding, hydrolase activity, nucleic acid binding, structural molecule activity, and molecular transducer activity are the top ones with the highest enrichment (Figure 7(a)). In addition, Kyoto Encyclopedia of Genes and Genomes (KEGG) pathway was used to exhibit the enrichment ratio of specific biological functions that contribute to the LUAD development. The top-ranked YTH-associated biological functions involved in the LUAD development were antigen processing and presentation, hemidesmosome assembly, formation of primary germ layer, and appendage development (Figure 7(b)).

3.5. Correlation between Immune Cell Infiltration and Each YTH Domain Family Member. Immune cell infiltration in
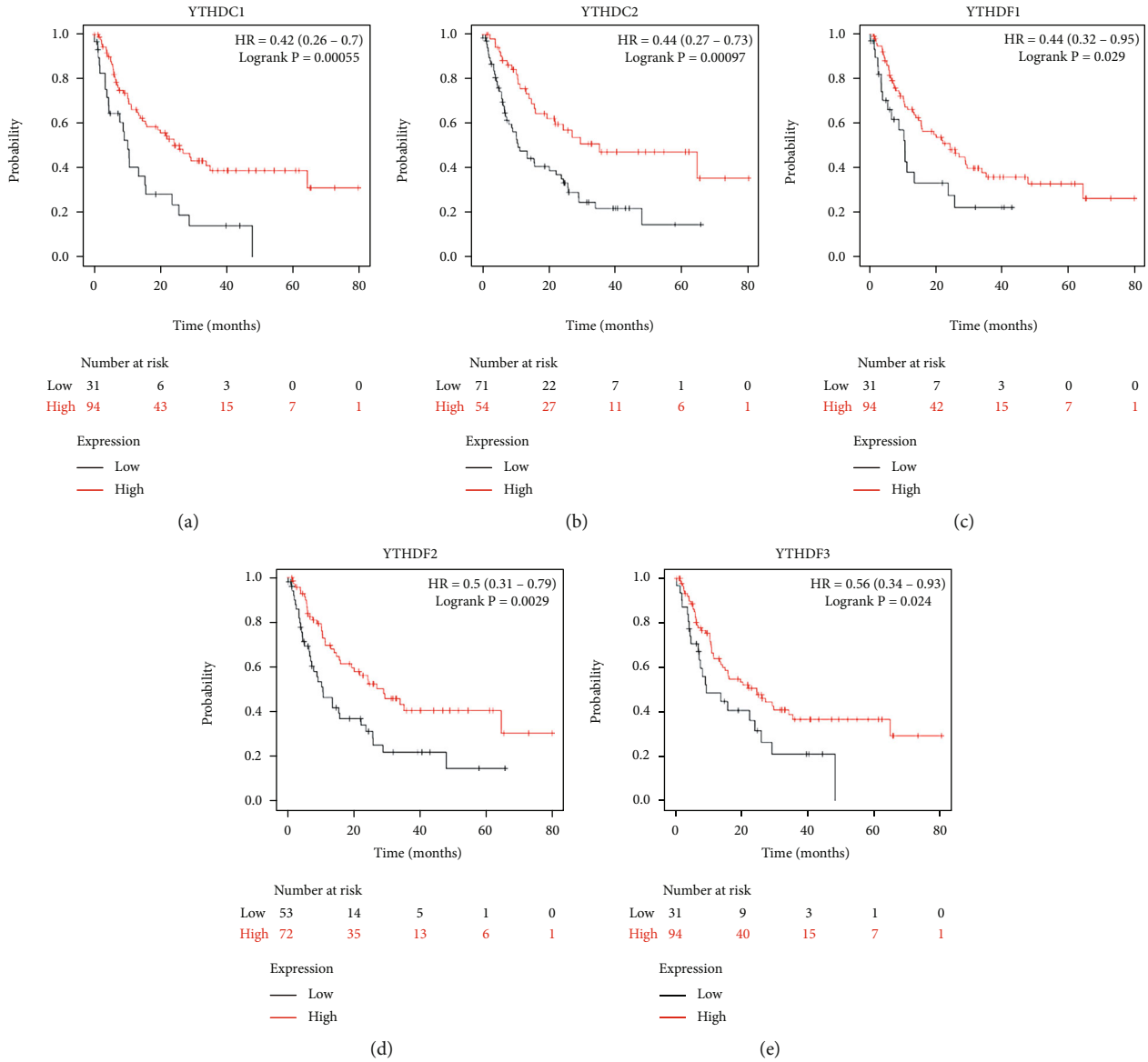
FIGURE 5: The correlations between the expression of YTH family members and postprogression survival (PPS) of LUAD patients were obtained from the Kaplan-Meier plotter website.

tumor is an indispensable component of tumor microenvironment and an independent index that reflects prognosis and lymphatic metastasis status [25–27]. Thus, we use the TIMER2.0 database to further illustrate the correlation between immune cell infiltration and each YTH domain family members. YTHDC1 expression was significantly correlated with infiltration of several types of immune cells ranging from macrophage (Rho = 0.146, $p = 1.14 \times 10^{-3}$) to neutrophil (Rho = 0.224, $p = 5.31 \times 10^{-7}$), CD4+ T cell (Rho = 0.233, $p = 1.77 \times 10^{-7}$), and CD8+ T cell (Rho = 0.224, $p = 5.32 \times 10^{-7}$) (Figure 8(a)). YTHDC2 expression was significantly associated with infiltration of macrophage (Rho = 0.145, $p = 1.25 \times 10^{-3}$), neutrophil (Rho = 0.313, $p = 1.09 \times 10^{-12}$), CD4+ T cell (Rho = 0.235, $p = 1.32 \times 10^{-7}$), CD8+ T cell (Rho = 0.185, $p = 3.69 \times 10^{-5}$), and dendritic cell (Rho = 0.146, $p = 5.22 \times 10^{-4}$)

(Figure 8(b)). In addition, in the cases of YTHDF1, YTHDF2, and YTHDF3, various immune infiltration signatures were observed to have a significant correlation (Figures 8(c)–8(e)). These data indicated the deep involvement of the YTH domain family in the immune cell infiltration in LUAD.

4. Discussion

RNA methylation is a vital posttranscriptional modification that participates in various human biological processes [28]. Recent researches on m6A RNA methylation have revealed its facilitating role in the initiation and development of various types of cancer, thus, has gradually become a new direction in oncology research and targeted drug development [29, 30]. All of the five YTH domain family members are m6A reader proteins—the key enzyme that
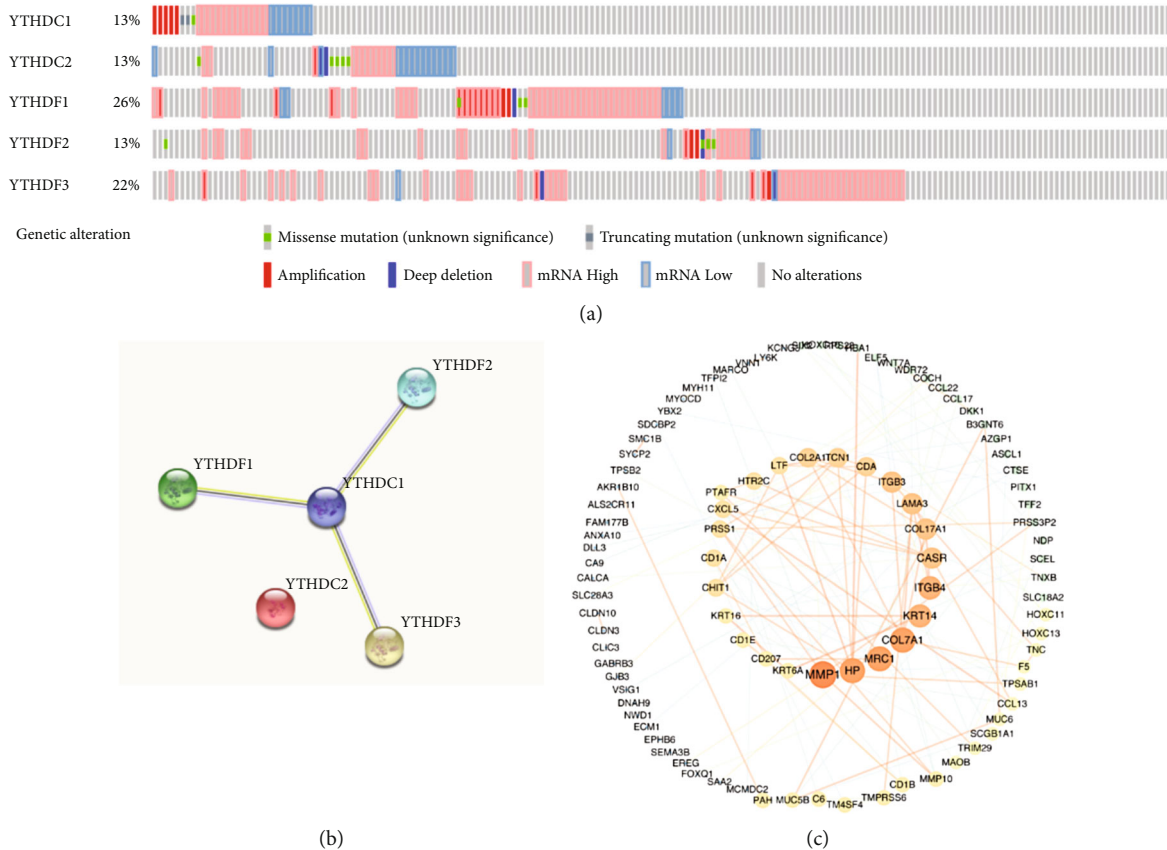
(a)

(b)

(c)

Figure 6: Genetic alterations analysis and molecular interaction analysis of the YTH family in LUAD. (a) Genetic alteration profiles of the YTH family in LUAD by using cBioPortal. (b) The interaction analysis within the YTH family from STRING. (c) The identification of 152 YTH-associated genes which was most frequently altered in LUAD through cBioPortal and Cytoscape.

regulates the methylation of target RNA by specific combination with m6A-containing mRNA. With huge potential value, there are multiple studies reporting the role of YTH family proteins in various cancer types. For instance, YTHDF1 was proved to be an oncogene in hepatocellular carcinoma (HCC) owing to its overexpression in HCC patients and association with poor prognosis [10, 31]. The oncogenic role of YTHDF1 may be achieved by the mechanisms of Snail-induced EMT [32] and m6A-dependent activation of the WNT/β-catenin pathway [33]. However, the role of YTHDF2 in HCC was found to be contradictory, which acted as either oncogene in a m6A-dependent manner or tumor suppressor gene through EGFR and ERK/MAPK pathway [34, 35]. In the case of ovarian cancer, YTHDF1 was also found to be overexpressed and associated with poor clinical outcome. YTHDF1 accelerated the growth and metastasis of ovarian cancer in vivo and in vitro by promoting the m6A-modified translation of EIF3C [36]. In the field of lung cancer, the expression of YTHDF2 was aberrantly higher and facilitated the proliferation and growth of cancer cells, ribose-5-phosphate, and NADPH induced by pentose phosphate pathway might be the mechanism underlies [37]. YTHDF1 was demonstrated to promote proliferation of cancer cells in nonsmall cell lung cancer (NSCLC), whereas paradoxically, better prognosis and chemotherapy sensitivity were correlated with high YTHDF1 expression

and implied the complicated and multiple mechanisms lurking beneath the phenomena observed above [38].

According to our knowledge, a study that systematically focused on the expression, prognostic value, and pathophysiological function of the YTH domain family in LUAD is still lacking. Hence, we preliminarily explore the expression profiles of the YTH domain family and found that only the expression of YTHDC2 is significantly lower in all of the LUAD datasets included in this study, while YTHDF1, YTHDF2, and YTHDF3 are proved to be significantly upregulated only in one dataset. Undoubtedly, YTHDC2 expression is more convincing because data retrieved from multiple datasets showed high concordance. These indicated that YTHDC2 might be the potential tumor suppressor gene. YTHDF1, YTHDF2, and YTHDF3 might as well act as the potential oncogenes with a lower level of evidence.

Then, we explored whether the prognostic value of YTH proteins was in line with their expression trend. Only YTHDC1 passed this round of screening cause its lower expression was correlated with poorer prognosis with statistical significance when using OS, FP, and PPS as the endpoints of survival. While higher expression of YTHDF1, YTHDF2, and YTHDF3 was associated with better clinical outcome, which is in contradiction with their expression profiles in LUAD compared with normal lung tissue. These results pushed YTHDC2 to the foreground as a novel
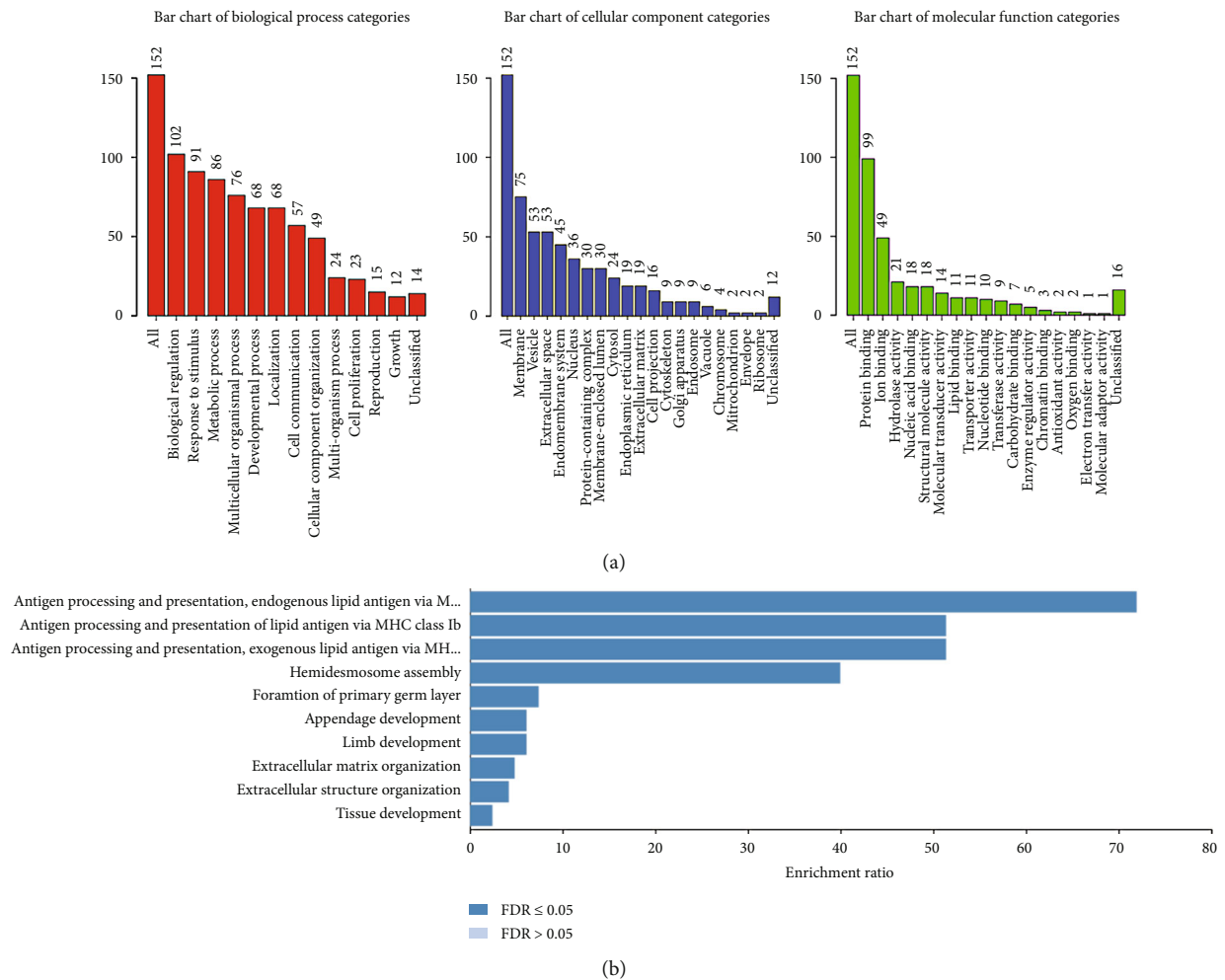
FIGURE 7: The biological pathway analysis of YTH family from WebGestalt database. (a) The biological process, cellular component, and molecular function which were associated with the YTH family were shown on the bar charts through Gene Ontology (GO) enrichment analysis. (b) Kyoto Encyclopedia of Genes and Genome (KEGG) enrichment analysis of YTH family.

potential target gene against LUAD. Of course, more solid evidence from experiments is needed.

To date, the role of YTHDF2 in lung cancer (especially in LUAD) remains to be further explored. YTHDC2 can promote 6PGD mRNA translation in lung cancer cells by means of m6A modification. We made a horizontal comparison of YTHDC2 in different types of cancer. Unlike the low expression of YTHDC2 in LUAD, YTHDC2 expression was increased in liver cancer and positively related to tumor malignancy [39]. Whereas opposite evidence of YTHDC2 as a tumor suppressor gene is also reported in liver cancer [35], covering the underneath mechanisms a heterogeneous veil. In addition, YTHDC2 exerts a promoting role in the colorectal cancer metastasis through the hypoxia/HIF-1α/Twist1 signaling pathway [40]. Our study also for the first time suggested that smoking habits may negatively reflect the expression of YTHDC2 level in LAUD patients. Further investigations based on it may have the opportunities to make breakthrough in targeted drug development and precision medicine of LAUD with smoking habit.

The functional enrichment analysis [41] in this study screens out the biological process and functional interpretation of genes around the YTH family, which further broaden our understanding of the role of the YTH family in the pathophysiological process of LUAD. The major functions of the YTH family seem to point in the direction of immunomodulation, especially antigen processing and presentation. This was in accordance with the finding of a published paper, showing that gene signature of antigen processing and presentation machinery may predict the therapeutic effect of immune checkpoint inhibitors such as anti-PD-1/PD-L1 [42]. Another study gave a similar conclusion that impaired antigen processing and presentation may account for the acquired resistance of immune checkpoint inhibitors and thus led to treatment failure [43] in lung cancer. Therefore, the relationship between the YTH family and antigen processing and presentation in LUAD is worthy of further exploration.

m6A methylation has been reported to play essential roles in tumor immunity. Furthermore, profiles of immune cells infiltration in tumor could act as novel biomarkers that effectively improved the diagnosis and prognosis of many
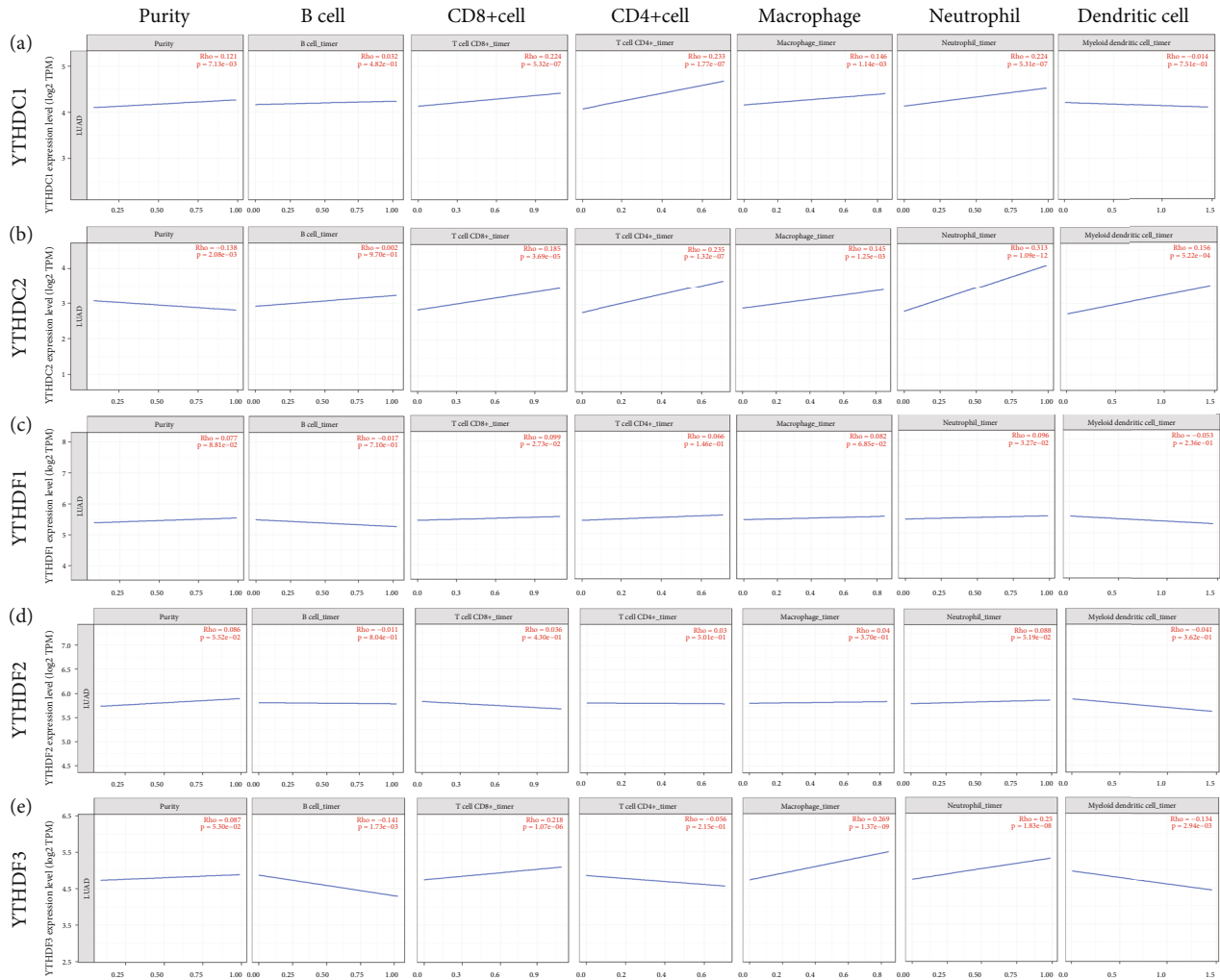
FIGURE 8: The correlation between immune cell infiltration and each YTH domain family member. The TIMER2.0 database was applied to explore the role of (a) YTHDC1, (b) YTHDC2, (c) YTHDF1, (d) YTHDF2, and (e) YTHDF3 in different immune cell infiltration (CD4+ T cells, CD8+ T cells, B cells, dendritic cells, macrophages, and neutrophils) around LUAD.

types of cancer [44, 45]. Our study found that in LUAD, most of the YTH family members were significantly correlated with the infiltration of CD4+ T cells, CD8+ T cells, macrophages, and neutrophils. A previous study presented that CD4+ T cells and CD8+ T cells were generally believed to control cancer outcome, while macrophages and neutrophils produce various factors that induce inflammation and stimulus tumor progression [46]. Taken together, the abnormal expression of YTH family members (especially YTHDC2) may alter the profiles of immune cell infiltration in LUAD through some kinds of specific mechanisms, thus influence the clinical outcome and the therapeutic effect of immunotherapy.

However, there were several limitations in our work. Our analysis in this study was mostly based on the data from the online databases, and further laboratory experiments were needed to verify these conclusions. Moreover, further research into the specific molecular mechanisms and molecules interactions would be needed in the future.

5. Conclusions

In conclusion, the molecular and expression profiles of the YTH family were dysregulated in LUAD. YTH family members (especially YTHDC2) are promising biomarkers and potential therapeutic targets that may bring benefit for patients with LUAD.

Data Availability

The original contributions presented in the study are included in the article/Supplementary Material, and further inquiries can be directed to the corresponding authors.

Conflicts of Interest

The authors declare no conflict of interest.

Authors' Contributions

Acknowledgments

Supplementary Materials

Supplementary 1. Supplementary Figure S1: the prognostic effect of YTHDC2 on smoking and nonsmoking patients with LUAD using Kaplan-Meier plotter.

Supplementary 2. Supplementary Table S1: summary of bioinformatics databases used in this study for analyzing the role of the YTH domain family in LUAD.

Supplementary 3. Supplementary Table S2: the YTH domain family associated coexpressed genes in LUAD.

Supplementary 4. Supplementary Table S3: the association between the expression of individual YTH family members and clinical characters in LUAD patients.

References

[1] E. N. Imyanitov, A. G. Iyevleva, and E. V. Levchenko, "Molecular testing and targeted therapy for non-small cell lung cancer: current status and perspectives," *Critical Reviews in Oncology/Hematology*, vol. 157, p. 103194, 2021.

[2] K. Zhu, L. Chen, C. He et al., "Prediction of pleural invasion in challenging non-small-cell lung cancer patients using serum and imaging markers," *Disease Markers*, vol. 2020, Article ID 6430459, 6 pages, 2020.

[3] Z. Q. Chen, L. S. Huang, and B. Zhu, "Assessment of seven clinical tumor markers in diagnosis of non-small-cell lung cancer," *Disease Markers*, vol. 2018, Article ID 9845123, 7 pages, 2018.

[4] E. L. Schenk, T. Patil, J. Pacheco, and P. A. Bunn, "2020 innovation-based optimism for lung cancer outcomes," *The Oncologist*, vol. 26, pp. e454–e472, 2021.

[5] T. Sun, R. Wu, and L. Ming, "The role of m6A RNA methylation in cancer," *Biomedicine & Pharmacotherapy*, vol. 112, p. 108613, 2019.

[6] Y. Yan, Z. Xu, Z. Li, L. Sun, and Z. Gong, "An insight into the increasing role of lncRNAs in the pathogenesis of gliomas," *Frontiers in Molecular Neuroscience*, vol. 10, p. 53, 2017.

[7] Z. Xu, Y. Yan, L. Qian, and Z. Gong, "Long non-coding RNAs act as regulators of cell autophagy in diseases (review)," *Oncology Reports*, vol. 37, no. 3, pp. 1359–1366, 2017.

[8] S. R. Jaffrey and M. G. Kharas, "Emerging links between m6A and misregulated mRNA methylation in cancer," *Genome Medicine*, vol. 9, no. 1, p. 2, 2017.

[9] S. Panneerdoss, V. K. Eedunuri, P. Yadav et al., "Cross-talk among writers, readers, and erasers of m6A regulates cancer growth and progression," *Science Advances*, vol. 4, no. 10, article eaar8263, 2018.

[10] X. Zhao, Y. Chen, Q. Mao et al., "Overexpression of YTHDF1 is associated with poor prognosis in patients with hepatocellular carcinoma," *Cancer Biomarkers*, vol. 21, no. 4, pp. 859–868, 2018.

[11] J. Chen, Y. Sun, X. Xu et al., "YTH domain family 2 orchestrates epithelial-mesenchymal transition/proliferation dichotomy in pancreatic cancer cells," *Cell Cycle*, vol. 16, no. 23, pp. 2259–2271, 2017.

[12] J. J. He, Z. Li, Z. X. Rong et al., "m6A reader YTHDC2 promotes radiotherapy resistance of nasopharyngeal carcinoma via activating IGF1R/AKT/S6 signaling axis," *Frontiers in Oncology*, vol. 10, p. 1166, 2020.

[13] Z. Tang, B. Kang, C. Li, T. Chen, and Z. Zhang, "GEPIA2: an enhanced web server for large-scale expression profiling and interactive analysis," *Nucleic Acids Research*, vol. 47, no. W1, pp. W556–W560, 2019.

[14] Á. Bartha and B. Győrffy, "TNMplot.com: a web tool for the comparison of gene expression in normal, tumor and metastatic tissues," *International Journal of Molecular Sciences*, vol. 22, no. 5, p. 2622, 2021.

[15] J. Li, K. Hu, D. He, L. Zhou, Z. Wang, and Y. Tao, "Prognostic value of PLXND1 and TGF-β1 coexpression and its correlation with immune infiltrates in hepatocellular carcinoma," *Frontiers in Oncology*, vol. 10, p. 604131, 2020.

[16] D. S. Chandrashekar, B. Bashel, S. A. H. Balasubramanya et al., "UALCAN: a portal for facilitating tumor subgroup gene expression and survival analyses," *Neoplasia*, vol. 19, no. 8, pp. 649–658, 2017.

[17] B. Gyorffy, A. Lánczky, and Z. Szállási, "Implementing an online tool for genome-wide validation of survival-associated biomarkers in ovarian-cancer using microarray data from 1287 patients," *Endocrine-Related Cancer*, vol. 19, no. 2, pp. 197–208, 2012.

[18] J. Gao, B. A. Aksoy, U. Dogrusoz et al., "Integrative analysis of complex cancer genomics and clinical profiles using the cBioPortal," *Science Signaling*, vol. 6, no. 269, p. pl1, 2013.

[19] J. Li, K. Hu, L. Zhou et al., "Spectrum of mesenchymal-epithelial transition aberrations and potential clinical implications: insights from integrative pancancer analysis," *Frontiers in Oncology*, vol. 10, p. 560615, 2020.

[20] D. Szklarczyk, J. H. Morris, H. Cook et al., "The STRING database in 2017: quality-controlled protein-protein association networks, made broadly accessible," *Nucleic Acids Research*, vol. 45, no. D1, pp. D362–D368, 2017.

[21] D. Szklarczyk, A. L. Gable, K. C. Nastou et al., "The STRING database in 2021: customizable protein-protein networks, and functional characterization of user-uploaded gene/measurement sets," *Nucleic Acids Research*, vol. 49, no. D1, pp. D605–D612, 2021.

[22] N. T. Doncheva, J. H. Morris, J. Gorodkin, and L. J. Jensen, "Cytoscape StringApp: network analysis and visualization of proteomics data," *Journal of Proteome Research*, vol. 18, no. 2, pp. 623–632, 2019.

[23] Y. Liao, J. Wang, E. J. Jaehnig, Z. Shi, and B. Zhang, "WebGestalt 2019: gene set analysis toolkit with revamped UIs and APIs," *Nucleic Acids Research*, vol. 47, no. W1, pp. W199–W205, 2019.

[24] T. Li, J. Fu, Z. Zeng et al., "TIMER2.0 for analysis of tumor-infiltrating immune cells," *Nucleic Acids Research*, vol. 48, no. W1, pp. W509–W514, 2020.

[25] W. Sun, H. Shi, Z. Yuan et al., "Prognostic value of genes and immune infiltration in prostate tumor microenvironment," *Frontiers in Oncology*, vol. 10, p. 584055, 2020.

[26] H. C. Wang, L. P. Chan, and S. F. Cho, "Targeting the immune microenvironment in the treatment of head and neck squamous cell carcinoma," *Frontiers in Oncology*, vol. 9, p. 1084, 2019.

[27] H. Liao, W. Chen, Y. Dai et al., "Expression of programmed cell death-ligands in hepatocellular carcinoma: correlation with immune microenvironment and survival outcomes," *Frontiers in Oncology*, vol. 9, p. 883, 2019.

[28] I. A. Roundtree, M. E. Evans, T. Pan, and C. He, "Dynamic RNA modifications in gene expression regulation," *Cell*, vol. 169, no. 7, pp. 1187–1200, 2017.

[29] Q. Lan, P. Y. Liu, J. L. Bell et al., "The emerging roles of RNA m6A methylation and demethylation as critical regulators of tumorigenesis, drug sensitivity, and resistance," *Cancer Research*, vol. 81, no. 13, pp. 3431–3440, 2021.

[30] W. Li, J. Liu, Z. Ma, X. Zhai, B. Cheng, and H. Zhao, "m6A RNA methylation regulators elicit malignant progression and predict clinical outcome in hepatocellular carcinoma," *Disease Markers*, vol. 2021, Article ID 8859590, 12 pages, 2021.

[31] Y. Zhou, Z. Yin, B. Hou et al., "Expression profiles and prognostic significance of RNA N6-methyladenosine-related genes in patients with hepatocellular carcinoma: evidence from independent datasets," *Cancer Management and Research*, vol. - Volume 11, pp. 3921–3931, 2019.

[32] X. Lin, G. Chai, Y. Wu et al., "RNA m6A methylation regulates the epithelial mesenchymal transition of cancer cells and translation of Snail," *Nature Communications*, vol. 10, no. 1, p. 2065, 2019.

[33] X. Liu, J. Qin, T. Gao et al., "YTHDF1 facilitates the progression of hepatocellular carcinoma by promoting FZD5 mRNA translation in an m6A-dependent manner," *Molecular Therapy-Nucleic Acids*, vol. 22, pp. 750–765, 2020.

[34] C. Zhang, S. Huang, H. Zhuang et al., "YTHDF2 promotes the liver cancer stem cell phenotype and cancer metastasis by regulating OCT4 expression via m6A RNA methylation," *Oncogene*, vol. 39, no. 23, pp. 4507–4518, 2020.

[35] L. Zhong, D. Liao, M. Zhang et al., "YTHDF2 suppresses cell proliferation and growth via destabilizing the EGFR mRNA in hepatocellular carcinoma," *Cancer Letters*, vol. 442, pp. 252–261, 2019.

[36] T. Liu, Q. Wei, J. Jin et al., "The m6A reader YTHDF1 promotes ovarian cancer progression via augmenting EIF3C translation," *Nucleic Acids Research*, vol. 48, no. 7, pp. 3816–3831, 2020.

[37] H. Sheng, Z. Li, S. Su et al., "YTH domain family 2 promotes lung cancer cell growth by facilitating 6-phosphogluconate dehydrogenase mRNA translation," *Carcinogenesis*, vol. 41, no. 5, pp. 541–550, 2020.

[38] Y. Shi, S. Fan, M. Wu et al., "YTHDF1 links hypoxia adaptation and non-small cell lung cancer progression," *Nature Communications*, vol. 10, no. 1, p. 4892, 2019.

[39] Z. Yang, J. Li, G. Feng et al., "MicroRNA-145 modulates N^6-methyladenosine levels by targeting the $3'$-untranslated mRNA region of the N^6-methyladenosine binding YTH

[40] A. Tanabe, K. Tanikawa, M. Tsunetomi et al., "RNA helicase YTHDC2 promotes cancer metastasis via the enhancement of the efficiency by which *HIF-1 α* mRNA is translated," *Cancer Letters*, vol. 376, no. 1, pp. 34–42, 2016.

[41] Gene Ontology Consortium, "The gene ontology resource: 20 years and still GOing strong," *Nucleic Acids Research*, vol. 47, no. D1, pp. D330–D338, 2019.

[42] J. C. Thompson, C. Davis, C. Deshpande et al., "Gene signature of antigen processing and presentation machinery predicts response to checkpoint blockade in non-small cell lung cancer (NSCLC) and melanoma," *Journal for Immunotherapy of Cancer*, vol. 8, no. 2, p. e000974, 2020.

[43] S. Gettinger, J. Choi, K. Hastings et al., "Impaired HLA class I antigen processing and presentation as a mechanism of acquired resistance to immune checkpoint inhibitors in lung cancer," *Cancer Discovery*, vol. 7, no. 12, pp. 1420–1435, 2017.

[44] R. Zhou, J. Zhang, D. Zeng et al., "Immune cell infiltration as a biomarker for the diagnosis and prognosis of stage I-III colon cancer," *Cancer Immunology, Immunotherapy*, vol. 68, no. 3, pp. 433–442, 2019.

[45] F. Klemm, R. R. Maas, R. L. Bowman et al., "Interrogation of the microenvironmental landscape in brain tumors reveals disease-specific alterations of immune cells," *Cell*, vol. 181, no. 7, pp. 1643–1660.e17, 2020, e17.

[46] Y. Wang, J. Dong, Q. Quan et al., "Immune cell infiltration of the primary tumor microenvironment predicted the treatment outcome of chemotherapy with or without bevacizumab in metastatic colorectal cancer patients," *Frontiers in Oncology*, vol. 10, p. 3181, 2020.

domain family 2 protein," *The Journal of Biological Chemistry*, vol. 292, no. 9, pp. 3614–3623, 2017.

Research Article

Ethacrynic Acid Enhances the Antitumor Effects of Afatinib in EGFR/T790M-Mutated NSCLC by Inhibiting WNT/Beta-Catenin Pathway Activation

Xuehui Zhang [iD],[1] **Chaoyuan Huang** [iD],[2] **Biyu Cui,**[3] **Yebin Pang,**[4] **Rong Liang,**[5] **and Xiaoling Luo** [iD][6]

[1]*Department of Nuclear Medicine, The Ninth Affiliated Hospital of Guangxi Medical University, Beihai People's Hospital, Beihai, Guangxi, China*
[2]*Department of Oncology, The Third Affiliated Hospital of Guangxi Medical University, Nanning, Guangxi, China*
[3]*Department of Endocrinology, The Affiliated LiuTie Central Hospital of Guangxi Medical University, Liuzhou, China*
[4]*Department of Gynecological Oncology, GuangXi Medical University Cancer Hospital, Nanning, Guangxi, China*
[5]*Department of Digestive Oncology, GuangXi Medical University Cancer Hospital, Nanning, Guangxi, China*
[6]*Research Department, GuangXi Medical University Cancer Hospital, Nanning, Guangxi, China*

Correspondence should be addressed to Xiaoling Luo; luoxiaoling67@126.com

Background. Despite afatinib as a new first-line treatment for EGFR L858R and exon 19 deletion or other rare EGFR-mutation patients, the acquired resistance or toxic effects associated with it limited its use clinically. The controlling of acquired resistance or optimization of the afatinib dosage in EGFR/T790M mutation-positive non-small-cell lung cancer (NSCLC) is still an important fundamental problem. Ethacrynic acid (EA) has been proved as a dual inhibitor of GST and WNT, and the α, β-unsaturated-keto structure of it is similar to that of irreversible tyrosine kinase inhibitors (TKIs). However, these beneficial effects of EA combined with afatinib have never been reported in NSCLC. Therefore, the antitumor effects of afatinib combined with EA in EGFR L858R/T790M-mutated NSCLC cells and related mechanisms were analyzed. Our *in vitro* and *in vivo* results showed that EA has strong synergistic antitumor effects with afatinib in EGFR L858R/T790M-mutated NSCLC cells, but has no cytotoxic effects in NSCLC cells when used it alone, i.e., the cytotoxic effects of afatinib (IC30) plus EA (IC30) were stronger than the effects of afatinib (IC50) alone. Our functional studies found that the antitumor mechanisms of afatinib when combined with EA mainly occurred by inhibiting WNT/β-catenin pathway activation and suppression of the secretion of anti-inflammatory factors. These results revealed that combination of afatinib with EA derivatives not only provided a new therapeutic approach for EGFR/T790M-mutated NSCLC patients but also offered a new idea for developing new drugs or optimizing the dose of afatinib in clinical use in future antitumor therapy.

1. Introduction

Lung cancer is the most prevalent and lethal type of cancer worldwide, and approximately 80% of all these cases are non-small-cell lung cancer (NSCLC). It is estimated that 135,720 (72,500 men and 63,220 women) deaths occur due to this disease in the year 2020 based on the report of *Cancer Statistics* [1]. Unfortunately, most of the lung cancer patients (about 50%) are diagnosed at advanced stages and have metastatic cancer, missing the opportunity of surgical treatment [2]. Although epithelial growth factor receptor (EGFR) mutation-positive advanced/recurrence NSCLC can receive

EGFR tyrosine kinase inhibitors (TKIs) as a promising targeted treatment; their 5-year relative survival rate is just 5% after treatment [1]. This meant that the current treatment strategies are not effective in suppressing the lung cancers. Thus, how to improve the therapeutic efficiency and prolong survival time is an urgent problem to be solved in lung cancer.

Afatinib is an irreversible, second-generation tyrosine kinase inhibitors (TKIs) and an effective first-line treatment strategy for patients with EGFR-mutant NSCLC [3]. Recent data from real-world studies and LUX-Lung 8 together revealed that afatinib has not only a good response rate and could prolong median progression-free survival (PFS) rate at 12 months but also benefit patients with rare or complex EGFR mutations and symptomatic brain metastases [4–7]. Moreover, a recent study showed that sequential treatment with afatinib and osimertinib in patients with EGFR-T790M mutant NSCLC demonstrated an overall median survival time of 27.6 months after treatment, 30.3 months in Del19-positive patients, and 46.7 months in Asians. Additionally, the 2-year overall survival (OS) rate is 78.9% [8]. These findings proved afatinib as a potent and highly selective drug for treating NSCLC in patients. Afatinib treatment is widely accepted due to its inhibition of epidermal growth factor receptors 1 (ErbB1; EGFR), 2 (ErbB2; HER2), and 4 (ErbB4; HER4) and certain EGFR mutants, including those caused by EGFR exon 19 deletion mutations or exon 21 (L858R) mutations. It is also associated with severe side effects in one-tenth of patients, and the most common side effects were diarrhea, paronychia, and fatigue [5, 9]. Additionally, similar to the first-generation TKIs, EGFR T790M mutation is regarded as the major mechanism of acquired resistance to afatinib [10]. Hence, it is essential to find new strategies to improve the therapeutic effects of afatinib and overcome acquired resistance or side effects.

Ethacrynic acid (EA) is a diuretic agent clinically and has been confirmed to act as a WNT and GST inhibitor. It has selective toxicity against chronic lymphocytic leukemia cells [11], multiple myeloma [12], and pancreatic cancer [13]. Recently, EA has been reported to have synergistic antitumor effects in breast cancer when combined with irreversible EGFR TKIs [14]. Moreover, one study revealed that β-catenin of the classical WNT pathway contributed to the development of lung tumors induced by EGFR-T790M mutations, and genetic deletion of β-catenin gene dramatically reduced lung tumor formation in EGFR-L858R-T790M transgenic mice [15]. These findings revealed EA as a WNT inhibitor and could help to resolve the problem of EGFR-TKI's acquired resistance. However, the antitumor effects of EA combined with afatinib in NSCLC have never been studied. Thus, we aimed to explore whether EA could enhance the antitumor effects of afatinib in NSCLC and reveal the relative mechanism.

2. Materials and Methods

2.1. Cell Lines and Cell Culture.
The human NSCLC cell lines A549 and H1975 were purchased from the Cell Biology of Chinese Academy of Science (Shanghai, China). The cells were cultured in RPMI-1640 (Gibco, USA) supplemented with 10% fetal bovine serum (BIOIND, Israel), 100 μg/ml streptomycin and 100 U/ml penicillin (Gibco, USA) at 37°C in a humidified 5% CO_2. The cells were passaged every 2-3 days by 0.25% trypsin (Gibco) and not cultured for more than 3 months.

2.2. Cytotoxicity Assay.
CCK8 assay was used to detect the drug cytotoxic effects. Briefly, the cells at a density of 5×10^3/well were plated in a 96-well plate and incubated for 24 h followed by treatment with afatinib with or without EA for 48 h. Next, the cells were stained with CCK8 (Dojindo, Japan) for 2 h. The absorbance was then measured at 450 nm using a microplate reader (Thermo, USA).

2.3. Drugs and Reagents.
Afatinib and EA were obtained from Melone Pharmaceutical Company (China) and Sigma (USA). These substances were diluted in DMSO and stocked at a concentration of 10 mm for afatinib and 100 mm for EA. These were diluted to five different concentrations to stimulate cells. The IC50 value was analyzed based on the data of cytotoxic effects after treatment for 48 hours at this time point. Additionally, the synergistic effect of the two drugs or the coefficient of drug interaction (CDI) was analyzed using the Calcusyn software [16]. CDI less than 0.7 (CDI < 1) indicates a significant synergistic effect; CDI = 1 represents that the two drugs have an additive effect; and CDI > 1 represents that the two drugs have antagonistic effects.

2.4. Cell Cycle and Apoptosis.
The cells at a concentration of 2×10^5/ml/well were plated in a 6-well plate and incubated overnight. The cells were treated with afatinib with EA or EA alone for 48 h. The cells were then harvested for the following analysis. The cells were fixed in 75% ethanol for overnight at 4°C and centrifugation followed by washing with cold PBS three times and treatment with 50 μl of RNase A at a final concentration of 100 μg/ml for 1 h at room temperature for cell cycle analysis. Propidium iodide staining buffer (PI, final concentration is 50 μg/ml) (Shanghai Yuanmu Biological Technology Co. Ltd, China) was then added to each well until it reaches a final volume of 500 ml. The cell cycle was then analyzed by flow cytometry (Beckman Counter, USA). Cell apoptosis was detected using an apoptosis Kit (Becton-Dickinson, USA) according to the kit protocol. After treatment with afatinib and with/without EA for 48 h, the cells and the supernatant were collected, incubated with FITC Annexin V and PI for 30 min, and measured using FACS Calibur flow cytometer (Becton-Dickinson, USA).

2.5. Animal Study.
Male BALB/C nude mice (4-5 weeks old, 16-20 g) were obtained from Guangxi Medical University (Nanning, China) and housed in Guangxi Medical University Laboratory Animal Center (Nanning, China). All animal experiments were conducted according to the Guangxi Medical College Animal Care Committee's ethical and animal experiment regulations. For tumor cell inoculation, A549 or H1975 cells (8×10^6 cells were suspended in 100 μl PBS) were injected subcutaneously into the left flank to produce subcutaneous tumors. The tumor-bearing mice, those that did not form tumors or the smallest tumors were removed, were randomly divided into four groups (six mice per group)

when the tumor size reached to 150 to 200 mm^3: (1) control group (100 μl PBS); (2) afatinib group (25 mg/kg/daily); (3) EA group (20 mg/kg/daily); and (4) afatinib+EA group (25 mg/kg/daily + 20 mg/kg/daily) [14, 17]. All mice were treated with the above-mentioned drugs by intragastric administration for 3 weeks. Finally, the tumor size and body weight were measured according to the formula Tumor volume = 0.5 × length × width^2.

2.6. RNA Extraction and Quantitative RT-PCR. Total RNA was extracted using trizol reagent (Invitrogen, Carlsbad, CA, USA) according to the manufacturer's instructions. cDNAs were synthesized using the ReverTra Ace qPCR RT kit (FSQ-101; Toyobo, Kagoshima, Japan). Real-time PCR analyses were performed with Thunderbird SYBR qPCR mix (QPS-201; Toyobo) on an MxPro Mx3000P Sequence Detection system (Stratagene, La Jolla, CA, USA). β-Catenin was used as an internal normalized reference, and fold changes were calculated by relative quantification ($2^{-\Delta\Delta Ct}$). The primer sequences are shown in supplemental Table 1.

2.7. Western Blotting. EGFR, WNT7B, β-catenin, RET, and GAPDH were purchased from Cell Signaling Technology (CST). The cells were harvested and lysed with RIPA protein extraction reagent supplemented with protease inhibitor cocktail. The protein concentrations were measured using the BCA assay (Pierce, CA, USA). Equal amounts of extracts were loaded and separated by electrophoresis on 8-10% SDS-PAGE and transferred onto nitrocellulose membranes (Bio-Rad). The membranes were blocked for 1 h at room temperature in Tris-buffered saline/0.1% Tween 20 (TBST) containing 5% (wt/vol) nonfat milk and then incubated with primary antibodies in TBST containing 5% (wt/vol) nonfat milk or 5% (wt/vol) BSA at 4°C overnight. The membranes were then incubated with an appropriate secondary antibody coupled to horseradish peroxidase, and the proteins were detected by ECL Supersignal West Pico Chemiluminescence Kit (Thermo Fisher Scientific).

2.8. RNA Sequencing and Data Analysis. The H1975 NSCLC cells after treatment with different drugs for 24 h were sent to Yucebio Company (Shenzhen, China) and underwent RNA sequence analysis. Meanwhile, for differential gene expression analysis, Gene Ontology (GO) and Kyoto Encyclopedia of Genes and Genomes (KEGG) pathways were analyzed. Briefly, differential expression analysis was performed using the DESeq (V1.6.3) and EdgeR (V3.4.6) Bioconductor package. The data were adjusted using the Benjamini and Hochberg approach for controlling the false discovery rate. The p value was set to $p < 0.05$ to detect the differentially expressed genes (DEGs). KEGG pathway analysis was used to harvest the pathway clusters of molecular interaction and reaction networks in differentially regulated gene profiling. In the present study, significant pathways were identified as those with a fold change of ≥2 and p values of <0.05.

2.9. Statistical Analysis. Data were presented as means ± standard deviation (S.D.) of one representative experiment. Unless otherwise noted, statistically significant differences were analyzed by one-way analysis of variance (ANOVA) when there were more than two groups. All analyses were performed using GraphPad Prism 8. In all analyses, $p < 0.05$ was considered as statistical significance.

3. Results

3.1. The Validation of the Cytotoxic Effects of Afatinib and EA in NSCLC Cells. To assess the cytotoxic effects of afatinib or EA on NSCLC cell lines, A549 cells (EGFR^{WT}) and H1975 cells (EGFR$^{L858R/T790M}$ mutation) were used. As shown in Figures 1(b) and 1(c), afatinib significantly inhibited the growth of NSCLC cells (A549 and H1975), and this inhibition was increased correspondingly with increasing drug concentrations and time. However, low concentrations of EA promoted H1975 cell proliferation even though high concentration of EA exerted cytotoxic effects in A549 cells and H1975 cells (Figures 1(d) and 1(e)). When the IC50 value was calculated using the data at 48 h, the results showed that the IC50 of EA in A549 or H1975 reached the highest to 87.03 μM or 99.54 μM, respectively (Figures 1(h) and 1(i)), indicating that the mean EA had little effect on NSCLC cells. In contrast, the cytotoxic effects of afatinib with EA were more significant in EGFR-L858R-mutated H1975 cells (IC50 = 5.03 μM) than that in EGFR-WT A549 cells (IC50 = 6.37 μM). These findings suggested that L858R-EGFR-mutated NSCLC cells were more sensitive to afatinib than WT-EGFR cells.

3.2. EA Combined with Afatinib Had Synergistic Cytotoxic Effects on EGFR$^{L858R/T790M}$-Mutated NSCLC Cells In Vitro. To further explore whether EA combined with afatinib has synergistic antitumor effects in NSCLC cells as previously reported in breast cancer [14], a dosage of IC30~50 of these two drugs was combined. As shown in Figures 2(a) and 2(b), EA combined with afatinib significantly inhibited H1975 cell proliferation when compared with afatinib alone, while this combination effect was not so obvious in EGFR-WT A549 cells. Besides these, Calcusyn software was used to analyze the combination drug index (CDI) in different cells. As shown in Table 1 and Figures 2(c) and 2(d), regardless of which concentration of EA (IC30–75μM or IC50–100μM) combined with 2 μM afatinib (IC30) or 6 μM afatinib (IC50), the CDI of afatinib combined with EA in H1975 cell was less than 0.2. On contrary, the CDI of afatinib plus EA in A549 cells was larger than 0.8, and even larger than 1 at times, which meant that they had antagonistic effects. These findings indicated that EA plays a synergistic role and enhanced the cytotoxic effects of afatinib in EGFR-mutated NSCLC cells.

3.3. Combination Treatment with EA and Afatinib Enhanced Antitumor Effects In Vivo. To evaluate whether combined treatment with EA and afatinib had stronger antitumor effects *in vivo*, A549 and H1975 NSCLC cells were implanted subcutaneously into the back of syngeneic Balb/c mice. When the tumor diameter of these reached to 5 mm, the mice were treated by intragastric administration with afatinib (25 mg/kg) alone or together with EA (20 mg/kg) for 3 weeks.
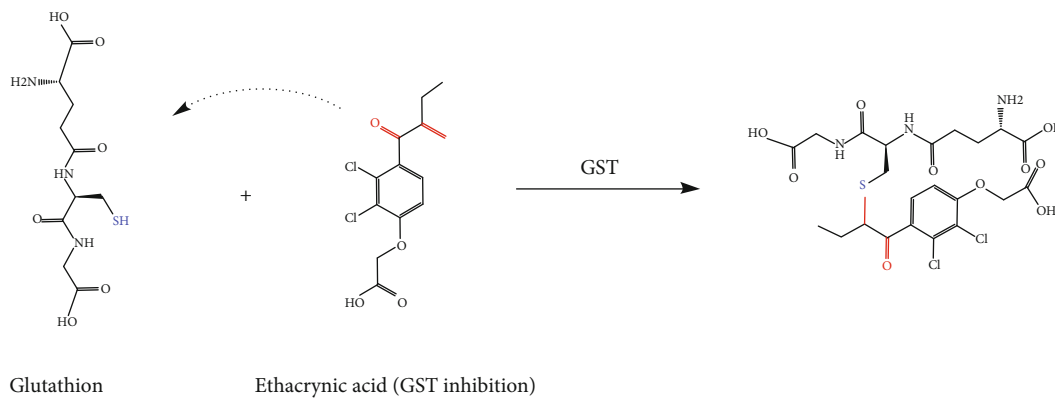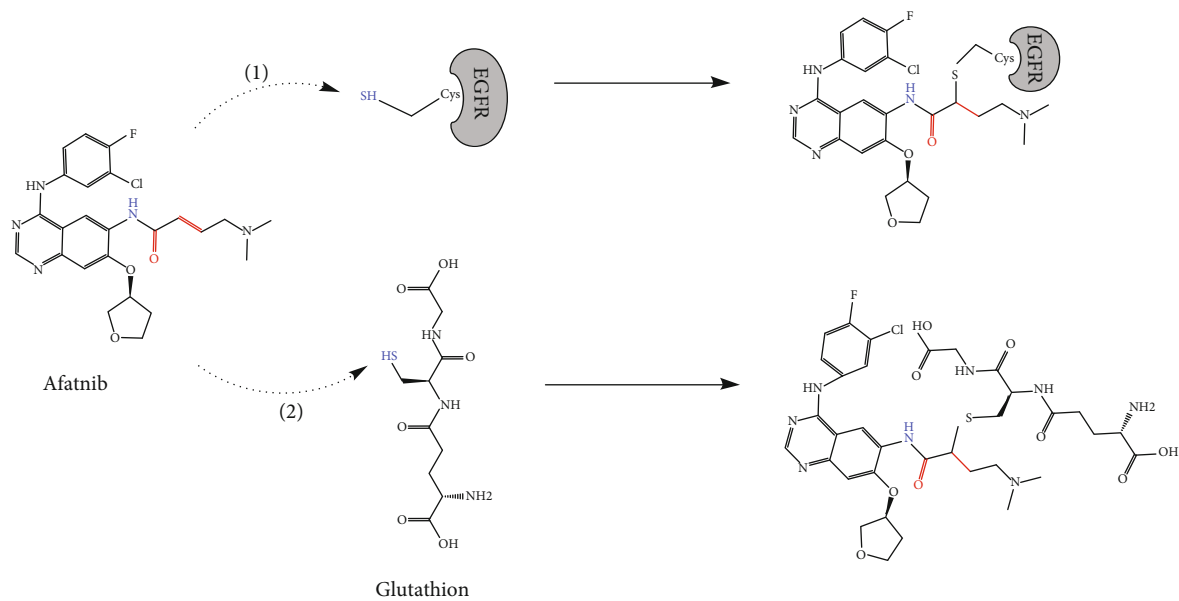
(a)
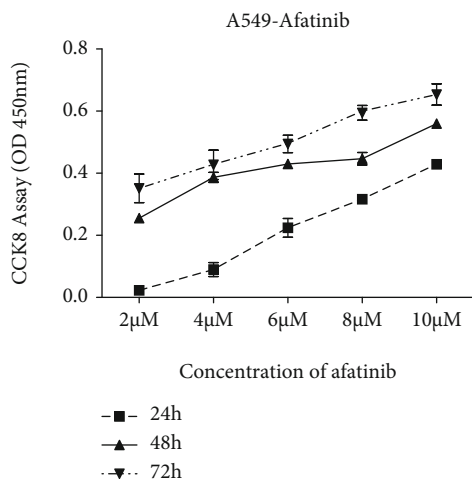
(b)
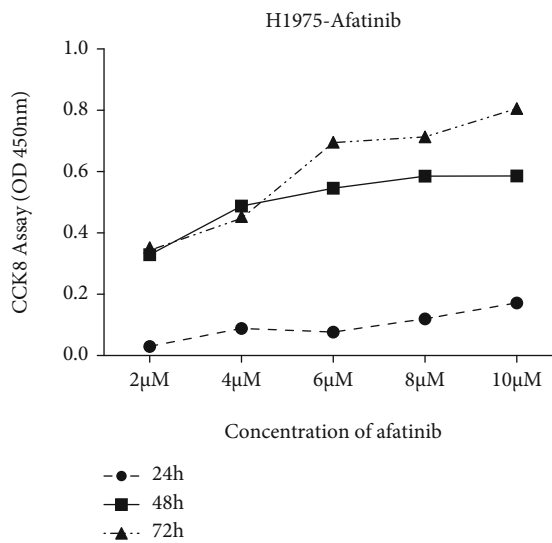
(c)

Figure 1: Continued.

(d)

(e)

(f)

(g)

(h)

(i)

FIGURE 1: The validation of cytotoxic effects of afatinib and EA in NSCLC cells. (a) Interaction between afatinib or ethacrynic acid and glutathione. (b–e) The cell proliferation of A549 or H1975 cells after treatment 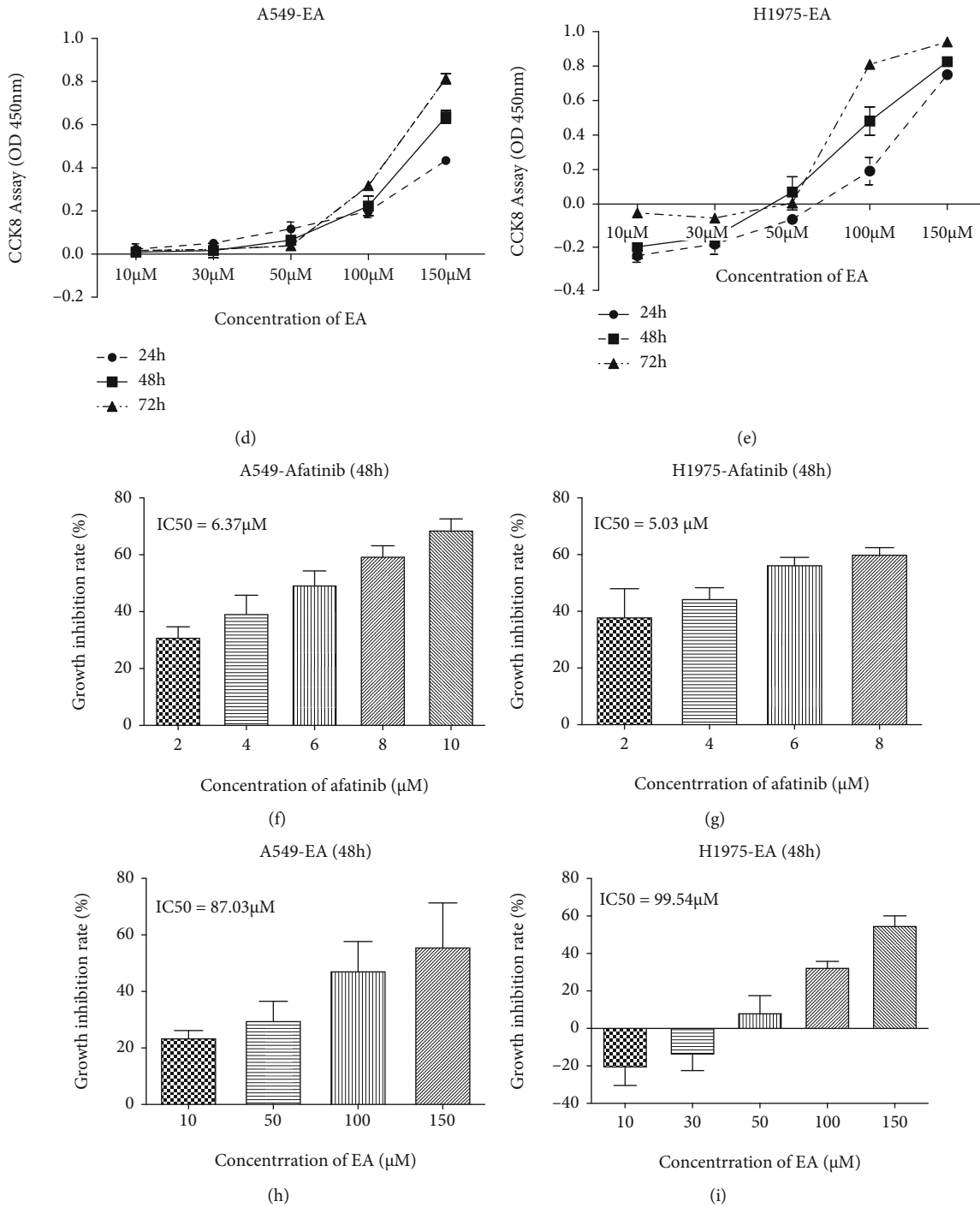with afatinib or EA at different time points. (f–i) IC50 value of afatinib or ethacrynic acid in different cells at 48 h. The IC50 value is the mean concentration of drug that reduced cell survival by 50%.

All the nude mice were put to death after anesthesia, the tumors were separated and weighed. The calculation formula of tumor inhibition rate is as follows: $(\mathrm{TW}_{\mathrm{Control\,group}} - \mathrm{TW}_{\mathrm{experimental\,group}})/\mathrm{TW}_{\mathrm{Control\,group}} \times 100\%$. The results as shown in Figure 3 and Table 2 revealed that the tumor rate in the combination group (84.12%) was significantly higher than that in the afatinib alone group (48.72%) in H1975-

tumor model, while the tumor inhibition rate in the combination group (69.76%) was increased slightly when compared to that in the afatinib group (51.75%).

3.4. EA Enhanced the Antitumor Effects of Afatinib by Inhibiting Cell Cycle Progression and Inducing Cell Apoptosis in EGFR L858R/T790M-Mutated NSCLC Cells. To investigate
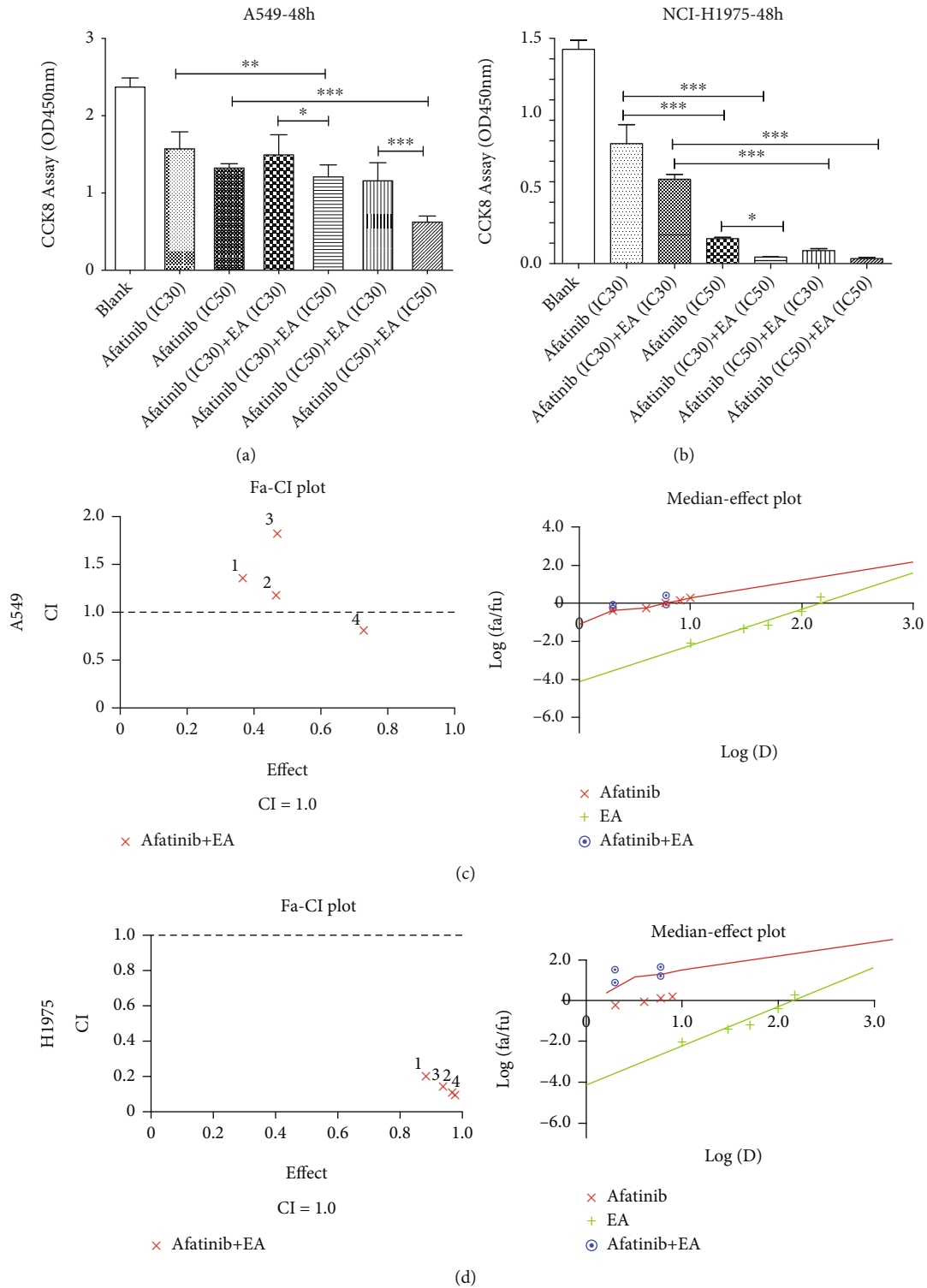
(a)

(b)

(c)

(d)

FIGURE 2: The effects of combination of EA and afatinib on A549 and H1975 cells. (a) The cytotoxic effects of afatinib combined with or without EA in A549 cells. (b) The cytotoxic effects of afatinib combined with or without EA in H1975 cells. The Calcusyn software was used to analyze the combination drug index (CDI) in A549 (c) or H1975 (d) cells. CI: coefficient index; Fa: the fraction affected by dose; Fu: The fraction unaffected; Fu = 1 − Fa. $^*p < 0.05$; $^{**}p < 0.01$; $^{***}p < 0.001$.

the effects of EA combined with afatinib on NSCLC cell function, a 30% ~50% inhibitory concentration of afatinib (6 μM) and EA (75 μM) was chosen for subsequent experiments. Thus, we examined if there were any changes in the cell cycle

and apoptotic rate that are associated with tumor cell growth. Cell cycle analysis revealed that EA combined with afatinib significantly reduced the G0/G1 phase (afatinib vs. afatinib +EA: 83.6% vs. 48.0%) and blocked the cell cycle at G2/M

TABLE 1: The coefficient index (CI) of afatinib combined with EA in NSCLC cells.

Drugs	A549 cell		H1975 cell	
	Fa	CI	Fa	CI
Combination 1: Afatinib (2 μM) + EA (75 μM)	0.366151	1.362	0.883641	0.200
Combination 2: Afatinib (2 μM) + EA (100 μM)	0.465099	1.182	0.969724	0.114
Combination 3: Afatinib (6 μM) + EA (75 μM)	0.471219	1.830	0.93933	0.146
Combination 4: Afatinib (6 μM) + EA (100 μM)	0.730376	0.812	0.97684	0.101

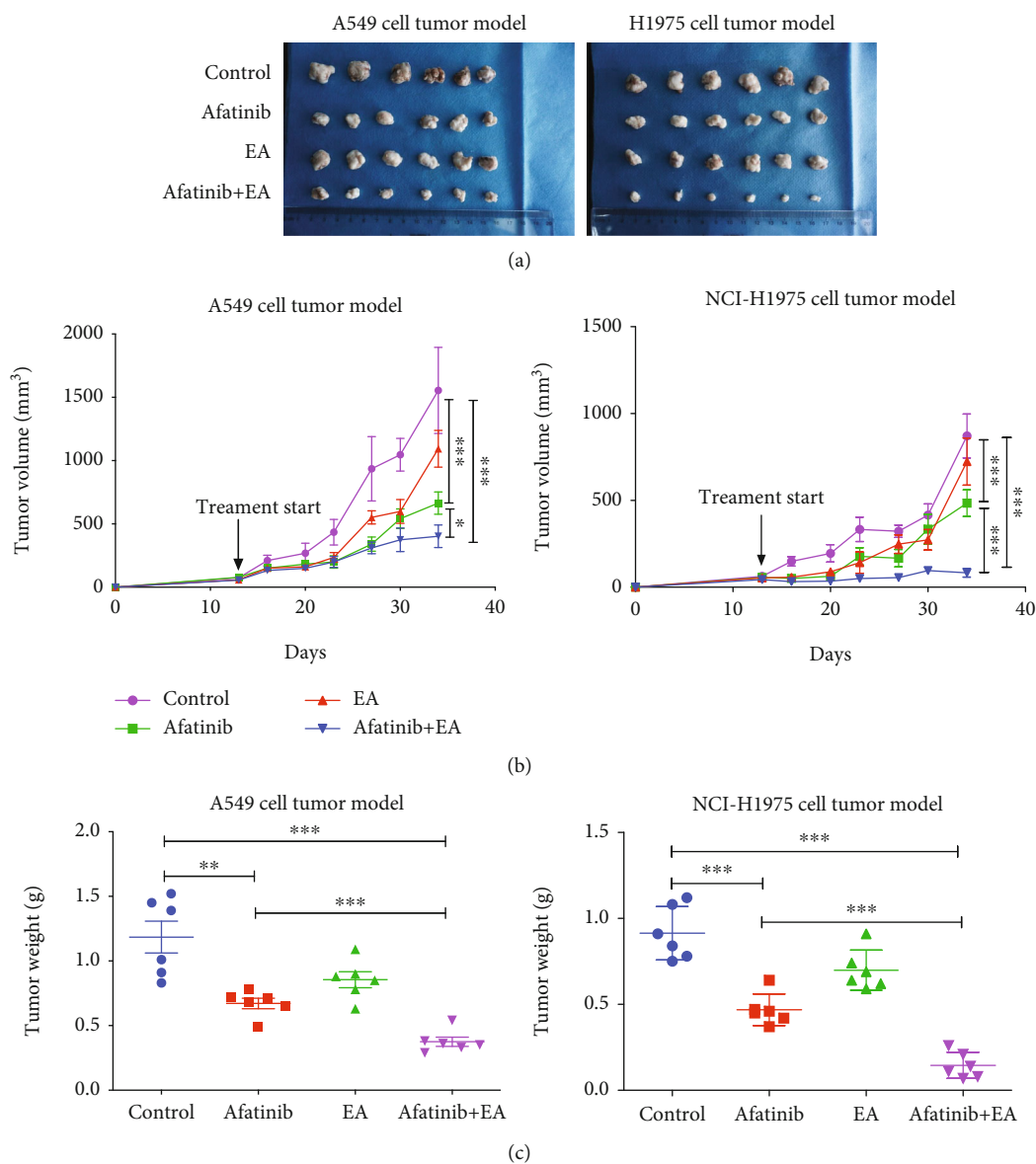CI: coefficient index; Fa: the fraction affected by dose; Fu: the unaffected fraction; Fu = 1 − Fa.

FIGURE 3: Combination of afatinib with EA suppressed tumor growth *in vivo*. (a) Image showing the method of tumor removal in a representative experiment. (b) The change in tumor volume of mice after treatment with different drugs. (c) Tumor weights of mice after treatment with different drugs. $^*p < 0.05$; $^{**}p < 0.01$; $^{***}p < 0.01$.

phase, controlling the cell division process (afatinib vs. afatinib +EA: 9.7% vs. 33.9%) (Figure 4). Additionally, apoptosis results revealed that the apoptotic rate of H1975 in EA combined with afatinib group was significantly higher than that in the afatinib alone group, and the apoptotic rate of combination group and afatinib alone was about 20% and 10%, respectively (Figure 5). However, the cell cycle results and apoptotic rate in the combination group showed no significant difference

TABLE 2: The antitumor effects of EA combined with afatinib *in vivo* ($n = 6$).

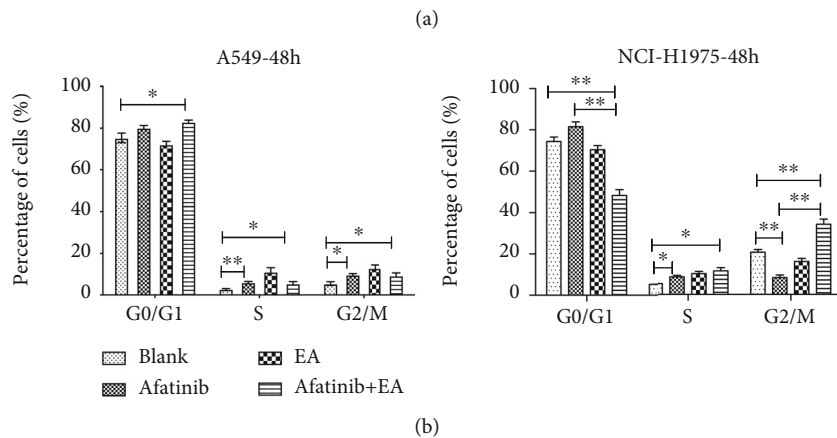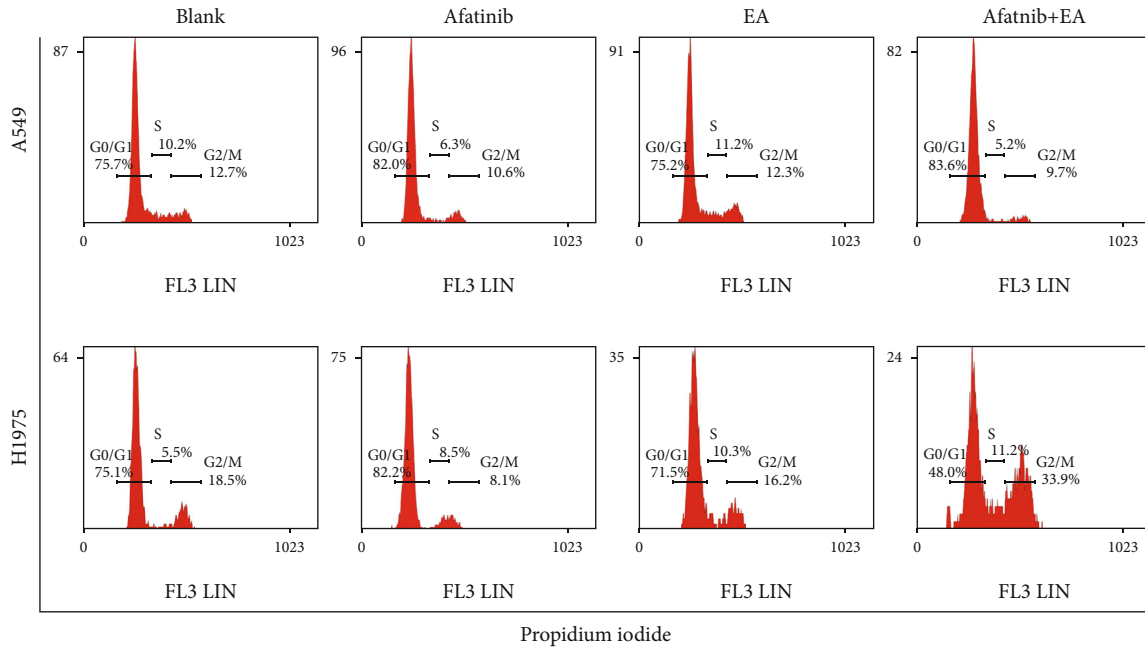| Group	A549		H1975	
	Tumor weight (mg)	Inhibition rate (%)	Tumor weight (mg)	Inhibition rate (%)
Control	1.18 ± 0.30	0	0.91 ± 0.16	0
Afatinib	0.57 ± 0.11	51.75 ± 9.17	0.47 ± 0.09	48.72 ± 10.02
EA	0.83 ± 0.12	29.25 ± 10.37	0.70 ± 0.12	23.54 ± 12.76
Afatinib+EA	0.36 ± 0.05	69.76 ± 4.25	0.15 ± 0.08	84.12 ± 8.27
F value	18.345		50.192	
p value	0.000		0.000	

(a)

(b)

FIGURE 4: The effect of combination afatinib with EA on cell cycle. (a) A549 and H1975 cells were treated with afatinib and with or without EA for 48 hours after the cells were harvested and analyzed by FACS. (b) The calculated cell cycle distribution. Data are presented as means ± SD ($n = 6$) of a representative experiment. Similar results were obtained in three experiments. $^*p < 0.05$; $^{**}p < 0.01$; $^{***}p < 0.001$.

when compared to afatinib alone group in A549 cells. These results were consistent with the results of tumor growth.

3.5. EA Enhanced the Antitumor Effects of Afatinib in NSCLC by Suppressing WNT/β-Catenin Pathway Activation. Previ-

ous studies have reported that EA acts as a dual inhibitor of GST and WNT, and afatinib can inhibit EGFR family, and so we examined whether the combination of EA and afatinib has enhanced antitumor effects in NSCLC by suppressing EGFR and WNT signaling pathways. The WNT proteins
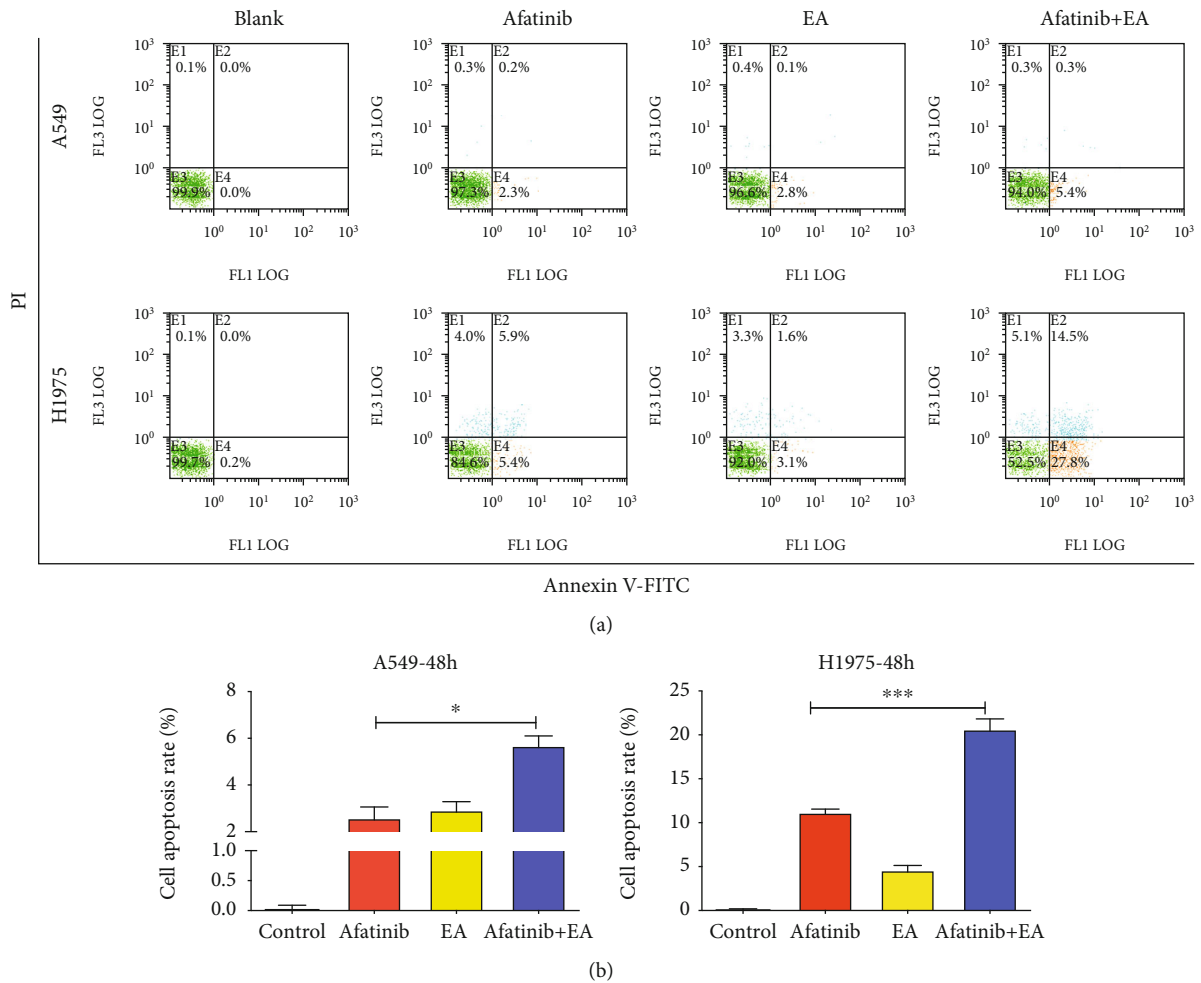
(a)

(b)

FIGURE 5: The effects of combination of afatinib with EA on cell apoptosis. (a) A549 and H1975 cells were treated with afatinib and with or without EA for 48 hours after the cells were harvested and analyzed by FACS. (b) The calculated cell cycle distribution. Data are shown as means ± SD ($n = 6$) of a representative experiment. Similar results were obtained in three experiments. $^*p < 0.05$; $^{**}p < 0.01$; $^{***}p < 0.001$.

were grouped as classical WNTs (WNT1) that activate the β-catenin-dependent (canonical) pathway and nonclassical WNTs (WNT5A) for inducing β-catenin-independent (non-canonical) signaling pathways [18]. The mRNA expression of EGFR and its downstream ERK1/2, WNT1, WNT5A, and β-catenin was detected in this study. As shown in Figure 6(a), compared to afatinib alone group, the combination of EA and afatinib has significantly cosuppressed the mRNA expression of EGFR/ERK1/2 and WNT1/β-catenin and WNT5A in H1975 cells, while there was no significant difference in the combination group when compared with the afatinib alone group in A549 cells. In addition, GST levels were also detected in this study using ELISA, but no matter what type of NSCLC cells, afatinib alone or combined treatment showed no change in the expression of GST protein (Figure 6(b)). Therefore, GST was hypothesized to be mainly synthesized and secreted by hepatocytes and its protein level remained very low in NSCLC cells, making it difficult to detect significant changes in protein expression. The above results indicated that the combination treatment was more effective in EGFR-L858R/T790M-mutated NSCLC cells than in EGFR-WT NSCLC. Hence, further exploration of the real

underlying mechanism of combined treatment in H1975 cells using RNA sequencing is warranted.

As shown in Figure 7(a), the heat map showed gene expression changes, in which the combination group reversed most of the gene expression changes when compared with the afatinib alone group. Similar significant gene profile changes were obtained in H1975 cells. Next, the DEGs between afatinib and afatinib combined with EA were focused on, and a volcano plot was used to show the DEGs with a fold change of ≥2 and p value of ≤0.05. As shown in Figure 7(b), there were 1351 upregulated genes and 1234 downregulated genes. David 6.8 was used as a functional annotation tool to enrich these DEGs and the results of Pathway Enrichment. The top 3 enrichment pathways were shown in cancer (19 genes), cytokine-cytokine receptor interaction (14 genes), and HTLV-I infection (14 genes), respectively ($p < 0.05$), (Figure 7(c)). Beyond this, the pathway in cancer revealed that most of the genes are relative to WNT pathway (WNT7B, WNT6, WNT10B, FZD6, FZD8, and LPAR5), and among these, WNT7B, WNT10B, FZD6, FZD8, and LPAR5 belonged to the classical WNT pathway. As cytokines have paracrine action and play an important role in the tumor
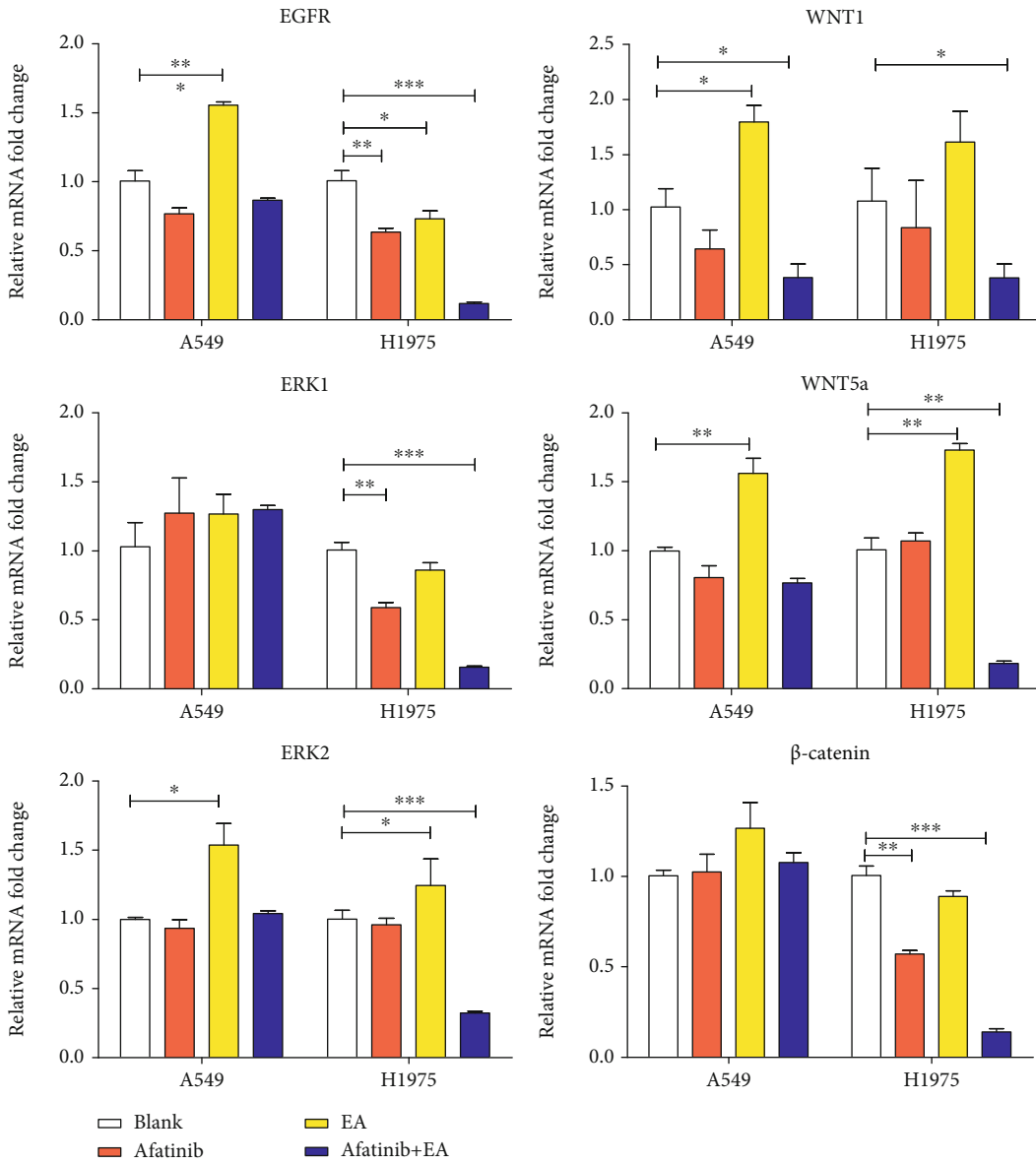
(a)
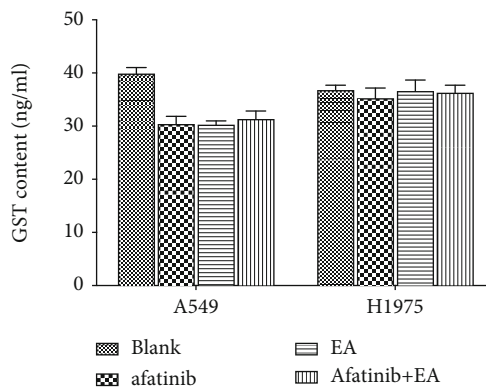
(b)

FIGURE 6: Combination with afatinib and EA inhibited EGFR pathway and WNT pathway. A549 and H1975 were analyzed by real-time qRT-PCR after stimulation with afatinib and with or without EA for 48 hours. (a) The impact on EGFR, ERK1, ERK2, WNT1, WNT5A, and β-catenin. (b) The change of GST protein in A549 or H1975 cells after treatment with afatinib and with or without EA. $^{*}p < 0.05$; $^{**}p < 0.01$; $^{***}p < 0.001$.
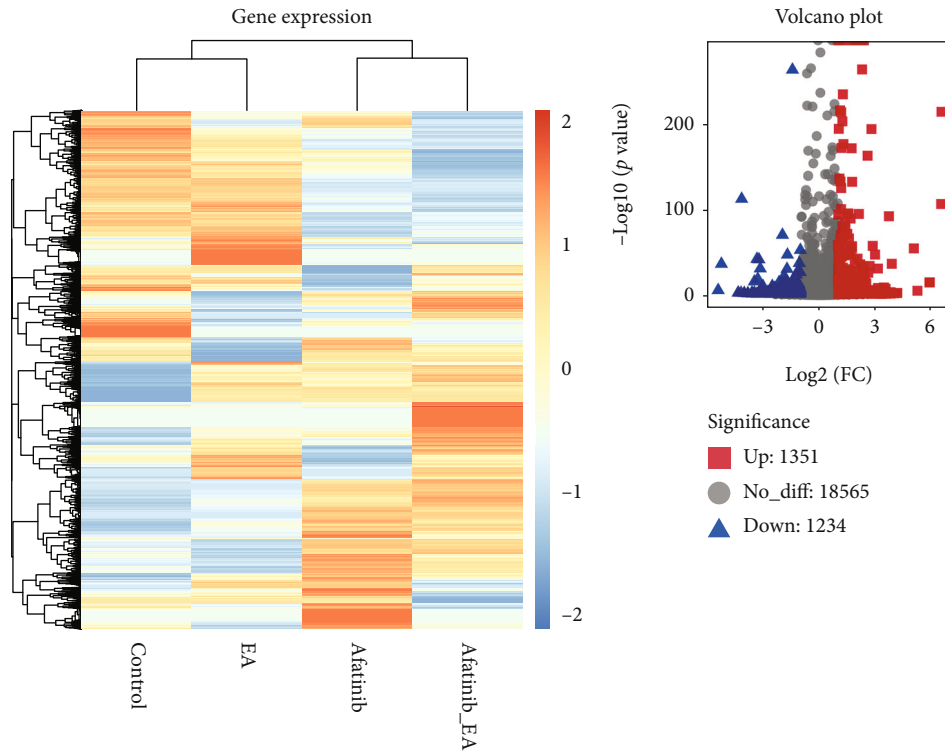
(a)

(b)
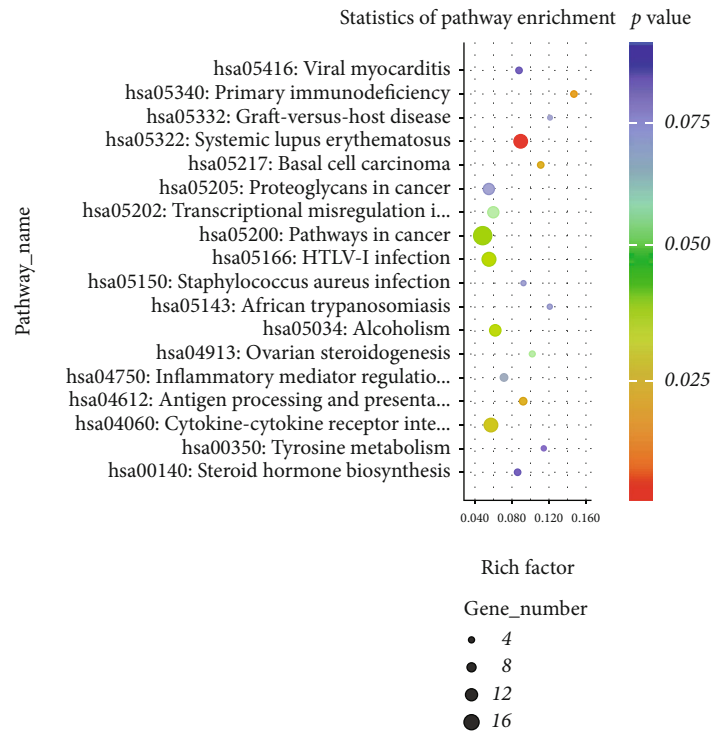
(c)

Figure 7: Continued.

(d)

(e)
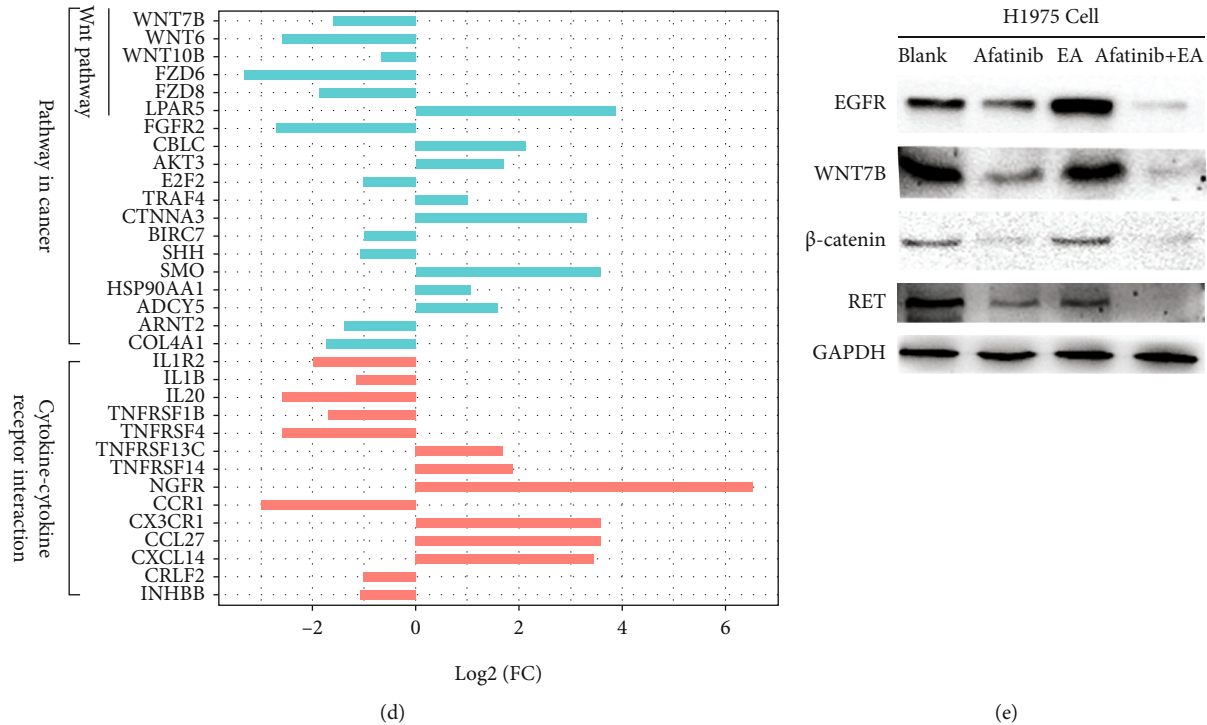
FIGURE 7: The mechanism of EA combined with afatinib had synergistic cytotoxic effects on H1975 cells. (a) The heat map showed gene expression of H1975 from RNA-seq after treatment with afatinib and with or without EA for 24 h. (b) Volcano plot showed the expression of differential genes in afatinib combined EA vs. afatinib alone. (c) Statistics of pathway enrichment on differential expressed genes were analyzed by KEGG (afatinib+EA vs. afatinib). (d) Relative expression of genes in the cancer and cytokine-cytokine receptor interaction pathways. (e) The change of protein expression in H1975 after treatment with afatinib and with or without EA were examined by western blotting.

microenvironment, the cytokine-cytokine receptor pathway was analyzed and found that many anti-inflammatory factors (IL1R2, IL1B, and IL20) were decreased. The above-mentioned DEGs in the combination group when compared to afatinib alone group were displayed in Figure 7(d). Finally, the expression of some proteins was validated by western blotting and found that the protein expression of EGFR, WNT7B, and RET, β-catenin in the combination treatment group was significantly decreased when compared to that in afatinib. RET gene is a new target closely related to the pathogenesis of NSCLC. It mainly induces oncoprotein production through KIF5B-RET, CCDC6RET, NCOA4RET, and TTlM33 genes and activates signal transduction pathways similar to ALK gene mutations and carcinogenesis. Mutations and fusions occur and are highly expressed in tumor tissues, thereby inducing NSCLC. As expected, the RET protein expression was significantly inhibited in the combination group than that in afatinib. Our findings demonstrated that combination with EA and afatinib enhanced the antitumor effects of afatinib and overcame T790M acquired resistance by suppressing WNT/β-catenin signaling pathway activation in NSCLC.

Furthermore, whether EGFR/ERK1/ERK2 or WNT1/WNT5A/WNT7B gene expression was potentially associated with the OS of lung cancer patients was assessed by Kaplan-Meier curve and Log-rank test. Kaplan-Meier curve plotter online tool (http://kmplot.com) included 1972 lung cancer patients for OS and 344 lung cancer patients for progression-

free survival (PFS) to analyze their correlation. However, except for WNT1, the WNT5A and WNT7B gene expressions showed significant positive correlation with OS (Figure 8(c)) and PFS (Figure 8(d)). These data suggested that WNT signaling pathway activation might contribute to lung cancer progression or EGFR TKIs resistance. Hence, these findings demonstrated that combining EA and afatinib enhanced the antitumor effects of afatinib and overcame T790M acquired resistance by suppressing WNT/β-catenin pathway activation in NSCLC patients.

4. Discussion

Acquired resistance is an inevitable question for the long-term use of TKIs, and so how to overcome resistance and prolong the duration of drug application is not only a hot topic in the current research but also an urgent problem to be resolved. Hence, in this study, a combination treatment with afatinib and EA was used in NSCLC and found that EA has synergistic effects on the antitumor activity of afatinib in EGFR L858R/T790M-mutated NSCLC cells.

Afatinib is a good and irreversible EGFR TKI, and recently, many clinical trials have proved that it can effectively prolong the median PFS and OS time in NSCLC patients when compared to the first-generation EGFR TKIs [19]. However, severe side effects and newer mutations induced acquired resistance, limiting its use clinically, and

EGFR (211551_at)

HR = 1.26 (1.11 − 1.43)
Log rank $P = 0.00041$

MAPK3 (212046_x_at)

HR = 1.18 (1.04 − 1.34)
Log rank $P = 0.0084$

MAPK1 (208351_s_at)

HR = 1.43 (1.26 − 1.63)
Log rank $P = 2.8e−08$

(a)

EGFR (211551_at)

HR = 1.06 (0.82 − 1.36)
Log rank $P = 0.67$

MAPK3 (212046_x_at)

HR = 1 (0.77 − 1.28)
Log rank $P = 0.97$

MAPK1 (208351_s_at)

HR = 1.1 (0.86 − 1.42)
Log rank $P = 0.45$

(b)

WNT1 (208570_at)

HR = 1.13 (1 − 1.29)
Log rank $P = 0.051$

WNT5A (205990_s_at)

HR = 0.82 (0.72 − 0.93)
Log rank $P = 0.0024$

LOC100289775 (217681_at)

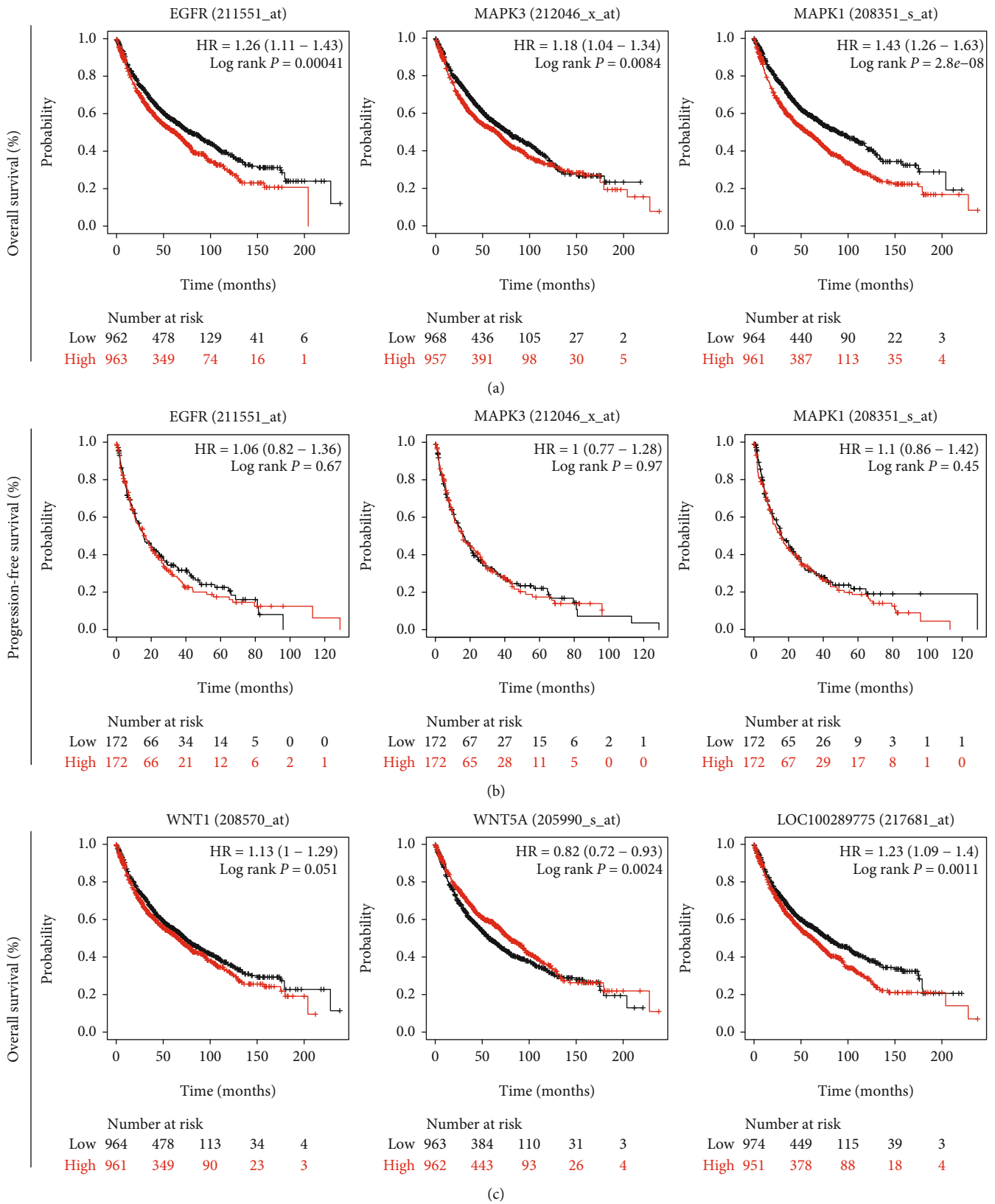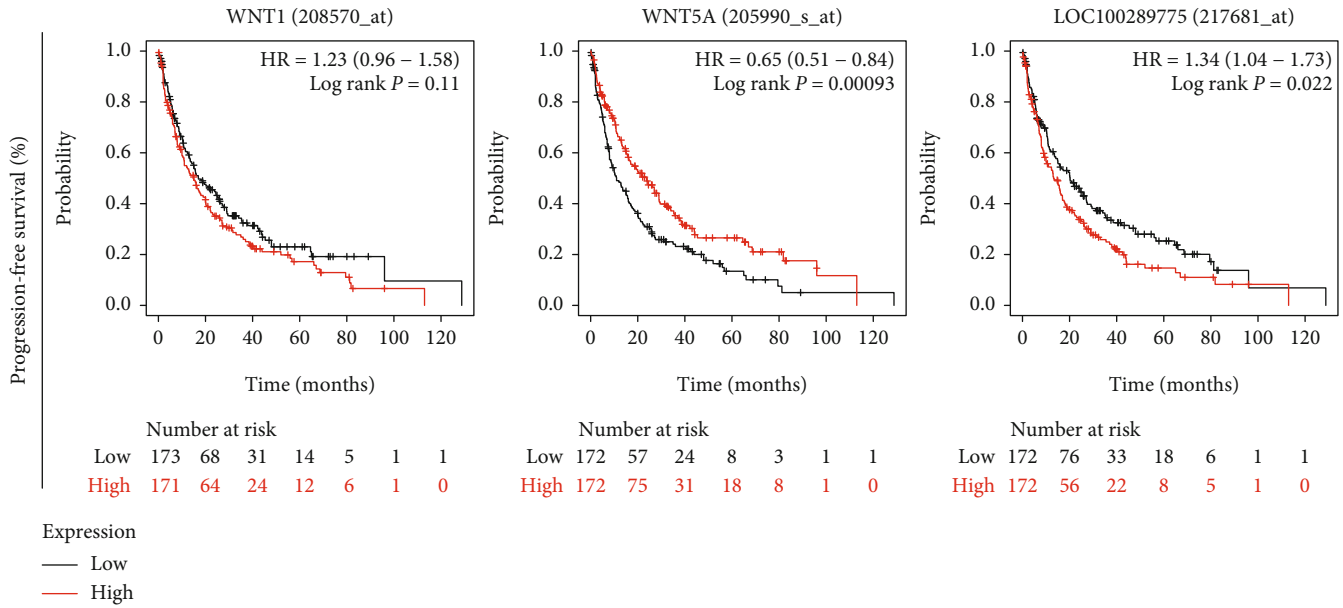HR = 1.23 (1.09 − 1.4)
Log rank $P = 0.0011$

(c)

Figure 8: Continued.

(d)

FIGURE 8: The effect of EGFR/ERK1/ERK2 OR WNT1/WNT5A/WNT7B gene expression on the OS and PFS of lung cancer patients by Kaplan-Meier curve and Log-rank test.

so some patients who acquired resistance to the first generation TKIs directly jumped to the third generation EGFR TKI treatment like osimertinib [20, 21]. Even though osimertinib has been approved for the treatment of EGFR-T790M mutant NSCLC patients, it is associated with drug resistance [22]. Thus, how to prolong the duration of second generation EGFR TKIs before the occurrence of T790M mutation or overcome the acquired resistance assists in improving the cure rate in patients and is the problem to be solved in our study. Afatinib combined with EA in NSCLC was studied due to two main reasons: one is a paper which revealed that β-catenin of the classical WNT signaling pathway contributed to lung tumor development induced by EGFR-T790M mutations, and genetic deletion of β-catenin gene dramatically reduced lung tumor formation in EGFR-L858R-T790M transgenic mice [15], and the other one is EA as a glutathione S-transferase P1-1(GSTP1-1) and WNT inhibitor can improve the antitumor effects of irreversible EGFR TKIs in breast cancer [14]. Thus, we inferred that EA combined with afatinib could improve the antitumor effects of afatinib in acquiring resistance in NSCLC. Besides these, there are two main types of EGFR-TKIs resistance: primary resistance and acquired resistance [23]. For primary resistance, it is said that approximately 30% EGFR-mutated NSCLC patients develop resistance at the beginning of EGFR-TKI treatment due to K-Ras mutation and PTEN deletion [24–27]. For acquired resistance, EGFR-T790M mutation, MET gene amplification, and HGF overexpression can cause this [28]. In the study, it was found that IL1R2 is more likely to act as a carcinogen in tumors, and it is only lowly expressed in a few tumors. IL-1B has strong proinflammatory activity and activates related signal pathways after binding to receptors on target cells. Such as MAPK, IL-1 signaling pathway, and STAT3 signaling pathway, which induce

tumor cell proliferation, migration, invasion, and metastasis [29, 30], IL-20 can activate the STAT signaling pathway as an effective angiogenesis, chemotaxis, and proinflammatory cytokine, which is related to chronic inflammatory diseases such as psoriasis, rheumatoid arthritis, osteoarthritis, cancer, and liver fibrosis [31]. A study showed that a single nucleotide polymorphism (SNP) of IL1R2 was found during the occurrence and development of NSCLC [32]. But their specific mechanisms affecting the process of lung cancer have not been reported in the literature. Among them, T790M mutation is considered the most important factor for secondary resistance to EGFR-TKIs, accounting for 50% of patients after EGFR-TKIs treatment [33]. Thus, A549 (EGFR wild-type and K-ras mutations) and H1975 (EGFR L858R and T790M mutations) NSCLC cells were chosen as research objects to better evaluate the antitumor effects of the combination of EA and afatinib [34]. Finally, our results showed that EA has no cytotoxic effects on NSCLC cells, and its IC50 value in A549 or H1975 cells reached to 87.03 μM or 99.54 μM, respectively. This high concentration does not meet the sensitivity and specificity requirements of drug development, and these results were not similar to those in leukemia [11, 35]. However, unexpectedly, regardless of whether 2 μm (IC30) or 6 μm (IC50) afatinib combined with 75 μm (IC30) EA was used, the antitumor effects of these combinations were stronger than that of the same dose of afatinib in H1975 cells both *in vitro* and *in vivo*, and their combination drug index (CDI) was less than 0.2. Conversely, the combination has little effect on primary drug resistance in A549 cells, meaning that EA really has a synergistic effect on the antitumor effects of afatinib in EGFR-T790M-mutated NSCLC.

For the mechanism regarding the combination of EFGR-T790M-mutated NSCLC, RNAseq was used to comprehensively analyze. The data of the transcriptome as shown in

the heat map revealed that the combination with afatinib and EA reversed most part of gene expression. Moreover, enriched and clustered analysis was performed for DEGs (log2 fold change > |1|, $p < 0.05$) and found that the pathway in cancer was significantly enriched. Among these genes, WNT7B, WNT10B, FZD6, FZD8, and LPAR5 are classical WNT signaling pathway genes, and most of them were significantly suppressed in the combination group. These results were similar to the study conducted by Nakayama's group [15], in which EA can enhance the antitumor effects of afatinib in NSCLC by suppressing the classical WNT signaling pathway activation. However, no changes in GST were detected in this study. A meta-analysis in 2018 reported that glutathione S-transferase gene polymorphism (GST-PI) gene mRNA was high in NSCLC and was involved in the pathogenesis and prognosis of NSCLC [36, 37]. In contrast, a study reported that the levels of GSH were low in EGFR-T790M NSCLC and increased GSH expression in acquired NSCLC cells resensitized by the EGFR TKIs [38]. Regarding these, it is hypothesized that liver cytochrome P450 enzymes, glutathione, and other drug metabolism-related enzymes are mainly synthesized and secreted by the liver, and only *in vivo* experiments can offer reliable results for the detection of the effects of these enzymes on EGFR TKIs. However, there are some deficiencies that still require improvement. For example, it is still a question as to which targets of WNT signaling pathway can truly reverse or overcome drug resistance? How do the WNT signaling pathway and EGFR-related signaling pathways interact in NSCLC. More animal experiments and molecular experiments should be carried out in the future.

In conclusion, our results demonstrated that EA has synergistic effects in enhancing the antitumor effects of afatinib in EGFR-T790M-mutated NSCLC both *in vitro* and *in vivo* by suppressing WNT/β-catenin pathway. These studies provide strong evidence and experimental basis to overcome the resistance of afatinib and the development of more effective strategies for clinical application in the future.

Data Availability

The data used to support the findings of this study is included within the article, and the data are available from the corresponding author request.

Conflicts of Interest

The authors declare that they have no conflict of interest.

Authors' Contributions

Xuehui Zhang performed the experiments and analyzed the results. Chaoyuan Huang designed the project and wrote the paper. Biyu Cui and Ye-Bin Pang helped to perform animal studies. Rong Liang revised the manuscript and assisted with the draft of the manuscript. Xiaoling Luo supervised the whole experimental work and revised the manuscript. All authors read and approved the final manuscript. Xuehui Zhang and Chaoyuan Huang contributed equally to this work.

Supplementary Materials

Supplementary 1. Supplementary Materials 1: pathways to cancer new.

Supplementary 2. Supplementary Materials 2: pathways of cytokines.

Supplementary 3. Supplemental Table 1: primer sequences for quantitative RT-PCR.

References

[1] R. L. Siegel, K. D. Miller, and A. Jemal, "Cancer statistics, 2020," *CA: a Cancer Journal for Clinicians*, vol. 70, no. 1, pp. 7–30, 2020.

[2] B. L. Liu, X. Y. Quan, C. G. Xu et al., "Lung cancer in young adults aged 35 years or younger: a full-scale analysis and review," *Journal of Cancer*, vol. 10, no. 15, pp. 3553–3559, 2019.

[3] A. Masood, R. K. Kancha, and J. Subramanian, "Epidermal growth factor receptor (EGFR) tyrosine kinase inhibitors in non-small cell lung cancer harboring uncommon EGFR mutations: focus on afatinib," *Seminars in Oncology*, vol. 46, no. 3, pp. 271–283, 2019.

[4] H. Tanaka, K. Taima, M. Itoga et al., "Real-world study of afatinib in first-line or re-challenge settings for patients with EGFR mutant non-small cell lung cancer," *Medical Oncology*, vol. 36, no. 6, 2019.

[5] G. F. Ho, C. S. Chai, A. Alip, C. K. Liam, and M. M. Yusof, "Real-world experience of first-line afatinib in patients with EGFR-mutant advanced NSCLC: a multicenter observational study," *BMC Cancer*, vol. 19, no. 1, p. 896, 2019.

[6] E. Felip, V. Hirsh, S. Popat et al., "Symptom and quality of life improvement in LUX-lung 8, an open-label phase III study of second-line afatinib versus erlotinib in patients with advanced squamous cell carcinoma of the lung after first-line platinum-based chemotherapy," *Clinical Lung Cancer*, vol. 19, no. 1, pp. 74–83.e11, 2018.

[7] K. Park, D. W. T. Lim, I. Okamoto, and J. C. H. Yang, "First-line afatinib for the treatment ofEGFRmutation-positive non-small-cell lung cancer in the 'real-world' clinical setting," *Therapeutic Advances in Medical Oncology*, vol. 11, p. 175883591983637, 2019.

[8] M. J. Hochmair, A. Morabito, D. Hao et al., "Sequential treatment with afatinib and osimertinib in patients withEGFRmutation-positive non-small-cell lung cancer: an observational study," *Future Oncology*, vol. 14, no. 27, pp. 2861–2874, 2018.

[9] M. Joshi, S. M. Rizvi, and C. P. Belani, "Afatinib for the treatment of metastatic non-small cell lung cancer," *Cancer Management and Research*, vol. 7, pp. 75–82, 2015.

[10] K. Tanaka, K. Nosaki, K. Otsubo et al., "Acquisition of the T790M resistance mutation during afatinib treatment in EGFR tyrosine kinase inhibitor-naïve patients with non-small cell lung cancer harboring EGFR mutations," *Oncotarget*, vol. 8, no. 40, pp. 68123–68130, 2017.

[11] D. Lu, J. X. Liu, T. Endo et al., "Ethacrynic acid exhibits selective toxicity to chronic lymphocytic leukemia cells by inhibition of the Wnt/beta-catenin pathway," *PLoS One*, vol. 4, no. 12, article e8294, 2009.

[12] L. C. Schmeel, F. C. Schmeel, Y. Kim, T. Endo, D. S. Lu, and G. H. Schmidt-Wolf Ingo, "Targeting the Wnt/beta-catenin pathway in multiple myeloma," *Anticancer Research*, vol. 33, no. 11, pp. 4719–4726, 2013.

[13] H. J. Byun, K. J. Kang, M. K. Park et al., "Ethacrynic acid inhibits sphingosylphosphorylcholine-induced keratin 8 phosphorylation and reorganization via transglutaminase-2 inhibition," *Biomolecules and Therapeutics*, vol. 21, no. 5, pp. 338–342, 2013.

[14] B. Liu, X. P. Huang, Y. L. Hu et al., "Ethacrynic acid improves the antitumor effects of irreversible epidermal growth factor receptor tyrosine kinase inhibitors in breast cancer," *Oncotarget*, vol. 7, no. 36, pp. 58038–58050, 2016.

[15] S. Nakayama, N. Sng, J. Carretero, R. Welner, and S. S. Kobayashi, "β-Catenin contributes to lung tumor development induced by EGFR mutations," *Cancer Research*, vol. 74, no. 20, pp. 5891–5902, 2014.

[16] T.-C. Chou and P. Talalay, "Quantitative analysis of dose-effect relationships: the combined effects of multiple drugs or enzyme inhibitors," *Advances in Enzyme Regulation*, vol. 22, pp. 27–55, 1984.

[17] C. L. Schwab, S. Bellone, D. P. English et al., "Afatinib demonstrates remarkable activity against HER2-amplified uterine serous endometrial cancer in vitro and in vivo," *British Journal of Cancer*, vol. 111, no. 9, pp. 1750–1756, 2014.

[18] J. Rapp, L. Jaromi, K. Kvell, G. Miskei, and J. E. Pongracz, "WNT signaling - lung cancer is no exception," *Respiratory Research*, vol. 18, no. 1, p. 167, 2017.

[19] B. Ricciuti, S. Baglivo, A. De Giglio, and R. Chiari, "Afatinib in the first-line treatment of patients with non-small cell lung cancer: clinical evidence and experience," *Therapeutic Advances in Respiratory Disease*, vol. 12, p. 175346661880865, 2018.

[20] W. H. Hsu, J. C. H. Yang, T. S. Mok, and H. H. Loong, "Overview of current systemic management of EGFR-mutant NSCLC," *Annals of Oncology*, vol. 29, suppl_1, pp. I3–I9, 2018.

[21] G. Recondo, F. Facchinetti, K. A. Olaussen, B. Besse, and L. Friboulet, "Making the first move in EGFR-driven or ALK-driven NSCLC: first-generation or next-generation TKI?," *Nature Reviews Clinical Oncology*, vol. 15, no. 11, pp. 694–708, 2018.

[22] T. Nagano, M. Tachihara, and Y. Nishimura, "Mechanism of resistance to epidermal growth factor receptor-tyrosine kinase inhibitors and a potential treatment strategy," *Cell*, vol. 7, 2018.

[23] A. Ayoola, A. Barochia, K. Belani, and C. P. Belani, "Primary and acquired resistance to epidermal growth factor receptor tyrosine kinase inhibitors in non-small cell lung cancer: an update," *Cancer Investigation*, vol. 30, no. 5, pp. 433–446, 2012.

[24] C. Mao, L.-X. Qiu, R.-Y. Liao et al., "KRAS mutations and resistance to EGFR-TKIs treatment in patients with non-small cell lung cancer: a meta-analysis of 22 studies," *Lung Cancer*, vol. 69, no. 3, pp. 272–278, 2010.

[25] G. Bidkhori, A. Moeini, and A. Masoudi-Nejad, "Modeling of tumor progression in NSCLC and intrinsic resistance to TKI in loss of PTEN expression," *PLoS One*, vol. 7, no. 10, article e48004, 2012.

[26] T. Onitsuka, H. Uramoto, N. Nose et al., "Acquired resistance to gefitinib: the contribution of mechanisms other than the T790M, MET, and HGF status," *Lung Cancer*, vol. 68, no. 2, pp. 198–203, 2010.

[27] E. Massarelli, M. Varella-Garcia, X. M. Tang et al., "KRAS mutation is an important predictor of resistance to therapy with epidermal growth factor receptor tyrosine kinase inhibitors in non-small cell lung cancer," *Clinical Cancer Research*, vol. 13, no. 10, pp. 2890–2896, 2007.

[28] W. Pao, V. Miller, M. Zakowski et al., "EGF receptor gene mutations are common in lung cancers from "never smokers" and are associated with sensitivity of tumors to gefitinib and erlotinib," *Proceedings of the National Academy of Sciences of the United States of America*, vol. 101, no. 36, pp. 13306–13311, 2004.

[29] M. Molgora, D. Supino, A. Mantovani, and C. Garlanda, "Tuning inflammation and immunity by the negative regulators IL-1R2 and IL-1R8," *Immunological Reviews*, vol. 281, no. 1, pp. 233–247, 2018.

[30] J. W. Long, Y. G. Xiang, X. H. Ma, Y. J. Hu, and M. L. Liu, "Advances in the mechanism of interleukin 1β activating signaling and transcription factor 3 to promote tumorigenesis," *Labeled Immunoassays and Clinical Medicine*, vol. 27, no. 11, pp. 2011–2015, 2020.

[31] L. Dumoutier, C. Leemans, D. Lejeune, S. V. Kotenko, and J.-C. Renauld, "Cutting edge: STAT activation by IL-19,IL-20 and mda-7 through IL-20 receptor complexes of two types," *Journal of Immunology*, vol. 167, no. 7, pp. 3545–3549, 2001.

[32] H. Edvardsen, P. F. Brunsvig, H. Solvang et al., "SNPs in genes coding for ROS metabolism and signalling in association with docetaxel clearance," *The Pharmaceutical Journal*, vol. 10, no. 6, pp. 513–523, 2010.

[33] R. Chen, T. T. An, J. Wang et al., "Non-invasive and quantitative analysis for EGFR T790M mutation in the patients with advanced non-small cell lung cancer received EGFR-TKI therapy," *Journal of Clinical Oncology*, vol. 31, 15_suppl, p. e19101, 2013.

[34] E. Giovannetti, M. Labots, H. Dekker et al., "Molecular mechanisms and modulation of key pathways underlying the synergistic interaction of sorafenib with erlotinib in non-small-cell-lung cancer (NSCLC) cells," *Current Pharmaceutical Design*, vol. 19, pp. 927–939, 2013.

[35] R. Wang, C. D. Liu, L. J. Xia et al., "Ethacrynic acid and a derivative enhance apoptosis in arsenic trioxide-treated myeloid leukemia and lymphoma cells: the role of glutathione S-transferase P1-1," *Clinical Cancer Research*, vol. 18, no. 24, pp. 6690–6701, 2012.

[36] P. P. Grimminger, M. K. H. Maus, P. M. Schneider et al.Glutathione S-transferase PI (GST-PI) mRNA expression and DNA methylation is involved in the pathogenesis and prognosis of NSCLC," *Lung Cancer*, vol. 78, no. 1, pp. 87–91, 2012.

[37] Z. Q. Zhong, H. Y. Li, H. Z. Zhong, T. B. Zhou, W. J. Xie, and Z. J. Lin, "A systematic review and meta-analyses of the relationship between glutathione S-transferase gene polymorphisms and renal cell carcinoma susceptibility," *BMC Medical Genetics*, vol. 19, no. 1, p. 98, 2018.

[38] H. Li, W. Stokes, E. Chater et al., "Decreased glutathione biosynthesis contributes to EGFR T790M-driven erlotinib resistance in non-small cell lung cancer," *Cell Discovery*, vol. 2, no. 1, 2016.